4th Generation aromatase inhibitors for the treatment of breast cancer:

design, synthesis, biochemical and molecular biology studies

A thesis submitted in partial fulfilment of the requirements for PhD degree

by

Ahmed Gamal Mohamed AbdAllah Eissa

Supervisors:

Dr. Claire Simons

Dr. Julia Gee

(December 2020)

Acknowledgements

Abbreviations

AI	Aromatase inhibitor
AJCC	American Joint Committee on Cancer
AKt	Protein kinase B
BRCA1	Breast cancer type 1 susceptibility protein gene
BRCA2	Breast cancer type 2 susceptibility protein gene
COX	Cyclooxygenase
DASI	Dual aromatase/sulfatase inhibitor
EGFR	Epidermal growth factor receptor
EPS	Extrapyramidal motor symptoms
ER	Oestrogen receptor
FAD	Flavin adenine dinucleotide
FMN	Flavin mononucleotide
HDACs	Histone deacetylases
HER	Human epidermal growth factor receptor
HIV	Human immunodeficiency virus
IGF-1	Insulin-like growth factor 1
IN	Integrase
MAPK	Mitogen activated protein kinase
MD	Molecular dynamics
MTDL	Multi-target directed ligand
mTOR	Mammalian target of rapamycin
NADP	Nicotinamide adenine dinucleotide phosphate
PI3K	Phosphatidylinositol 3-kinase
PR	Progesterone receptor
RT	Reverse transcriptase
SAR	Structure activity relationship
SERM	Selective oestrogen receptor modulator
STS	Sulfatase enzyme
TNBC	Triple negative breast cancer
UICC	Union for international Cancer Control
VEGFR	Vascular endothelial growth factor receptor

Table of contents

iv

xiv

List of tables

List of figures

Abstract

Breast cancer is one of the most common forms of cancer worldwide with 11.6% of all cancer incidence in 2018. One in every eight women will be diagnosed with breast cancer during their lifetime and approximately 70% of all patients are oestrogen receptor (ER) positive depending upon oestrogen for their growth. Oestrogens are synthesised from androgens through three steps, the last of which is catalysed by aromatase enzyme (CYP19A1), accounting for third generation aromatase inhibitors being the mainstay in the treatment of ER-positive breast cancer. Despite the success of current aromatase inhibitors, acquired resistance occurs after prolonged therapy. Although the precise mechanisms of resistance are not known, lack of cross resistance among aromatase inhibitors drives the need for a newer generation of inhibitors to overcome this resistance alongside minimising toxicity and adverse effects.

Novel inhibitors including 22 triazole-based compounds and 12 pyridine-based compounds were designed based on previously published parent compounds (**6a**, **6d**, **36a** and **36b**) by our group, making use of the now available crystal structure of CYP19A1 (PDB 3S79), to make modifications at specific sites to explore the potential of dual binding of both the active site and the access channel. Modifications included adding long chain substituents e.g. but-2-ynyloxy and pent-2-ynyloxy at different positions. The designed compounds were synthesised through various synthetic pathways and were fully characterised to ensure the effectiveness of the methods and quality of the products including the most active compound **23c** with IC_{50} value in the picomolar range (0.09 nM). Aromatase inhibition results paired with the molecular dynamics studies provided a clear structure activity relationship and favourable dual binding mode was verified.

Also, 11 sulfamate-based compounds were designed by the incorporation of the sulfamate group into the aromatase inhibitors to explore the aromatase/sulfatase dual inhibition. Six of these compounds (**47-51**) were based on the triazole scaffold, however biological evaluation revealed no sulfatase inhibitory activity despite the potent aromatase inhibition. Modifications led to the synthesis of the other five compounds (**56**) to achieve a balanced aromatase/sulfatase inhibition. However, the synthetic scheme for these compounds was not optimal either owing to poor reactivity of starting material and/or questionable purity of the products. This requires more investigation by working with larger scale and/or modifications to the structural design to overcome the low yield produced and the extensive purification process.

Proliferation assays and CYP selectivity profile studies for the most active compounds will be performed to select the best candidate for further development and investigations.

Chapter 1: General introduction

1.1. Incidence of breast cancer

Breast cancer is a heterogenous complex collection of neoplastic diseases originating from the epithelial cells lining the milk ducts rather than one single disease (Vargo-Gogola and Rosen 2007; Polyak 2011). Breast cancer is the most common form of cancer in women worldwide with more than 1.68 million women diagnosed in 2012 (Ferlay *et al.*, 2015; Cancer Research UK, 2017). Even more tragic, about 2.1 million women were estimated to be newly diagnosed with breast cancer in 2018 representing 11.6% of all cancer cases worldwide, the second most common cancer after lung cancer (**Figure 1.1a**) (Bray *et al.* 2018). On narrowing the comparison to only female cancer cases, this percentage changes into more than 24%, putting breast cancer above all cancers, with the second most common, colorectal cancer, with 9.5% (**Figure 1.1b**) (Bray *et al.* 2018). Breast cancer incidence rates shows intergender variations with 1 in 8 women and 1 in 870 men diagnosed with breast cancer during their lifetime (Ferlay *et al.* 2015; Cancer Research UK 2017). In most countries (154 out of 185), breast cancer is the highest diagnosed cancer e.g.; in the UK, breast cancer has the highest incidence (26.7%) and mortality rates (14.3%) among all female cancer cases (Bray *et al.* 2018; Ferlay *et al.* 2018).
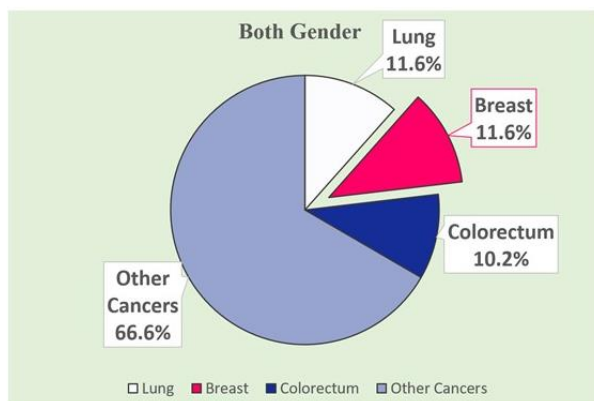
Figure (1.1a): Incidence of different cancer types worldwide (2018).
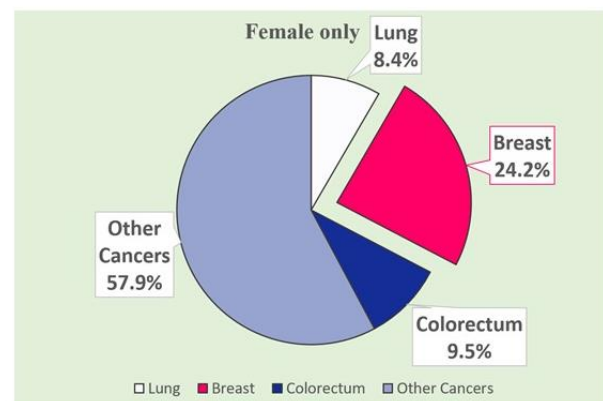
Figure (1.1b): Incidence of different cancer types worldwide (2018) (Female only cases).

1.2. Risk factors of breast cancer

Aetiology of breast cancer includes both genetic and non-genetic factors. While genetic factors, demonstrated by the tendency to cluster in some families attributed to high percentage

mutations e.g. BRCA1 or BRCA2 mutation (Mavaddat *et al.* 2010), underpin only a small proportion of breast cancer, most breast cancers are sporadic with non-genetic factors including age, smoking, alcohol consumption, physical inactivity, early menarche or late menopause (Mojaddami *et al.* 2017). Many of the risk factors are thought to be linked to the female hormone oestrogen (Mavaddat *et al.* 2010; Mojaddami *et al.* 2017). There is also a large difference in breast cancer susceptibility among different populations, for example, breast cancer shows a higher incidence rate in European women than African Americans, but the disease is more aggressive and hits at a younger age in the African American group (Mavaddat *et al.* 2010). Collectively risk factors can be categorised into modifiable and non-modifiable risk factors. Non-modifiable includes all genetic factors, age, race and menstrual history, while modifiable includes lifestyle elements such as external hormone administration, physical inactivity, smoking, alcohol and food consumption (Maas *et al.* 2019).

1.3. Classification of breast cancer

Different classification and staging systems have been addressed to organise the heterogenicity of breast cancer. Histologically, breast cancers can be either *in situ* or invasive, ductal or lobular (**Figure 1.2**) (Malhotra *et al.* 2010).
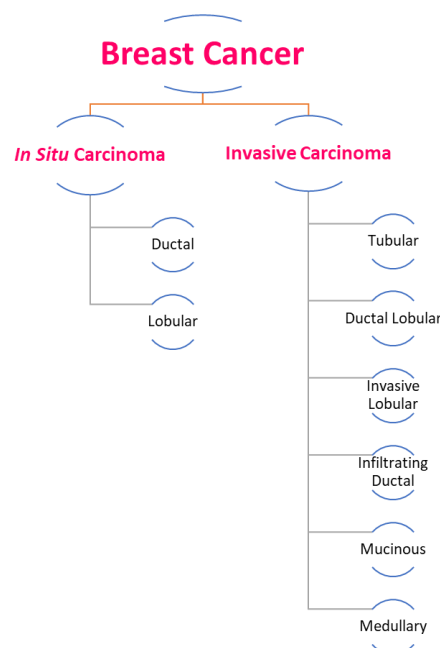
Figure (1.2): Histological classification of breast cancer subtypes (adapted from Malhotra *et al.* 2010).

For staging, the American Joint Committee on Cancer (AJCC) and the International Union for Cancer Control (UICC) maintains a coding system called TNM indicating the extent and size of the tumour (T), lymph nodes involved (N) and distant metastases (M) (Edge and Compton 2010). Stage I anatomically represents tumours smaller than 2 cm without the involvement of lymph nodes, while distant metastases is stage IV (Waks and Winer 2019).

With respect to molecular or clinical criteria, oestrogen receptor-alpha (ERα), progesterone receptor (PR) and human epidermal growth factor receptor 2 (HER2) are well-established immunohistochemical markers and provide the basis for traditional clinical classification of breast cancer (**Figure 1.3**) into (i) ER-positive, (ii) HER2-positive and (iii) triple negative (ER$^-$/PR$^-$/HER2$^-$) (De Abreu *et al.* 2014).
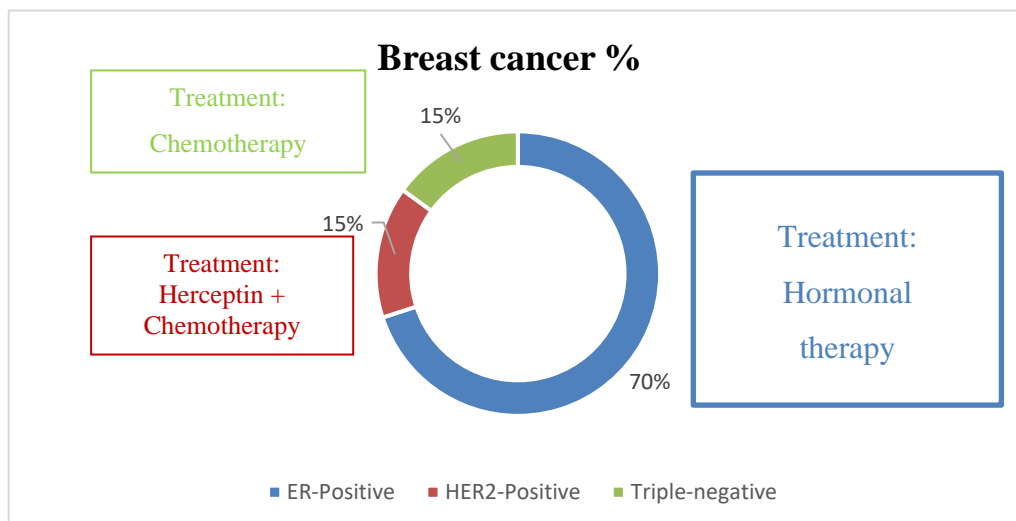
Figure (1.3): ER+, HER2+ and triple negative breast cancer percentage and first line treatment.

1.3.1. ER-positive breast cancer

Approximately 70% of all breast cancer patients are ER positive and commonly show dependence on oestrogen/ER signalling for their growth (Kang *et al.* 2018). Also most breast cancers affect postmenopausal women with 80% of them ER positive (Hiscox *et al.* 2009; Di Matteo *et al.* 2016). Oestrogens are synthesised from androgens by the act of aromatase enzyme. The ER is then activated by these steroidal oestrogenic sex hormones, which upon binding triggers ER conformational changes. The ligand-bound ER forms a dimer, which is able to bind DNA to activate the oestrogen response element sequence, with resultant ER regulated gene

expression (**Figure 1.4**). Such genes not only include the progesterone receptor (PR), but also other genes such as MYC, cyclin D1 and bcl-2 that lead to oestrogenic effects in breast cancer including proliferation and cell survival (Tokunaga *et al.* 2014; De Abreu *et al.* 2014; Hayashi and Kimura 2015).

There are two isoforms of ER; ER-α and ER-β, both are expressed in normal healthy mammary gland. In pathological conditions such as breast cancer, ER-α is often directly involved in tumour growth providing the basis for two different classes of antihormonal therapy (**Figure 1.4**); selective oestrogen receptor modulators (SERMs) that are competitive inhibitors of the ER e.g. tamoxifen, and oestrogen deprivation using aromatase inhibitors (AIs) e.g. anastrozole and exemestane (De Abreu *et al.* 2014).
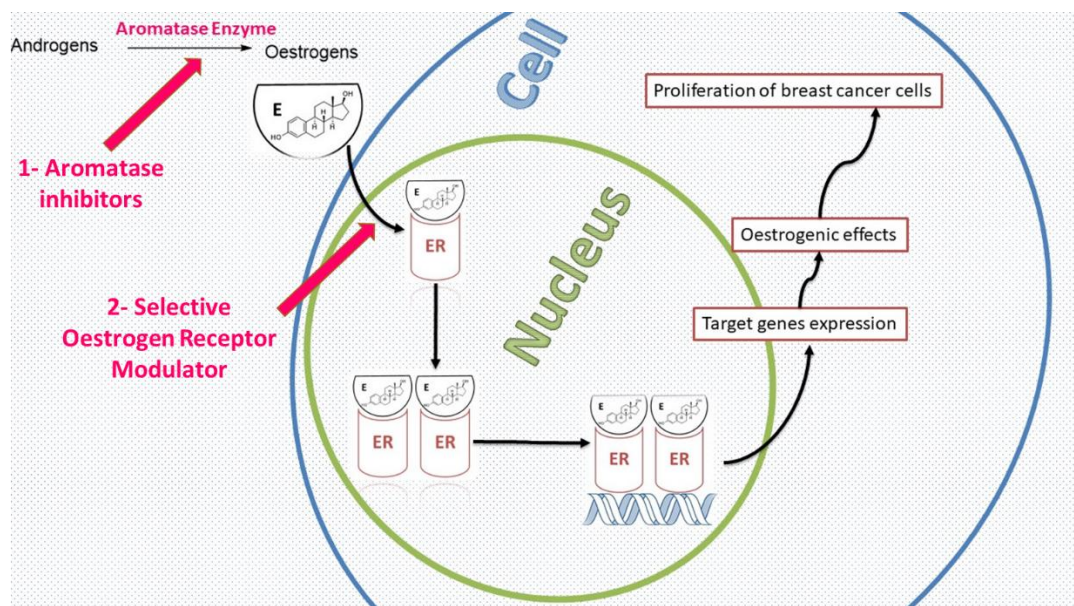
Figure (1.4): Oestrogen signalling pathway indicating treatment options for ER-positive breast cancer.

In premenopausal women, oestrogen is synthesised in the ovaries. In postmenopausal women, the main source is peripheral conversion of androgens to oestrogens by the action of aromatase enzyme. In total, this makes aromatase inhibitors the standard oestrogen deprivation treatment for ER positive breast cancer in postmenopausal women (Chumsri *et al.* 2011).

1.3.2. HER2-positive breast cancer

The human epidermal growth factor receptor (HER) family includes HER1, HER2, HER3 and HER4. HER2 (now known as ErbB2) is a transmembrane receptor tyrosine kinase, which has an important role in regulation of cell proliferation and survival in some breast cancers (Waks and Winer 2019). HER2 can be expressed in ER+ or in ER- disease. HER2 overexpression is found in 15-20 % of all breast cancer cases. In this type of breast cancer, targeting HER2 causes inhibition of cancer cell growth and apoptosis (De Abreu *et al.* 2014). One of the main agents used is trastuzumab (Herceptin), which is a monoclonal antibody for the HER2 extracellular domain causing HER2 downregulation (De Abreu *et al.* 2014). Apart from ErbB2 antibodies, small molecule tyrosine kinase inhibitors e.g. lapatinib and neratinib are another targeted option for treating this subclass of breast cancer (Waks and Winer 2019).

1.3.3. Triple negative breast cancer

Triple negative breast cancer (TNBC), lacking ER, PR and HER2, is a more aggressive class and has a poor prognosis and clinical outcome. This type of breast cancer partially responds to chemotherapy with no clinically approved targeted therapy, however TNBC represents around 15-20 % of all breast cancer cases. (De Abreu *et al.* 2014).

1.4. Molecular profile of breast cancer

The immunohistochemical and histological features of breast cancer can now be enhanced by the advances in molecular biology techniques such as microarrays, gene expression and sequencing studies, which has resulted in an expansion of different subtypes of the disease. In 2000, four subtypes of breast cancer were revealed based on their molecular profile (Perou *et al.* 2000). This includes: (i) luminal (ER positive and PR Positive), (ii) HER2 overexpressing (ER negative, PR negative, HER2 positive), (iii) basal-like (triple negative disease: ER negative, PR negative, HER2 negative) and (iv) normal breast-like. In 2006, this classification was extended to divide the luminal subclass into luminal A (HER2 negative) and luminal B (HER2 positive or highly proliferative as detected by Ki67 immunostaining) (Hu *et al.* 2006). More recently in 2007, a further triple negative subtype (Claudin-low) was also reported (Herschkowitz *et al.* 2007). Molecular profiling for breast cancer did not reach clinical

implementation but it was able to identify to date at least five clinically important subtypes (**Table 1.1**) (Cetin and Topcul 2014; De Abreu *et al.* 2014).

Table (1.1): Molecular subtypes of breast cancer with immunohistochemical markers

Subclass	Luminal A	Luminal B	HER2-positive	TNBC	
				Basal-like	Claudin-low
Percentage	**50 -60 %**	**10-20 %**	15-20 %	10-20 %	12-14 %
Receptors	**ER⁺/PR⁺**				
		HER2⁺			
Therapy	**Hormonal therapy (SERMs & AIs)**				
		HER2-targeted therapy (Herceptin)			
	Chemotherapy				

1.5. Oestrogen synthesis through steroidogenesis

Oestrogen has a vital role in the pathological processes of ER-positive breast cancer (De Abreu *et al.* 2014; Hayashi and Kimura 2015). Sex hormones including oestrogen are synthesised via the steroidogenic pathway from cholesterol (**Figure 1.5**). Many of the enzymes involved in steroid biosynthesis are cytochrome P450 enzymes (Miller and Auchus 2011).
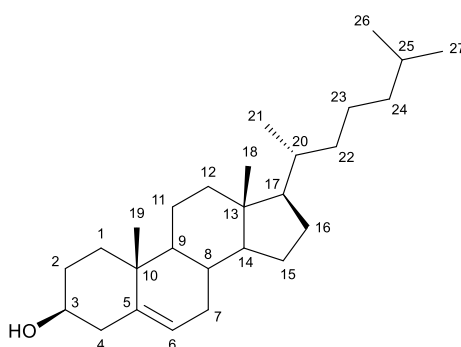
Figure (1.5): Structure of cholesterol with numbering.

Each cytochrome P450 has the ability to metabolise multiple substrates, catalysing a broad range of predominantly oxidation reactions. Six cytochrome P450s have roles in steroidogenesis (**Figure 1.6**) three of which are mitochondrial (P450scc and the two isozymes

of P450c11). P450scc (cholesterol side-chain cleavage enzyme) catalyses the series of reactions known as 20,22-desmolase. P450 c11β (11β-hydroxylase) and c11AS (aldosterone synthase), catalyse 11β-hydroxylase, 18-hydroxylase, and 18-methyl oxidase activities. The other three are bound to the endoplasmic reticulum. P450c17 catalyses 17-hydroxylase and 17,20-lyase activities, while P450c21 is responsible for 21-hydroxylation in the synthesis of glucocorticoids and mineralocorticoids. Last but not least is the unique P450arom (aromatase enzyme) which catalyses aromatisation of androgens to oestrogens i.e. androstenedione to oestrone and testosterone to oestradiol (Miller and Auchus 2011).
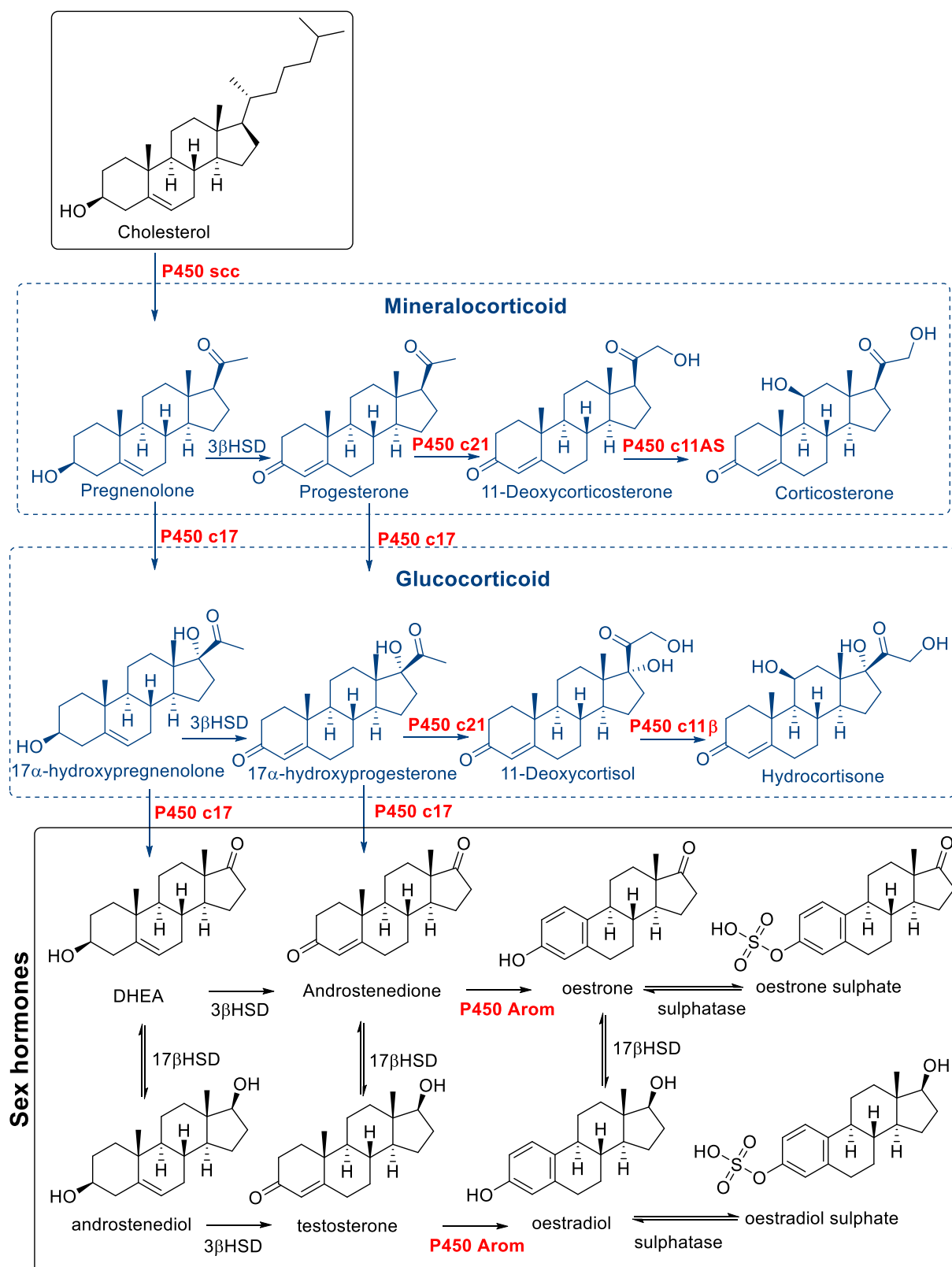
Figure (1.6): Steroidogenesis pathway of the human sex hormones with cytochrome P450 enzymes denoted in red.

1.6. Treatment options for breast cancer

Treatment options for breast cancer can be either local or systemic depending on whether the tumour is metastatic or not. Local therapy includes surgery and radiotherapy, while systemic therapy includes chemotherapy and antihormonal treatment or HER2 directed therapy (**Figure 1.7**).
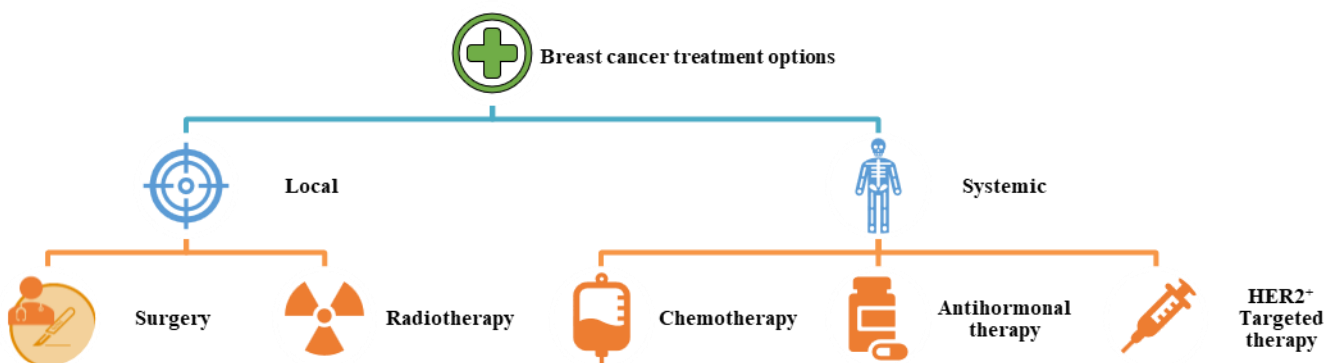
Figure (1.7): Breast cancer treatment options.

In non-metastatic breast cancer, the main objectives are to eradicate the tumour from the breast and the involved regional lymph nodes through surgery with or without postoperative radiation and to prevent recurrence through systemic therapy. The adjuvant or neoadjuvant systemic therapy component is guided by the subtype of breast cancer (Waks and Winer 2019). Oestrogen dependant breast cancer requires antihormonal treatment, while HER2+ tumours require trastuzumab. In an adjuvant setting, the antihormonal treatment can be either AIs or SERMs followed by AIs for 5 years. Neoadjuvant setting refers to treatment applied before surgery to down-stage the tumour including any chemotherapy, antihormonal therapy or even radiation (Chumsri *et al.* 2011). TNBC systemic treatment is generally achieved by chemotherapy, however some patients from other subtypes may require chemotherapy as well. In metastatic tumours, systemic therapy is the mainstay to relieve some of the symptoms and to prolong life as it is virtually incurable and local therapies have very little effect (Waks and Winer 2019).

1.7. History of Hormonal therapy

The history of breast cancer antihormonal treatment starts with Sir George Beatson in the 1890s who reported response to oophorectomy highlighting the role of ovarian hormones in breast cancer (Beatson 1896). Afterwards, other surgical interventions such as adrenalectomy and hypophysectomy were also tried for the control of breast cancer (Chumsri *et al.* 2011). By 1937 diethylstilbestrol was synthesised demonstrating anti-cancer activity but was discontinued owing to its severe side effects (Dixon 2014).

Diethylstilbestrol
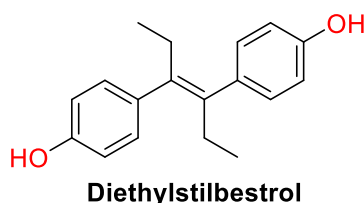
In the 1970s, there was a breakthrough with the approval of the first drug to target the oestrogen signalling pathway, a triphenyl ethylene compound first synthesised in the 1960s, known as Tamoxifen providing the backbone of breast cancer therapy for the following three decades ahead (Cole *et al.* 1971). Competitively blocking the oestrogen receptor made the nonsteroidal antioestrogen Tamoxifen the first member of a class called selective oestrogen receptor modulators (SERMs) (Chumsri *et al.* 2011; Dixon 2014; Begam *et al.* 2017).

**Tamoxifen
(Trans isomer)**
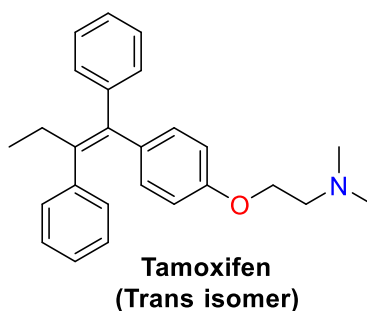
Around the same time an anti-epileptic non-steroidal drug, aminoglutethimide, gained attention as a treatment for breast cancer owing to its ability to inhibit the aromatase enzyme as part of its multiple cytochrome P450 enzyme inhibitory action and became the first known potent aromatase inhibitor (AI). Although aminoglutethimide use for treatment of breast cancer was not favoured because of a lack of aromatase selectivity and significant side effects, it paved the way for subsequent generations of AIs (Chumsri *et al.* 2011; Ghosh *et al.* 2016).
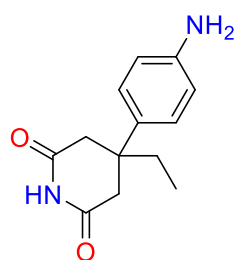
Aminoglutethimide

In the 1980s, a by-product, 4-hydroxy-4-androstene-3,17-dione, from a synthetic pathway for 2-hydroxy-steroid-4-en-3-ones at Angela Brodie's laboratory at the University of Maryland gained attention and underwent clinical trials for the treatment of breast cancer (Brodie *et al.* 1981). Being one of the most promising second generation AIs, it was renamed formestane and was found to be the first selective steroidal AI (Chumsri *et al.* 2011; Ghosh *et al.* 2016). Another AI, fadrozole, was approved in Japan as a more potent and specific nonsteroidal AI compared with the parent aminoglutethimide. Despite being the leading second generation AI, fadrozole was never approved in the USA as a drug (Ghosh *et al.* 2016).
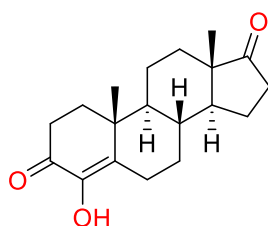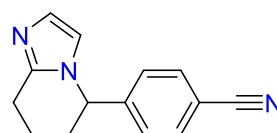
Formestane   **Fadrozole**

In the late 1990s, third generation AIs stepped into the forefront after the FDA approval of three drugs, namely; Anastrozole (Arimidex), Letrozole (Femara) and Exemestane (Aromasin) (Ghosh *et al.* 2016; Brodie and Njar 1998; Miller 1999). Based upon the difference in their structural skeleton, current AIs can be categorised into two distinct subclasses, namely androgen-like steroidal (e.g. Exemestane) and non-steroidal inhibitors (e.g. Anastrozole and Letrozole) (Chumsri *et al.* 2011; Kang *et al.* 2018).

Anastrozole

Letrozole

Exemestane
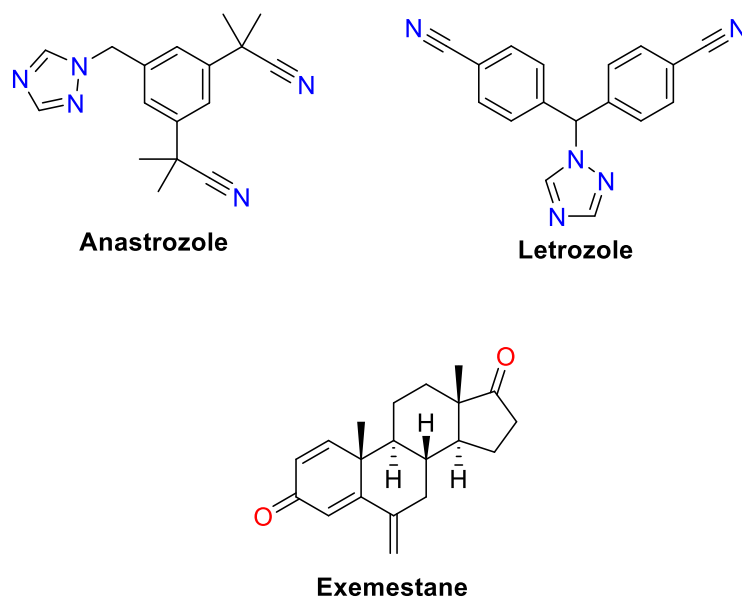
The 3rd generation steroidal and non-steroidal AIs, after a long history of development of the antihormonal therapy (**Figure 1.8**), constitute the current front line treatment for ER positive postmenopausal breast cancer in women (Miller and Larionov 2012; Kang *et al.* 2018).
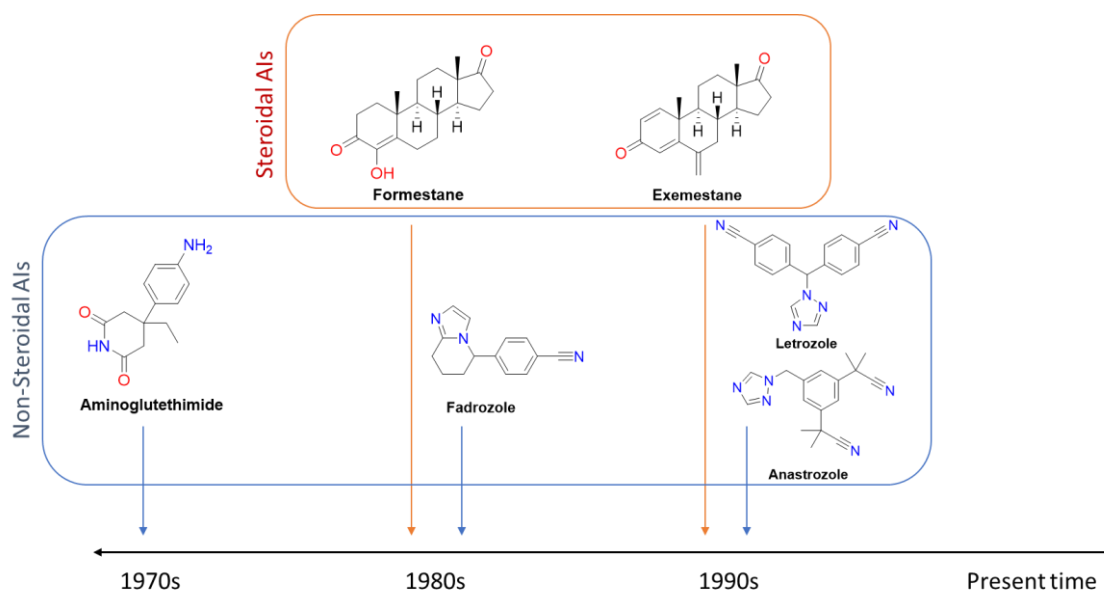
Figure (1.8): Timeline of development of aromatase inhibitors.

Being more potent than previous generation AIs and also SERMs (e.g. Tamoxifen), all three third generation AIs were found to be equally effective in head to head trials with no evidence of superiority of either steroidal or non-steroidal over the other (Ghosh *et al.* 2016; Goss *et al.*

2013; Murray *et al.* 2009). Despite high efficacy and selectivity, some cross-activity to other cytochrome P450 family members (e.g. Anastrozole's inhibition of CYP1A2, Letrozole's inhibition of CYP2A6) and some androgenic along with weak ERα agonistic activity are two drawbacks of the current third generation AIs (Ghosh *et al.* 2016).

1.8. The need for a new generation of aromatase inhibitors

Despite the success of currently available aromatase inhibitors in ER+ postmenopausal breast cancer, acquired resistance to aromatase inhibitors eventually occurs after prolonged therapy (Hiscox *et al.* 2009; Dixon 2014). Although the precise mechanisms of aromatase inhibitor resistance are not known, and many mechanisms have been implicated and are being studied, of particular note are three major mechanistic categories comprising (**Figure 1.9**): (i) aromatase-independent supply of oestrogens e.g. the action of sulfatase enzyme as described in steroidogenesis (**Figure 1.6**) (ii) oestrogen-independent activation of ER, and (iii) ER-independent cancer cell proliferation (Hayashi and Kimura 2015).
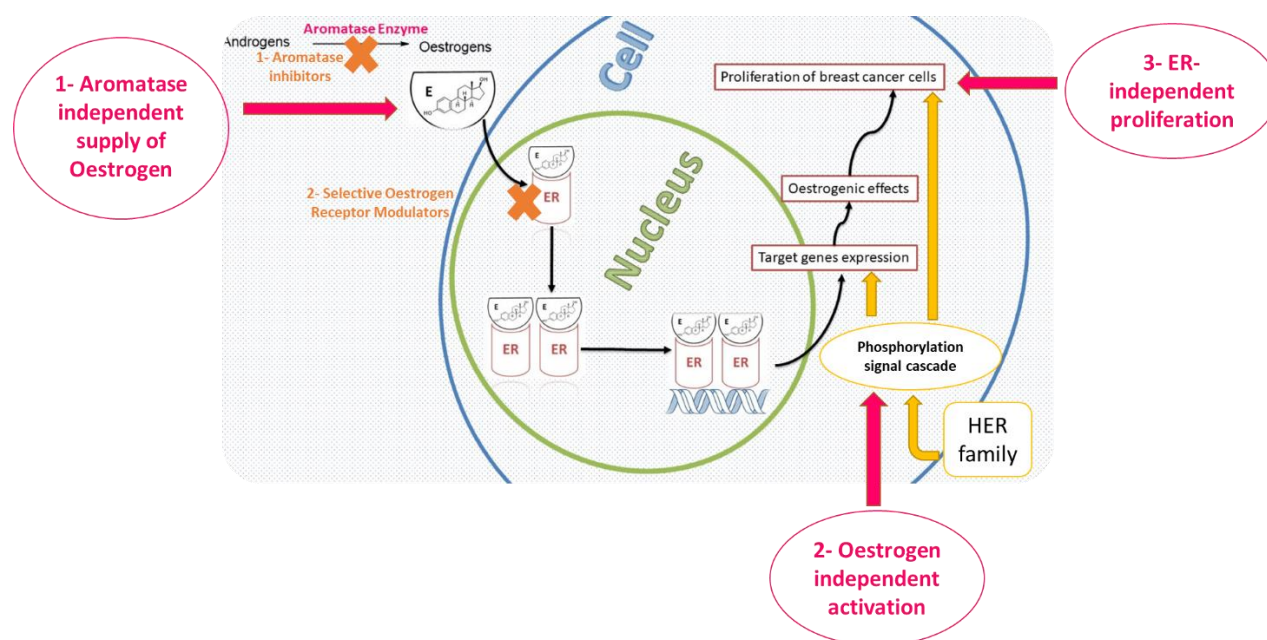
Figure (1.9): The three categories of aromatase inhibitor resistance (adapted from Hayashi and Kimura 2015).

The mechanisms of this resistance are versatile and differ from one AI to another, however they are usually related to crosstalk between oestrogen signalling and pathways of one of the growth factors (**Figure 1.10**). For example, in relation to resistance mechanisms involving

deregulated growth factor pathways that can activate ER independent of oestrogen levels, in Letrozole resistant breast cancer, significant upregulation of the HER2/mitogen activated protein kinase (MAPK) signalling pathway has been observed leading to ligand-independent phosphorylation and thus activation of oestrogen receptor (Chumsri *et al.* 2011). However, in the case of anastrozole resistance, upregulation of insulin-like growth factor 1 (IGF-1) receptor and the phosphatidylinositol 3-kinase (PI3K)/ protein kinase B (AKt)/mammalian target of rapamycin (mTOR) pathway leading to oestrogen independent activation of ER has been reported (Macedo *et al.* 2008). Other resistance mechanisms include mutation or truncation of ERα (Chumsri *et al.* 2011). Moreover, hypersensitivity of ER to residual amounts of oestrogen has been suggested to cause resistance to aromatase inhibitors (Dixon 2014).
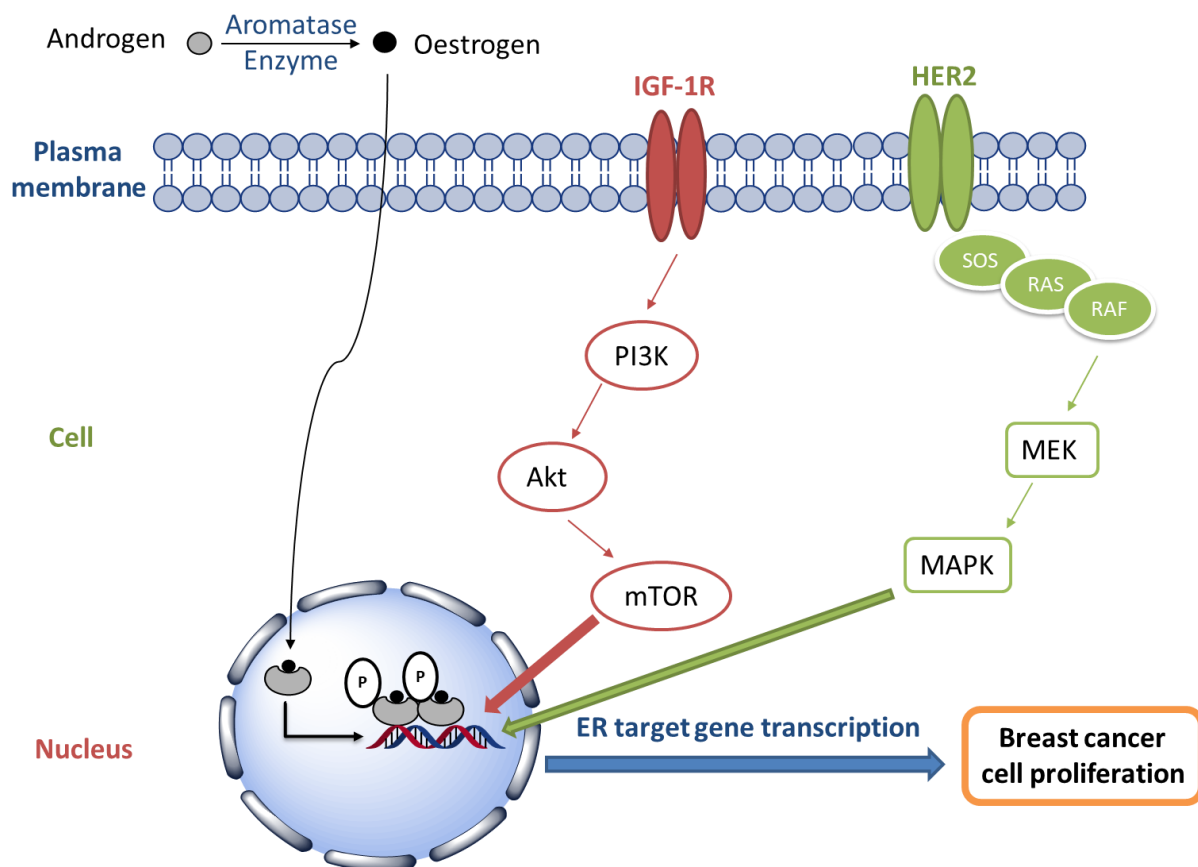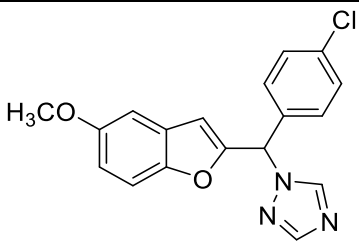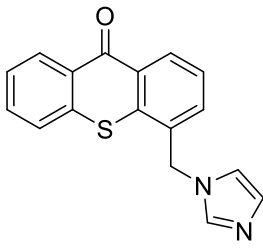
Figure (1.10): Crosstalk between ER signalling pathway, IGF-1 and HER2 pathways (adapted from Hayashi and Kimura 2015).
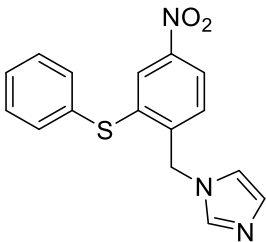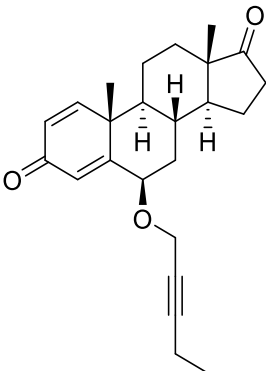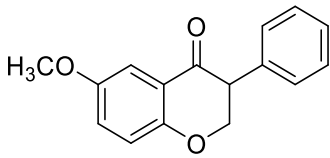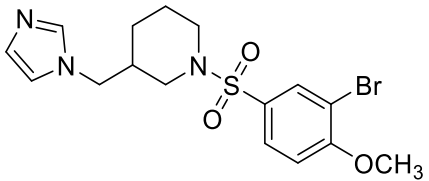
Interestingly, evidence also indicates that resistance can emerge to one aromatase inhibitor while the tumour remains responsive to another as there is a lack of cross resistance among aromatase inhibitors (Miller and Larionov 2012; Chumsri *et al.* 2011).
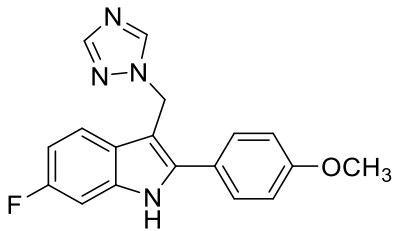
Therefore the design and synthesis of a new generation of inhibitors is needed to widen the therapeutic options facing the risk of resistance towards available drugs, minimise toxicity and reduce the non-specific and adverse effects by increasing aromatase selectivity (Mojaddami *et al.* 2017; Kang *et al.* 2018; Ghosh *et al.* 2016).

Great efforts have been made to date in relation to the design of further compounds, some with improved IC_{50} values compared with the clinically-approved reference compounds and so with promising AI activity. This is the case either for steroidal or nonsteroidal AIs especially after the crystal structure of aromatase (PDB 3EQM) was published (Ghosh *et al.* 2009). There is chemical diversity among the reported compounds e.g. azole derivatives, quinoline, flavone, coumarins and other compounds with different chemical structures. Some of the steroidal and non-steroidal reported compounds are summarised in **Table 1.2.**

Table (1.2): Some of the previously reported compounds with promising AI activity with IC_{50} data

Compound	IC_{50} (nM)	Type of assay	Reference compound (IC_{50})	Reference
1-((4-chlorophenyl)(5-methoxybenzofuran-2-yl)methyl)-1*H*-1,2,4-triazole	44	Placental microsomes aromatase inhibitory measuring produced tritiated water	Anastrozole (0.6 µM)	(Saberi *et al.* 2006)
4-((1*H*-imidazol-1-yl)methyl)-9*H*-thioxanthen-9-one	3.98	Placental microsomes aromatase inhibitory measuring produced tritiated water	Fadrozole (52 nM)	(Gobbi *et al.* 2010)

Compound	IC$_{50}$ (nM)	Type of assay	Reference compound (IC$_{50}$)	Reference
 1-(4-nitro-2-(phenylthio)benzyl)-1*H*-imidazole	5.59	Placental microsomes aromatase inhibitory measuring produced tritiated water	Fadrozole (52 nM)	(Gobbi *et al.* 2010)
 (6*R*,8*R*,9*S*,10*R*,13*S*,14*S*)-10,13-dimethyl-6-(pent-2-yn-1-yloxy)-7,8,9,10,11,12,13,14,15,16-decahydro-3*H*-cyclopenta[*a*]phenanthrene-3,17(6*H*)-dione	11.8	Placental microsomes aromatase inhibitory measuring produced tritiated water	Exemestane (50.1 nM)	(Ghosh *et al.* 2012)
 6-methoxy-3-phenylchroman-4-one	0.26 μM	Fluorometric substrate (7-methoxy-trifluoromethylcoumarin) and human CYP19 aromatase	Ketoconazole (1.3 μM)	(Bonfield *et al.* 2012)
 3-((1*H*-imidazol-1-yl)methyl)-1-((3-bromo-4-methoxyphenyl)sulfonyl)piperidine	6	Recombinant human aromatase and a fluorometric substrate, 7-methoxy-4-trifluoromethyl coumarin (MFC)	Letrozole (4 nM)	(Di Matteo *et al.* 2016)

Compound	IC$_{50}$ (nM)	Type of assay	Reference compound (IC$_{50}$)	Reference
3-((1*H*-1,2,4-triazol-1-yl)methyl)-6-fluoro-2-(4-methoxyphenyl)-1*H*-indole	14.1	Placental microsomes aromatase inhibitory using ELISA estrone kit	Letrozole (49.5 nM)	(Kang *et al.* 2018)

1.9. Gaps and new concepts for future designs to target oestrogen synthesis

There is an absence of experimentally determined structural data on binding modes of the non-steroidal AIs, which makes the widely reported docking studies to the aromatase active site provisional. This represents a major limitation to the design of novel AIs. There is experimental evidence that the non-steroidal agent anastrozole binding mode to the active site of aromatase does not include any interaction between the triazole and Asp309 of the enzyme, which in contrast is thought to be a crucial residue for steroidal AI binding (Ghosh *et al.* 2016). Hyperfine sublevel correlation spectroscopy studies (HYSCORE) showed that the N4 atom of the triazole in anastrozole directly coordinates with the iron of the haem as the sixth ligand displacing the water molecule (Maurelli *et al.* 2011). This means that anastrozole is suggested to bind as a pseudo-substrate of the aromatase enzyme (**Figure 1.11**) (Gilardi and Di Nardo 2017).
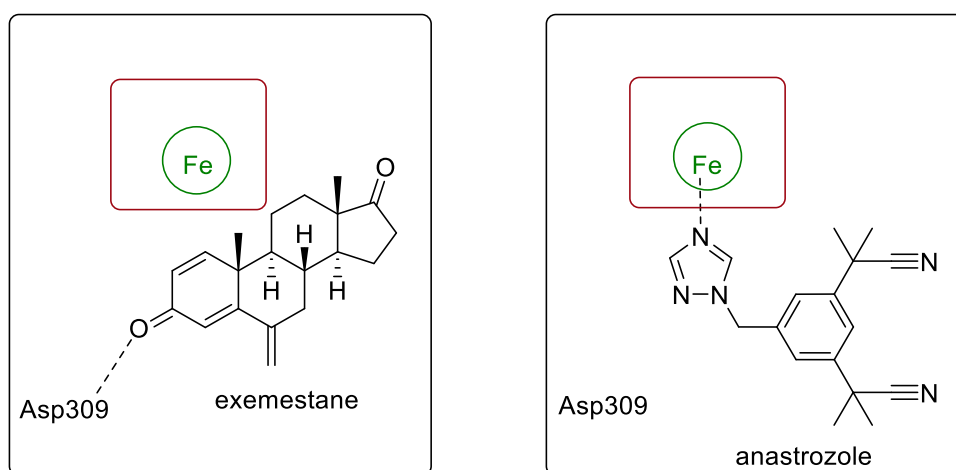
Figure (1.11): Binding of anastrozole vs exemestane.

Another aspect is a dual-binding mode for some of the recently reported compounds (Ghosh *et al.* 2012). Computational studies for these compounds has shown that for steroidal inhibitors, a C6 substitution with a methyl or longer derivatives e.g. pent-2-ynyl, gave the compounds an ability to bind in the access channel as an allosteric binding site as well as the active site pocket in the enzyme introducing a new insight into aromatase inhibition (Ghosh *et al.* 2016).

A totally different area is the study of sulfatase enzyme (STS) inhibition. STS is an enzyme that catalyses the hydrolysis of steroid sulfates to the biologically active forms, so the steroid sulfates can act as a reservoir for oestrogens as indicated in the steroidogenesis pathway (**Figure 1.6**). In breast cancer, STS activity is at least 50 times greater when compared with normal breast tissues making it a possible target in the fight against hormone dependant breast cancer (Begam *et al.* 2017). In this regard, oestrone-*O*-sulfamate (EMATE) was designed by replacing the oestrogen sulfate OH group with an amino group to provide a potent STS inhibitor (Purohit and Foster 2012).

EMATE
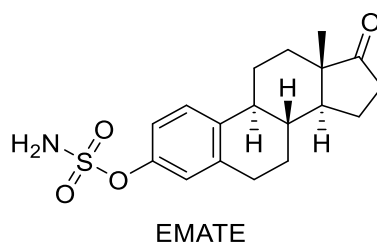
More interestingly, dual aromatase-sulfatase inhibition is a rising concept in the field of hormone dependent breast cancer. Comparing dual inhibition to a multi-drug approach shows some advantages in terms of avoiding drug-drug interactions or as a way to circumvent resistance that may arise for either one of the two enzyme targets. The initial idea of dual aromatase-sulfatase inhibitor design is based on sulfomylation of compounds with initial aromatase inhibitor properties (Wood et al. 2011).

1.10.   Aim and Objectives

Resistance towards available AIs as antihormonal treatment for oestrogen dependant breast cancer, with the side effects produced due to cross reactivity of current AIs towards other CYP enzymes drives an urgent need for developing new generation of AIs to overcome these problems. The absence of experimentally determined structural data on binding modes of the non-steroidal AIs represents a knowledge gap facing the design of new AIs, however new insights represented in the dual binding concept of both the active site and its access channel may present the molecular basis for the design of a 4th generation of aromatase inhibitors with the aim of filling this knowledge gap. Also, dual aromatase-sulfatase inhibition as a rising concept in the field of hormone dependent breast cancer provides another dimension in the attempts to circumvent the hormonal treatment resistance, leading to a clear research question or hypothesis for the thesis.

Aims: To design and synthesise new chemical molecules that will function as aromatase (CYP19A1) inhibitors or dual aromatase-sulfatase inhibitors with potential as anti-breast cancer agents.

Objectives:

1- To understand the binding requirements of the androgen specific active site and potential allosteric binding sites of aromatase and use of the knowledge gained to design selective non-steroidal aromatase inhibitors with the aid of computational tools; docking and molecular dynamics (MD).

2- To design novel compounds having the structural requirements for acting as dual aromatase-sulfatase inhibitors (DASI).

3- To develop synthetic routes to synthesise the novel inhibitors.

4- To perform biological assays (aromatase inhibitory activity and sulfatase inhibitory activity) to assess the efficacy of novel inhibitors.

5- To perform toxicological studies (MTT assays) to evaluate the safety index of the novel inhibitors.

Chapter 2: triazole-based dual binding aromatase inhibitors

2.1. Background

2.1.1. Aromatase (CYP19A1) as part of the cytochrome P450 family

The aromatase enzyme (CYP19A1) is a member of the cytochrome P450 family also known as oestrogen synthase. Aromatase is a class II P450, which is expressed by the *CYP19A1* gene. Aromatase is an endoplasmic reticulum membrane-bound enzyme, which can be found in many tissues and organs including gonads, brain, adipose tissue, placenta, blood vessels, skin, muscles, bone and endometrium (Chumsri *et al.* 2011). Aromatase catalyses with a high degree of substrate specificity the final and rate limiting step of oestrogen biosynthesis, that is the conversion of androgens to oestrogens. Aromatase has an important role in sex dimorphism, development and reproduction besides being crucial in some oestrogen dependant pathologies such as breast cancer and endometriosis (Chumsri *et al.* 2011; Gilardi and Di Nardo 2017; Di Nardo and Gilardi 2013). Interestingly the wide expression in many organs e.g., brain, accounts for aromatase involvement in other physiological and behavioural processes including neuroplasticity, cell growth, influence learning, memory, sexual behaviour, mood and a central role in neuroprotection in brain stroke, Alzheimer's and Parkinson's diseases (Gilardi and Di Nardo 2017; Di Nardo and Gilardi 2013).

2.1.2. Cytochrome P450 enzyme family

Cytochrome P450s were first reported in the 1960s (Omura and Sato 1962). Their catalytic activity is of great importance in fields such as drug-drug interactions and endocrinology as they are involved in the metabolism of drugs, steroids, fat soluble vitamins, carcinogens and other types of chemicals (Guengerich *et al.* 2016). Cytochrome P450 enzymes are responsible for around 75% of the enzymatic reactions that occur in drug metabolism and growing interest in this field of research led to the discovery of 57 P450s in humans, five of which alone play a significant role in the metabolism of around 90% of the small-molecule drugs to date (Guengerich *et al.* 2016).

Cytochrome P450s are generally oxygenases transferring electrons to oxygen and catalysing the oxidation of organic chemicals (Guengerich *et al.* 2016). The cytochrome P450

enzyme family is characterised by their spectral properties with the unique absorption band around 450 nm when complexed with carbon monoxide (Omura and Sato 1962).

Cytochrome P450 enzymes are widely spread throughout nature as they are found ubiquitously in animals, plants, fungi and bacteria (Guengerich *et al.* 2016; Manikandan and Nagini 2018). The total number of P450 enzymes identified to date is more than 40 thousand (Mak and Denisov 2018; Manikandan and Nagini 2018). All human P450s discovered are membrane-bound proteins. Of the 57 human cytochrome P450s, 50 are bound in the endoplasmic reticulum while only 7 are in the mitochondrial membrane. Human P450s can be classified based on their substrate as shown in **Table 2.1** (Guengerich *et al.* 2016).

Table (2.1): Classification of discovered human cytochrome P450 enzymes based upon their substrate (Guengerich 2015).

Xenobiotics	Sterols	Fatty acids	Vitamins	Eicosanoids	Unknown
1A1	1B1	2J2	2R1	4F2	2A7
1A2	7A1	2U1	24A1	4F3	2S1
2A6	7B1	4A11	26A1	4F8	2W1
2A13	8B1	4B1	26B1	5A1	4A22
2B6	11A1	4F11	26C1	8A1	4F22
2C8	11B1	4F12	27B1		4X1
2C9	11B2	4V2	27C1		4Z1
2C18	17A1				20A1
2C19	19A1				
2D6	21A2				
2E1	27A1				
2F1	39A1				
3A4	46A1				
3A5	51A1				
3A7					
3A43					

Cytochrome P450s can be classified according to the interactions with redox partners into four different classes illustrating the way electrons are delivered from NADPH to the catalytic site. Class I needs a FAD (flavin adenine dinucleotide)-containing reductase and an iron sulfur redoxin. Class II enzymes, which are the most common among eukaryotes, only require P450 reductase containing FAD and FMN (Flavin mononucleotide) for electron transfer e.g. aromatase enzyme (**Figure 2.1**). Class III are self-sufficient requiring no electron donor, while in class IV electrons transfer directly from NADPH (Werck-Reichhart and Feyereisen 2000).
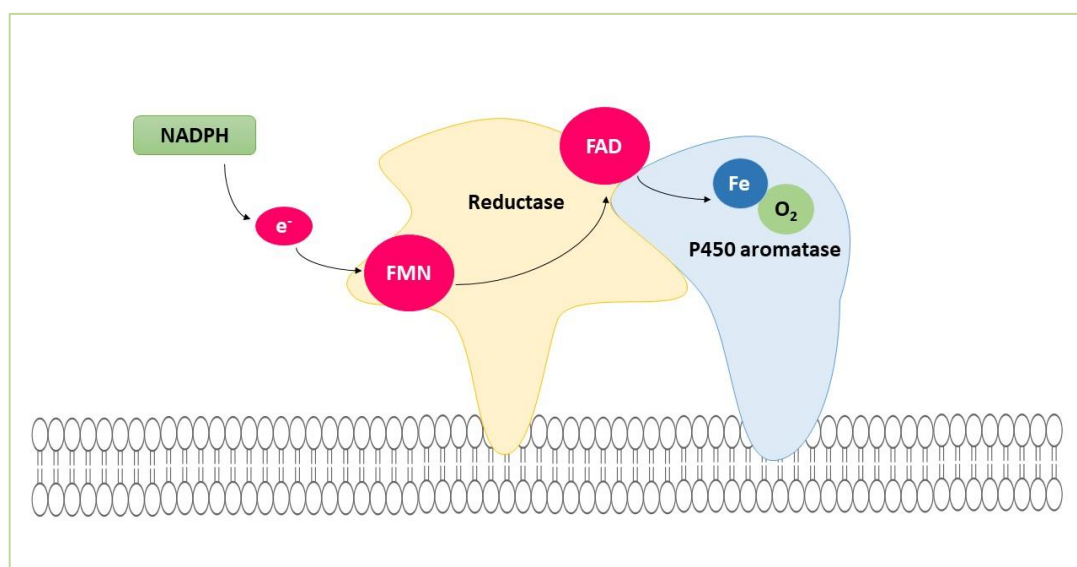
Figure (2.1): Schematic diagram of aromatase enzyme complex with the redox partner cytochrome P450 oxidoreductase (reductase) anchored on microsomal membrane (adapted from Conley and Hinshelwood 2001).

2.1.3. Nomenclature of cytochrome P450s

The nomenclature of cytochrome P450 enzymes follows a general rule. The name starts with letters "CYP" as abbreviation for the cytochrome P450 superfamily followed by Arabic numerals indicating the CYP family e.g., CYP1, CYP2, CYP3. The subfamily is designated after that by a letter e.g., CYP1A followed by another Arabic numeral representing the individual gene/isoenzyme/isoform e.g., CYP1A1. This nomenclature system should be written in italics (*CYP1A1*) when representing the gene or cDNA but it is used in regular uppercase (CYP1A1) when denoting the encoded mRNA or the protein itself. (Manikandan and Nagini 2018).

2.1.4. General structure of cytochrome P450s

Cytochrome P450s share a common structure containing around 400-500 amino acid residues bound to a single haem prosthetic group (Fe – protoporphyrin **IX**) (**Figure 2.2**). The amino acid sequences show 55% identity within the same subfamily and 40% homology within the same family. The iron atom is coordinated with a cysteine residue forming a haem-thiolate ligand and a water molecule represents the sixth ligand of the iron in the substrate free state (Gilardi and Di Nardo 2017; Manikandan and Nagini 2018).
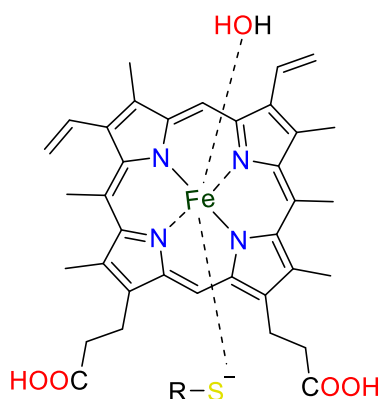
Figure (2.2): Structure of protoporphyrin **IX**.

2.1.5. General considerations of cytochrome P450s catalysis

Cytochrome P450 enzymes catalyse a wide range of oxidation-reduction reactions including hydroxylation, dealkylation, epoxidation, desaturation and other reactions. The typical P450 catalysed general carbon hydroxylation reaction is:

$$NADPH + H^+ + RH + O_2 \longrightarrow NADP^+ + H_2O + ROH$$
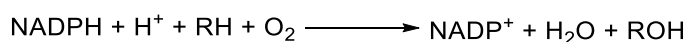
where RH is the substrate of the enzyme and NADPH is the source of electrons.

Generally, cytochrome P450 chemistry is similar, with some exceptions, but still catalytically specific. This specificity is driven by a number of factors such as the size, shape of the active site and how the enzyme positions the substrate in the pocket of the active site (Guengerich *et al.* 2016). The sizes vary considerably, some of them may be as small as 190 $Å^3$ as seen in human CYP2E1 (PDB 3E6I) (Porubsky *et al.* 2008) and some larger such as in human CYP2C8 (PDB 2NNI) (Schoch *et al.* 2008) with an active site volume of 1438 $Å^3$. A bacterial

P450 was even found to have an active site size of 2446 $Å^3$ (Takahashi *et al.* 2014). The active site shape of CYP3A4 (PDB 1TQN) (Yano *et al.* 2004), which is wider and more open compared to the L-shape of CYP2C8 (PDB 2NNI) (Schoch *et al.* 2008), may account for the wider catalytic specificity. P450s involved in steroid reactions have key residues, which make hydrogen and ionic bonds to assure the appropriate positioning of the substrate, for example Asp309 in CYP19A1 and Asn202 in CYP17A1 can hydrogen bond the 3-keto group of the steroid structure (Guengerich *et al.* 2016).

2.1.6. Catalytic cycle of cytochrome P450 enzymes

Cytochrome P450s are extraordinary catalysts with great ability to perform a versatile range of reactions with high regio and stereoselectivity. This is carried out through a sophisticated catalytic cycle (**Figure 2.3**). In the first step, binding of the substrate (RH) displaces the water molecule as the sixth ligand converting the haem to the five coordinated conformation. The change in the iron electronic state towards the five coordination results in more positive reduction potential. In the second step, reduction by an electron from NADPH transforms the iron from ferric (Fe^{3+}) state to ferrous (Fe^{2+}) state. The third step involves binding of an oxygen molecule as the sixth ligand forming the hexa-coordinated ferric peroxide ($Fe^{3+}-OO^-$). The reduction by a second electron in the fourth step results in the ferric peroxo anion ($Fe^{3+}-OO^{2-}$). The fifth step is formation of hydroperoxide intermediate ($Fe^{3+}-OOH^-$) by the entrance of a proton. Entrance of a second proton during the sixth step leads to elimination of a molecule of water producing the highly reactive oxoferryl species ($Fe^{4+}=O$), which abstracts a proton from the substrate in step 7 to give hydroxyferryl ($Fe^{4+}-OH$) which hydroxylates the substrate. Finally, the product is released with a water molecule coordinating as the sixth ligand to regenerate the resting state of the enzyme (Gilardi and Di Nardo 2017; Mak and Denisov 2018).
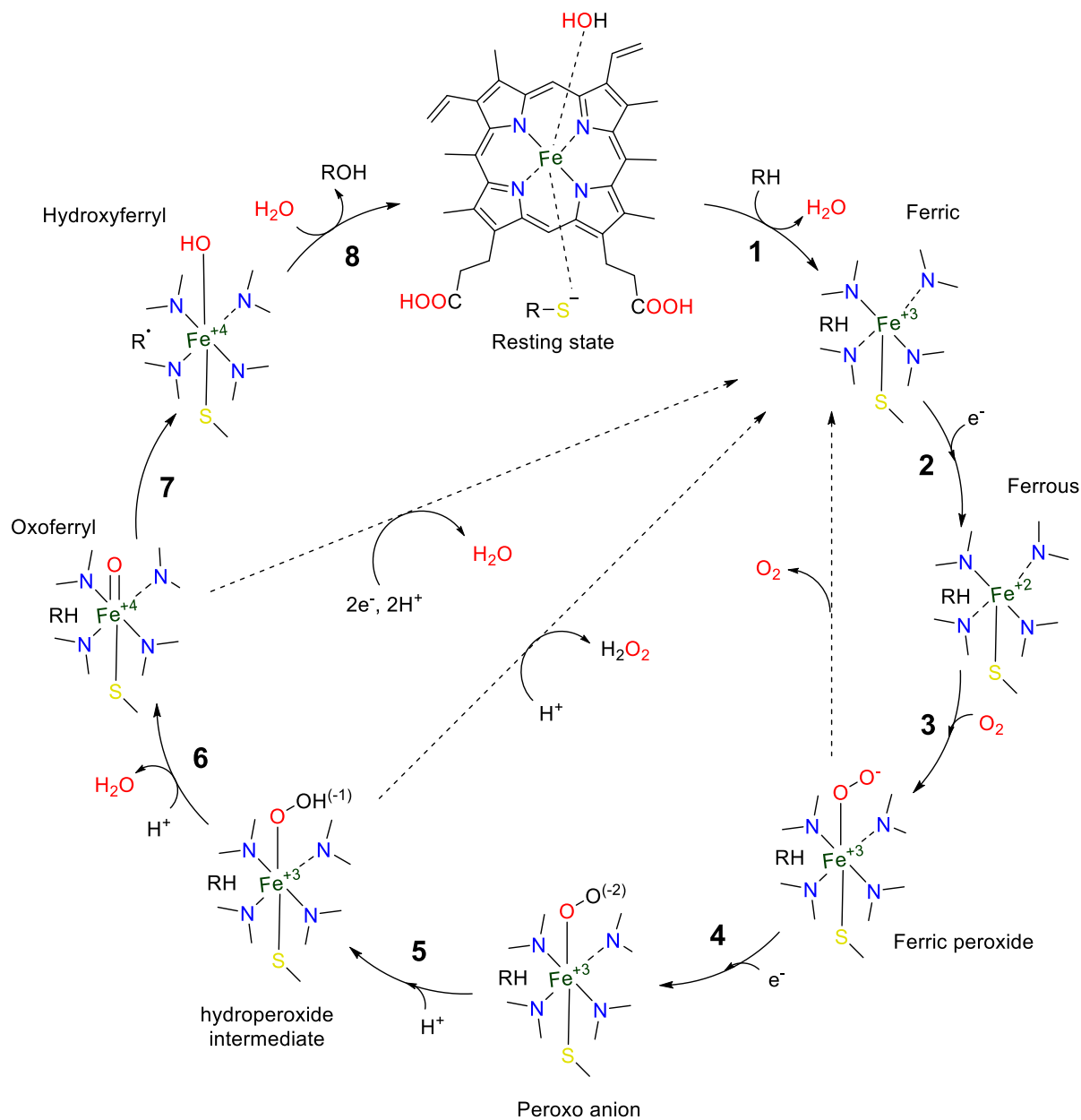
Figure (2.3): Schematic presentation of cytochrome P450 catalytic cycle showing the different intermediates and the uncoupling routes (dashed arrows).

2.1.7. **Structure of human aromatase**

Structural knowledge of cytochrome P450 enzymes is extremely important because besides being involved in predicting drug metabolism, several cytochrome P450 enzymes are drug targets themselves e.g., aromatase (CYP19A1). Although structures of important human P450s involved in drug metabolism began to be reported in 2004, it was not until 2009 that a crystal structure for the aromatase enzyme was published (Guengerich *et al.* 2016; Ghosh *et al.* 2009). Research was greatly hindered by the absence of a crystal structure for aromatase enzyme until 2009 and, as a result, many homology modelling studies were carried out based on other P450s structures. Unfortunately, none of them could explain the unique nature of aromatase catalysed reactions (Ghosh *et al.* 2016; Chumsri *et al.* 2011).

The crystal structure of aromatase complexed with its natural substrate androst-4-ene-3,17-dione (PDB 3EQM) was originally determined at a resolution of 2.9 Å (Ghosh *et al.* 2009), which was later extended to 2.75 Å (PDB 3S79) (**Figure 2.4**). These recent crystal structures have provided extraordinary insights into the molecular basis for its substrate specificity revolutionising novel aromatase inhibitor research (Ghosh *et al.* 2012).
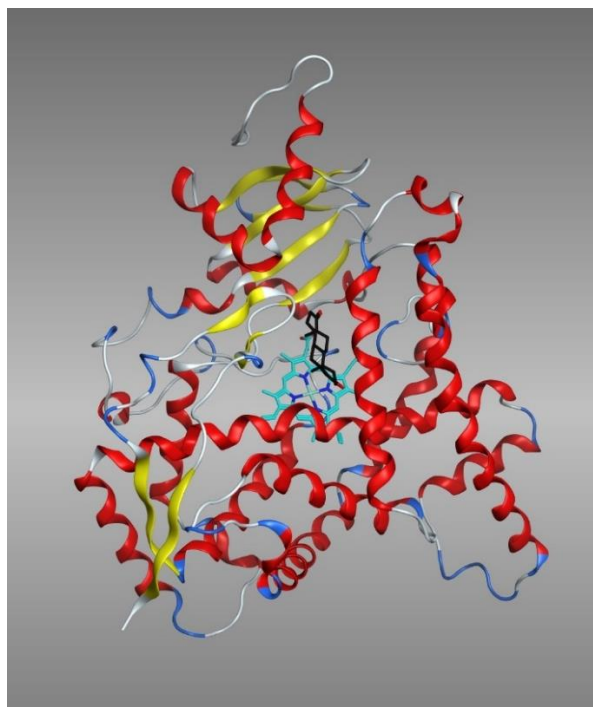
Figure (2.4): Aromatase crystal structure (PDB 3S79): Helices (red), strands (gold), haem molecule (Cyan) and natural substrate androstenedione (black).

Aromatase follows the typical fold of cytochrome P450s as the 503 amino acids constituting the polypeptide chain are organised in 12 α-helices (A – L) and 10 β-strands (1 -10). Aromatase contains a unique residue among other P450s (Pro308), which causes a distortion in helix I creating a relatively small substrate-binding pocket (400 $Å^3$) when compared with other human cytochrome P450s such as CYP3A4 (530 $Å^3$) (Williams 2004) and CYP2D6 (540 $Å^3$) (Rowland *et al.* 2006). A haem cofactor is accommodated inside this active site (**Figure 2.5**) with the iron atom bound to Cys437 as the fifth ligand. Arg192, Val313 and Glu483 line the access channel to the active site. The Met374 residue forms a hydrogen bond with the 17-keto oxygen of androstenedione while the 3-keto oxygen forms a hydrogen bond with Asp309. These two residues with other residues such as Arg115, Ile133, Phe134, Val370, Val373 and Leu477 constitute the tight boundaries of the active site, but more interestingly Ala306 and Thr310 form a pair which is involved in all three catalytic steps of aromatase (Ghosh *et al.* 2009; Gilardi and Di Nardo 2017; Di Nardo and Gilardi 2013).
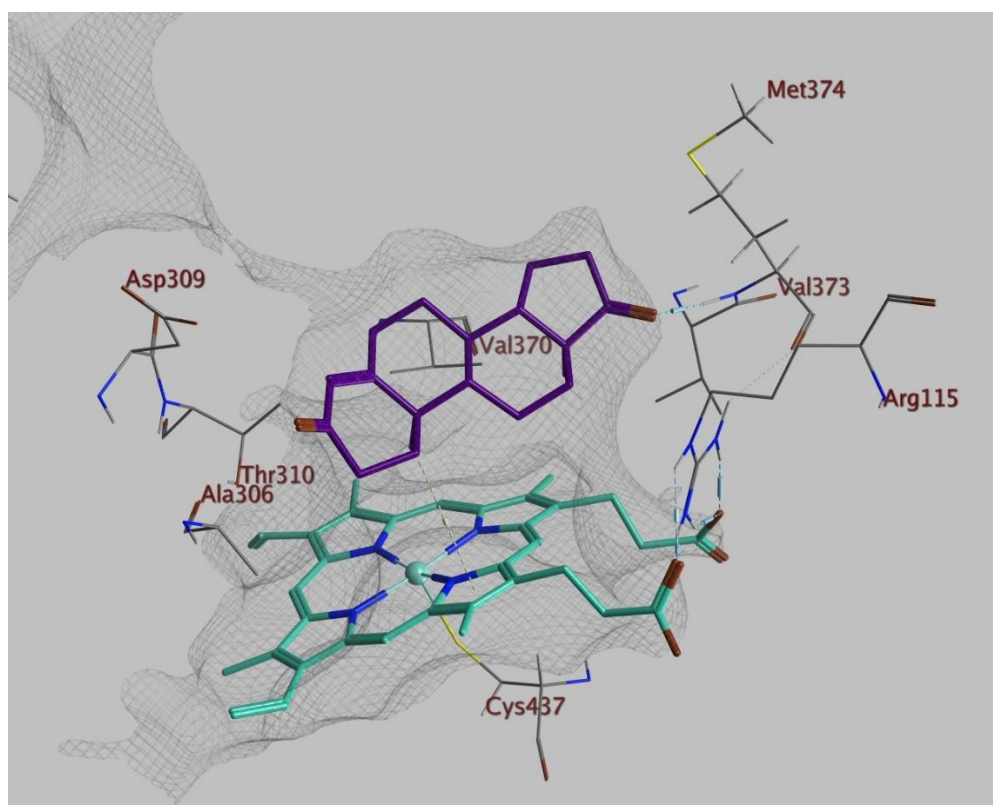
Figure (2.5): Active site of aromatase showing the haem molecule (Cyan) and some of the main residues of the active site with androstenedione inside (purple).

2.1.8. The catalytic mechanism of human aromatase

Human aromatase shows a complicated multi-step reaction mechanism catalysing the conversion of androstenedione, testosterone and 16α-hydroxytestosterone into oestrone, 17β-oestradiol and 17β,16α-oestriol respectively. The overall reaction happens in three steps (**Figure 2.6**), requiring one oxygen molecule and electrons provided by NADPH for each step (Ghosh *et al.* 2016; Gilardi and Di Nardo 2017).
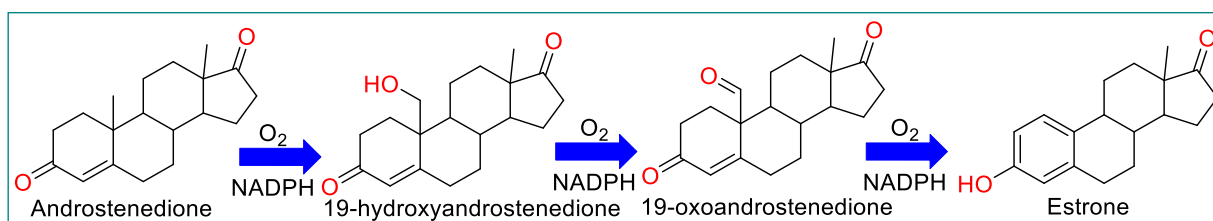
Figure (2.6): Three steps for conversion of androstenedione into estrone showing the two intermediates.

Aromatase is known to be the only vertebrate enzyme capable of catalysing aromatisation of a six-membered ring, however the mechanism of action of this enzyme is still not completely understood (Chumsri *et al.* 2011). The first two steps of this reaction are hydroxylation at C19 of the androgen producing two stable intermediates; 19-hydroxy and 19-oxo respectively. After a first oxidation reaction at C19 to give the first intermediate 19-hydroxyandrogen, a second hydroxylation at C19 produces 19-gem-diol as an unstable intermediate which spontaneously produces the 19-oxo-androgen by the loss of one mole of H_2O (Gilardi and Di Nardo 2017). The biochemistry behind the third step is still unclear and several mechanisms have been proposed. One proposal (**Figure 2.7**) is that the ferric peroxide (**Fe^{3+}-OO⁻**) acts as a nucleophile and attacks the C19 carbonyl group. Then peroxide fragmentation with the 1β proton causes aromatisation of ring A and one oxygen atom is incorporated into formic acid (Akhtar *et al.* 1982).
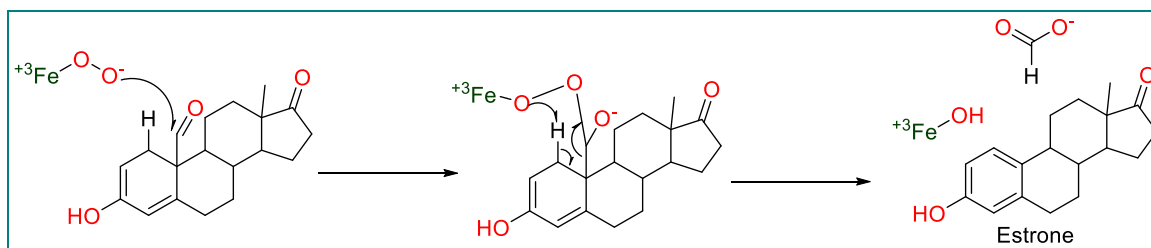
Figure (2.7): Proposed mechanism by Akhtar and co-workers for the third step using ferric peroxide intermediate (Akhtar *et al.* 1982).

Another proposed mechanism (**Figure 2.8**) is that the highly reactive oxoferryl species (**Fe⁴⁺=O**) abstracts the 1β proton from the gem-diol intermediate then one electron is transferred to the iron from ring A. A second hydrogen from the gem-diol is abstracted releasing C19 as a formic acid (Hackett *et al.* 2005).
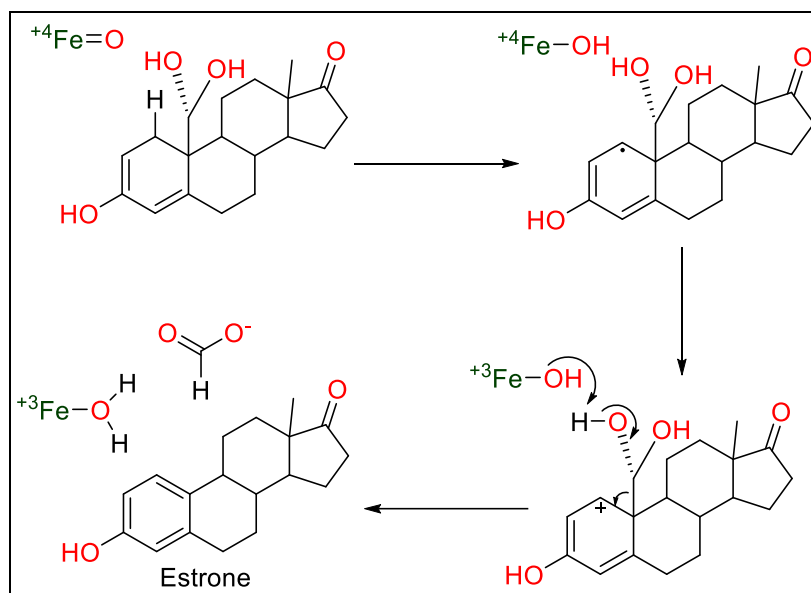
Figure (2.8): Second proposed mechanism by Hackett and co-workers for the third step using oxoferryl species (Hackett *et al.* 2005).

From the crystal structure data a key catalytic role was assigned to the Thr310-Ala306 carbonyl pair, which could be responsible for the 2,3-enolisation in the aromatisation step through a nucleophilic attack on H2β-C along with an electrophilic attack on the C3-carbonyl by a protonated Asp309 promoting H2β-C subtraction, however the 1β proton is directed closely to the haem Fe (4.2 Å) indicating it may be subtracted by ferric peroxide (**Fe³⁺-OO⁻**) nucleophilic attack as previously reported by Akhtar and co-workers (Akhtar *et al.* 1982) on the formed carbonyl at C19 (Ghosh *et al.* 2009).

One of the more recent studies using molecular dynamics and hybrid quantum mechanics/molecular mechanics (QM/MM) simulations proposed that the most kinetically advantageous mechanism (**Figure 2.9**) is through cleavage of the C10-C19 bond by the act of peroxide species. A peroxohemiacetal intermediate is first formed then a peroxoformate. The cleavage of the bond between the two oxygens produces the highly reactive oxoferryl species (**Fe⁴⁺=O**), which abstracts a proton on C1 followed by electron transfer mediated by

hydroxyferryl (**Fe^{4+}-OH**). The produced carbocation then loses a proton to Asp309 at C3 to produce the keto group. Finally, enolisation and aromatisation happens on abstraction of the 2β-proton (Sen and Hackett 2012).
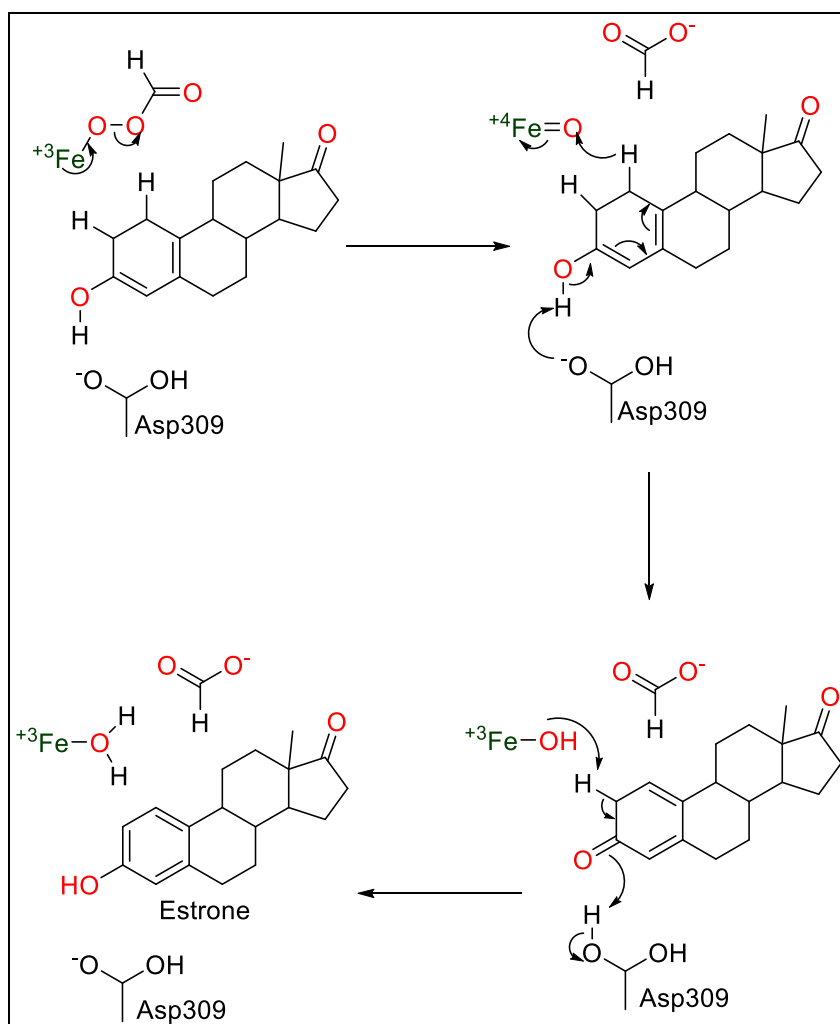
Figure (2.9): Recent mechanism proposed by molecular dynamics and hybrid quantum mechanics/molecular mechanics simulations for the third catalytic step of aromatase enzyme (Sen and Hackett 2012).

Another aspect of the aromatase mechanism of catalysis as a multi-step enzyme is whether it has the ability to retain the substrate and following intermediates in the active site for processing in order and to only release the final product, a manner known as processive reaction or follow the distributive reaction in which the intermediates can freely dissociate and re-bind to be further processed (Gilardi and Di Nardo 2017). Pulse-chase experiments using radiolabelled

androstenedione were performed and on addition of 19-hydroxyandrostenedione and 19-oxoandrostenedione to the reaction mixture, showed a decrease in radiolabelled estrone. These results suggest a distributive mechanism rather than processive (Sohl and Guengerich 2010). In 2015, similar results were obtained from bio-electrochemical studies in which electrode driven catalysis for immobilised enzyme on glassy carbon electrodes was conducted at both high concentrations of substrate (excess) and low concentrations (non-saturating). With the substrate in excess, the enzyme only produced the first intermediate. At lower concentrations, the final product was detected. This indicates that aromatase has higher affinity to the substrate and if its concentrations are high, aromatase prefers to process the substrate. Only when the substrate concentrations are low, the first intermediate starts to compete for enzyme binding. This provides evidence for a distributive mechanism of reaction for aromatase three-step catalysis (Di Nardo *et al.* 2015).

2.1.9. Allosteric inhibition of human aromatase

Letrozole and one of the metabolites of tamoxifen; namely endoxifen, was reported to have the potential of non-competitive/ mixed inhibition for aromatase (Jessie *et al.* 2012; Egbuta *et al.* 2014). This type of inhibition indicates the presence and identification of allosteric sites in the aromatase enzyme. Three potential allosteric sites were identified through computational studies including the haem proximal site along with two access channels connected to the active site (Spinello *et al.* 2019; Magistrato *et al.* 2017; Sgrignani *et al.* 2014). The front door access channel gated by Asp309 was identified in the crystal structure published in 2009 (Ghosh *et al.* 2009). On the other side of the active site, a backdoor channel gated with ser314 was discovered through the crystal structure published in 2018, which is postulated to be involved in the passage of catalytic water (Ghosh *et al.* 2009; Ghosh *et al.* 2018).
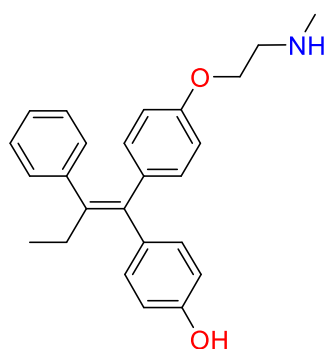
Endoxifen

Allosteric non-competitive inhibition of the aromatase enzyme offers major advantages over conventional inhibitors in terms of reaching maximum inhibition without the complete blockage of oestrogen production, which causes reduction in side effects and delaying or avoidance of the onset of resistance along with better selectivity being less conserved across other enzymes. Also, they are not outcompeted by high concentrations of androgens as natural substrate, making this approach appealing for rational drug discovery (Spinello *et al.* 2019). Even though there is no reported effective allosteric inhibitor of the aromatase enzyme, some novel compounds with a dual-binding ability for the access channel and the active site were reported in 2012 (**Figure 2.10**). These potent inhibitors were characterised by a long alkyne side chain at C6 of the steroidal scaffold to be able to fit through the narrow hydrophobic access channel giving rise to the concept of 4th generation steroidal aromatase inhibitors with dual binding capacity. This may be extendable to the non-steroidal AI class and so may present the molecular basis for the design of 4th generation non-steroidal aromatase inhibitors (Spinello *et al.* 2019; Ghosh *et al.* 2012).
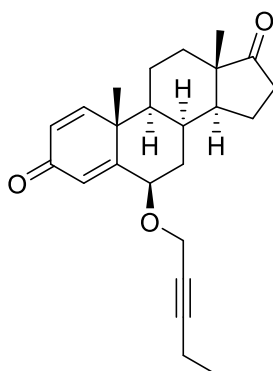
Figure (2.10): Example of novel dual-binding steroidal aromatase inhibitors: (6*R*,8*S*,9*S*,10*R*,13*S*,14*S*)-10,13-dimethyl-6-(pent-2-yn-1-yloxy)-7,8,9,10,11,12,13,14,15,16-decahydro-3*H*-cyclopenta-[*a*]phenanthrene-3,17(6*H*)-dione (IC$_{50}$=11.8 nM).

2.2. Objectives of this chapter

In order to design novel dual-binding non-steroidal compounds in the absence of a crystal structure for aromatase enzyme co-crystallised with a non-steroidal compound, proper understanding of the binding requirements and establishment of clear SAR for the non-steroidal compounds is very challenging. This requires an iterative design process with feedback through the design/synthesis/enzyme inhibition cycle to optimise the novel inhibitors (**Figure 2.11**).
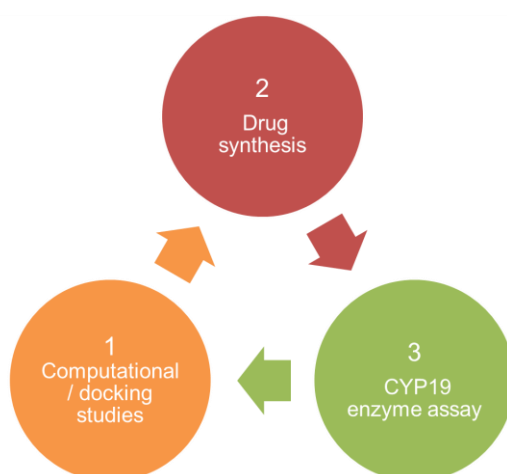
Figure (2.11): Iterative design cycle.

Objectives to be fulfilled by the end of this chapter:

1- To understand the binding requirements of the androgen specific active site and the access channel of aromatase and use of the knowledge gained to design dual-binding selective non-steroidal aromatase inhibitors, with the aid of computational tools; docking and MD studies.

2- To develop synthetic routes to synthesise the novel inhibitors.

3- To perform aromatase inhibitory assays to assess the efficacy of novel inhibitors.

4- To establish a clear SAR for the compounds in this study to help further development of novel inhibitors.

5- To perform toxicological studies (MTT assays) to evaluate the safety index of the prepared inhibitors.

From previous published work in our lab (Saberi *et al.* 2006), the main lead compounds having a benzofuran scaffold were identified based on their CYP19A1 activity and toxicity profile (**Figure 2.12**). Further modifications and substitutions will be investigated in order to optimise activity, selectivity and toxicity profiles for the prepared compounds to constitute the 4th generation of non-steroidal aromatase inhibitors.

3-secondary substitution

1-Position

2-length

IC_{50} (µM) = 0.044

LC_{50} (µM) = 50

LC_{50}/IC_{50} = 1136
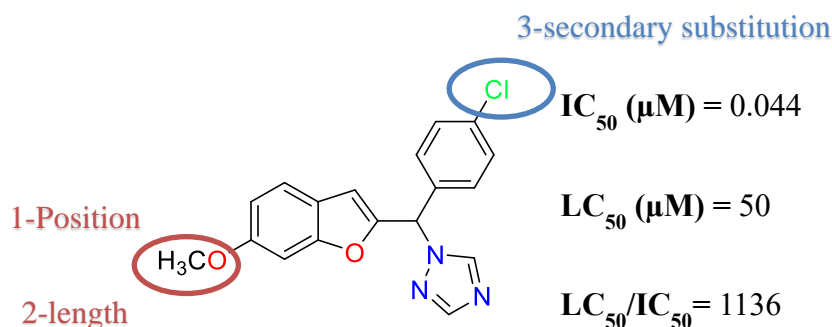
Figure (2.12): Parent compound with benzofuran/triazole scaffold showing the variants of these studies (Saberi *et al.* 2006), IC_{50} evaluated using placental microsomes aromatase inhibitory assay measuring tritiated water, LC_{50} evaluated using lactate dehydrogenase retention in rat liver hepatocytes.

In the quest for optimising the lead compound, modifications for these variants ought to be studied to address answers for three major criteria: 1) the position of substituent needed to fill the access channel, 2) the required nature of that substituent, and 3) optimal substituents on other possible sites. Proper understanding of the binding requirements was needed with the underlying SAR of the compounds to show optimal activity. Different compounds were designed to answer each question separately.

A series of 12 compounds, divided into three categories, were designed to compare the optimal position of the substituent required for access channel binding. The three categories are 6-substituted benzofuran, 5- substituted benzofuran and 4- substituted phenyl (**Figure 2.13**). Each category contained four compounds with different substituent nature to exploit the full possibilities of binding. Hydroxy and methoxy derivatives represented the short substituents to show binding to the active site only. A pent-2-yne substituent was investigated as a starting point of long chain substituents required for binding the access channel. A morpholine 4-carboxylate substituent was designed to check the possibility of bulkier and more hydrophilic substituent.

6-substitued benzofuran   **5-substituted benzofuran**   **4-substituted phenyl**

	6-substitued benzofuran	5-substituted benzofuran	4-substituted phenyl
R_1 = CH$_3$	6a	6b	6c
R_1 = H	11	12	17
R_1 =	27a	30	32
R_1 =	29a	31	33
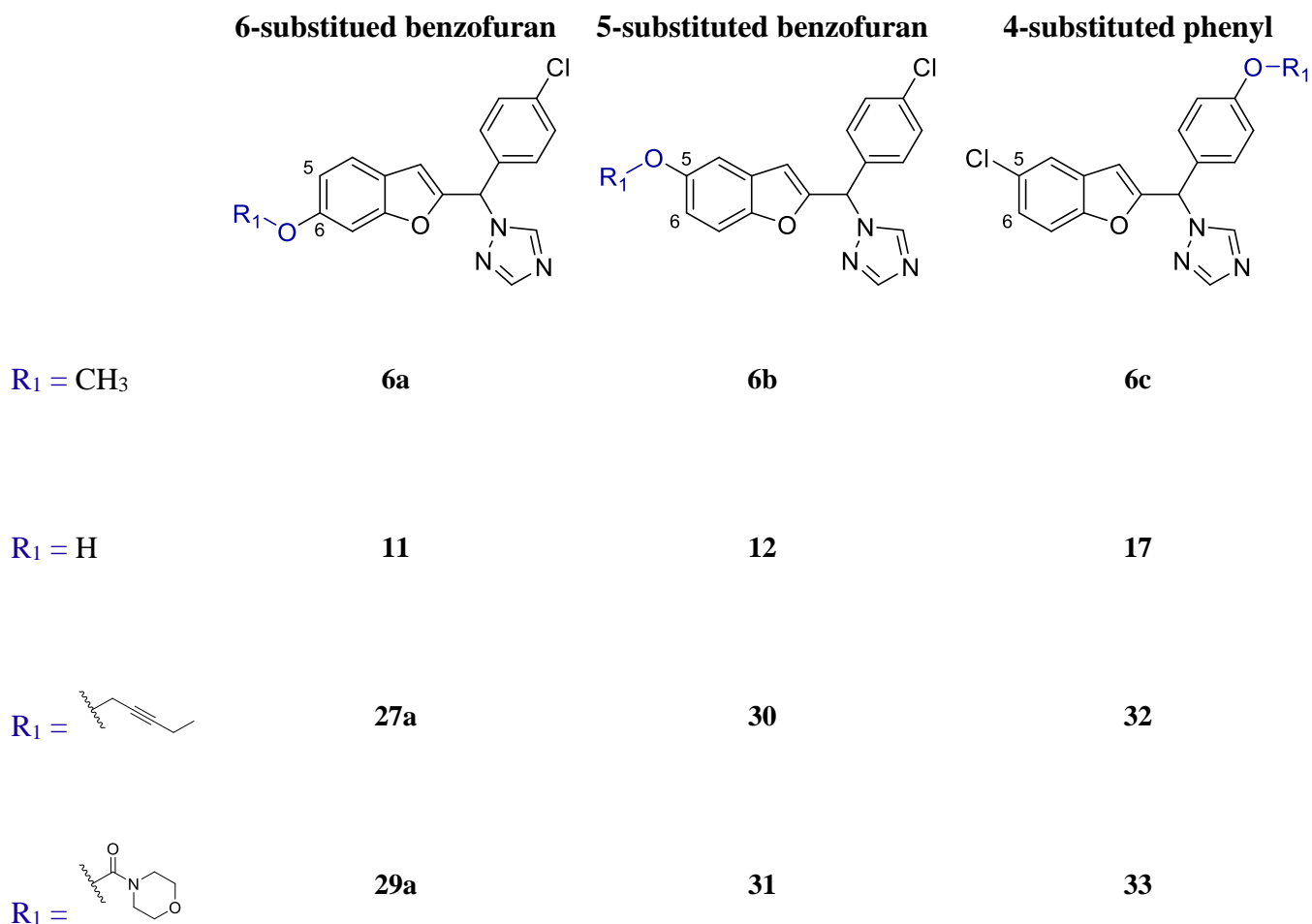
Figure (2.13): Members of the preliminary series addressing the position and nature of the substituent required for access channel binding.

For the second question about the length of the substituent, three more compounds were prepared to fill the gap between the methoxy and the pentyne, with the substituent varying from ethyl to propyne and butyne to form a series of compounds covering the full range from hydroxy to pentynyloxy (**Figure 2.14**). All compounds of this series belonged to the 6-substituted benzofuran category and all had a constant secondary substituent on the phenyl side which was a chloro group.
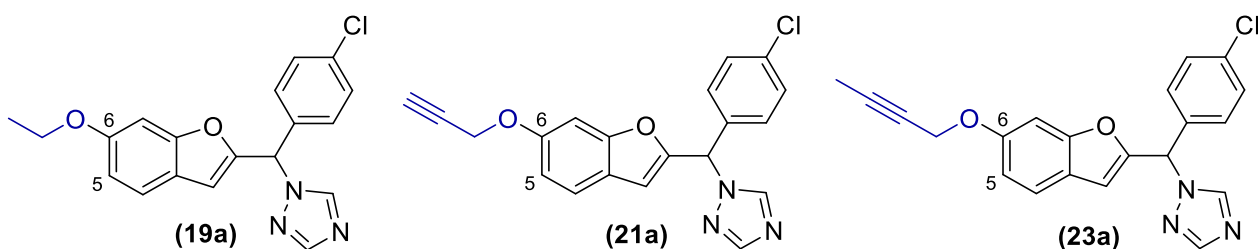
Figure (2.14): A series of varying length of the alkyl chain on the 6-benzofuran position.

To approach the question about the nature of the secondary substituent on the phenyl group, a series of six compounds were prepared. Three of them were fluoro derivatives and the other three were nitrile derivatives. These six compounds constituted the required comparison to the chloro analogues to determine the optimal group(s) for activity. (**Figure 2.15**).

$R_1 = CH_3$	**6d**	**6e**
$R_1 = H$	**13**	**14**
$R_1 =$ pent-2-ynyl	**27b**	**27c**
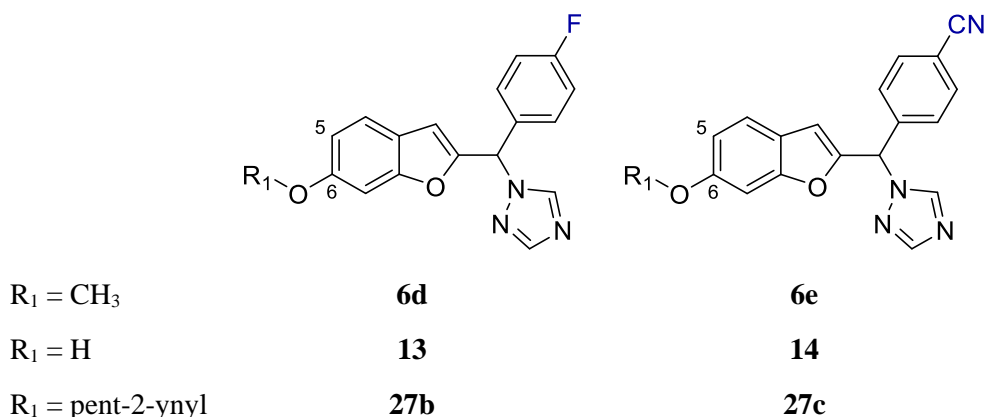
Figure (2.15): Varying substituents on the phenyl side of the compounds.

Finally, based on the biological results obtained, it was found that the butyne chain on the 6-benzofuran position is optimal for activity and the benzonitrile derivatives were proposed to be superior. As a result, Compound **23c**, having these two features, was synthesised, and evaluated for biological activity.
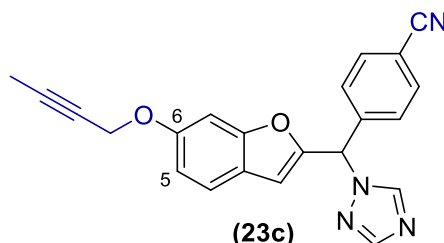
Figure (2.16): 4-((6-(But-2-yn-1-yloxy)benzofuran-2-yl)(1*H*-1,2,4-triazol-1-yl)methyl)benzonitrile (**23c**) with the two important structural features (but-2-ynyl and nitrile groups) labelled in blue.

2.3. Results & discussion

2.3.1. Computational Studies

Preparation of protein: The crystal structure of human placental aromatase, (CYP19A1) refined at 2.75 Å (PDB 3S79) (Ghosh et al. 2012), was downloaded from the protein data bank (https://www.rcsb.org). Missing hydrogens were added, and the charge and geometry of the iron atom were adjusted. Using the site finder tool in molecular operating environment software (MOE),

the active site was chosen to contain the main amino acid residues and the haem molecule. The amino acids constituting the wall of the active site contained Arg115, Ile133, Phe134, Phe221, Trp224, Ile305, Ala306, Asp309, Thr310, Val370, Leu372, Val373, Met374, Leu477, Ser478.

Preparation of ligands: The 3D structures of compounds (*R* and *S* enantiomers) were generated using MOE builder, energy minimised and saved in a dataset ready for docking studies.

Molecular Dynamics: The complexes for MD studies were prepared by docking the compounds using MOE. The best poses were selected based upon the 3D visual inspection and the score value of the complex and subjected to 150 ns MD simulations using Desmond.

Regarding the position of the substituent, it was obvious that 6-substituted benzofurans e.g. **27a** formed more stable complexes than the 5-substituted analogues e.g. **30** (**figure 2.17**), however the 4-substituted phenyl derivatives were comparable to the 6-substituted benzofurans.

27a R= 6-pent-2-ynyloxy
30 R= 5-pent-2-ynyloxy
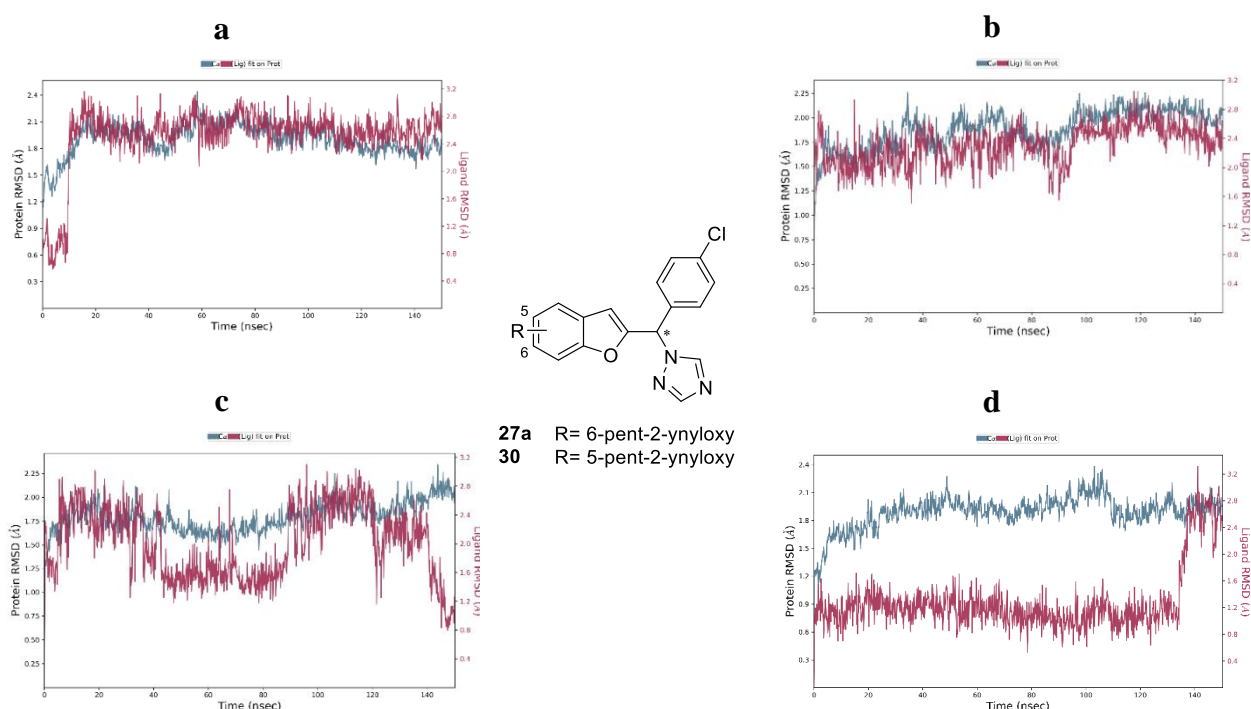
Figure (2.17): Comparing the complexes stability through protein-ligand RMSD over 150 ns MD simulation for (a) *S*-enantiomer of **27a** (b) *R*-enantiomer of **27a** (c) *S*-enantiomer of **30** (d) *R*-enantiomer of **30,** ligand RMSD in red and protein RMSD in blue.

Studying the binding profile through the simulation time indicated that the *S*-enantiomer had reasonable interactions with the key amino acid residues and more importantly formed a robust

interaction with the haem iron through the N4 of the triazole ring. On the other hand, the R-enantiomer shifted the interaction with the haem iron towards the N2 of the triazole ring either in part or all of the simulation time (**figure 2.18**). These results comply with literature findings for the structurally similar compound (vorozole) indicating that the *S*-enantiomer is the active form (Wouters *et al.* 1994), this will need to be further verified by separating the two enantiomers and testing each separately to reach a final conclusion.
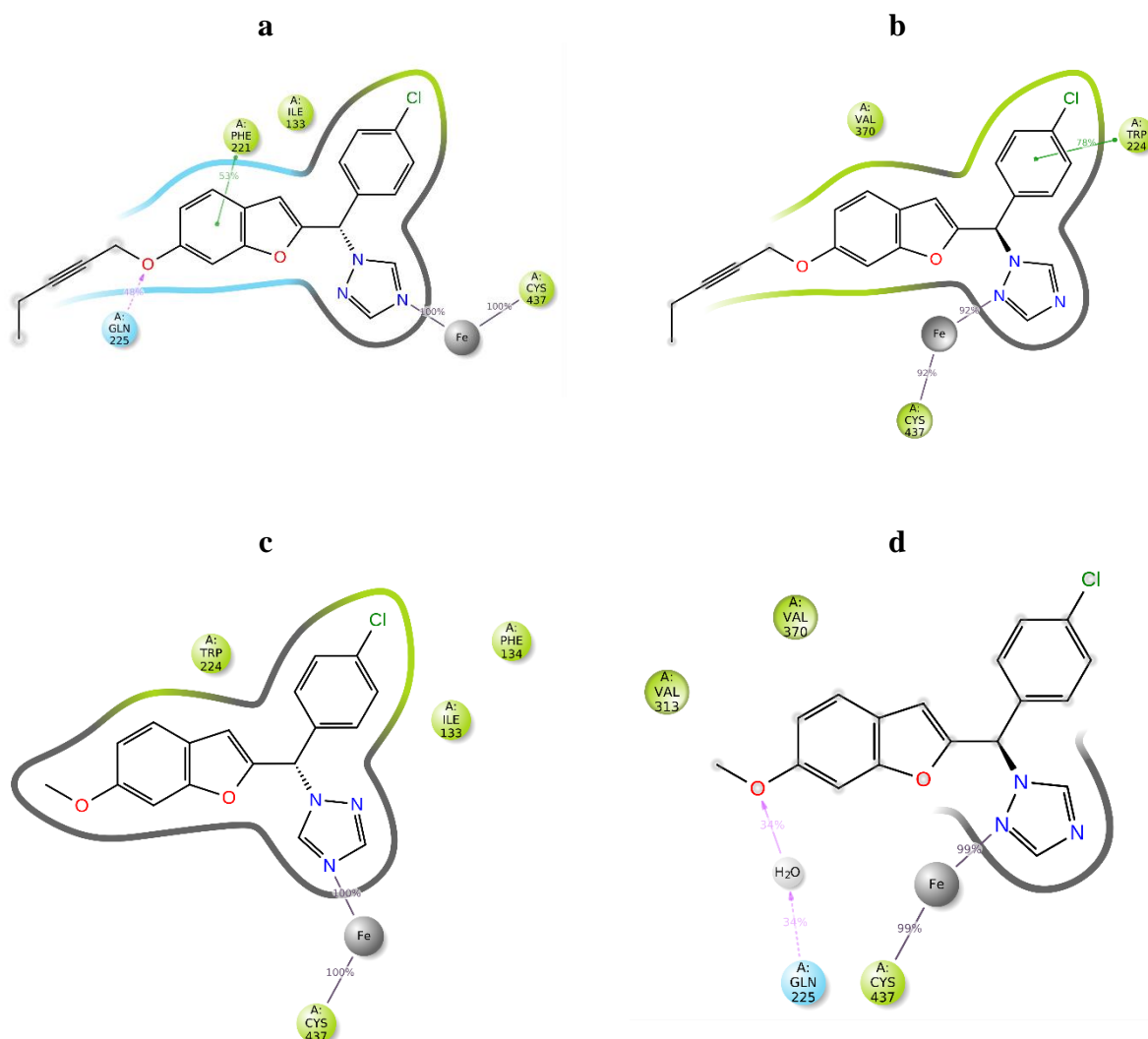
Figure (2.18): Comparing the binding profile showing haem binding over 150 ns MD simulation for (a) *S*-enantiomer of **27a** (b) *R*-enantiomer of **27a** (c) *S*-enantiomer of **6a** (d) *R*-enantiomer of **6a**.

Varying the length of the alkyl chain substituent did not show a significant difference in the stability of the complex and all compounds showed adequate 3D fitting, with the methoxy derivatives fitting in the active site pocket e.g. **6a**, and the long chain substituted derivatives fitting both the active site and the access channel e.g. **23a** (**figure 2.19**).
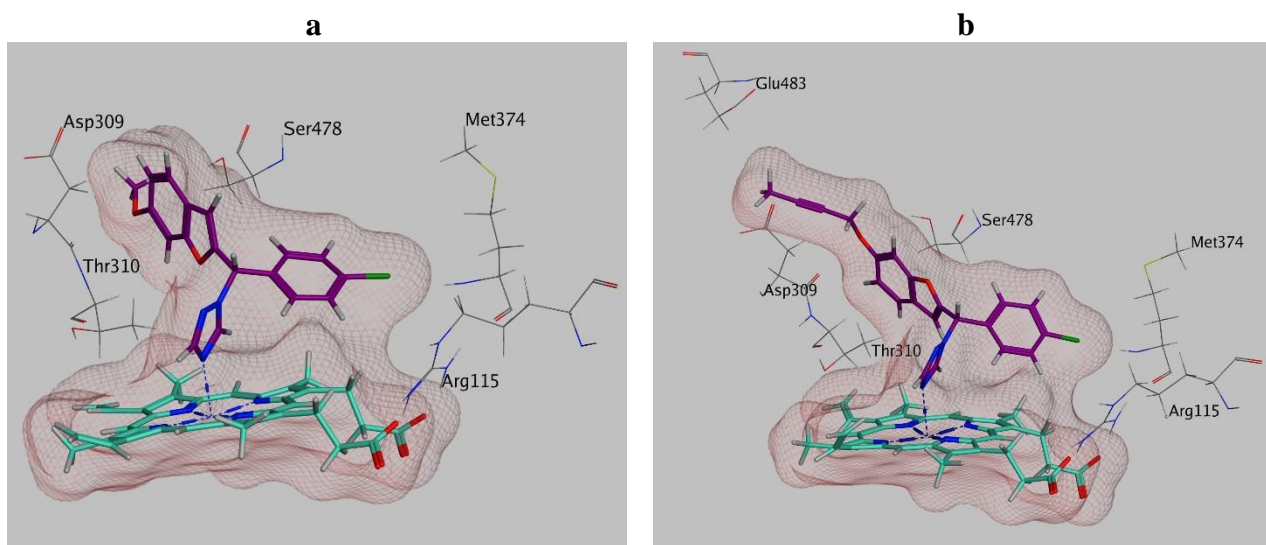
Figure (2.19): 3D fitting of the final frame after 150 ns MD simulations in the active site of the aromatase enzyme for (a) *S*-enantiomer of **6a** (b) *S*-enantiomer of **23a**.

Comparing the secondary substituent on the phenyl ring showed that the nitrile group (**27c**) had the potential to form a hydrogen bond with the key amino acid residue Met374 for the whole simulation time, however the chloro (**27a**) and fluoro (**27b**) derivatives showed moderate potential of interactions with a variety of key amino acid residues e.g. Gln225 for the chloro and Ser478 for the fluoro (**figure 2.20**).
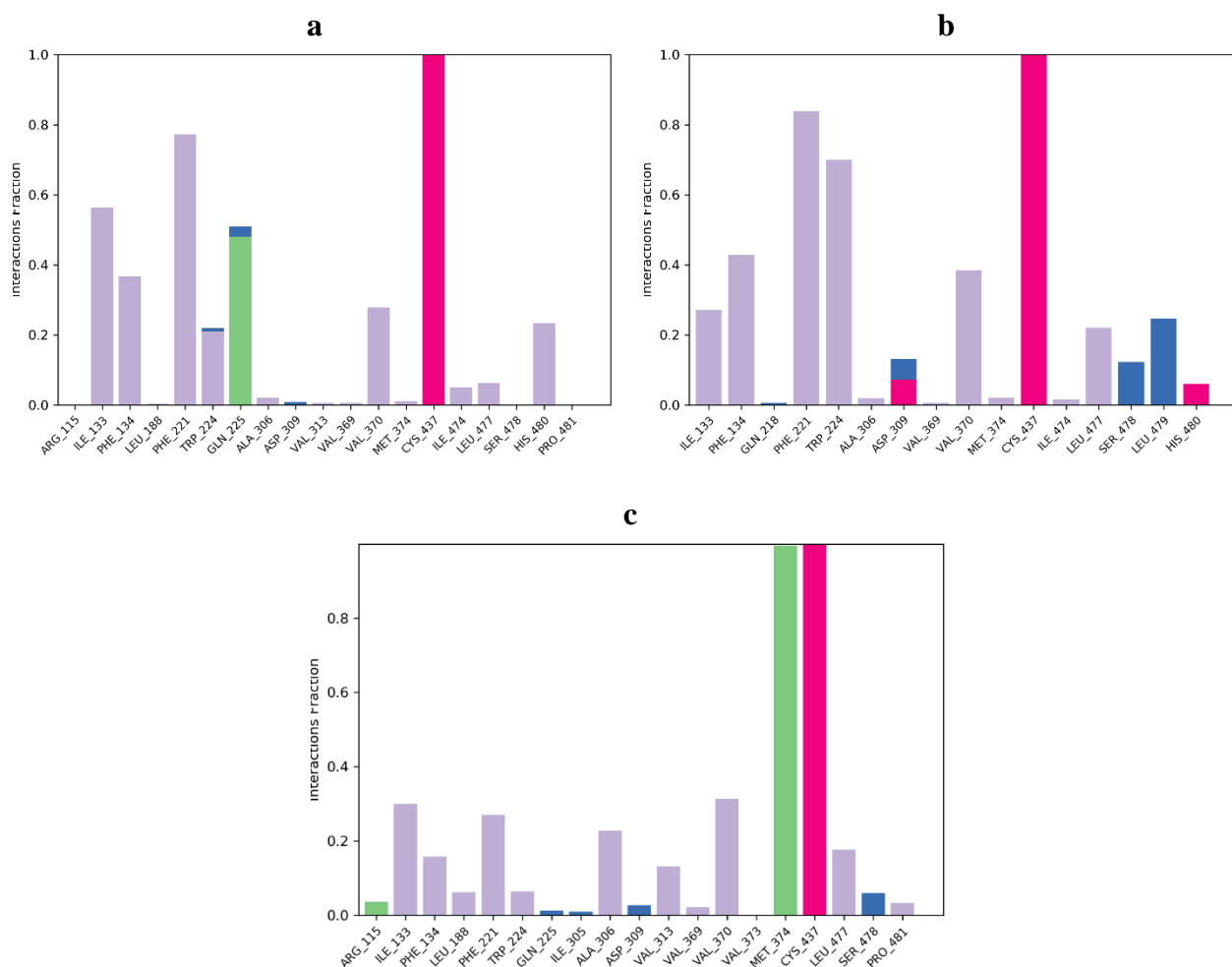
Figure (2.20): Comparing the protein-ligand contact through 150 ns MD simulation for (a) *S*-enantiomer of **27a** (b) *S*-enantiomer of **27b** (c) *S*-enantiomer of **27c**.

2.3.2. Chemistry

In this part, different synthetic routes for the target compounds as well as unsuccessful attempts to prepare synthetically inaccessible target compounds will be discussed in detail. Apart from the classification of compounds into three series based on the position of substituent, chemically these compounds were divided into four classes based on the similarity and differences in the synthetic procedure followed to prepare them namely:

➢ Class 1: (methoxy-substituted compounds).
➢ Class 2: (hydroxybenzofuran compounds).
➢ Class 3: (hydroxyphenyl compound).
➢ Class 4: (all the extended compounds regardless of the position of substituent).

2.3.2.1. Synthetic pathway for Class 1 (methoxy-substituted benzofurans):

This synthetic pathway follows the published preparation of the lead compound (**6a**) (Saberi *et al.* 2006) with modifications discussed where applicable. The scheme consists of three steps; the first of which is the formation of benzofuran ketone species followed by reduction of the carbonyl group into a secondary alcohol in the second step. The final step is the substitution of the alcohol group with the triazole ring leading to the successful preparation of the lead compound (**6a**) along with the 5-methoxy analogue (**6b**) and the methoxyphenyl analogue (**6c**).
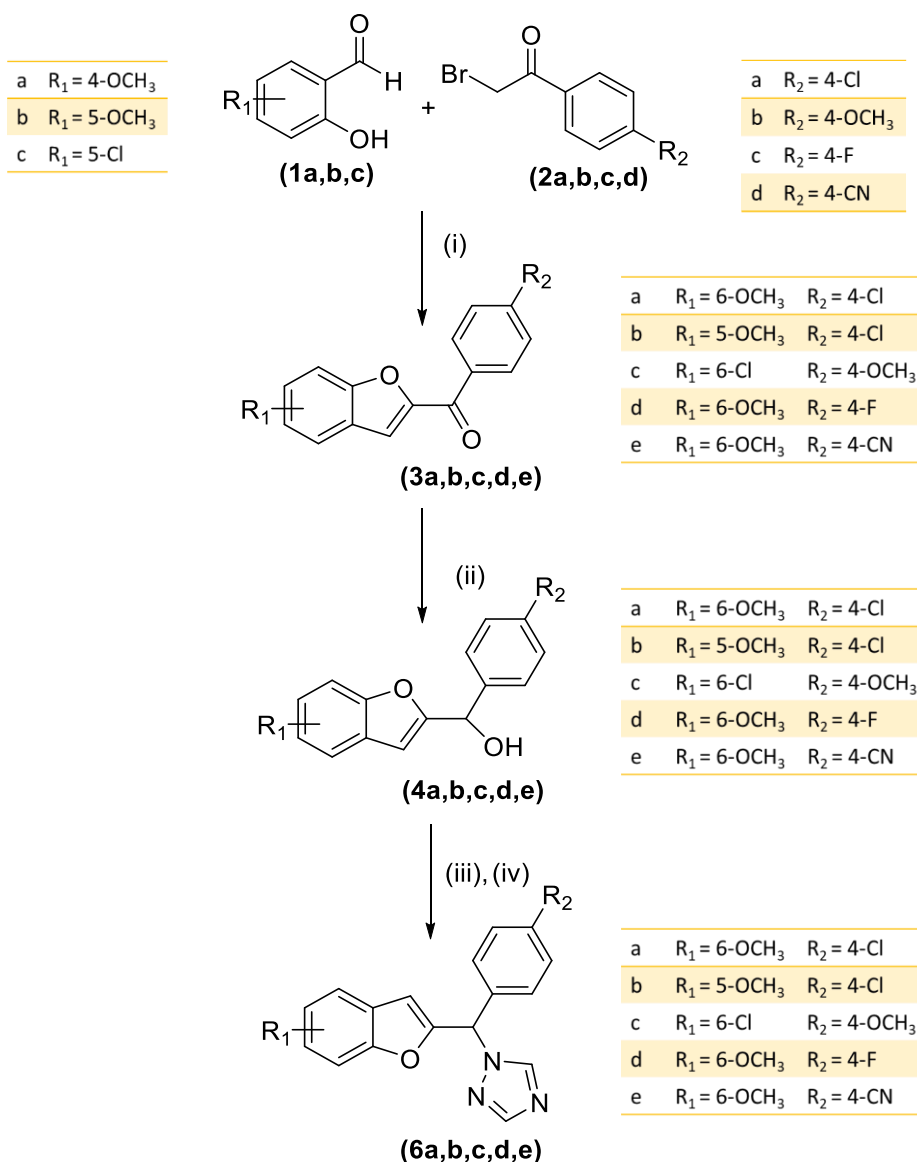
Scheme (2.1): (i) K_2CO_3, CH_3CN, 70 ℃, 3 h (ii) $NaBH_4$, dioxane, 2h (iii) $SOCl_2$, triazole, CH_3CN, 0 ℃, 1 h (iv) K_2CO_3, r.t, 5 days.

2.3.2.1.1. First step: synthesis of (4-substitutedphenyl)(5- or 6-substitutedbenzofuran-2-yl) methanone (3a,b,c,d,e)
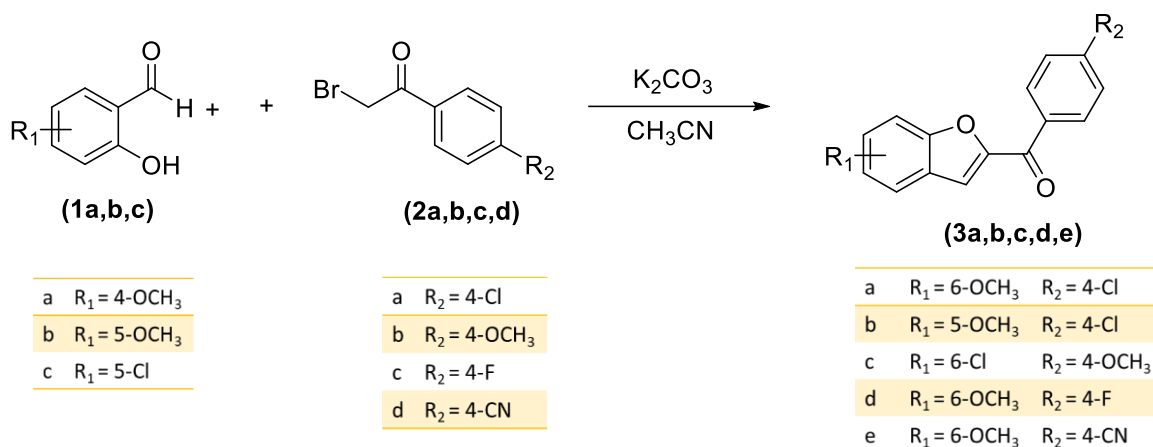
This reaction is a Rap-Stoermer reaction (Pestellini *et al.* 1988; Mahboobi *et al.* 2007) (**Figure 2.21**) where potassium carbonate is used as a base to deprotonate the phenolic OH group of 2-hydroxy substituted benzaldehyde (**1a,b,c**)**,** which then makes a nucleophilic attack towards the methylene group of 2-bromo-4′-substituted acetophenone (**2a,b,c,d**). Under the basic conditions of the reaction an intramolecular cyclisation occurs to produce the desired benzofuran moiety.
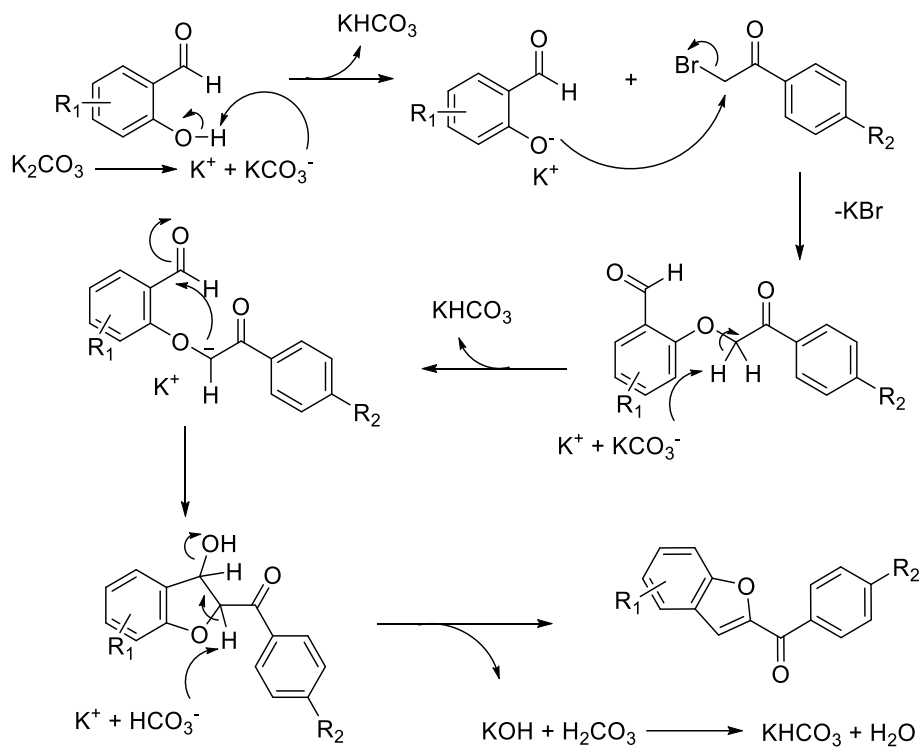
Figure (2.21): Mechanism for the synthesis of (phenyl)(benzofuran-2-yl)methanone derivatives.

This reaction was monitored by TLC, however it was not conclusive as the starting materials had the same R_f as the product. Five compounds were successfully prepared with yield and melting points indicated in **table 2.2**.

Table (2.2): Yield and melting points of compounds **3a-e**

Compound	Yield	Melting point (ºC)
3a	95%	184-186 (lit. m.p. = 174-176) (Saberi *et al.* 2006)
3b	87%	141-143
3c	80%	140-142 (lit. m.p. = 147-148) (Yoshizawa *et al.* 2003)
3d	96%	164-166 (lit. m.p. = 156-158) (Saberi *et al.* 2006)
3e	90%	192-194 (lit. m.p. = 192-194) (Saberi *et al.* 2006)

^{1}H NMR showed the two doublets of the para-substituted phenyl ring with separate peaks for each of the four protons of the benzofuran ring (**Figure 2.22**). Regardless of the shifts in the relative position of each of these peaks, depending on the environment of the compound, this fingerprint ^{1}H NMR was consistent throughout except for the fluoro-substituted compounds, with a more complex peak profile in the aromatic area. ^{13}C NMR for **3b** and **3c** confirmed the correct number of carbon atoms
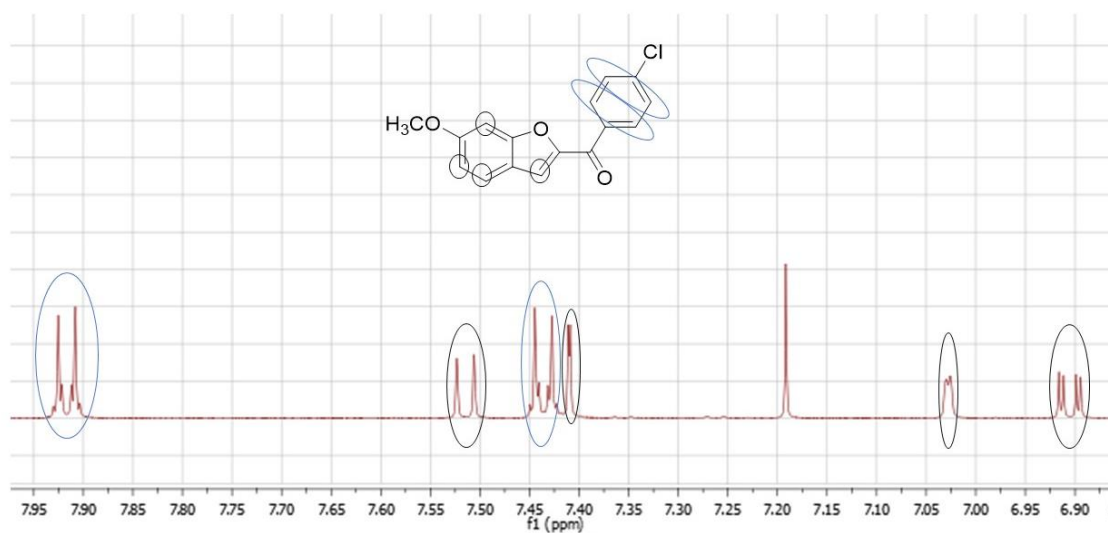
Figure (2.22): Magnification of the aromatic area of the ^{1}H NMR for (4-chlorophenyl)(6-methoxybenzofuran-2-yl)methanone (**3a**) showing the peaks of phenyl ring circled in blue and benzofuran peaks circled in black.

This reaction was attempted at first using NaH as base instead of K_2CO_3 conforming with the literature method of preparation (Pestellini *et al.* 1988; Saberi *et al.* 2006), however this provided the 5-methoxy derivative in a less pure form, which needed recrystallisation using ethanol lowering the yield to around 60%.

2.3.2.1.2. Second step: synthesis of (4-substitutedphenyl)(5- or 6-substituted benzofuran-2-yl)methanol (4a,b,c,d,e)

a	R_1 = 6-OCH$_3$	R_2 = 4-Cl
b	R_1 = 5-OCH$_3$	R_2 = 4-Cl
c	R_1 = 6-Cl	R_2 = 4-OCH$_3$
d	R_1 = 6-OCH$_3$	R_2 = 4-F
e	R_1 = 6-OCH$_3$	R_2 = 4-CN
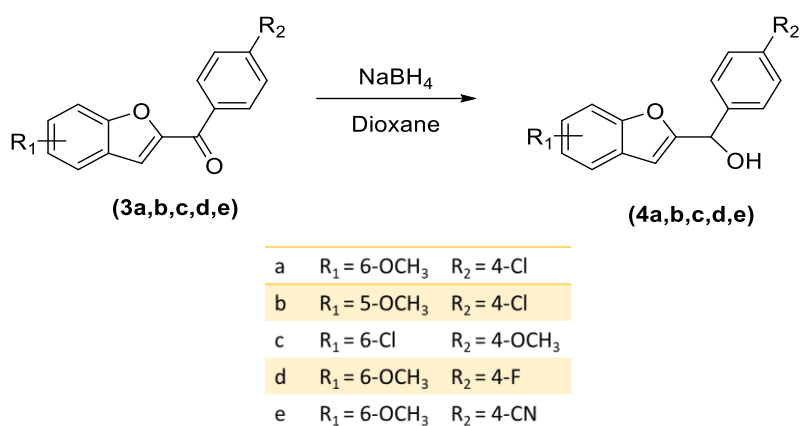
This reaction is a sodium borohydride reduction of ketone compounds to carbinols (**Figure 2.23**) in which ideally each mole of sodium borohydride reacts with four moles of ketone, however excess sodium borohydride was used to push the reaction to completion to avoid any purification complications.
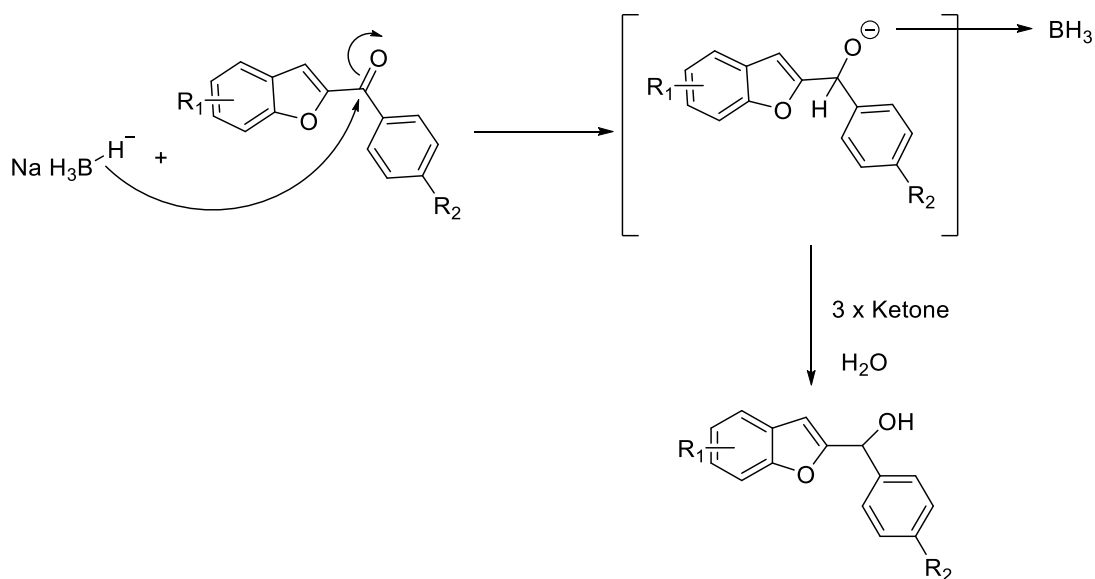
Figure (2.23): Mechanism for the preparation of (4-substituted phenyl)(substituted benzofuran-2-yl)methanol.

The identity of the compounds was confirmed by ^{1}H NMR, which showed the appearance of a singlet signal at around 5.8 ppm indicating the benzylic proton and a broad singlet at around 3.1 ppm indicating the formation of alcoholic OH. Also ^{13}C NMR performed for compound **4b** as an example showed the disappearance of one quaternary carbon with the formation of a new CH peak for the benzylic carbon at around 70.0 ppm (**Figure 2.24**). The oily carbinols were usually obtained in quantitative yield and used directly in the next step without any further characterisation owing to their poor stability.
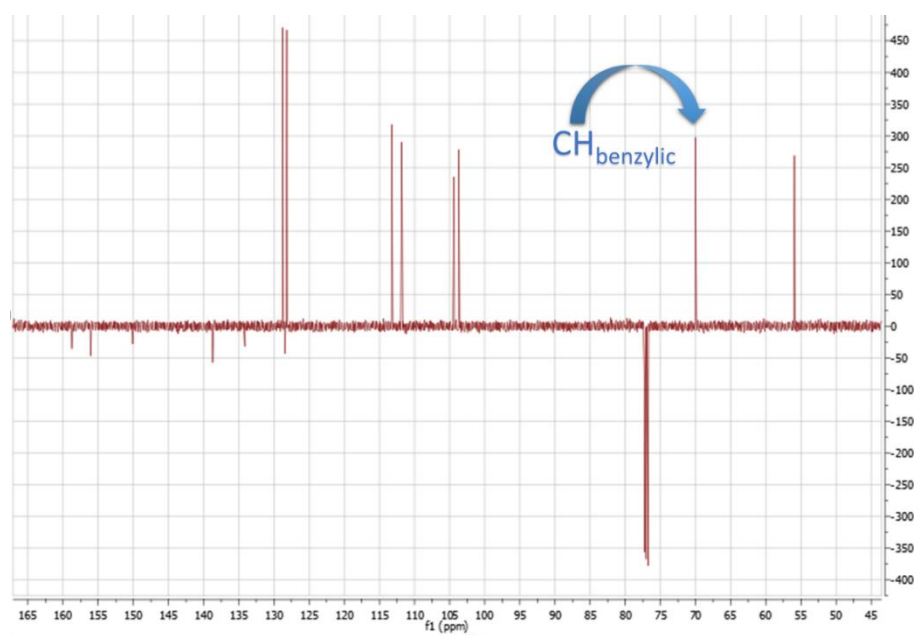
Figure (2.24): Magnification of the ^{13}C NMR for (4-chlorophenyl)(5-methoxybenzofuran-2-yl)methanol (**4a**) indicating the appearance of the CH signal.

2.3.2.1.3. Third step: synthesis of 1-((4-substituted phenyl)(5- or 6-substituted benzofuran-2-yl) methyl)-1*H*-1,2,4-triazole (6a,b,c,d,e)

a	$R_1 = 6\text{-OCH}_3$	$R_2 = 4\text{-Cl}$
b	$R_1 = 5\text{-OCH}_3$	$R_2 = 4\text{-Cl}$
c	$R_1 = 6\text{-Cl}$	$R_2 = 4\text{-OCH}_3$
d	$R_1 = 6\text{-OCH}_3$	$R_2 = 4\text{-F}$
e	$R_1 = 6\text{-OCH}_3$	$R_2 = 4\text{-CN}$
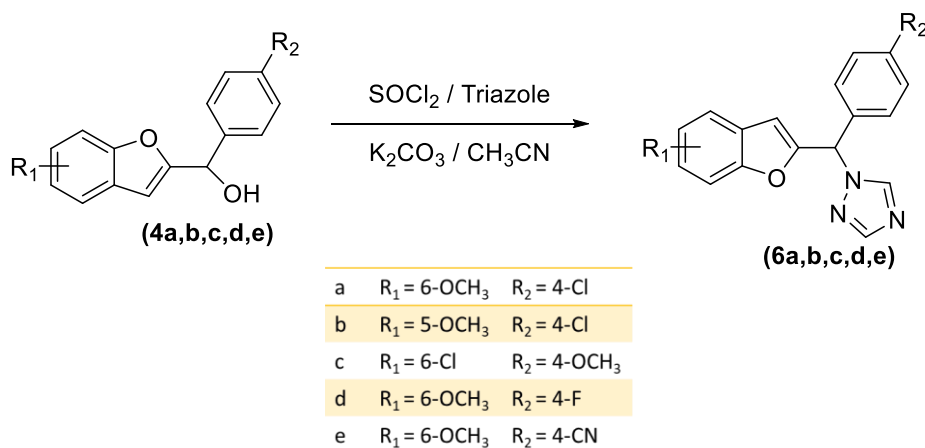
In this reaction (**Figure 2.25**) thionyl chloride reacts with triazole forming the activated electrophile *in situ* and then K_2CO_3 increases the nucleophilicity of the hydroxyl group of the carbinols to form a racemic mixture of the final compound (**6**). This reaction is very slow taking 5 days and never goes to completion and in the attempts to overcome this, 1,1′-carbonyl-di(1,2,4-triazole) was used instead of using $SOCl_2$/triazole mixture to produce the activated triazole *in situ*. Unfortunately, it was not successful with a very complex mixture observed by TLC. However, later during the course of this work due to complications in the formation of other derivatives, several modifications to the method (discussed later) were attempted and found that raising the equivalents of thionyl chloride from 1 to 1.6 led to the completion of the reaction in 16 hours only.
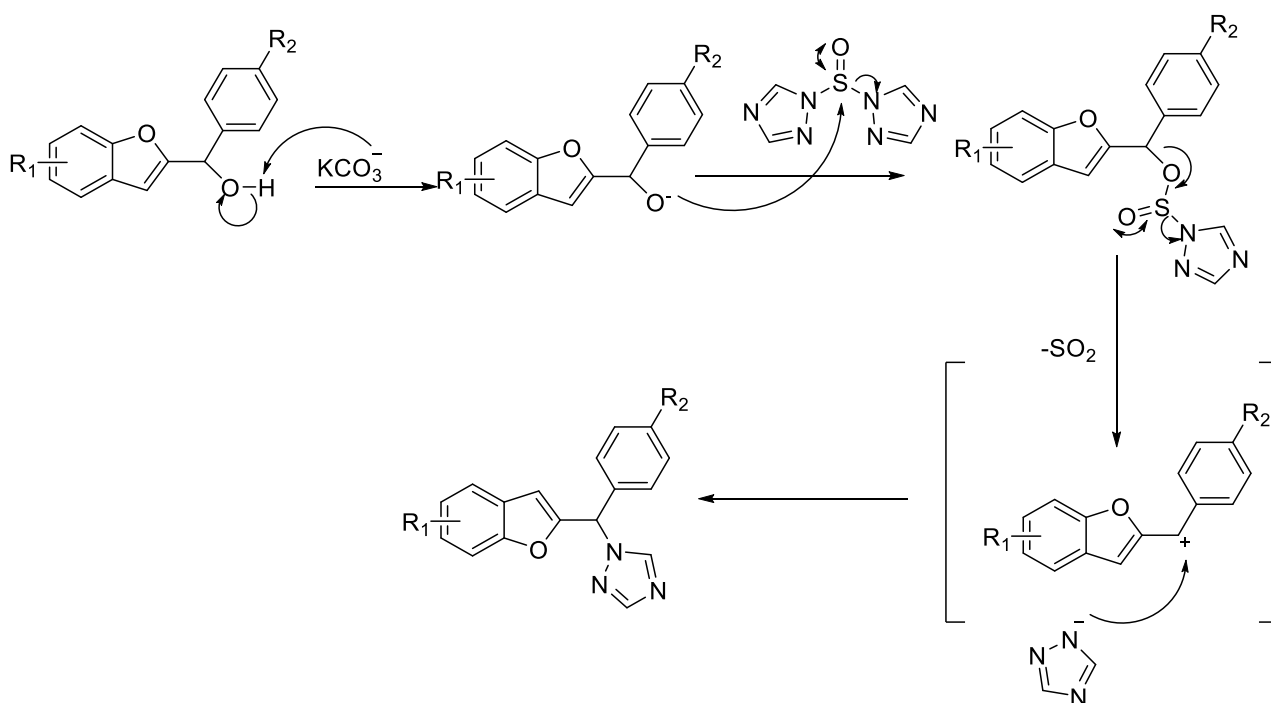
Figure (2.25): Mechanism for the synthesis of 1-((4-substituted phenyl)(5- or 6-substituted benzofuran-2-yl)methyl)-1*H*-1,2,4-triazole.

The identity of the compounds was indicated by two new aromatic signals of the triazole CH at around 8.0 and 8.1 ppm in ^{1}H NMR and at around 152.6 and 143.3 ppm in ^{13}C NMR. The ^{13}C signals of the triazole ring had lower intensity when compared to other signals even during longer experiment times (**Figure 2.26**). In some cases, one or both did not appear in the ^{13}C NMR but the ^{1}H signals were always consistent confirming with high degree of confidence the identity of the formed compounds.
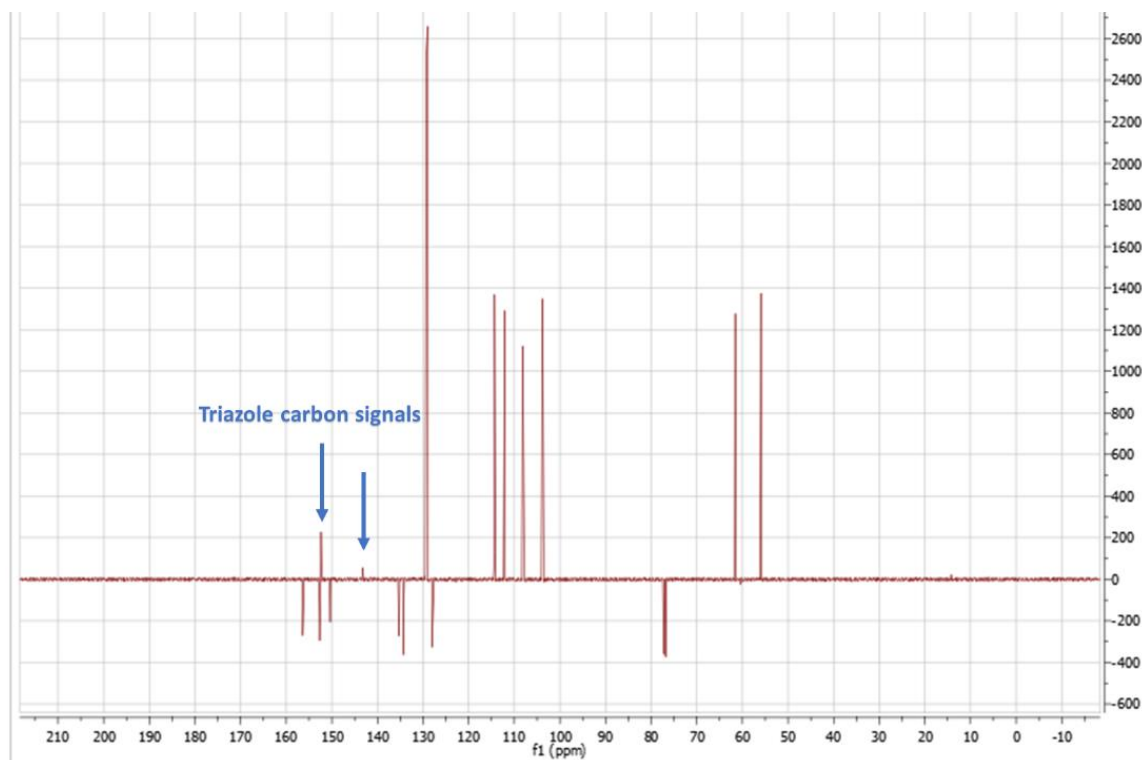
Figure (2.26): Magnification of the ^{13}C NMR for 1-((4-chlorophenyl)(5-methoxybenzofuran-2-yl) methyl)-1*H*-1,2,4-triazole (**6b**) showing the low intensity of the triazole carbon signal.

2.3.2.2. Synthetic pathway for Class 2 (hydroxybenzofuran compounds):

This synthetic pathway followed the published preparation of 2-((4-chlorophenyl)(1*H*-1,2,4-triazol-1-yl)methyl)benzofuran-6-ol (**11**) and 4-((6-hydroxybenzofuran-2-yl)(1*H*-1,2,4-triazol-1-yl)methyl)benzonitrile (**14**) (Saberi *et al.* 2006) with modifications discussed where applicable. The scheme consists of four steps starting with the selective pyran protection of one of the phenolic hydroxy groups of the dihydroxybenzaldehyde (**1**) then applying the same three steps of the scheme under class 1; 1) benzofuran ketone species formation, 2) reduction to carbinols, 3) substitution of the hydroxy group by triazole. This scheme resulted in successful preparation of four compounds (**11-14**) (**scheme 2.2**).

| 1d | 4-OH |
| 1e | 5-OH |

| 8a | 4-OPy |
| 8b | 5-OPy |

a	R_2 = 4-Cl
c	R_2 = 4-F
d	R_2 = 4-CN

a	R_1 = 6-OPy	R_2 = 4-Cl
b	R_1 = 5-OPy	R_2 = 4-Cl
c	R_1 = 6-OPy	R_2 = 4-F
d	R_1 = 6-OPy	R_2 = 4-CN

a	R_1 = 6-OPy	R_2 = 4-Cl
b	R_1 = 5-OPy	R_2 = 4-Cl
c	R_1 = 6-OPy	R_2 = 4-F
d	R_1 = 6-OPy	R_2 = 4-CN

11	R_1 = 6-OH	R_2 = 4-Cl
12	R_1 = 5-OH	R_2 = 4-Cl
13	R_1 = 6-OH	R_2 = 4-F
14	R_1 = 6-OH	R_2 = 4-CN
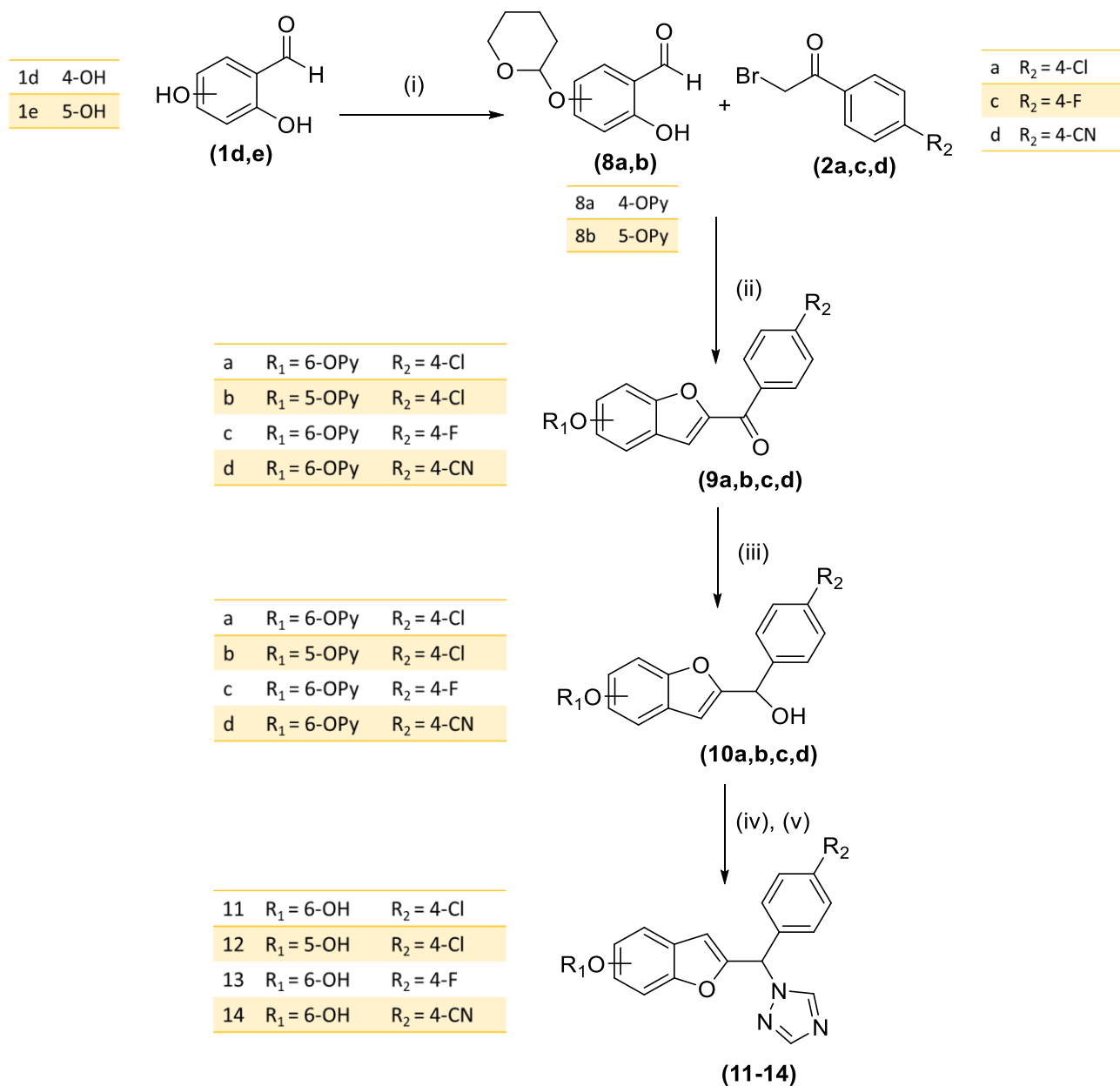
Scheme (2.2): (i) 3,4-dihydro-2*H*-pyran, *p*-toluenesulfonic acid, Et$_2$O, r.t, 3h (ii) K$_2$CO$_3$, CH$_3$CN, 70 ℃, 3 h (iii) NaBH$_4$, dioxane, 2 h (iv) SOCl$_2$, triazole, CH$_3$CN, 0 ℃, 1 h (v) K$_2$CO$_3$, r.t, 16h.

2.3.2.2.1. First step: synthesis of 2-hydroxy-4/5-((tetrahydro-2*H*-pyran-2-yl)oxy)benzaldehyde (8a,b)

1d	4-OH
1e	5-OH

8a	4-OPy
8b	5-OPy
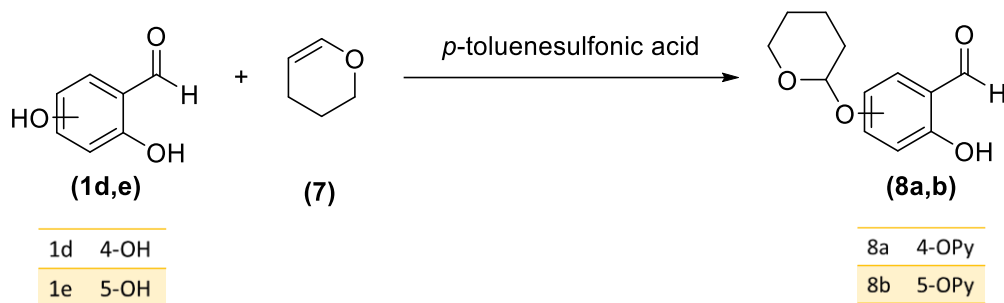
This is a selective pyran protection of the *para-* or *meta-* phenolic OH in which *p*-toluenesulfonic acid is used as the acid catalyst. In this reaction (**Figure 2.27**) the *ortho* position is less reactive owing to intramolecular hydrogen bond formation with the adjacent aldehyde group leading to reaction on the *para* or *meta* position only.
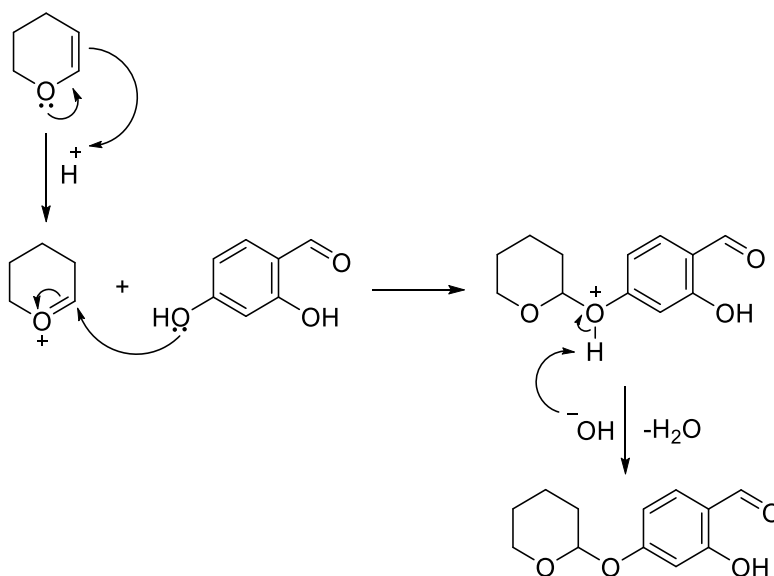
Figure (2.27): Mechanism for the acid catalysed pyran protection of 2,4-dihydroxybenzaldehyde.

The produced colourless oil (**8a,b**) was obtained with yield range (40-50%) and was of pure enough quality as indicated by ^{1}H NMR, which showed the appearance of the pyran peaks, which are a triplet at 5.5 ppm for the CH-pyran that is directly attached to the phenolic oxygen and multiplets at around 3.8, 3.6 and 2.0 to represent the CH_2 groups.

2.3.2.2.2. Second step: synthesis of (4-substituted phenyl)((((tetrahydro-2*H*-pyran-2-yl)oxy)benzofuran-2-yl)methanone derivatives (9a,b,c,d)
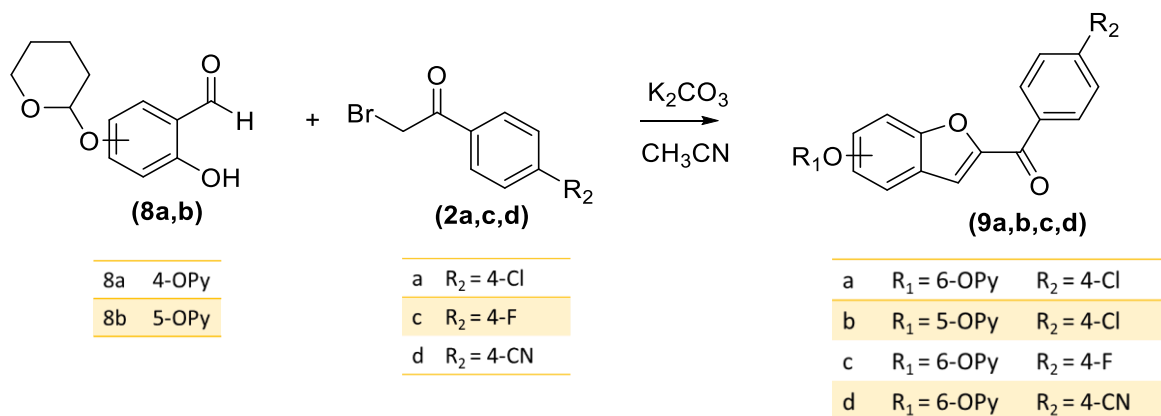
This reaction is a Rap-Stoermer formation (**Figure 2.21**) as described for preparation of (**3**) but this time the product purity was not sufficient and purification by recrystallisation from methanol was needed to afford (4-chlorophenyl)(6-((tetrahydro-2*H*-pyran-2-yl)oxy)benzofuran-2-yl)methanone (**9a**) with a yield of 52 %, and from ethanol to afford both (4-chlorophenyl)(5-((tetrahydro-2*H*-pyran-2-yl)oxy)benzofuran-2-yl)methanone (**9b**) and 4-(6-((tetrahydro-2*H*-pyran-2-yl)oxy)benzofuran-2-carbonyl)benzonitrile (**9d**) with a yield of 68% and 70% respectively. Only (4-fluorophenyl)(6-((tetrahydro-2*H*-pyran-2-yl)oxy)benzofuran-2-yl)methanone (**9c**) was obtained in 95% yield pure enough to be used directly in the next step.

2.3.2.2.3. Third step: synthesis of (4-substituted-phenyl)(5-/6-((tetrahydro-2*H*-pyran-2-yl)oxy) benzofuran-2-yl)methanol (10a,b,c,d)
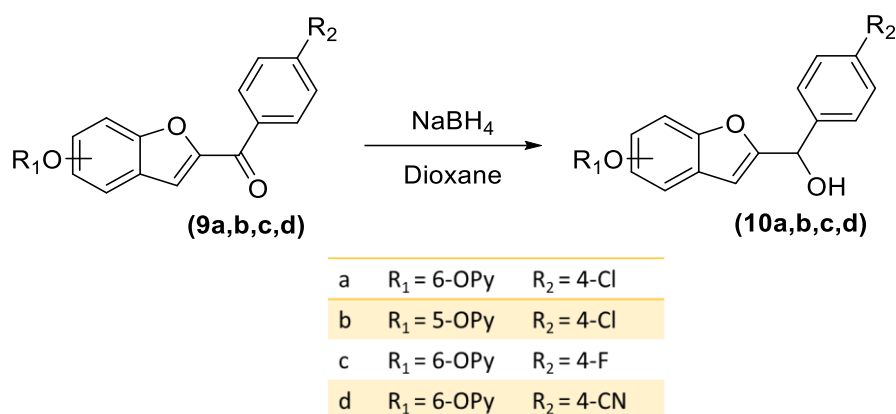
This reaction is a sodium borohydride reduction of ketone compounds to carbinols as described under synthesis of (**4**) (**Figure 2.23**). The identity of the compounds was confirmed by ^{1}H NMR,

which showed the appearance of a singlet signal at around 5.8 ppm indicating the benzylic proton and a broad signal at around 2.7 ppm indicating the formation of alcoholic OH. The oily colourless carbinols were obtained in quantitative yield. These compounds suffered from extreme instability indicated by fast degradation and formation of colourful oils ranging from pink to blue or purple (**Figure 2.28**) and therefore needed to be used directly in the next step.
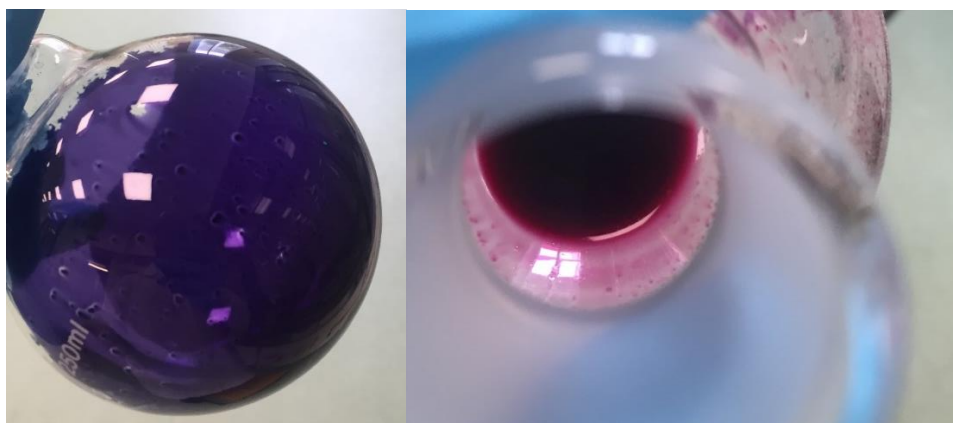
Figure (2.28): Pink and blue colours of the degradation products of (4-chlorophenyl)(6-((tetrahydro-2*H*-pyran-2-yl)oxy)benzofuran-2-yl)methanol (**10a**).

2.3.2.2.4. Fourth step: synthesis of 2-((4-substituted phenyl)(1*H*-1,2,4-triazol-1-yl)methyl) benzofuranol (11-14)

a	R$_1$ = 6-OPy	R$_2$ = 4-Cl
b	R$_1$ = 5-OPy	R$_2$ = 4-Cl
c	R$_1$ = 6-OPy	R$_2$ = 4-F
d	R$_1$ = 6-OPy	R$_2$ = 4-CN

11	R$_1$ = 6-OH	R$_2$ = 4-Cl
12	R$_1$ = 5-OH	R$_2$ = 4-Cl
13	R$_1$ = 6-OH	R$_2$ = 4-F
14	R$_1$ = 6-OH	R$_2$ = 4-CN
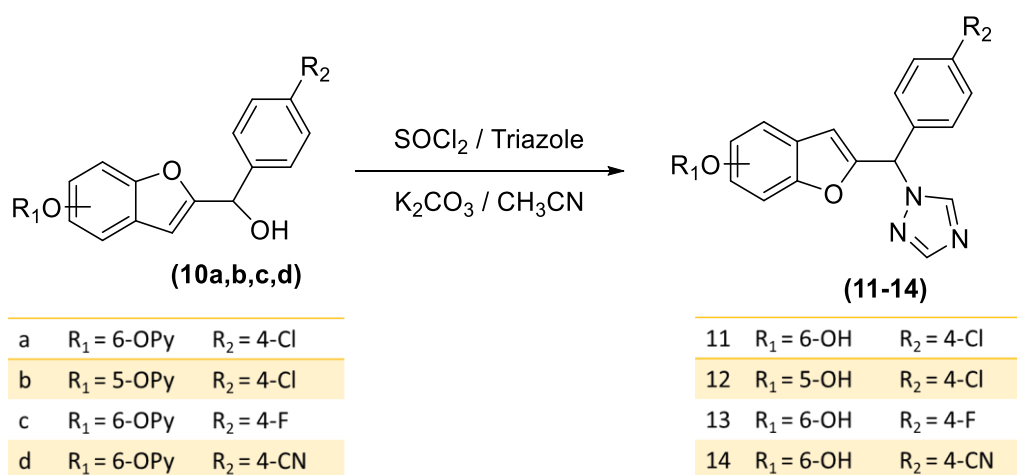
This reaction follows the same mechanism as described for the preparation of (**6**) in the addition of triazole but it has a totally new aspect, that is the deprotection of the pyran moiety under the reaction conditions providing a racemic mixture of the final compounds (**11-14**). At first, this reaction suffered

from two drawbacks; the slow progress and poor yield with the major side product produced found to be 2-((4-substituted-phenyl)(hydroxy)methyl)benzofuranol as identified by ^{1}H NMR by the absence of triazole protons and the presence of phenolic OH peak (**Figure 2.29**).
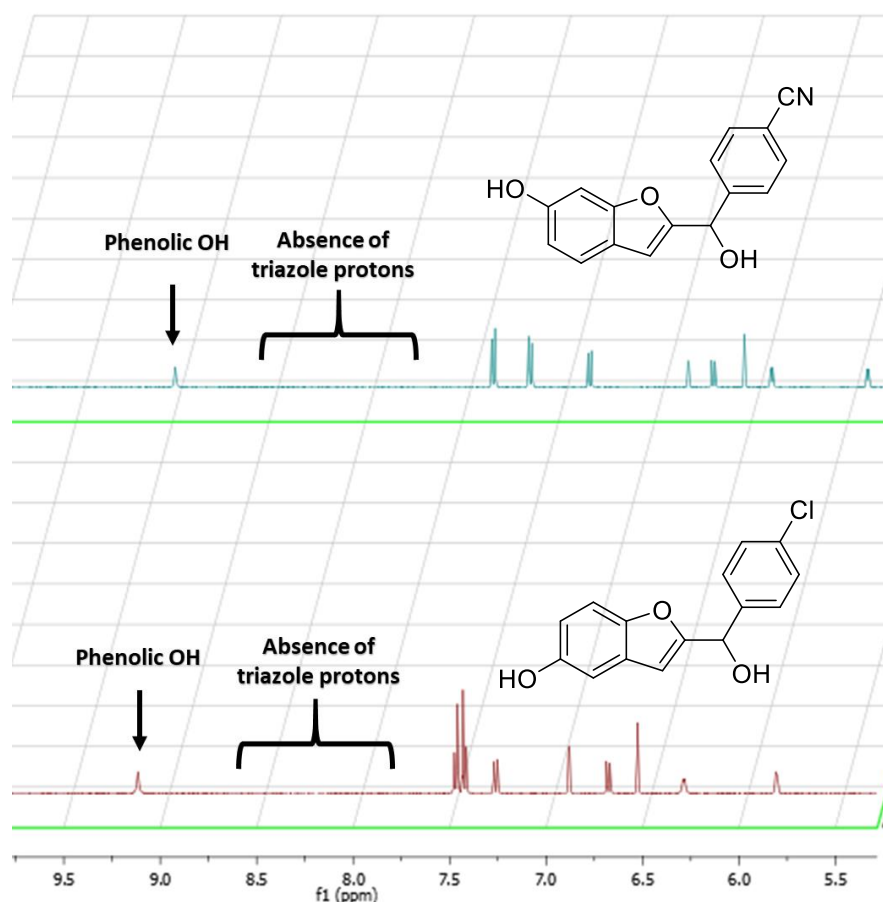
Figure (2.29): Magnification of ^{1}H NMR for two different 2-((4-substituted-phenyl)(hydroxy)methyl)benzofuranol separated as the side products.

Modifications to the method, including changing the order of addition or the equivalents of reactants, one at a time, revealed that raising the equivalent of thionyl chloride from 1 to 1.6 led to complete reaction in 16 hours only and significantly improved the yield to 70-90% without the formation of the side product. The identity of the compound was confirmed by two new aromatic signals of the triazole CH at around 8.0 and 8.1 ppm in ^{1}H NMR and at around 151.7 and 143.1 ppm in ^{13}C NMR.

2.3.2.3. **Synthetic pathway for Class 3 (hydroxyphenyl compound):**

This synthetic pathway used (4-chlorophenyl) (5-methoxybenzofuran-2-yl) methanone (**3c**) previously prepared in scheme one. Demethylation to form free phenolic hydroxy group then protection with pyran represent the first two steps. The final two steps are typically the same in the previous schemes; one and two, which are reduction of the ketone to carbinol then triazole substitution of the alcoholic hydroxy group providing 4-((5-chlorobenzofuran-2-yl)(1*H*-1,2,4-triazol-1-yl)methyl)phenol (**17**).
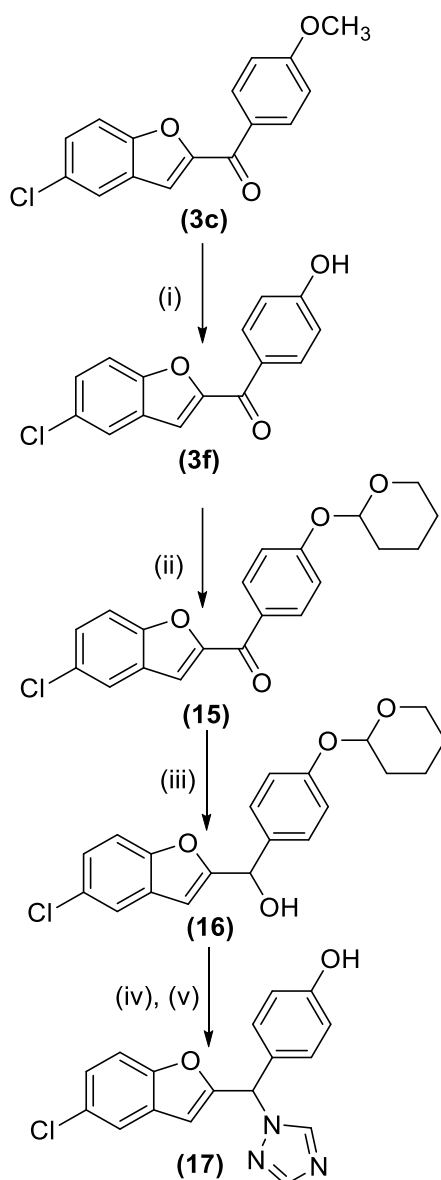
Scheme (2.3): (i) HBr, CH₃COOH, 110 ℃, 16 h (ii) 3,4-dihydro-2*H*-pyran, *p*-toluenesulfonic acid, Et₂O, r.t, 3h (iii) NaBH₄, dioxane, 2 h (iv) SOCl₂, triazole, CH₃CN, 0 ℃, 1 h (v) K₂CO₃, r.t, 16h.

2.3.2.3.1. First Step: synthesis of (5-chlorobenzofuran-2-yl)(4-hydroxyphenyl) methanone (3f)
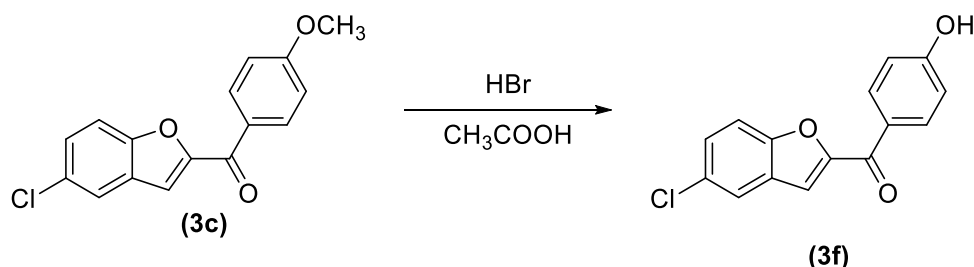
Several methods were tried to prepare this compound (**Table 2.3**). At first a mixture of BCl$_3$ and tetrabutylammonium iodide (Brooks *et al.* 1999) was used but no reaction was observed. Then the common demethylation protocol with BBr$_3$ (Salomé *et al.* 2014) was employed but was shown to be unsuccessful. Finally, a method refluxing for 6 h with HBr in acetic acid (Plattner *et al.* 1985) was used to provide the desired product in a poor yield (around 10 %) suggesting that the reaction needed more time. Increasing the reflux time to 16 h significantly raised the yield to 55-75%. Although, crystallisation from CH$_3$CN provided the compound as brown crystals, column chromatography was the ideal choice providing the product as a white solid in a purer form indicated by HPLC analysis. The identity of the compound was confirmed through the disappearance of the methyl group signals from both ^{1}H and ^{13}C NMR and the presence of a new singlet signal in the ^{1}H NMR representing the phenolic group.

Table (2.3): Different methods for preparing (5-chlorobenzofuran-2-yl)(4-hydroxyphenyl) methanone (**3f**)

Reagent	Yield
BCl$_3$	No reaction
BBr$_3$	No reaction
HBr/CH$_3$COOH/110 ℃/6 h	10%
HBr/CH$_3$COOH/110 ℃/16 h	55-75%

2.3.2.3.2. Second step: synthesis of (5-chlorobenzofuran-2-yl)(4-((tetrahydro-2*H*-pyran-2-yl)oxy)phenyl)methanone (15)
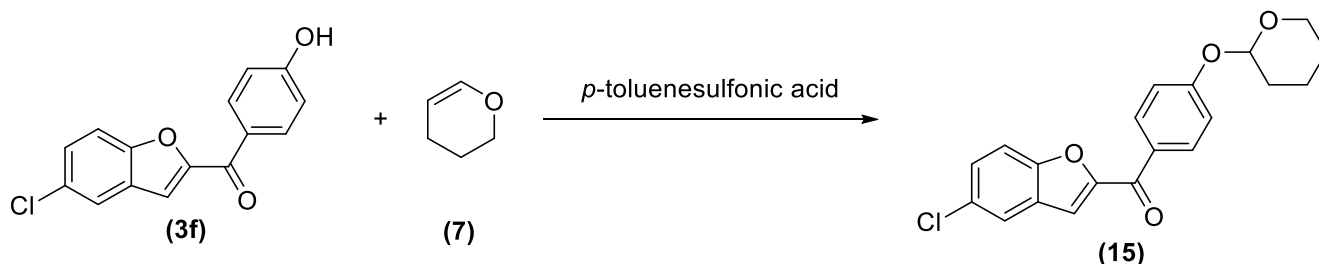
This is a pyran protection of phenolic OH as discussed before (**Figure 2.27**). Following the same conditions using Et$_2$O resulted in poor reactivity owing to limited solubility in this solvent. The solvent was switched to EtOAc, which completely solubilised the reactants, and provided the product in significantly better yield (70-80%). Purification using column chromatography provided the required product as a white solid confirmed by ^{1}H NMR, which showed the appearance of the pyran peaks which are a triplet at 5.5 ppm for the CH-pyran that is directly attached to the phenolic oxygen and multiplets at around 3.8, 3.6 and 2.0 to represent the CH$_2$ groups.

2.3.2.3.3. Third step: synthesis of (5-chlorobenzofuran-2-yl)(4-((tetrahydro-2*H*-pyran-2-yl)oxy)phenyl)methanone (16)
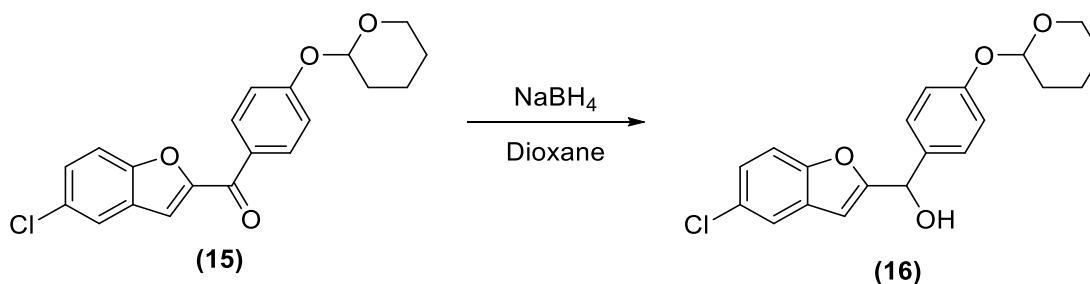
This reaction is a sodium borohydride reduction of ketone compounds to carbinols as described under synthesis of (**4**) (**Figure 2.23**). The identity of the compound was confirmed by ^{1}H NMR, which showed the appearance of a singlet signal at around 5.8 ppm indicating the benzylic proton and a broad signal at around 2.9 ppm indicating the formation of alcoholic OH. The oily colourless carbinol was obtained in quantitative yield and was used without any further purification.

2.3.2.3.4. Fourth step: synthesis of 4-((5-chlorobenzofuran-2-yl)(1*H*-1,2,4-triazol-1-yl)methyl) phenol (17)

(16) → SOCl₂ / Triazole, K₂CO₃ / CH₃CN → **(17)**
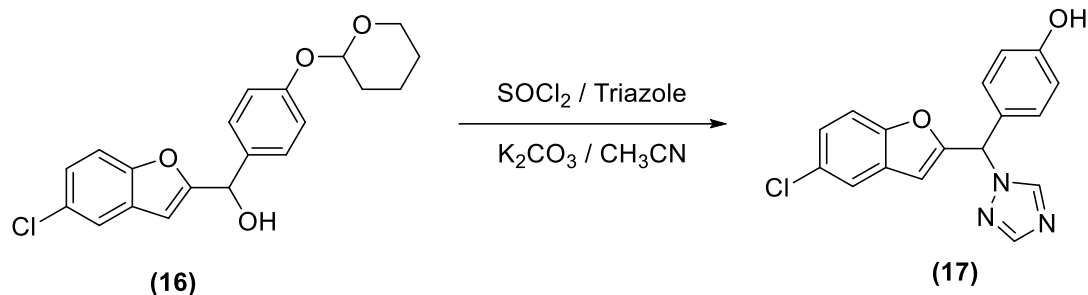
This reaction follows the same mechanism as described for compounds (**11-14**) with deprotection of the pyran moiety under the reaction conditions providing a racemic mixture of the final compound (**17**). The only difference was the solubility of the produced compound. Being poorly soluble in CH₃CN, the formed compound precipitated from the reaction mixture. The work-up and purification was simpler as it only needed stepwise filtration. At first, filtering to remove of any remaining impurities in the solvent leaving the residue, which was composed of K₂CO₃, triazole and the product, further washing with EtOAc gave the product in fairly good yield (45%) by collecting the filtrate and evaporating the solvent. The identity of the compound was confirmed by two new aromatic signals of the triazole CH at around 8.0 and 8.1 ppm in ¹H NMR and at around 151.7 and 143.1 ppm in ¹³C NMR.

2.3.2.4. Class 4 (all the extended compounds regardless of the position of substituent):

Class four simply encompass using the free phenolic hydroxy group of compounds from Class two and three to make different substitutions whether morpholino-carboxyl group or a whole range of aliphatic chains (ethyl, propynyl, butynyl and pentynyl) in a one step reaction. Although the simple nucleophilic reaction was used to prepare all the compounds in this class, they can be divided into three distinct subclasses based on the position of this substitution (6-substituted benzofuran, 5-substituted benzofuran and 4-substituted phenyl).

2.3.2.4.1. Sub-class A (6-substituted benzofuran compounds):
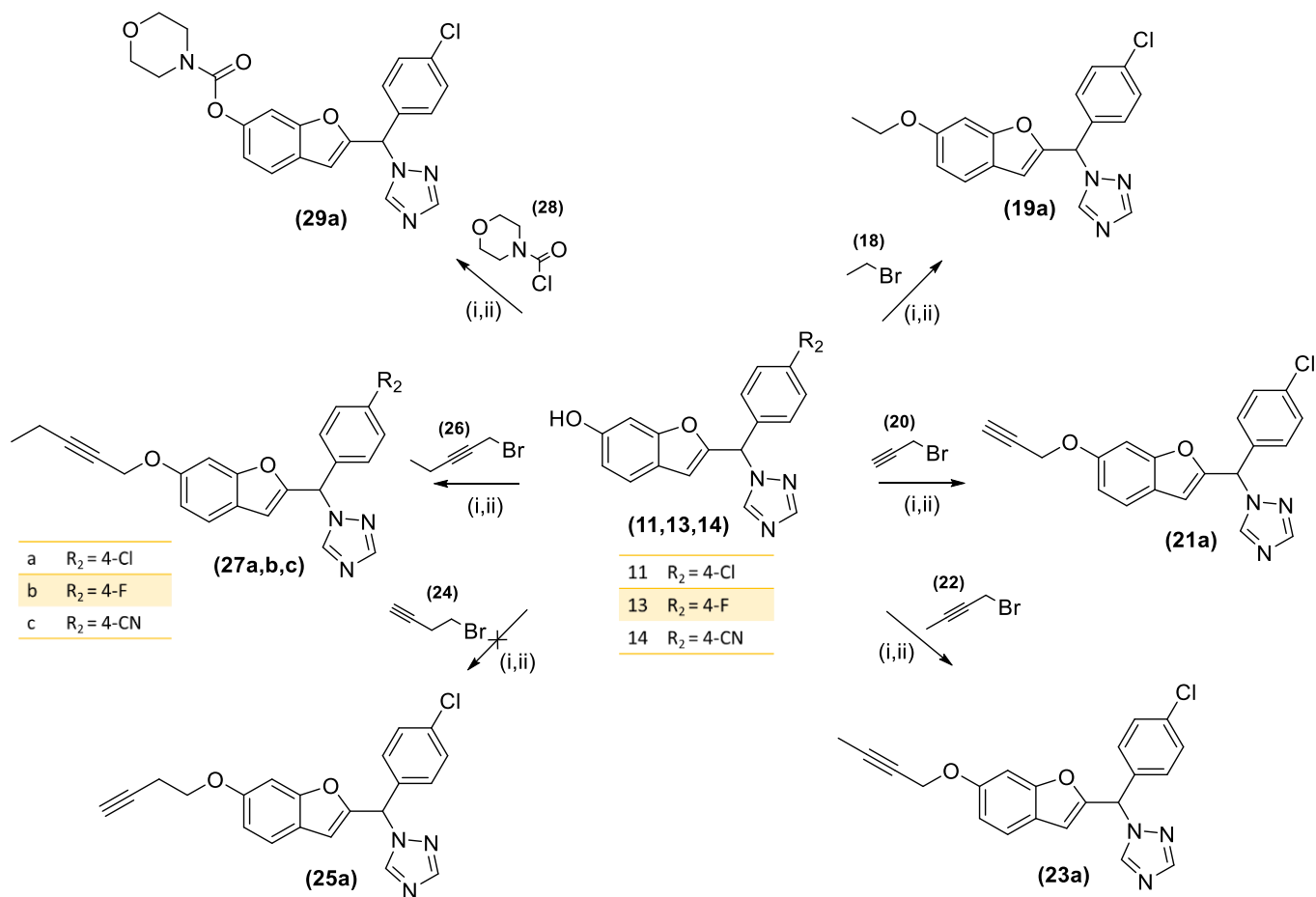
Scheme (2.4): (i) K$_2$CO$_3$, CH$_3$CN, 40 °C, 1h (ii)RX, r.t, 16h (where X = Cl or Br).

2.3.2.4.1.1. Synthesis of 1-((4-chlorophenyl)(6-ethoxybenzofuran-2-yl)methyl)-1*H*-1,2,4-triazole (19a)
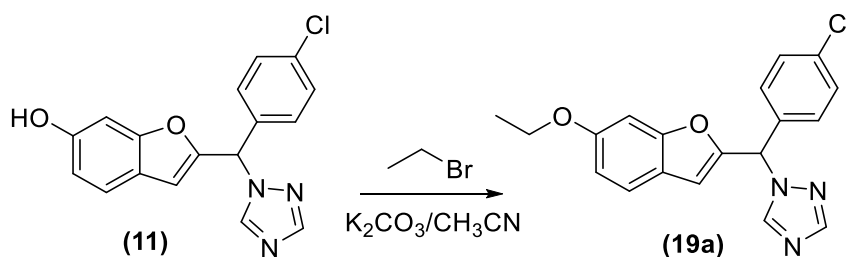
In this reaction the acidic phenolic OH of compound **11** is deprotonated by a base, which can then make a nucleophilic attack and substitute the bromide of ethyl bromide (**18**). The choice of K$_2$CO$_3$ as the base will be discussed later under the synthesis of 1-((4-chlorophenyl)(6-(pent-2-yn-1-

yloxy)benzofuran-2-yl)methyl)-1*H*-1,2,4-triazole (**27**). Although this reaction is an equimolar reaction, excess of the alkyl halide was needed due to its volatility. The identity of the compound was confirmed by ^{1}H NMR as indicated by the appearance of two peaks at around 1.4 and 4.0 ppm for the methyl and methylene groups respectively. ^{13}C NMR also showed the appearance of the two peaks corresponding to the ethyl group at around 15 and 64 ppm.

2.3.2.4.1.2. Synthesis of 1-((4-chlorophenyl)(6-(prop-2-yn-1-yloxy)benzofuran-2-yl)methyl)-1*H*-1,2,4-triazole (21a)
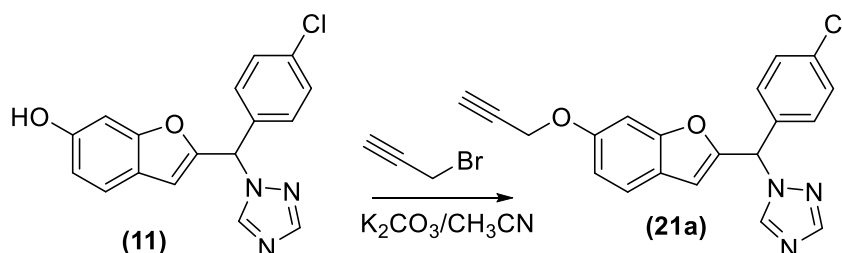
The same method described for compound (**19a**) was used with excess of the propargyl bromide (**20**) (solution in toluene) due to its volatility. ^{1}H NMR indicated the formation of the required compound by the appearance of two peaks at around 2.4 ppm as triplet and 4.6 ppm as doublet for the terminal CH and methylene groups respectively due to long range coupling across the triple bond (**Figure 2.30**).
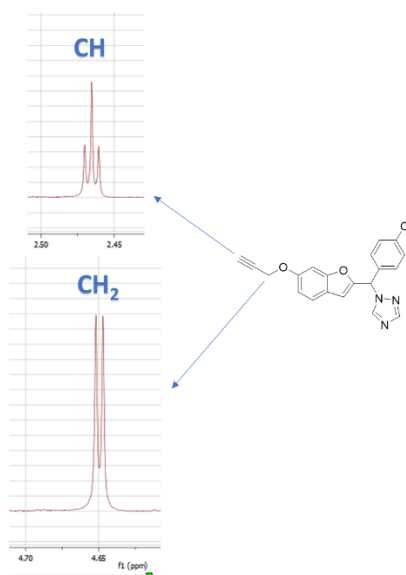
Figure (2.30): Magnification of ^{1}H NMR for (**21a**) showing the splitting of the peaks involved in long range coupling.

In APT ^{13}C NMR, all signals were in place except the terminal CH, that appeared in the negative side of the chart. Using DEPT135 showed the CH peak in the positive side as would normally be excepted, however the quaternary alkyne carbon was surprisingly observed and in the positive side of the chart. This confusing and unexcepted behaviour is attributed to the exceptionally large coupling constant of the alkyne carbons (240-250 Hz) (Claridge 2009). HSQC experiment was used to indicate the correlation between the proton peak of the CH group at 2.4 ppm and the carbon peaks at 76 and 78 ppm corresponding to the CH and quaternary carbon of the triple bond (**Figure 2.31**).
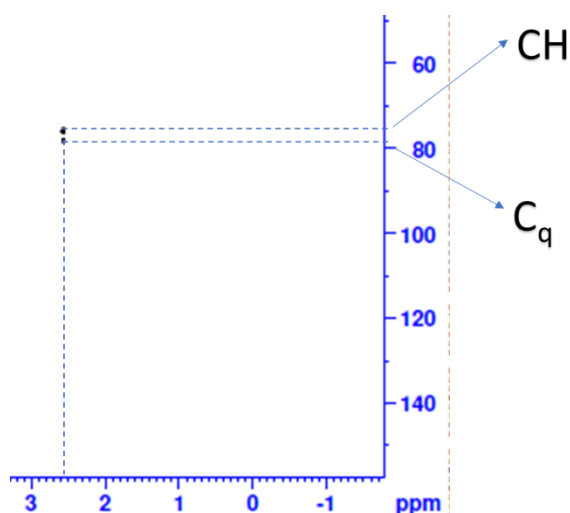
Figure (2.31): Magnification of HSQC for (**21a**) showing the correlation of the two carbons of the terminal alkyne.

2.3.2.4.1.3. Synthesis of 1-(((6-(but-2-yn-1-yloxy)benzofuran-2-yl)(4-substitutedphenyl)methyl)-1*H*-1,2,4-triazole (23a, c)

11	R= Cl
14	R= CN

a	R= Cl
c	R= CN
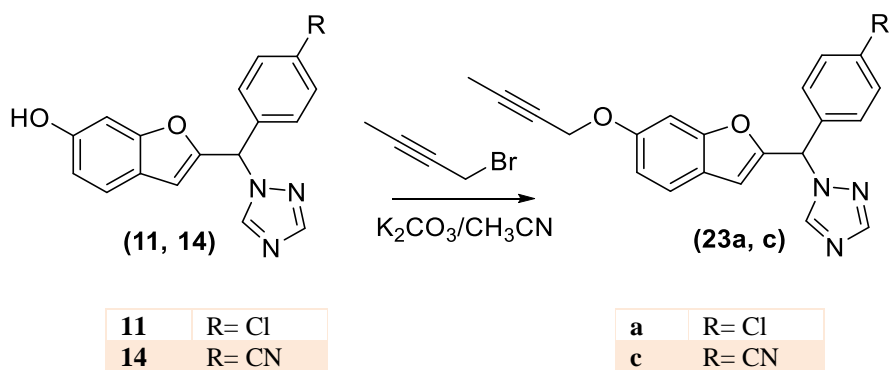
This was a straightforward reaction using the same method described for compound (**19a**) but a much lower excess of the butyne bromide was required due to having lower volatility when compared to lower molecular weight alkyl halides. The structure of the prepared compound was confirmed by ^{1}H and ^{13}C NMR. The nitrile derivative (**23c**) was obtained in a very poor yield (7%) compared to the good yield of the chloro analogue (**23a**) (76%) as a result of a very complex reaction as reflected by the numerous spots in TLC.

2.3.2.4.1.4. Synthesis of 1-((6-(but-3-yn-1-yloxy)benzofuran-2-yl)(4-chlorophenyl)methyl)-1*H*-1,2,4-triazole (25a)
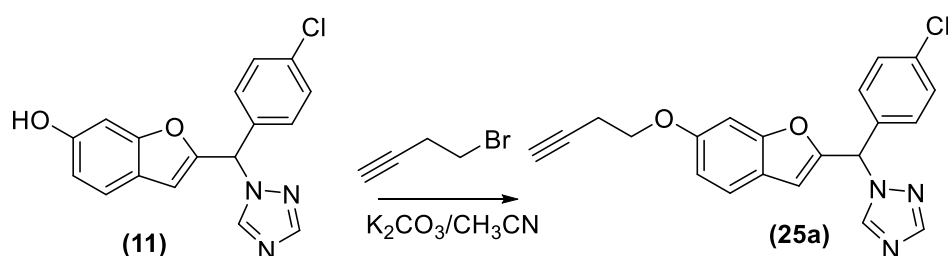
Although this reaction was expected to follow the rest of the series, the compound was not obtained no matter what conditions were used. Trying the usual conditions with room temperature stirring overnight in CH_3CN showed no progress in the reaction. Shifting to heating at different temperature ranging from 40-70 ℃ in an attempt to push the reaction forward was not successful. This poor reactivity may be attributed to the flexibility of the 4-bromo-1-butyne (**24**), which may hinder nucleophilic substitution for the halide atom.

2.3.2.4.1.5. Synthesis of 1-((4-substituted phenyl)(6-(pent-2-yn-1-yloxy) benzofuran-2-yl)methyl)-1*H*-1,2,4-triazole (27a, b, c)

a	R= Cl
b	R= F
c	R= CN
di	R=Cl
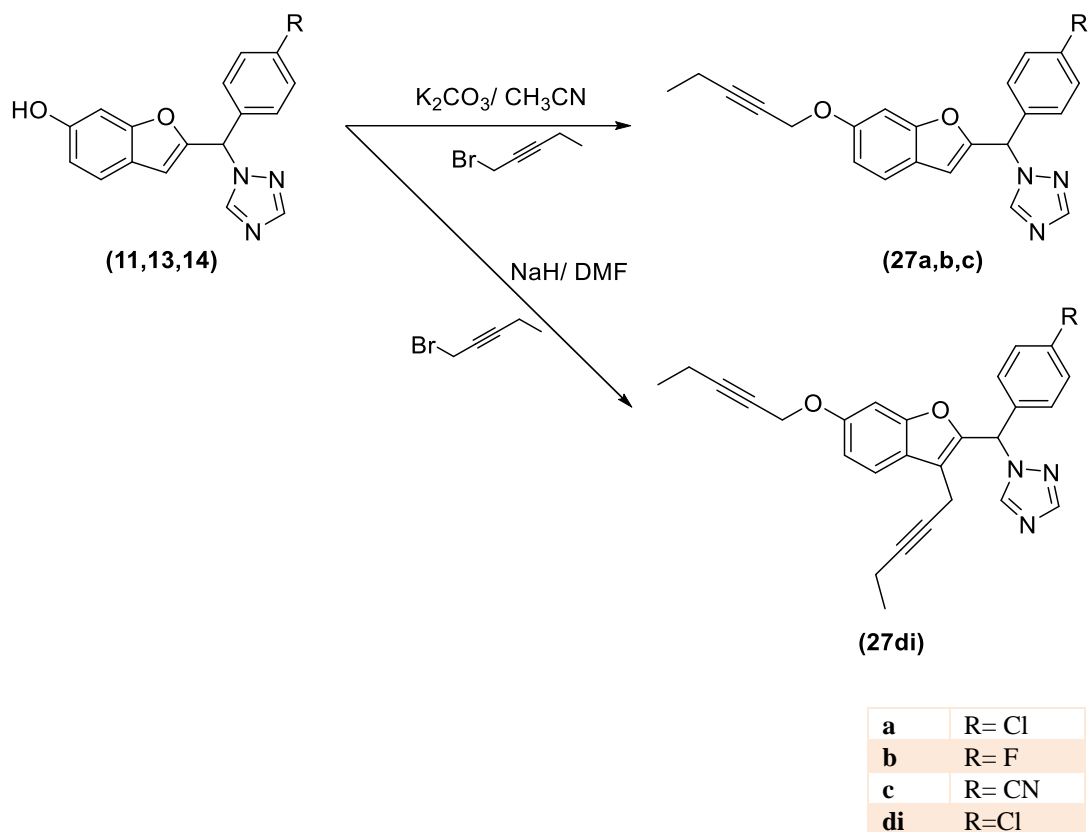
This reaction followed the exact same method for preparing the other members of the series as described for compound (**19a**), however it was actually the first reaction to be done in this series. At first, NaH was tried as the base in this reaction and after a complex column to separate the major product it was found to form a di-substitution owing to the acidity of the furan proton to form 1-((4-chlorophenyl)(3-(pent-2-yn-1-yl)-6-(pent-2-yn-1-yloxy)benzofuran-2-yl)methyl)-1*H*-1,2,4-triazole (**27di**). The identity of the formed compound was revealed by the duplication of signals of pentyne in ^{1}H NMR at around 4.6, 3.6, 2.2 and 1.9 ppm for the four CH_2 groups and 0.9 and 1.1 for the CH_3 groups along with the absence of one singlet signal from the aromatic region to prove the di-substitution assumption. As a result, a milder base e.g., potassium carbonate was suggested to selectively deprotonate the more acidic phenolic OH alone and was then applied to all the series members. ^{1}H and ^{13}C NMR confirmed the structure of the products.

2.3.2.4.1.6. Synthesis of 2-((4-chlorophenyl)(1*H*-1,2,4-triazol-1-yl)methyl) benzofuran-6-yl morpholine-4-carboxylate (29a)
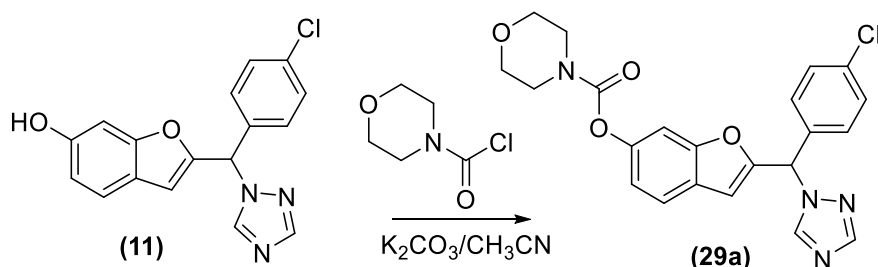
This compound was prepared also through nucleophilic substitution reaction using 4-morpholinecarbonyl chloride (**28**). The product was confirmed by ^{1}H and ^{13}C NMR with 2 multiplet peaks each for two of the morpholine CH$_2$ in the ^{1}H NMR and 4 distinct signals at around 66 and 44 ppm in the ^{13}C NMR.

In summary, eight compounds for the 6-substituted extended class were prepared and with yield and physical characteristics indicated in **table 2.4**.

Table (2.4): Yield and physical characteristics of 6-substituted extended compounds (**Class 4A**)

Compound	Yield	Physical characteristics
19a	67%	Yellow oil
21a	90%	Yellow oil
23a	76%	Yellow oil
23c	7%	Yellow oil
25a	0%	Not obtained
27a	75%	Yellow oil
27b	50%	Yellow oil
27c	17%	Yellow oil
29a	65%	White solid (m.p. = 150-154 ºC)

2.3.2.4.2. Sub-class B (5-substituted benzofuran compounds) and sub-class C (4-substituted phenyl):
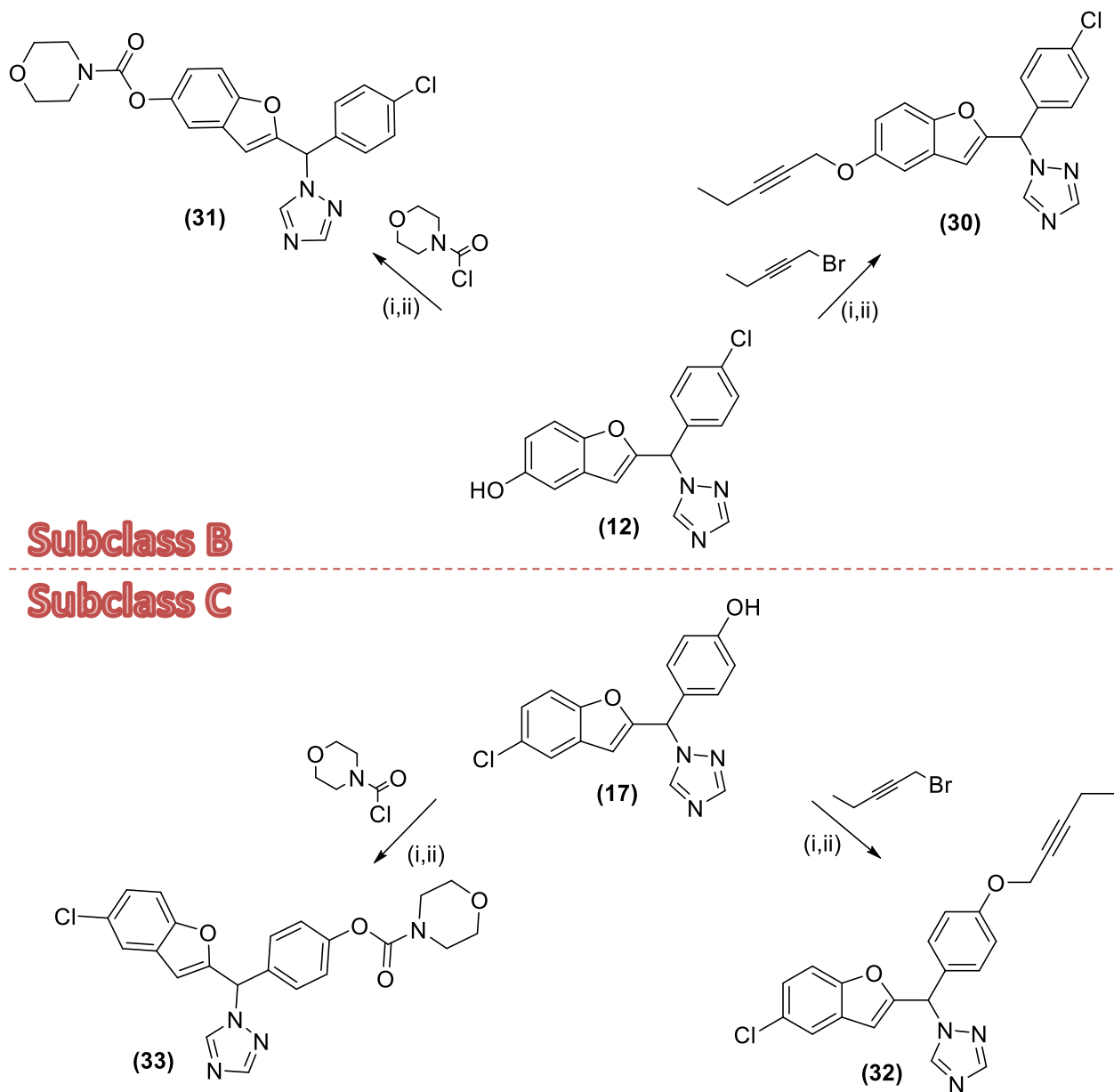
Scheme (2.5): (i) K$_2$CO$_3$, CH$_3$CN, 40 ℃, 1h (ii)RX, r.t, 16h.

The members of these two subclasses were prepared by the method described for compound (**19a**). All the four compounds were confirmed by ^{1}H and ^{13}C NMR.

In total, four compounds were prepared and with yield and physical characteristics indicated in **table 2.5**.

Table (2.5): Yield and physical characteristics of class 4B and class 4C compounds

Compound	Yield	Physical characteristics
30	50%	Yellow oil
31	81%	White solid (m.p. = 158-162 ºC)
32	44%	Yellow oil
33	60%	Yellow oil

2.3.3. Aromatase enzyme inhibition

As an iterative process, twelve compounds divided into three series were evaluated for CYP19A1 inhibitory activity, performed by Dr. Paul Foster of Birmingham University. Each of the three series contained four members as shown in **figure 2.32**.
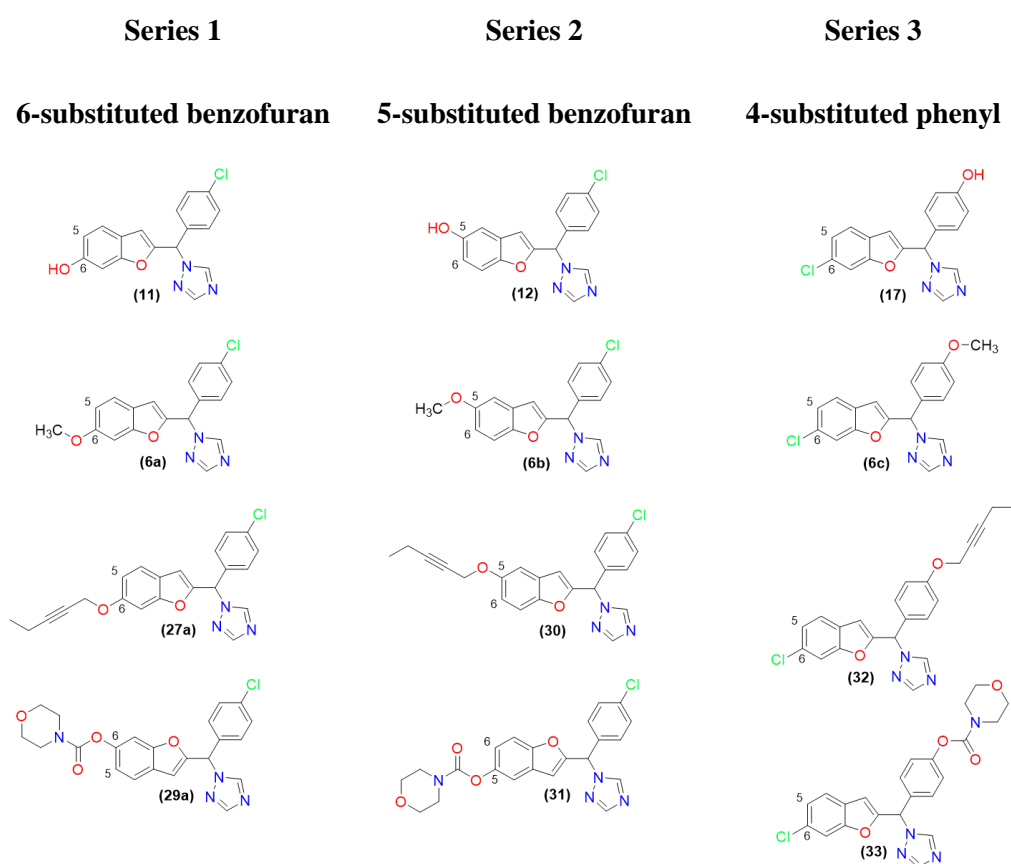
Figure (2.32): The members of the three series.

All compounds were first tested at a single concentration (1 µM) to narrow down the selection to the most active compounds (**Figure 2.33**). Seven of the twelve compounds were found to have promising activity and proceeded to IC_{50} determination.
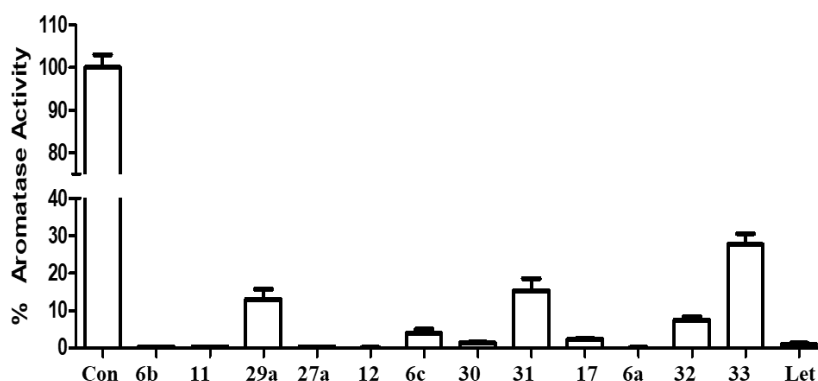
Figure (2.33): Aromatase activity at 1µM concentration of the twelve compounds.

Testing the compounds at different concentrations provided the IC_{50} for the seven compounds (**Figure 2.34**). Head to head comparisons indicated that 6-substituted series was a clear winner.
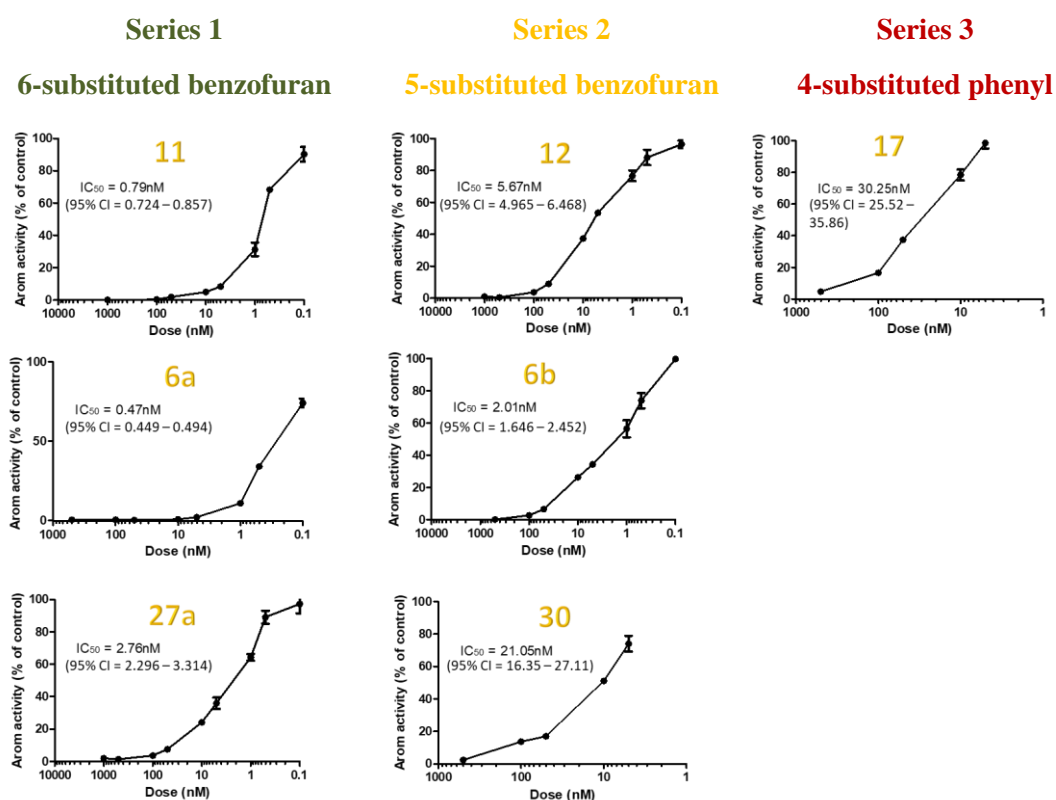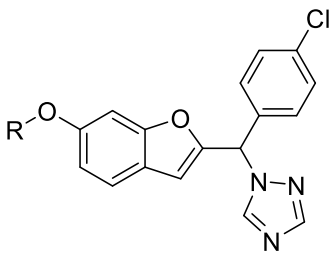
Figure (2.34): IC_{50} values of the most active compounds of the basic three series (nM) with 95% confidence intervals (95% CI) (letrozole IC_{50} = 0.5 nM).

Testing the rest of the compounds to compare the length of the hydrophobic tail at different concentrations provided the IC_{50} indicating that the butyne group was the optimal length for activity among the extended substituents required for the dual binding as indicated from head to head comparison of compounds **19a, 21a, 23a, 25a and 27a** (**Table 2.6**).

Table (2.6): IC_{50} values of the compounds **19a, 21a, 23a and 27a**.
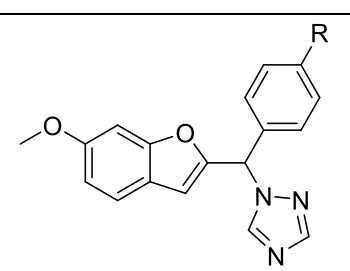
Compound	R	IC_{50} (nM)	95% Confidence interval (nM)	
19a	ethyl	0.46	0.378 - 0.562	
21a	Prop-3-yne	1.03	0.674 - 1.573	
23a	but-2-yne	0.53	0.479 - 0.589	
27a	pent-2-yne	2.76	2.296 - 3.314	

Also comparing the secondary substituent on the 4-phenyl position indicated that the nitrile and fluoro groups showed better activity compared with the chloro as indicated by head to head comparison of the methoxy derivatives (compounds **6a, d, e**) (**Table 2.7**).

Table (2.7): IC_{50} values of the compounds **6a, d, e**.

Compound	R	IC_{50} (nM)	95% Confidence interval (nM)	
6a	Cl	0.47	0.449 - 0.494	
6d	F	0.15	0.101 - 0.215	
6e	CN	0.11	0.092 - 0.126	

These results led to the decision to prepare compound **23c** with both the butyne and nitrile substituents (**figure 2.35**) and testing showed activity of 0.09 nM.

(**23c**) $IC_{50} = 0.09$ nM
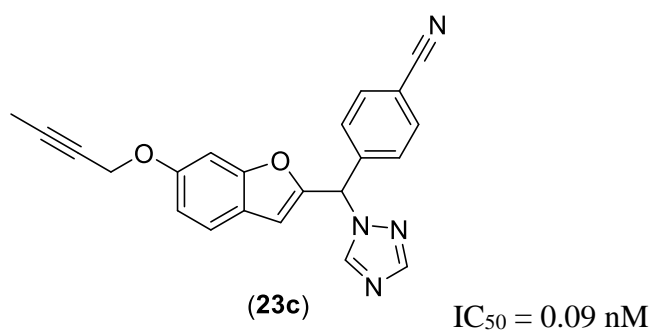
Figure (2.35): 4-((6-(But-2-yn-1-yloxy)benzofuran-2-yl)(1*H*-1,2,4-triazol-1-yl)methyl)benzonitrile (**23c**) with IC_{50}.

Subsequent biological results of the other fluoro and nitrile substituted compounds (**table 2.8**) lead to a conclusion that, even with an extended substitution e.g. pent-2-ynyloxy or but-2-ynyloxy, a fluoro derivatives still showed comparable inhibitory activity to nitrile analogues and therefore, compound **23b** should be prepared as future work.

Table (2.8): IC_{50} values of the compounds **13**, **14**, **27b** and **27c**.

Compound	R_1	R_2	IC_{50} (nM)	95% Confidence interval (nM)
13	OH	F	0.39	0.359 -0.431
14	OH	CN	0.56	0.504 - 0.612
27b	Pent-2-yloxy	F	0.51	0.419 - 0.619
27c	Pent-2-yloxy	CN	0.72	0.677 - 0.759
23b	But-2-yloxy	F	TBD	TBD

2.3.4. Drug toxicity

Examples of the compounds, namely **13**, **6d**, **23c**, and **27b**, were tested at 1 µM over 48 hours along with doxorubicin as positive control by bromodeoxyuridine (BrdU) proliferation assay, performed by Dr. Paul Foster of Birmingham University, to evaluate the toxicity against non-oestrogen dependent cells (MDA-MB-231). Statistics using one-way ANOVA followed by a Tukey's Multiple Comparison test comparing all compounds against control showed no significant difference between the tested compounds and the negative control indicating that the compounds had no impact on MDA-MB-231 growth (**Figure 2.36**). These results suggest possible limited off-target effects.
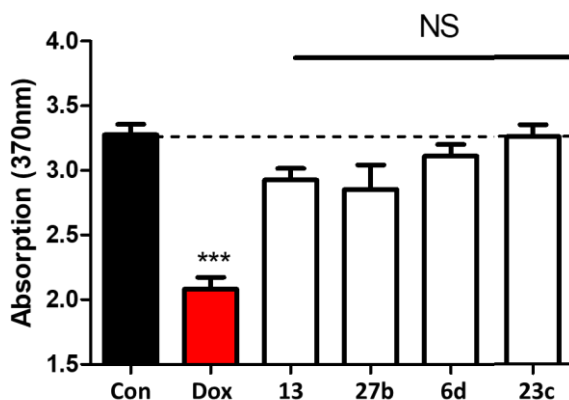
Figure (2.36): Toxicity of final compounds tested at 1 µM for 48 hours treatment followed by BrdU proliferation assay. Stats are one-way ANOVA followed by a Tukey's Multiple Comparison test comparing all compounds against control. Data represents n = 6 technical replicates ± SEM. *** p < 0.001 compared to control. NS – Non-significant compared to control.

2.4. Conclusion and future work

Studying the CYP19A1 crystal structure (PDB 3S79) (Ghosh *et al.* 2012) and the binding interactions of the natural substrate showed that hydrogen bonds for the 3- and 17-keto oxygen with Asp309 and Met374 respectively are key ligand interactions along with the other hydrophobic interactions of the ligand with the boundaries of the active site constituted by other residues including Arg115, Ile133, Phe134, Val370, Val373 and Leu477. Docking studies using MOE generated ligand-protein complexes that showed a good fit within the active site pocket. More interestingly, the long chain substitutions with but-2-ynyloxy or pent-2-ynyloxy groups on either the benzofuran or phenyl side were able to theoretically fit in the access channel of the active site, which is lined with Arg192, Val313 and Glu483. MD simulations for the generated complexes showed that generally the 6-position of the benzofuran ring was optimal for long chain substitution to target the access channel. Also, the *S*-enantiomer of the compounds showed better binding than the *R*-enantiomer in terms of binding to the haem through N4 of the triazole ring.

Synthetic pathways were developed for the designed compounds and modified when needed. Synthesis of class 1 compounds, with simple changing of the position of substitutions on the benzofuran side of the parent compound (**6a**) and also the nature of the secondary substitution on the phenyl ring, was found to be successful providing five final compounds (**6a-**

e). Synthesis of class 2 compounds with the hydroxy group on the benzofuran ring was very successful in all the steps in good yields, providing the required compounds (**11-14**). Class 3 only included one compound (**17**), which was prepared successfully with minor modifications in the work-up steps. Three subclasses of class 4 containing in total 12 compounds were successfully prepared through a one-step scheme starting from the compounds obtained from class 2 and 3, however the reaction required modification due to the formation of a di-substitution as in compound **27di** upon using NaH as base. Changing NaH to a milder base, K_2CO_3, proved to be optimal for this reaction avoiding the di-substitution and providing the required products.

In general, 22 final compounds were successfully prepared and fully characterised. The aromatase inhibitory activity of the tested compounds ranged from low nanomolar range to picomolar active compounds with the dual binding capacity e.g. 4-((6-(But-2-yn-1-yloxy)benzofuran-2-yl)(1*H*-1,2,4-triazol-1-yl)methyl)benzonitrile (**23c**). A clear SAR could be concluded from the biological results with the alkyl chain substituent on the 6-position of the benzofuran ring optimal for activity. The secondary substituent on the phenyl side showed comparable aromatase inhibitory activity for the nitrile and fluoro, which is better than the chloro analogues. For the length of the alkynyl chain, it was found that the butyne is the optimal length for dual binding compounds.

❖ **Future work:**

1- Representative examples of the compounds will be tested for selectivity (CYP panel e.g. 1A2, 2C9, 2C19, 2D6 and 3A4).

2- Aromatase inhibitors that 'pass' these assays will be subject to more detailed cell/molecular biology investigations to investigate the antiproliferative activity (using aromatase-transfected breast cancer cell line MCF7-AROM (Macaulay *et al.* 1994)).

3- Resistant Cell lines for known AIs based on MCF7-AROM will be developed and the compounds evaluated against these resistant cell lines to determine whether they are effective against the resistant cell lines of clinically used AIs.

4- Resistance for the synthesised compounds will be studied to identify the course and mechanism of resistance (if any).

2.5. Experimental

2.5.1. General considerations:

All reagents and solvents were of general purpose or analytical grade and purchased from Sigma-Aldrich, Alfa Aesar, VWR or Acros. Solvents were appropriately dried over molecular sieves (4 Å).

^{1}H and ^{13}C-NMR spectra were recorded on a Bruker Advance DP500 spectrometer operating at 500 MHz and 125 MHz, respectively. NMR solvents were chloroform-d (CDCl$_3$), DMSO-d6 ((CD$_3$)$_2$SO). Chemical shifts are given in parts per million (ppm) relative to the internal standard tetramethylsilane (Me$_4$Si). Coupling constants (*J*-value) were calculated in hertz (Hz). The following abbreviations were used in describing the splitting of the peaks in the ^{1}H NMR spectra as shown in the table:

Abbreviation	Meaning
s	Singlet
bs	Broad singlet
d	Doublet
t	Triplet
q	Quartet
dd	Doublet of doublet
m	Multiplet

All NMR characterisations were made by comparison with previous NMR spectra of the appropriate structure class and/or predictions from ChemDraw ™.

Melting points were determined using a Gallenkamp melting point apparatus and were uncorrected. HPLC/MS were either performed by Shaun Reeksting, Department of Pharmacy & Pharmacology, University of Bath, Bath, UK on a zobrax Eclipse plus C18 Rapid resolution 2.1 x 50 mm, 1.8 µm particle size using gradient (methanol: H$_2$O) with 0.1% formic acid (method A) or in house on a Shimadzu LC-2030C Plus C18 Rapid resolution 250 x 4.6mm, 5 µm particle size using isocratic 80:20 (methanol: H$_2$O) (method B). For column chromatography, a glass column was slurry packed in the appropriate eluent with silica gel (Fluka Kieselgel 60), flash column chromatography was performed with the aid of a bellow. Analytical thin layer

chromatography (TLC) was carried out on precoated silica plates (ALUGRAM® SIL G/UV254) with visualisation via UV light (254 nm).

2.5.2. Computational studies

Preparation of protein and ligands: The crystal structure of human placental aromatase cytochrome P450 (CYP19A1) refined at 2.75 Å (PDB 3S79) (Ghosh et al. 2012) was downloaded from the protein data bank (https://www.rcsb.org). Missing hydrogens were added, and the charge and geometry of the iron atom were adjusted to Fe^{3+} and d_2sp_3 respectively. The 3D structures of compounds were generated using MOE (Molecular Operating Environment (MOE), 2019.01) builder then energy minimised and saved in a dataset ready for docking studies.

MOE Docking: The docking process was performed with the amino acid sequence and haem chain selected as the receptor atoms and the active site was selected using the site finder tool in MOE. The resulting databases were inspected visually for 3D fitting and the distance between the iron of the haem and the nitrogen of the triazole ring were measured using MOE to make sure that only poses with distances of around ≤ 3 Å were considered as a viable result.

Molecular Dynamics: Using the pdb files containing the selected docking poses, the structures were optimised with protein preparation wizard (Sastry *et al.* 2013). The volume of space in which the simulation takes place, the global cell, is built up by regular 3D simulation boxes. The orthorhombic water box allowed for a 10 Å buffer region between protein atoms and box sides. Overlapping water molecules were deleted, and the systems were neutralised with Na+ ions and salt concentration 0.15 M. Molecular dynamics (150 ns simulations) were performed using OPLS_2005 forcefield at 300 K and constant pressure (1 bar) using Schrödinger Desmond programme (Bowers *et al.* 2006).

2.5.3. Chemistry:

2.5.3.1. **General procedure for the synthesis of benzofuran-2-yl(phenyl)methanone derivatives (3a-e)** (Mahboobi *et al.* 2007)
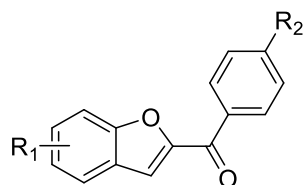
(3a-e)

a	R_1 = 6-OCH$_3$	R_2 = 4-Cl
b	R_1 = 5-OCH$_3$	R_2 = 4-Cl
c	R_1 = 6-Cl	R_2 = 4-OCH$_3$
d	R_1 = 6-OCH$_3$	R_2 = 4-F
e	R_1 = 6-OCH$_3$	R_2 = 4-CN

To a solution of salicylaldehyde derivatives (**1a,b,c**) (1 m.eq.) in dry CH$_3$CN (3 mL/mmol of salicylaldehyde) was added K$_2$CO$_3$ (2.2 m.eq.) and 2-bromo acetophenone derivatves (**2a-d**) (1 m.eq.). The reaction mixture was stirred at 70 ºC for 3 h. The solvent was then evaporated under reduced pressure and the residue dissolved in EtOAc (100 mL) and washed with H$_2$O (3 x 50 mL). The organic layer was dried (MgSO$_4$) and concentrated under reduced pressure to afford benzofuran-2-yl(phenyl)methanone derivatives (**3a-e**) as white to pale yellow solids.

2.5.3.1.1. **(4-Chlorophenyl)(6-methoxybenzofuran-2-yl)methanone (3a)**

Chemical formula: C$_{16}$H$_{11}$ClO$_3$, molecular Weight: 286.71

Prepared using 2-hydroxy-4-methoxybenzaldehyde (**1a**) (0.5 g, 3.28 mmol) and 2-bromo-4′-chloroacetophenone (**2a**) (0.77 g, 3.29 mmol) to provide the product as a white solid. Yield = 0.9 g (95%).

Melting Point: 184-186 ºC (lit. m.p. = 174-176 ºC) (Saberi *et al.* 2006).

TLC: Petroleum ether – EtOAc 3:1 v/v, R$_f$ = 0.5

^{1}H NMR (CDCl$_3$) δ: 7.92 (d, *J* = 8.6 Hz, 2H, Ar), 7.52 (d, *J* = 8.6 Hz, 1H, Ar), 7.44 (d, *J* = 8.6 Hz, 2H, Ar), 7.41 (d, *J* = 1.1 Hz, 1H, Ar), 7.03 (d, *J* = 2.3 Hz, 1H, Ar), 6.91 (dd, *J* = 2.2, 8.7 Hz, 1H, Ar), 3.82 (s, 3H, OCH$_3$).

^{13}C NMR (CDCl$_3$) δ: 182.45 (C), 161.41 (C), 157.73 (C), 151.70 (C), 139.10 (C), 135.76 (C), 130.78 (2 x CH), 128.84 (2 x CH), 123.71 (CH), 120.29 (C), 117.26 (CH), 114.74 (CH), 95.61 (CH), 55.78 (CH$_3$).

2.5.3.1.2. (4-Chlorophenyl)(5-methoxybenzofuran-2-yl)methanone (3b)
Chemical formula: C$_{16}$H$_{11}$ClO$_3$, molecular Weight: 286.71

Prepared using 2-hydroxy-5-methoxybenzaldehyde (**1b**) (0.41 mL, 3.29 mmol) and 2-bromo-4′-chloroacetophenone (**2a**) (0.77 g, 3.29 mmol) to provide the product as a pale yellow solid. Yield = 0.88 g (87%).

Melting Point: 141-143 ºC.

TLC: Petroleum ether – EtOAc 3:1 v/v, R$_f$ = 0.52

^{1}H NMR (DMSO-d_6) δ: 8.02 (d, *J* = 8.6 Hz, 2H, Ar), 7.73 (s, 1H, Ar), 7.69 (m, 3H, Ar), 7.31 (d, *J* = 2.6 Hz, 1H, Ar), 7.19 (dd, *J* = 2.7, 9.1 Hz, 1H, Ar), 3.82 (s, 3H, OCH$_3$).

^{13}C NMR (DMSO-d_6) δ: 182.61 (C), 156.77 (C), 152.40 (C), 150.98 (C), 138.45 (C), 135.89 (C), 131.55 (2 x CH), 129.33 (2 x CH), 127.88 (C), 119.15 (CH), 117.71 (CH), 113.56 (CH), 104.97 (CH), 56.12 (CH$_3$).

HPLC (method A): 97.78 % at R.T.= 4.74 min
HRMS (ESI): Calculated 287.0474 [M+H]$^+$, Found 287.0472 [M+H]$^+$.

2.5.3.1.3. (5-Chlorobenzofuran-2-yl)(4-methoxyphenyl)methanone (3c)
Chemical formula: C$_{16}$H$_{11}$ClO$_3$, molecular Weight: 286.71

Prepared using 5-chloro-2-hydroxybenzaldehyde (**1c**) (0.5 mL, 3.19 mmol) and 2-bromo-4′-methoxyacetophenone (**2b**) (0.73 g, 3.19 mmol) to provide the product as a pale yellow solid. Yield = 0.73 g (80%).

Melting Point: 140-142 ºC (lit. m.p. = 147-148 ºC) (Yoshizawa *et al.* 2003).

TLC: Petroleum ether – EtOAc 3:1 v/v, R$_f$ = 0.47

¹H NMR (CDCl₃) δ: 8.14 (d, *J* = 9.0 Hz, 2H, Ar), 7.72 (d, *J* = 2.2 Hz, 1H, Ar), 7.59 (d, *J* = 8.8 Hz ,1H, Ar), 7.48 (d, *J* = 0.9 Hz, 1H, Ar), 7.47 (dd, *J* = 2.1, 8.8 Hz, 1H, Ar), 7.06 (d, *J* = 9.0 Hz, 2H, Ar), 3.94 (s, 3H, OCH₃).

¹³C NMR (CDCl₃) δ: 182.49 (C), 163.83 (C), 154.08 (C), 153.90 (C), 132.05 (2 x CH), 129.53 (C), 129.51 (C), 128.31 (C), 128.29 (CH), 122.47 (CH), 114.46 (CH), 113.95 (2 x CH), 113.58 (CH), 55.59 (CH₃).

2.5.3.1.4. (4-Fluorophenyl)(6-methoxybenzofuran-2-yl)methanone (3d)

Chemical formula: C₁₆H₁₁FO₃, molecular Weight: 270.26

Prepared using 2-hydroxy-6-methoxybenzaldehyde (**1a**) (0.35 g, 2.3 mmol) and 2-bromo-4′-fluoroacetophenone (**2c**) (0.5 g, 2.3 mmol) to provide the product as a white solid. Yield = 0.6 g (96%).

Melting Point: 164-166 ℃ (lit. m.p. = 156-158 ℃) (Saberi *et al.* 2006).

TLC: Petroleum ether – EtOAc 3:1 v/v, R$_f$ = 0.57

¹H NMR (CDCl₃) δ: 8.09 (m, 2H, Ar), 7.75 (d, *J* = 0.9 Hz, 1H, Ar), 7.74 (d, *J* = 8.6 Hz, 1H, Ar), 7.44 (t, *J* = 8.8 Hz, 2H, Ar), 7.37 (d, *J* = 2.5 Hz, 1H, Ar) 7.04 (dd, *J* = 2.2, 8.7 Hz, 1H, Ar), 3.87 (s, 3H, OCH₃).

¹³C NMR (CDCl₃) δ: 181.85 (C), 166.24 (d, $^1J_{C,F}$ = 250 Hz, CF), 161.51 (C), 157.56 (C), 151.37 (C), 134.08 (d, $^4J_{C,F}$ = 2.5 Hz, C), 132.47 (d, $^3J_{C,F}$ = 10 Hz, 2 x CH), 124.71 (CH), 120.50 (C), 118.27 (CH), 116.33 (d, $^2J_{C,F}$ = 21.25 Hz, 2 x CH), 114.98 (CH), 96.23 (CH), 56.32 (CH₃).

2.5.3.1.5. 4-(6-Methoxybenzofuran-2-carbonyl)benzonitrile (3e)

Chemical formula: C₁₇H₁₁NO₃, molecular Weight: 277.28

Prepared using 2-hydroxy-6-methoxybenzaldehyde (**1a**) (0.5 g, 3.3 mmol) and 2-bromo-4′-cyanoacetophenone (**2d**) (0.74 g, 3.3 mmol) to provide the product as a white solid. Yield = 0.82 g (90%).

Melting Point: 192-194 ℃ (lit. m.p. =192-194 ℃) (Saberi *et al.* 2006)

TLC: Petroleum ether – EtOAc 3:1 v/v, R$_f$ = 0.47

¹H NMR (CDCl₃) δ: 8.11 (m, 4H, Ar), 7.78 (d, J = 0.8 Hz, 1H, Ar), 7.74 (d, J = 8.7 Hz, 1H, Ar), 7.38 (d, J = 1.7 Hz, 1H, Ar), 7.04 (dd, J = 2.2, 8.7 Hz, 1H, Ar), 3.87 (s, 3H, OCH₃).

2.5.3.2.   General procedure for the synthesis of benzofuran-2-yl(phenyl)methanol derivatives (4a-e) (Saberi *et al.* 2006)
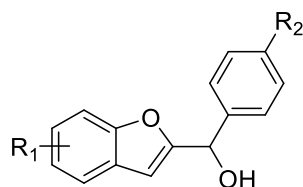
(4a-e)

a	R₁ = 6-OCH₃	R₂ = 4-Cl
b	R₁ = 5-OCH₃	R₂ = 4-Cl
c	R₁ = 6-Cl	R₂ = 4-OCH₃
d	R₁ = 6-OCH₃	R₂ = 4-F
e	R₁ = 6-OCH₃	R₂ = 4-CN

To a cooled solution of benzofuran-2-yl(phenyl)methanone derivatives (**3a-e**) (1 m.eq.) in dry dioxane (3 mL/mmol) at 0 ºC was added sodium borohydride (1.2 m.eq.). The reaction mixture was then stirred at r.t. for 2 h. The solvent was evaporated under reduced pressure, aq. HCl (1M, 10 mL) was added to the residue and extracted with Et₂O (2 x 50 mL). The combined organic layer was washed with H₂O (2 x 50 mL) then dried (MgSO₄) and concentrated under reduced pressure to afford benzofuran-2-yl(phenyl)methanol derivatives (**4a-e**) as colourless to yellow oils in quantitative yield. The products were used immediately in the next step without further purification.

2.5.3.2.1.   (4-Chlorophenyl)(6-methoxybenzofuran-2-yl)methanol (4a)

Chemical formula: C₁₆H₁₃ClO₃, molecular Weight: 288.73

Prepared using (4-chlorophenyl)(6-methoxybenzofuran-2-yl)methanone (**3a**) (0.9 g, 3.14 mmol) to provide a colourless oil.

TLC: Petroleum ether – EtOAc 3:1 v/v, R_f = 0.32

¹H NMR (CDCl₃) δ: 7.46 (d, J = 8.2 Hz, 2H, Ar), 7.40 (m, 3H, Ar), 7.00 (d, J = 2.3 Hz, 1H, Ar), 6.88 (dd, J = 2.3, 8.5 Hz, 1H, Ar), 6.45 (t, J = 0.8 Hz, 1H, Ar), 5.92 (s, 1H, CH), 3.85 (s, 3H, OCH₃), 2.56 (bs,1H, OH).

2.5.3.2.2.   (4-Chlorophenyl)(5-methoxybenzofuran-2-yl)methanol (4b)

Chemical formula: $C_{16}H_{13}ClO_3$, molecular Weight: 288.73

Prepared using (4-chlorophenyl)(5-methoxybenzofuran-2-yl)methanone (**3b**) (0.79 g, 2.75 mmol) to provide the product as a pale yellow oil.

TLC: Petroleum ether – EtOAc 3:1 v/v, $R_f = 0.32$

¹H NMR (CDCl₃) δ: 7.28 (m, 4H, Ar), 6.83 (d, $J = 2.7$ Hz, 1H, Ar), 6.75 (dd, $J = 2.6, 9.0$ Hz, 1H, Ar), 6.31 (s, 1H, Ar), 5.72 (s, 1H, CH), 3.69 (s, 3H, OCH₃), 3.12 (bs,1H, OH).

¹³C NMR (CDCl₃) δ: 158.75 (C), 156.05 (C), 150.10 (C), 138.71 (C), 134.16 (C), 128.77 (2 x CH), 128.44 (C), 128.16 (2 x CH), 113.21 (CH), 111.80 (CH), 104.36 (CH), 103.71 (CH), 70.00 (CH), 56.12 (CH₃).

2.5.3.2.3.   (5-Chlorobenzofuran-2-yl)(4-methoxyphenyl)methanol (4c)

Chemical formula: $C_{16}H_{13}ClO_3$, molecular Weight: 288.73

Prepared using (5-chlorobenzofuran-2-yl)(4-methoxyphenyl)methanone (**3c**) (0.5 g, 1.74 mmol) to provide the product as a yellow oil.

TLC: Petroleum ether – EtOAc 3:1 v/v, $R_f = 0.32$

¹H NMR (CDCl₃) δ: 7.40 (d, $J = 2.1$ Hz, 1H, Ar), 7.32 (d, $J = 8.4$ Hz, 2H, Ar), 7.27 (d, $J = 8.7$ Hz ,1H, Ar), 7.13 (dd, $J = 2.1, 8.7$ Hz, 1H, Ar), 6.85 (d, $J = 8.5$ Hz, 2H, Ar), 6.42 (s, 1H, Ar), 5.80 (s, 1H, CH), 3.74 (s, 3H, OCH₃), 2.41 (bs, 1H, OH).

2.5.3.2.4.   (4-Fluorophenyl)(6-methoxybenzofuran-2-yl)methanol (4d)

Chemical formula: $C_{16}H_{13}FO_3$, molecular Weight: 272.28

Prepared using (4-fluorophenyl)(6-methoxybenzofuran-2-yl)methanone (**3d**) (0.5 g, 1.85 mmol) to provide the product as a pale yellow oil which changed quickly into a brown sticky oil, which was used immediately without any further characterisation.

TLC: Petroleum ether – EtOAc 3:1 v/v, $R_f = 0.32$

2.5.3.2.5. 4-(Hydroxy(6-methoxybenzofuran-2-yl)methyl)benzonitrile (4e)

Chemical formula: $C_{17}H_{11}NO_3$, molecular Weight: 279.30

Prepared using 4-(6-methoxybenzofuran-2-carbonyl)benzonitrile (**3e**) (0.5 g, 1.8 mmol) to provide the product as a colourless oil.

TLC: Petroleum ether – EtOAc 3:1 v/v, R_f = 0.22

¹H NMR (CDCl₃) δ: 7.70 (d, J = 8.5 Hz, 2H, Ar), 7.64 (d, J = 8.1 Hz, 2H, Ar), 7.41 (d, J = 8.6 Hz ,1H, Ar), 6.98 (d, J = 2.04 Hz, 1H, Ar), 6.89 (dd, J = 2.3, 8.6 Hz, 1H, Ar), 6.49 (app. s, 1H, Ar), 5.99 (s, 1H, CH), 3.84 (s, 3H, OCH₃), 2.77 (bs, 1H, OH).

2.5.3.3. General procedure for synthesis of 1-(benzofuran-2-yl(phenyl)methyl)-1*H*-1,2,4-triazole (6a-e) (Saberi *et al.* 2006)
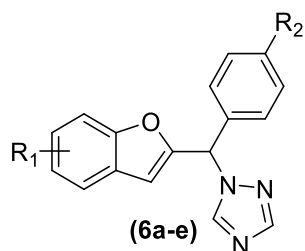
a	R₁ = 6-OCH₃	R₂ = 4-Cl
b	R₁ = 5-OCH₃	R₂ = 4-Cl
c	R₁ = 6-Cl	R₂ = 4-OCH₃
d	R₁ = 6-OCH₃	R₂ = 4-F
e	R₁ = 6-OCH₃	R₂ = 4-CN

To a cooled suspension of triazole (**5**) (4 m.eq.) in dry CH₃CN (3 mL/mmol of benzofuran-2-yl(phenyl)methanol (**4a-e**)) was added a solution of thionyl chloride (1.6 m.eq.) in dry CH₃CN (2 mL/mmol of **4a-e**). The mixture was stirred at 0 ºC for 1 h then K₂CO₃ (1 m.eq.) was added followed by a solution of benzofuran-2-yl(phenyl)methanol (**4a-e**) (1 m.eq.) in dry CH₃CN (3 mL/mmol of **4a-e**) and the reaction stirred at room temperature for 16 h. The reaction mixture was then filtered to remove any insoluble substances. The filtrate was diluted with EtOAc (100 mL) and washed with H₂O (3 x 50 mL). The organic layer was dried (MgSO₄) and concentrated under reduced pressure. The residue was purified by gradient column chromatography to give 1-(benzofuran-2-yl(phenyl)methyl)-1*H*-1,2,4-triazole (**6a-e**) at 60% EtOAc in petroleum ether (v/v) as a yellow oil.

2.5.3.3.1. 1-((4-Chlorophenyl)(6-methoxybenzofuran-2-yl)methyl)-1*H*-1,2,4-triazole (6a)

Chemical formula: $C_{18}H_{14}ClN_3O_2$, molecular Weight: 339.78

Prepared using (4-chlorophenyl)(6-methoxybenzofuran-2-yl)methanol (**4a**) (0.9 g, 3.14 mmol) to provide the product as a yellow oil. Yield = 0.6 g (56%).

TLC: Petroleum ether – EtOAc 3:1 v/v, R_f = 0.25

¹H NMR (CDCl₃) δ: 8.24 (s, 1H, CH-triazole), 7.99 (s, 1H, CH-triazole), 7.33 (m, 3H, Ar), 7.18 (m, 2H, Ar), 6.90 (d, *J* = 2.1 Hz, 1H, Ar), 6.82 (dd, *J* = 2.2, 8.5 Hz, 1H, Ar), 6.74 (s, 1H, Ar), 6.45 (t, *J* = 0.8 Hz, 1H, CH), 3.76 (s, 3H, OCH₃).

¹³C NMR (CDCl₃) δ: 158.84 (C), 156.52 (C), 151.75 (CH), 150.57 (C), 143.06 (CH), 135.26 (C), 134.20 (C), 129.33 (2 x CH), 129.97 (2 x CH), 121.74 (CH), 120.44 (C), 112.82 (CH), 108.21 (CH), 95.92 (CH), 61.71 (CH), 55.73 (CH₃).

HPLC (method B): 96.6% at R.T.= 6.35 min

2.5.3.3.2. 1-((4-Chlorophenyl)(5-methoxybenzofuran-2-yl)methyl)-1*H*-1,2,4-triazole (6b)

Chemical formula: $C_{18}H_{14}ClN_3O_2$, molecular Weight: 339.78

Prepared using (4-chlorophenyl)(5-methoxybenzofuran-2-yl)methanol (**4b**) (0.3 g, 1.04 mmol) to provide the product as a yellow oil. Yield = 0.26 g (63%).

TLC: Petroleum ether – EtOAc 2:1 v/v, R_f = 0.1

¹H NMR (CDCl₃) δ: 8.16 (s, 1H, CH-triazole), 8.05 (s, 1H, CH-triazole), 7.41 (d, *J* = 8.6 Hz, 2H, Ar), 7.37 (d, *J* = 8.9 Hz, 1H, Ar), 7.25 (d, *J* = 8.4 Hz, 2H, Ar), 7.01 (d, *J* = 2.6 Hz, 1H, Ar), 6.96 (dd, *J* = 2.6, 8.9 Hz, 1H, Ar), 6.81 (s, 1H, Ar), 6.55 (s, 1H, CH), 3.84 (s, 3H, OCH₃).

¹³C NMR (CDCl₃) δ: 156.38 (C), 152.66 (C), 152.36 (CH), 150.35 (C), 143.26 (CH), 135.25 (C), 134.22 (C), 129.33 (2 x CH), 129.02 (2 x CH), 127.92 (C), 114.33 (CH), 112.08 (CH), 108.14 (CH), 103.82 (CH), 61.57 (CH), 55.93 (CH₃).

HPLC (method A): 99.91 % at R.T.= 8.9 min

HRMS (ESI): Calculated 362.0672 [M+Na]$^+$, Found 362.0681 [M+Na]$^+$.

2.5.3.3.3. 1-((5-Chlorobenzofuran-2-yl)(4-methoxyphenyl)methyl)-1*H*-1,2,4-triazole (6c)

Chemical formula: $C_{18}H_{14}ClN_3O_2$, molecular Weight: 339.78

Prepared using (5-chlorobenzofuran-2-yl)(4-methoxyphenyl)methanol (**4c**) (0.5 g, 1.74 mmol) to provide the product as a yellow oil. Yield = 0.18 g (31%).

TLC: Petroleum ether – EtOAc 3:1 v/v, R$_f$ = 0.25

^{1}H NMR (CDCl₃) δ: 8.30 (s, 1H, CH-triazole), 8.01 (s, 1H, CH-triazole), 7.43 (d, *J* = 1.7 Hz, 1H, Ar), 7.30 (d, *J* = 8.6 Hz, 1H, Ar), 7.23 (d, *J* = 8.7 Hz, 2H, Ar), 7.20 (dd, obscured by CDCl₃, 1H, Ar), 6.88 (d, *J* = 8.7 Hz, 2H, Ar), 6.75 (s, 1H, Ar), 6.45 (s, 1H, CH), 3.75 (s, 3H, OCH₃).

^{13}C NMR (CDCl₃) δ: 160.47 (C), 154.29 (C), 153.66 (C), 151.06 (CH), 129.35 (2 x CH), 128.99 (C), 128.84 (C), 126.64 (C), 125.51 (CH), 121.08 (CH), 114.66 (2 x CH), 112.56 (CH), 107.08 (CH), 62.02 (CH), 56.35 (CH₃).

HPLC (method B): 97.8% at R.T.= 6.33 min

2.5.3.3.4. 1-((4-Fluorophenyl)(6-methoxybenzofuran-2-yl)methyl)-1*H*-1,2,4-triazole (6d)

Chemical formula: $C_{18}H_{14}FN_3O_2$, molecular Weight: 323.33

Prepared using (4-fluorophenyl)(6-methoxybenzofuran-2-yl)methanol (**4d**) (0.5 g, 1.84 mmol) to provide the product as a yellow oil. Yield = 0.37 g (62%).

TLC: Petroleum ether – EtOAc 3:1 v/v, R$_f$ = 0.42

^{1}H NMR (DMSO-*d₆*) δ: 8.71 (s, 1H, CH-triazole), 8.08 (s, 1H, CH-triazole), 7.53 (m, 2H, Ar), 7.49 (d, *J* = 8.5 Hz, 1H, Ar), 7.32 (s, 1H, Ar), 7.30 (t, *J* = 8.9 Hz, 2H, Ar), 7.19 (d, *J* = 2.1 Hz, 1H, Ar), 6.88 (dd, *J* = 2.2, 8.6 Hz, 1H, Ar), 6.56 (t, *J* = 1.1 Hz, 1H, CH), 3.77 (s, 3H, OCH₃).

^{13}C NMR (DMSO-*d₆*) δ: 163.56 (d, $^1J_{C,F}$ = 243.75 Hz, CF), 158.52 (C), 156.19 (C), 152.95 (C), 152.47 (CH), 144.68 (CH), 133.19 (d, $^4J_{C,F}$ = 2.5 Hz, C), 130.66 (d, $^3J_{C,F}$ = 7.5 Hz, 2 x CH), 122.18

(CH), 120.88 (C), 116.25 (d, $^2J_{C,F}$ = 22.5 Hz, 2 x CH), 112.72 (CH), 107.34 (CH), 96.44 (CH), 59.82 (CH), 56.05 (CH$_3$).

HPLC (method B): 100 % at R.T.= 5.22 min

2.5.3.3.5.   4-((6-Methoxybenzofuran-2-yl)(1*H*-1,2,4-triazol-1-yl)methyl)benzonitrile (6e)

Chemical formula: C$_{19}$H$_{14}$N$_4$O$_2$, molecular Weight: 330.35

Prepared using 4-(hydroxy(5-methoxybenzofuran-2-yl)methyl)benzonitrile (**4e**) (0.5 g, 1.8 mmol) to provide the product as yellow oil.

TLC: Petroleum ether – EtOAc 3:1 v/v, R$_f$ = 0.27

^{1}H NMR (CDCl$_3$) δ: 8.19 (s, 1H, CH-triazole), 8.06 (s, 1H, CH-triazole), 7.73 (d, *J* = 8.5 Hz, 2H, Ar), 7.44 (d, *J* = 8.5 Hz, 1H, Ar), 7.39 (d, *J* = 8.3 Hz, 2H, Ar), 7.00 (d, *J* = 2.1 Hz, 1H, Ar), 6.93 (dd, *J* = 2.2, 8.6 Hz, 1H, Ar), 6.87 (s, 1H, Ar), 6.58 (s, 1H, CH), 3.86 (s, 3H, OCH$_3$).

^{13}C NMR (CDCl$_3$) δ: 159.03 (C), 156.59 (C), 152.60 (CH), 149.61 (C), 143.40 (CH), 141.01 (C), 132.81 (2 x CH), 128.22 (2 x CH), 121.85 (CH), 120.26 (C), 118.08 (C), 113.03(C), 113.03 (CH), 108.62 (CH), 95.92 (CH), 61.57 (CH), 55.74 (CH$_3$).

HPLC (method B): 100 % at R.T.= 4.35 min.

2.5.3.4.   General procedure for the synthesis of 2-hydroxy-4/5-((tetrahydro-2*H*-pyran-2-yl)oxy)benzaldehyde (8a,b) (Saberi *et al.* 2006)
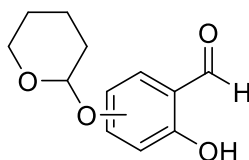
(8a,b)

8a	4-OPy
8b	5-OPy

To a solution of 2,4/5-dihydroxybenzaldehyde (**1d,e**) (1 m.eq.) in dry Et$_2$O (1 mL/mmol) was added 3,4-dihydro-2*H*-pyran (**7**) (1 m.eq.) and *p*-toluenesulfonic acid (0.1 m.eq.). The reaction was

stirred for 3 h at room temperature then quenched by 2 % aqueous KOH solution (50 mL). The ether layer was separated, washed with H_2O (2 x 50 mL), dried ($MgSO_4$) and concentrated under reduced pressure to provide the crude product. The residue was purified by gradient column chromatography to afford 2-hydroxy-4/5-((tetrahydro-2*H*-pyran-2-yl)oxy) benzaldehyde (**8a,b**) at 20% EtOAc in petroleum ether (v/v).

2.5.3.4.1. 2-Hydroxy-4-((tetrahydro-2*H*-pyran-2-yl)oxy)benzaldehyde

(8a) (Saberi *et al.* 2006)

Chemical Formula: $C_{12}H_{14}O_4$, molecular Weight: 222.24

Prepared using 2,4-dihydroxybenzaldehyde (**1d**) (5g, 36.20 mmol) to provide the product as a colourless oil. Yield = 4.15 g (51%).

TLC: Petroleum ether – EtOAc 3:1 v/v, R_f = 0.6

¹H NMR (CDCl₃) δ: 11.38 (s, 1H, OH), 9.74 (s, 1H, CHO), 7.46 (d, *J* = 8.6 Hz, 1H, Ar), 6.68 (dd, *J* = 2.3, 8.5 Hz, 1H, Ar), 6.64 (d, *J* = 2.3 Hz, 1H, Ar), 5.52 (t, *J* = 3.1 Hz, 1H, CH-pyran), 3.87 (m, 1H, CH_2-pyran), 3.67 (m, 1H, CH_2-pyran), 2.06 (m, 6H, 3 x CH_2-pyran).

2.5.3.4.2. 2-Hydroxy-5-((tetrahydro-2*H*-pyran-2-yl)oxy)benzaldehyde

(8b) (Schmidt *et al.* 2014)

Chemical Formula: $C_{12}H_{14}O_4$, molecular Weight: 222.24

Prepared using 2,5-dihydroxybenzaldehyde (**1e**) (1.24g, 9 mmol) to provide the product as yellow solid. Yield = 0.83 g (41%).

TLC: Petroleum ether – EtOAc 3:1 v/v, R_f = 0.57

Melting point: 72-76 ℃ (no lit. m.p.)

¹H NMR (CDCl₃) δ: 10.61 (s, 1H, CHO), 9.77 (d, *J* = 0.6 Hz, 1H, OH), 7.20 (m, 2H, Ar), 6.86 (m, 1H, Ar), 5.27 (t, *J* = 3.3 Hz, 1H, CH-pyran), 3.86 (m, 1H, CH_2-pyran), 3.57 (m, 1H, CH_2-pyran), 1.95 (m, 3H, CH_2-pyran), 1.66 (m, 3H, CH_2-pyran).

¹³C NMR (CDCl₃) δ: 196.31 (CHO), 156.65 (C), 150.08 (C), 127.37 (CH), 120.24 (C), 119.52 (CH), 118.45 (CH), 97.42 (CH-pyran), 62.05 (CH_2), 30.35 (CH_2), 25.15 (CH_2), 18.67 (CH_2).

HPLC (method B): 96.5 % at R.T.= 5.20 min.

2.5.3.5. Synthesis of phenyl(5/6-((tetrahydro-2*H*-pyran-2-yl)oxy)benzofuran-2-yl)methanone derivatives (9a-d) (Saberi *et al.* 2006)

(9a,b,c,d)
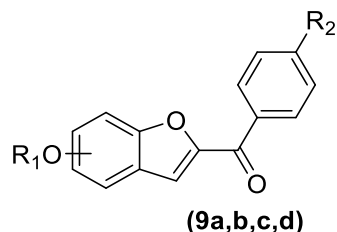
a	R_1 = 6-OPy	R_2 = 4-Cl
b	R_1 = 5-OPy	R_2 = 4-Cl
c	R_1 = 6-OPy	R_2 = 4-F
d	R_1 = 6-OPy	R_2 = 4-CN

2.5.3.5.1. (4-Chlorophenyl)(6-((tetrahydro-2*H*-pyran-2-yl)oxy)benzofuran-2-yl)methanone (9a) (Saberi *et al.* 2006)

Chemical Formula: $C_{20}H_{17}ClO_4$, molecular Weight: 356.80

Prepared as described for (**3a-e**) using 2-hydroxy-4-((tetrahydro-2*H*-pyran-2-yl)oxy) benzaldehyde (**8a**) (2 g, 9.00 mmol) and 2-bromo-4′-chloroacetophenone (**2a**) (2.10 g, 9.00 mmol). The formed solid was purified by recrystallisation from MeOH to afford (4-chlorophenyl)(6-((tetrahydro-2*H*-pyran-2-yl)oxy)benzofuran-2-yl)methanone (**9a**) as a white solid. Yield = 1.66 g (52%).

Melting Point: 174-177 °C (lit m.p. = 142-146 °C) (Saberi *et al.* 2006).

TLC: Petroleum ether – EtOAc 3:1 v/v, R_f = 0.57

¹H NMR (CDCl₃) δ: 8.03 (d, *J* = 8.7 Hz, 2H, Ar), 7.62 (d, *J* = 8.8 Hz, 1H, Ar), 7.53 (m, 3H, Ar), 7.36 (s,1H, Ar), 7.10 (dd, *J* = 2.1, 8.7 Hz, 1H, Ar), 5.52 (t, *J* = 3.1 Hz, 1H, CH-pyran), 3.95 (m, 1H, CH₂-pyran), 3.69 (m, 1H, CH₂-pyran), 2.08 (m, 6H, 3 x CH₂-pyran).

2.5.3.5.2. (4-Chlorophenyl)(5-((tetrahydro-2*H*-pyran-2-yl)oxy)benzofuran-2-yl)methanone (9b)

Chemical Formula: $C_{20}H_{17}ClO_4$, molecular Weight: 356.80

Prepared as described for (**3a-e**) using 2-hydroxy-5-((tetrahydro-2*H*-pyran-2-yl)oxy) benzaldehyde (**8b**) (0.67 g, 3.01 mmol) and 2-bromo-4′-chloroacetophenone (**2a**) (0.70 g, 3.01 mmol). The formed solid was purified by recrystallisation from EtOH to afford (4-chlorophenyl)(5-((tetrahydro-2*H*-pyran-2-yl)oxy)benzofuran-2-yl)methanone (**9b**) as a yellow solid. Yield = 0.83 g (77%).

Melting Point: 138-142 ºC.

TLC: Petroleum ether – EtOAc 3:1 v/v, R_f = 0.6

¹H NMR (CDCl₃) δ: 7.95 (d, *J* = 8.7 Hz, 2H, Ar), 7.46 (m, 3H, Ar), 7.41 (d, *J* = 0.7 Hz, 1H, Ar), 7.31 (d, *J* = 2.3 Hz, 1H, Ar), 7.17 (dd, *J* = 2.5, 9.0 Hz, 1H, Ar), 5.36 (t, *J* = 3.2 Hz, 1H, CH-pyran), 3.89 (m, 1H, CH₂-pyran), 3.58 (m, 1H, CH₂-pyran), 1.98 (m, 1H, CH₂-pyran), 1.84 (m, 2H, CH₂-pyran), 1.67 (m, 3H, CH₂-pyran).

¹³C NMR (CDCl₃) δ: 182.86 (C), 154.04 (C), 152.78 (C), 151.74 (C), 139.39 (C), 135.46 (C), 130.96 (2 x CH), 128.88 (2 x CH), 127.48 (C), 120.12 (CH), 116.65 (CH), 113.01 (CH), 108.50 (CH), 97.35 (CH), 62.14 (CH₂), 30.45 (CH₂), 25.20 (CH₂), 18.79 (CH₂).

2.5.3.5.3. (4-Fluorophenyl)(6-((tetrahydro-2*H*-pyran-2-yl)oxy)benzofuran-2-yl)methanone (9c)

Chemical Formula: $C_{20}H_{17}FO_4$, molecular Weight: 340.35

Prepared as described for (**3a-e**) using 2-hydroxy-4-((tetrahydro-2*H*-pyran-2-yl)oxy) benzaldehyde (**8a**) (2 g, 9.00 mmol) and 2-bromo-4′-chloroacetophenone (**2c**) (2.10 g, 9.00 mmol) to afford (4-fluorophenyl)(6-((tetrahydro-2*H*-pyran-2-yl)oxy)benzofuran-2-yl)methanone (**9c**) as a white solid. Yield = 0.64 g (95%).

Melting Point: 136-138 ºC

TLC: Petroleum ether – EtOAc 3:1 v/v, R_f = 0.6

¹H NMR (CDCl₃) δ: 8.09 (m, 2H, Ar), 7.76 (m, 2H, Ar), 7.45 (m, 3H, Ar), 7.12 (dd, J = 2.1, 8.7 Hz, 1H, Ar), 5.63 (t, J = 2.9 Hz, 1H, CH-pyran), 3.80 (m, 1H, CH₂-pyran), 3.62 (m, 1H, CH₂-pyran), 1.93 (m, 3H, CH₂-pyran), 1.67 (m, 3H, CH₂-pyran).

¹³C NMR (CDCl₃) δ: 181.95 (C), 166.27 (d, $^1J_{C,F}$ = 252.5 Hz, CF), 158.32 (C), 157.06 (C), 151.64 (C), 134.00 (C), 132.52 (d, $^3J_{C,F}$ = 10 Hz, 2 x CH), 124.70 (CH), 121.35 (C), 118.07 (CH), 116.35 (d, $^2J_{C,F}$ = 22.5 Hz, 2 x CH), 115.96 (CH), 99.48 (CH), 96.60 (CH), 62.14 (CH₂), 30.13 (CH₂), 25.07 (CH₂), 18.98 (CH₂).

HPLC (method B): 97.8 % at R.T.= 10.42 min.

2.5.3.5.4. 4-(6-((Tetrahydro-2*H*-pyran-2-yl)oxy)benzofuran-2-carbonyl)benzonitrile (9d) (Saberi *et al.* 2006)

Chemical Formula: C₂₁H₁₇NO₄, molecular Weight: 347.37

Prepared as described for (**3a-e**) using 2-hydroxy-4-((tetrahydro-2*H*-pyran-2-yl)oxy) benzaldehyde (**8a**) (0.99 g, 4.46 mmol) and 2-bromo-4′-chloroacetophenone (**2d**) (1 g, 4.46 mmol). The formed solid was purified by recrystallisation from EtOH to afford 4-(6-((tetrahydro-2H-pyran-2-yl)oxy)benzofuran-2-carbonyl)benzonitrile (**9d**) as a white solid. Yield = 1.1 g (70%).

Melting Point: 203-206 ºC (lit m.p. = 158-160 ºC) (Saberi *et al.* 2006).

TLC: Petroleum ether – EtOAc 3:1 v/v, R$_f$ = 0.38

¹H NMR (CDCl₃) δ: 8.05 (d, J = 8.6 Hz, 2H, Ar), 7.62 (d, J = 8.5 Hz, 1H, Ar), 7.53 (d, J = 8.6 Hz, 1H, Ar), 7.45 (d, J = 0.9 Hz, 1H, Ar), 7.18 (s, 1H, Ar), 7.02 (dd, J = 2.1, 8.6 Hz, 1H, Ar), 5.43 (t, J = 3.1 Hz, 1H, CH-pyran), 3.84 (m, 1H, CH₂-pyran), 3.59 (m, 1H, CH₂-pyran), 1.98 (m, 1H, CH₂-pyran), 1.85 (m, 2H, CH₂-pyran), 1.68 (m, 3H, CH₂-pyran).

2.5.3.6.   Synthesis of phenyl (6-((tetrahydro-2*H*-pyran-2-yl)oxy)benzofuran-2-yl)methanol (10a-d) (Saberi *et al.* 2006)
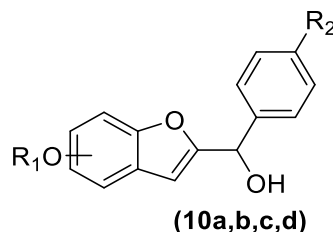
a	R$_1$ = 6-OPy	R$_2$ = 4-Cl
b	R$_1$ = 5-OPy	R$_2$ = 4-Cl
c	R$_1$ = 6-OPy	R$_2$ = 4-F
d	R$_1$ = 6-OPy	R$_2$ = 4-CN

2.5.3.6.1.   (4-Chlorophenyl)(6-((tetrahydro-2*H*-pyran-2-yl)oxy)benzofuran-2-yl)methanol (10a) (Saberi *et al.* 2006)

Chemical Formula: C$_{20}$H$_{19}$ClO$_4$, molecular Weight: 358.82

Prepared as described for (**4a-e**) using (4-chlorophenyl)(6-((tetrahydro-2*H*-pyran-2-yl)oxy)benzofuran-2-yl)methanone (**9a**) (0.88 g, 2.46 mmol) to afford (4-chlorophenyl)(6-((tetrahydro-2*H*-pyran-2-yl)oxy)benzofuran-2-yl)methanol (**10a**) as a colourless oil in quantitative yield.

TLC: Petroleum ether – EtOAc 3:1 v/v, R$_f$ = 0.35

^{1}H NMR (CDCl$_3$) δ: 7.45 (m, 5H, Ar), 7.21 (s, 1H, Ar), 6.98 (dd, *J* = 2.1, 8.5 Hz, 1H, Ar), 6.44 (d, *J* = 2.6 Hz, 1H, CH), 5.89 (s, 1H, CH), 5.41 (app. s, 1H, CH-pyran), 3.96 (m, 1H, CH$_2$-pyran), 3.64 (m, 1H, CH$_2$-pyran), 2.75 (bs, 1H, OH), 2.06 (m, 6H, 3 x CH$_2$-pyran).

2.5.3.6.2.   (4-Chlorophenyl)(5-((tetrahydro-2*H*-pyran-2-yl)oxy)benzofuran-2-yl)methanol (10b)

Chemical Formula: C$_{20}$H$_{19}$ClO$_4$, molecular Weight: 358.82

Prepared as described for (**4a-e**) using (4-chlorophenyl)(5-((tetrahydro-2*H*-pyran-2-yl)oxy)benzofuran-2-yl)methanone (**9b**) (0.72 g, 2.01 mmol) to afford (4-chlorophenyl)(5-((tetrahydro-2*H*-pyran-2-yl)oxy)benzofuran-2-yl)methanol (**10b**) as a yellow oil in quantitative yield.

TLC: Petroleum ether – EtOAc 3:1 v/v, R$_f$ = 0.35

¹H NMR (CDCl₃) δ: 7.33 (d, *J* = 8.3 Hz, 2H, Ar), 7.27 (d, *J* = 8.3 Hz, 2H, Ar), 7.23 (d, *J* = 9.0 Hz, 1H, Ar), 7.11 (d, *J* = 2.27 Hz, 1H, Ar), 6.91 (dd, *J* = 2.4, 8.9 Hz, 1H, Ar), 6.36 (s, 1H, CH), 5.79 (s, 1H, CH), 5.28 (t, *J* = 3.3 Hz, 1H, CH-pyran), 3.88 (m, 1H, CH₂-pyran), 3.53 (m, 1H, CH₂-pyran), 2.68 (bs, 1H, OH), 1.96 (m, 1H, CH₂-pyran), 1.80 (m, 2H, CH₂-pyran), 1.96 (m, 3H, CH₂-pyran).

2.5.3.6.3. (4-Fluorophenyl)(6-((tetrahydro-2*H*-pyran-2-yl)oxy)benzofuran-2-yl)methanol (10c)

Chemical Formula: C₂₀H₁₉FO₄, molecular Weight: 342.37

Prepared as described for (**4a-e**) using (4-chlorophenyl)(6-((tetrahydro-2*H*-pyran-2-yl)oxy)benzofuran-2-yl)methanone (**9c**) (0.6 g, 1.76 mmol) to afford (4-fluorophenyl)(6-((tetrahydro-2*H*-pyran-2-yl)oxy)benzofuran-2-yl)methanol (**10c**) as a yellow oil in quantitative yield.

TLC: Petroleum ether – EtOAc 3:1 v/v, R$_f$ = 0.4

¹H NMR (CDCl₃) δ: 7.40 (m, 2H, Ar), 7.30 (d, *J* = 8.5 Hz, 1H, Ar), 7.12 (d, *J* = 1.9 Hz, 1H, Ar), 7.01 (t, *J* = 8.7 Hz, 1H, Ar), 6.89 (dd, *J* = 2.1, 8.5 Hz, 1H, Ar), 6.35 (m, 1H, CH), 5.82 (s, 1H, CH), 5.32 (t, *J* = 3.3 Hz, 1H, CH-pyran), 3.87 (m, 1H, CH₂-pyran), 3.54 (m, 1H, CH₂-pyran), 2.46 (bs, 1H, OH), 1.97 (m, 1H, CH₂-pyran), 1.81 (m, 2H, CH₂-pyran), 1.65 (m, 3H, CH₂-pyran).

2.5.3.6.4. 4-(Hydroxy(6-((tetrahydro-2*H*-pyran-2-yl)oxy)benzofuran-2-yl)methyl)benzonitrile (10d) (Saberi *et al.* 2006)

Chemical Formula: C₂₁H₁₉NO₄, molecular Weight: 349.39

Prepared as described for (**4a-e**) using 4-(6-((tetrahydro-2*H*-pyran-2-yl)oxy)benzofuran-2-carbonyl)benzonitrile (**9d**) (0.88 g, 2.46 mmol) to afford 4-(hydroxy(6-((tetrahydro-2*H*-pyran-2-yl)oxy)benzofuran-2-yl)methyl)benzonitrile (**10d**) as a white foam in quantitative yield.

TLC: Petroleum ether – EtOAc 3:1 v/v, R$_f$ = 0.32

¹H NMR (CDCl₃) δ: 7.59 (d, *J* = 8.4 Hz, 2H, Ar), 7.53 (d, *J* = 8.1 Hz, 2H, Ar), 7.30 (d, *J* = 8.6 Hz, 1H, Ar), 7.10 (m, 1H, Ar), 6.89 (dd, *J* = 2.1, 8.4 Hz, 1H, Ar), 6.38 (s, 1H, CH, Ar), 5.88 (s, 1H, CH), 5.32 (t, *J* = 3.3 Hz, 1H, CH-pyran), 3.85 (m, 1H, CH₂-pyran), 3.54 (m, 1H, CH₂-pyran), 2.70 (bs, 1H, OH), 1.97 (m, 1H, CH₂-pyran), 1.81 (m, 2H, CH₂-pyran), 1.64 (m, 3H, CH₂-pyran).

2.5.3.7. Synthesis of phenyl(1*H*-1,2,4-triazol-1-yl)methyl)benzofuran-6-ol (11-14) (Saberi *et al.* 2006)
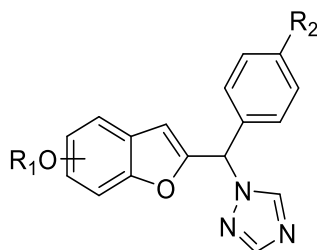
(11-14)

11	R₁ = 6-OH	R₂ = 4-Cl
12	R₁ = 5-OH	R₂ = 4-Cl
13	R₁ = 6-OH	R₂ = 4-F
14	R₁ = 6-OH	R₂ = 4-CN

2.5.3.7.1. 2-((4-Chlorophenyl)(1*H*-1,2,4-triazol-1-yl)methyl)benzofuran-6-ol (11) (Saberi *et al.* 2006)

Chemical Formula: $C_{17}H_{12}ClN_3O_2$, molecular Weight: 325.75

Prepared as described for (**6a-e**) using (4-chlorophenyl)(6-((tetrahydro-2*H*-pyran-2-yl)oxy)benzofuran-2-yl)methanol (**10a**) (0.88 g, 2.45 mmol). Purification by gradient column chromatography afforded 2-((4-chlorophenyl)(1*H*-1,2,4-triazol-1-yl)methyl)benzofuran-6-ol (**11**) at 90% EtOAc in petroleum ether (v/v) as a yellow waxy solid. Yield = 0.35 g (44%).

TLC: Petroleum ether – EtOAc 1:1 v/v, R_f = 0.25

¹H NMR (CDCl₃) δ: 8.11 (s, 1H, CH-triazole), 8.00 (s, 1H, CH-triazole), 7.81 (bs, 1H, OH), 7.32 (d, *J* = 8.6 Hz, 2H, Ar), 7.28 (d, *J* = 8.4 Hz, 1H, Ar), 7.14 (d, *J* = 8.5 Hz, 2H, Ar), 6.83 (d, *J* = 2.2 Hz, 1H, Ar), 6.76 (dd, *J* = 2.2, 8.4 Hz, 1H, Ar), 6.70 (s, 1H, Ar), 6.43 (s, 1H, CH).

¹³C NMR (CDCl₃) δ: 156.44 (C), 155.68 (C), 151.75 (CH), 149.98 (C), 143.07 (CH), 135.28 (C), 134.12 (C), 129.34 (2 x CH), 128.88 (2 x CH), 121.99 (CH), 120.06 (C), 113.36 (CH), 108.55 (CH), 98.20 (CH), 61.80 (CH).

HPLC (method B): 93.7 % at R.T.= 4.56 min.

2.5.3.7.2. 2-((4-Chlorophenyl)(1*H*-1,2,4-triazol-1-yl)methyl)benzofuran-5-ol (12)

Chemical Formula: $C_{17}H_{12}ClN_3O_2$, molecular Weight: 325.75

Prepared as described for (**6a-e**) using (4-chlorophenyl)(5-((tetrahydro-2*H*-pyran-2-yl)oxy)benzofuran-2-yl)methanol (**10b**) (0.71 g, 1.97 mmol). Purification by gradient column chromatography afforded 2-((4-chlorophenyl)(1*H*-1,2,4-triazol-1-yl)methyl)benzofuran-5-ol (**12**) at 70% EtOAc in petroleum ether (v/v) as a yellow sticky oil. Yield = 0.5 g (78%).

TLC: Petroleum ether – EtOAc 1:1 v/v, R_f = 0.2

¹H NMR (DMSO-*d₆*) δ: 9.22 (bs, 1H, OH), 8.72 (s, 1H, CH-triazole), 8.09 (s, 1H, CH-triazole), 7.52 (d, *J* = 8.6 Hz, 2H, Ar), 7.47 (d, *J* = 8.5 Hz, 2H, Ar), 7.33 (m, 2H, Ar), 6.92 (d, *J* = 2.46 Hz, 1H, Ar), 6.75 (dd, *J* = 2.5, 8.7 Hz, 1H, Ar), 6.51 (t, *J* = 0.95 Hz, 1H, CH).

¹³C NMR (DMSO-*d₆*) δ: 154.20 (C), 153.97 (C), 152.53 (CH), 149.23 (C), 144.82 (CH), 135.83 (C), 133.94 (C), 130.30 (2 x CH), 129.32 (2 x CH), 128.62 (C), 114.19 (CH), 111.94 (CH), 107.47 (CH), 106.32 (CH), 59.86 (CH).

HPLC (method B): 95.6 % at R.T.= 4.36 min.

2.5.3.7.3. 2-((4-Fluorophenyl)(1*H*-1,2,4-triazol-1-yl)methyl)benzofuran-6-ol (13) (Saberi *et al.* 2006)

Chemical Formula: $C_{17}H_{12}FN_3O_2$, molecular Weight: 309.30

Prepared as described for (**6a-e**) using (4-fluorophenyl)(6-((tetrahydro-2*H*-pyran-2-yl)oxy)benzofuran-2-yl)methanol (**10c**) (0.71 g, 1.97 mmol). Purification by gradient column chromatography afforded 2-((4-fluorophenyl)(1*H*-1,2,4-triazol-1-yl)methyl)benzofuran-6-ol (**13**) at 70% EtOAc in petroleum ether (v/v) as a yellow sticky wax. Yield = 0.46 g (86%).

TLC: Petroleum ether – EtOAc 1:1 v/v, R_f = 0.22

¹H NMR (DMSO-*d₆*) δ: 9.61 (bs, 1H, OH), 8.70 (s, 1H, CH-triazole), 8.08 (s, 1H, CH-triazole), 7.52 (m, 2H, Ar), 7.38 (d, *J* = 8.5 Hz, 1H, Ar), 7.29 (t, *J* = 8.9 Hz, 3H, Ar), 6.75 (d, *J* = 1.9 Hz, 1H, Ar), 6.75 (dd, *J* = 2.1, 8.4 Hz, 1H, Ar), 6.49 (t, *J* = 1.0 Hz, 1H, CH).

¹³C NMR (DMSO-d_6) δ: 161.42 (d, $^1J_{C,F}$ = 243.75 Hz, C), 154.34 (C), 154.18 (C), 150.32 (CH), 150.08 (C), 142.53 (CH), 131.17 (d, $^4J_{C,F}$ = 3.75 Hz, C), 128.49 (d, $^3J_{C,F}$ = 8.75 Hz, 2 x CH), 120.01 (CH), 117.60 (C), 114.10 (d, $^2J_{C,F}$ = 21.25 Hz, 2 x CH), 110.90 (CH), 105.35 (CH), 95.91 (CH), 57.77 (CH).

HPLC (method B): 98.3 % at R.T.= 4.04 min.

2.5.3.7.4.   4-((6-Hydroxybenzofuran-2-yl)(1*H*-1,2,4-triazol-1-yl)methyl) benzonitrile (14) (Saberi *et al.* 2006)

Chemical Formula: $C_{18}H_{12}N_4O_2$, molecular Weight: 316.32

Prepared as described for (**6a-e**) using 4-(hydroxy(6-((tetrahydro-2*H*-pyran-2-yl)oxy)benzofuran-2-yl)methyl)benzonitrile (**10d**) (0.85 g, 2.43 mmol). Purification by gradient column chromatography afforded 4-((6-hydroxybenzofuran-2-yl)(1*H*-1,2,4-triazol-1-yl)methyl)benzonitrile (**14**) at 80% EtOAc in petroleum ether (v/v) as a yellow solid. Yield = 0.6 g (78%).

TLC: Petroleum ether – EtOAc 1:1 v/v, R_f = 0.2

Melting point: 80-84 ºC

¹H NMR (CDCl₃) δ: 8.25 (s, 1H, CH-triazole), 8.12 (s, 1H, CH-triazole), 7.96 (bs, 1H, OH), 7.73 (d, *J* = 8.5 Hz, 2H, Ar), 7.40 (m, 3H, Ar), 6.93 (d, *J* = 1.9 Hz, 1H, Ar), 6.88 (s, 1H, Ar), 6.87 (dd, *J* = 2.1, 8.5 Hz, 1H, Ar), 6.56 (s, 1H, CH).

¹³C NMR (CDCl₃) δ: 156.53 (C), 155.94 (C), 151.98 (CH), 148.84 (C), 143.27 (CH), 140.70 (C), 132.86 (2 x CH), 128.20 (2 x CH), 122.16 (CH), 119.86 (C), 118.02 (C), 113.62 (CH), 113.20 (C), 109.08 (CH), 98.20 (CH), 61.83 (CH).

HPLC (method B): 96.6 % at R.T.= 3.66 min.

2.5.3.8.   (5-Chlorobenzofuran-2-yl)(4-hydroxyphenyl)methanone (3f)

Chemical Formula: $C_{15}H_9ClO_3$, molecular Weight: 272.68

(3f)
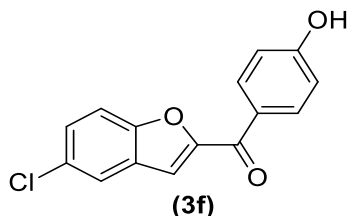
To a solution of (5-chlorobenzofuran-2-yl)(4-methoxyphenyl)methanone (**3c**) (0.23 g, 0.8 mmol) in acetic acid (7 mL) was added HBr (48% w/w aq. solution, 14 mL). The reaction mixture was stirred at 110 °C for 16 h. The solvent was evaporated under reduced pressure to about half the original volume. The residue was diluted with H_2O (30 mL) and extracted with EtOAc (2 x 100 mL). The organic layer was washed with sat. aq. $NaHCO_3$ (3 x 75 mL), dried ($MgSO_4$) and concentrated under reduced pressure and purified by gradient column chromatography to afford (5-chlorobenzofuran-2-yl)(4-hydroxyphenyl)methanone (**3f**) at 40% EtOAc in petroleum ether (v/v) as a white solid. Yield = 0.12 g (57%).

TLC: Petroleum ether – EtOAc 3:1 v/v, R_f = 0.25

Melting point: 198-200 °C

^{1}H NMR (DMSO-*d_6*) δ: 10.57 (bs, 1H, OH), 7.98 (d, *J* = 8.8 Hz, 2H, Ar), 7.92 (d, *J* = 2.1 Hz, 1H, Ar), 7.82 (d, *J* = 8.8 Hz, 1H, Ar), 7.70 (d, *J* = 0.9 Hz, 1H, Ar), 7.58 (dd, *J* = 2.3, 8.8 Hz, 1H, Ar), 6.96 (d, *J* = 8.8 Hz, 1H, Ar).

^{13}C NMR (DMSO-*d_6*) δ: 181.91 (C), 163.06 (C), 153.95 (C), 153.60 (C), 132.57 (2 x CH), 128.90 (C), 128.74 (C), 128.52 (CH), 127.93 (C), 123.23 (CH), 116.01 (2 x CH), 115.23 (CH), 114.46 (CH).

HPLC (method B): 100 % at R.T.= 6.10 min.

2.5.3.9. (5-Chlorobenzofuran-2-yl)(4-((tetrahydro-2*H*-pyran-2-yl)oxy)phenyl) methanone (15)

Chemical Formula: $C_{20}H_{17}ClO_4$, Molecular Weight: 356.80

(15)
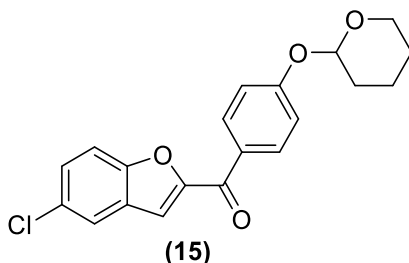
Prepared as described for preparation of (**8a,b**) using (5-chlorobenzofuran-2-yl)(4-hydroxyphenyl)methanone (**3f**) (0.5 g, 1.83 mmol) to provide the crude product. The residue was purified by gradient column chromatography to afford (5-chlorobenzofuran-2-yl)(4-((tetrahydro-2*H*-pyran-2-yl)oxy)phenyl)methanone (**15**) at 30% EtOAc in petroleum ether (v/v) as a white solid. Yield = 0.48 (73%).

Melting Point: 102-107 ℃

TLC: Petroleum ether – EtOAc 3:1 v/v, R_f = 0.65

¹H NMR (CDCl₃) δ: 8.04 (d, *J* = 8.9 Hz, 2H, Ar), 7.93 (d, *J* = 1.8 Hz, 1H, Ar), 7.84 (d, *J* = 8.8 Hz, 1H, Ar), 7.74(d, *J* = 0.92 Hz, 1H, Ar), 7.6 (dd, *J* = 2.3, 8.8 Hz, 1H, Ar), 7.23 (d, *J* = 8.9 Hz, 2H, Ar), 5.68 (t, *J* = 3.0 Hz, 1H, CH-pyran), 4.84 (m, 1H, CH₂-pyran), 3.75 (m, 2H, CH₂-pyran), 3.63 (m, 1H, CH₂-pyran), 3.45 (m, 1H, CH₂-pyran), 1.92 (m, 3H, CH₂-pyran).

¹³C NMR (CDCl₃) δ: 182.25 (C), 161.18 (C), 154.06 (C), 153.36 (C), 132.05 (2 x CH), 130.11 (C), 128.89 (C), 128.81 (C), 128.74 (CH), 123.35 (CH), 116.70 (2 x CH), 115.82 (CH), 114.52 (CH), 93.71 (CH), 62.12 (CH₂), 30.59 (CH₂), 25.47 (CH₂), 19.60 (CH₂).

HPLC (method A): 100 % at R.T.= 5.04 min.

HRMS (ESI): Calculated 379.0713 [M+Na]⁺, Found 379.0708 [M+Na]⁺.

2.5.3.10.   (5-Chlorobenzofuran-2-yl)(4-((tetrahydro-2*H*-pyran-2-yl)oxy)phenyl)methanol (16)

Chemical Formula: $C_{20}H_{17}ClO_4$, Molecular Weight: 356.80
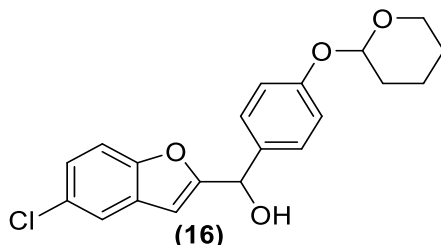
Prepared as described for (**4a-e**) using (5-chlorobenzofuran-2-yl)(4-((tetrahydro-2*H*-pyran-2-yl)oxy)phenyl)methanone (**15**) (0.47 g, 1.32 mmol) to afford (5-chlorobenzofuran-2-yl)(4-((tetrahydro-2*H*-pyran-2-yl)oxy)phenyl)methanol (**16**) as a pale yellow oil in quantitative yield.

TLC: Petroleum ether – EtOAc 3:1 v/v, R_f = 0.34

^{1}H NMR (CDCl$_3$) δ: 7.36 (d, *J* = 2.2 Hz, 1H, Ar), 7.27 (d, *J* = 8.6 Hz, 2H, Ar), 7.23 (d, *J* = 8.7 Hz, 1H, Ar), 7.1 (dd, *J* = 2.2, 8.8 Hz, 1H, Ar), 6.97 (d, *J* = 8.7 Hz, 2H, Ar), 6.38 (s, 1H, Ar), 5.74 (s, 1H, CH), 5.32 (m, 1H, CH-pyran), 3.82 (m, 1H, CH$_2$-pyran), 3.51 (m, 1H, CH$_2$-pyran), 2.97 (bs, 1H, OH), 1.94 (m, 1H, CH$_2$-pyran), 1.77 (m, 2H, CH$_2$-pyran), 1.58 (m, 3H, CH$_2$-pyran).

2.5.3.11.   4-((5-Chlorobenzofuran-2-yl)(1*H*-1,2,4-triazol-1-yl)methyl)phenol (17)

Chemical Formula: $C_{17}H_{12}ClN_3O_2$, molecular Weight: 325.75
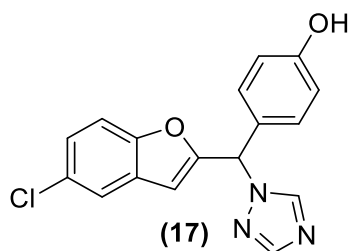
Prepared as described for (**6a-e**) using (5-chlorobenzofuran-2-yl)(4-((tetrahydro-2*H*-pyran-2-yl)oxy)phenyl)methanol (**16**) (0.47 g, 1.31 mmol) to afford 4-((5-chlorobenzofuran-2-yl)(1*H*-1,2,4-triazol-1-yl)methyl)phenol (**17**) as a white solid. Yield = 0.19 g (45%).

Melting Point: 240-242 ºC

TLC: Petroleum ether – EtOAc 1:1 v/v, R_f = 0.17

¹H NMR (DMSO-d_6) δ: 9.69 (bs, 1H, OH), 8.68 (s, 1H, CH-triazole), 8.06 (s, 1H, CH-triazole), 7.71 (d, *J* = 2.1 Hz, 1H, Ar), 7.59 (d, *J* = 8.7 Hz, 1H, Ar), 7.34 (dd, *J* = 2.2, 8.7 Hz, 1H, Ar), 7.31 (d, *J* = 8.6 Hz, 2H, Ar), 7.20 (s, 1H, Ar), 6.81 (d, *J* = 8.6 Hz, 1H, Ar), 6.61 (t, *J* = 1.0 Hz, 1H, CH).

¹³C NMR (DMSO-d_6) δ: 158.36 (C), 156.80 (C), 153.49 (C), 152.37 (CH), 144.55 (CH), 129.91 (2 x CH), 129.67 (C), 127.96 (C), 126.68 (C), 125.21 (CH), 121.46 (CH), 115.97 (2 x CH), 113.31 (CH), 106.75 (CH), 60.15 (CH).

HPLC (method B): 100 % at R.T.= 4.69 min.

2.5.3.12. 1-((4-Chlorophenyl)(6-ethoxybenzofuran-2-yl)methyl)-1*H*-1,2,4-triazole (19a)

Chemical Formula: $C_{19}H_{16}ClN_3O_2$, molecular Weight: 353.81

(19a)
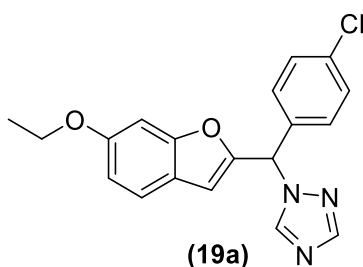
To a solution of 2-((4-chlorophenyl)(1*H*-1,2,4-triazol-1-yl)methyl)benzofuran-6-ol (**11**) (0.2 g, 0.61 mmol) in dry CH_3CN (8 mL), K_2CO_3 (0.1 g, 0.73 mmol) was added and the mixture stirred for 1 h at 40 ºC then ethylbromide (**18**) (0.25 mL, 3.4 mmol) was added and the reaction mixture stirred at room temperature for 16 h. The reaction mixture was concentrated under reduced pressure and the residue dissolved in EtOAc (100 mL). The organic layer was washed with H_2O (3 x 50 mL), dried ($MgSO_4$) and concentrated under reduced pressure. Purification by gradient column chromatography afforded 1-((4-chlorophenyl)(6-ethoxybenzofuran-2-yl)methyl)-1*H*-1,2,4-triazole (**19a**) at 60% EtOAc in petroleum ether (v/v) as a yellow oil. Yield = 0.147 g (67%).

TLC: Petroleum ether – EtOAc 1:1 v/v, R_f = 0.4

¹H NMR (CDCl₃) δ: 8.05 (s, 1H, CH-triazole), 7.94 (s, 1H, CH-triazole), 7.32 (m, 3H, Ar), 7.14 (d, *J* = 8.2 Hz, 2H, Ar), 6.89 (d, *J* = 2.1 Hz, 1H, Ar), 6.81 (dd, *J* = 2.2, 8.6 Hz, 1H, Ar), 6.70 (s, 1H, Ar), 6.42 (t, *J* = 0.9 Hz, 1H, CH), 3.99 (q, *J* = 6.9 Hz, 2H, CH₂), 1.37 (t, *J* = 6.9 Hz, 3H, CH₃).

¹³C NMR (CDCl₃) δ: 158.10 (C), 156.50 (C), 152.35 (CH), 150.68 (C), 143.22 (CH), 135.15 (C), 134.41 (C), 129.28 (2 x CH), 128.92 (2 x CH), 121.67 (CH), 120.36 (C), 113.24 (CH), 108.12 (CH), 96.56 (CH), 64.02 (CH₂), 61.57 (CH), 14.77 (CH₃).

HPLC (method B): 100 % at R.T.= 7.56 min.

2.5.3.13. 1-((4-Chlorophenyl)(6-(prop-2-yn-1-yloxy)benzofuran-2-yl)methyl)-1*H*-1,2,4-triazole (21a)

Chemical Formula: C₂₀H₁₄ClN₃O₂, molecular Weight: 363.80
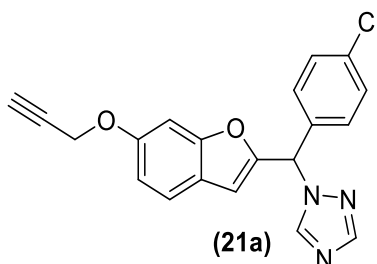
Prepared as described for 1-((4-chlorophenyl)(6-ethoxybenzofuran-2-yl)methyl)-1*H*-1,2,4-triazole (**19a**) using 2-((4-chlorophenyl)(1*H*-1,2,4-triazol-1-yl)methyl)benzofuran-6-ol (**11**) (0.2 g, 0.61 mmol) and propargyl bromide (80 wt % in toluene) (**20**) (0.2 mL, 1.84 mmol) to afford 1-((4-chlorophenyl)(6-(prop-2-yn-1-yloxy)benzofuran-2-yl)methyl)-1*H*-1,2,4-triazole (**21a**) as a yellow oil. Yield = 0.2 g (90%).

TLC: Petroleum ether – EtOAc 1:1 v/v, R$_f$ = 0.37

¹H NMR (CDCl₃) δ: 8.06 (s, 1H, CH-triazole), 7.95 (s, 1H, CH-triazole), 7.36 (d, *J* = 8.6 Hz, 1H, Ar), 7.32 (d, *J* = 8.5 Hz, 2H, Ar), 7.15 (d, *J* = 8.4 Hz, 2H, Ar), 7.02 (d, *J* = 2.1 Hz, 1H, Ar), 6.88 (dd, *J* = 2.3, 8.5 Hz, 1H, Ar), 6.71 (s, 1H, Ar), 6.45 (t, *J* = 0.9 Hz, 1H, CH), 4.65 (d, *J* = 2.4 Hz, 2H, CH₂), 2.47 (t, *J* = 2.4 Hz, 1H, CH).

^{13}C NMR (CDCl$_3$) δ: 156.55 (C), 156.15 (C), 152.39 (CH), 151.29 (C), 143.23 (CH), 135.23 (C), 134.27 (C), 129.32 (2 x CH), 128.95 (2 x CH), 121.83 (CH), 121.36 (C), 113.35 (CH), 108.02 (CH), 97.52 (CH), 78.24 (C), 75.93 (CH), 61.53 (CH), 56.41 (CH$_2$).

HPLC (method B): 100 % at R.T.= 5.78 min.

2.5.3.14. 1-((6-(But-2-yn-1-yloxy)benzofuran-2-yl)(4-chlorophenyl)methyl)-1*H*-1,2,4-triazole (23a)

Chemical Formula: C$_{21}$H$_{16}$ClN$_3$O$_2$, molecular Weight: 377.83
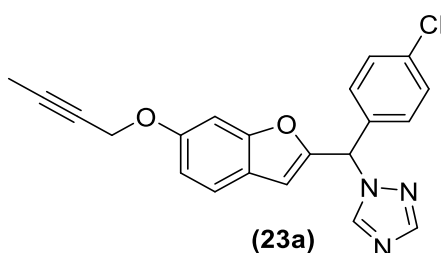
(23a)

Prepared as described for 1-((4-chlorophenyl)(6-ethoxybenzofuran-2-yl)methyl)-1*H*-1,2,4-triazole (**19a**) using 2-((4-chlorophenyl)(1*H*-1,2,4-triazol-1-yl)methyl)benzofuran-6-ol (**11**) (0.22 g, 0.67 mmol) and 1-bromobut-2-yne (**22**) (0.12 mL, 1.35 mmol) to afford 1-((6-(but-2-yn-1-yloxy)benzofuran-2-yl)(4-chlorophenyl)methyl)-1*H*-1,2,4-triazole (**23a**) as a yellow oil. Yield = 0.19 g (76%).

TLC: Petroleum ether – EtOAc 1:1 v/v, R$_f$ = 0.3

^{1}H NMR (CDCl$_3$) δ: 8.15 (s, 1H, CH-triazole), 8.05 (s, 1H, CH-triazole), 7.44 (d, *J* = 8.6 Hz, 1H, Ar), 7.41 (d, *J* = 8.5 Hz, 2H, Ar), 7.25 (d, *J* = 8.2 Hz, 2H, Ar), 7.10 (d, *J* = 2.1 Hz, 1H, Ar), 6.96 (dd, *J* = 2.2, 8.6 Hz, 1H, Ar), 6.81 (s, 1H, Ar), 6.54 (t, *J* = 0.8 Hz, 1H, CH), 4.70 (q, *J* = 2.2 Hz, 2H, CH$_2$), 1.89 (t, *J* = 2.3 Hz, 3H, CH$_3$).

^{13}C NMR (CDCl$_3$) δ: 156.91 (C), 156.25 (C), 152.38 (CH), 151.05 (C), 143.26 (CH), 135.20 (C), 134.33 (C), 129.31 (2 x CH), 128.94 (2 x CH), 121.72 (CH), 121.01 (C), 113.39 (CH), 108.08 (CH), 97.29 (CH), 84.17 (C), 73.71 (C), 61.56 (CH), 57.01 (CH$_2$), 3.74 (CH$_3$).

HPLC (method B): 100 % at R.T.= 7.35 min.

2.5.3.15. 4-((6-(But-2-yn-1-yloxy)benzofuran-2-yl)(1*H*-1,2,4-triazol-1-yl)methyl) benzonitrile (23c)

Chemical Formula: $C_{22}H_{16}N_4O_2$, Molecular Weight: 368.40
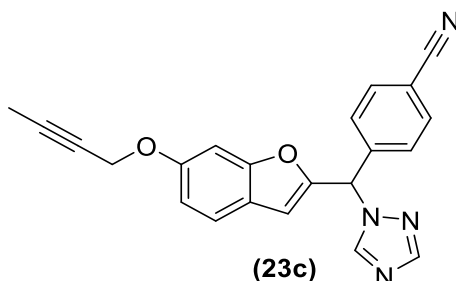
(23c)

Prepared as described for 1-((4-chlorophenyl)(6-ethoxybenzofuran-2-yl)methyl)-1*H*-1,2,4-triazole (**19a**) using 4-((6-hydroxybenzofuran-2-yl)(1*H*-1,2,4-triazol-1-yl)methyl)benzonitrile (**14**) (0.2 g, 0.63 mmol) and 1-bromobut-2-yne (**22**) (0.11 mL g, 1.26 mmol). Gradient column chromatography afforded 4-((6-(but-2-yn-1-yloxy)benzofuran-2-yl)(1*H*-1,2,4-triazol-1-yl)methyl)benzonitrile (**23c**) at 70% EtOAc further purified by preparative TLC to afford the product as a yellow oil. Yield = 0.017 g (7%).

TLC: Petroleum ether – EtOAc 1:1 v/v, R_f = 0.27

¹H NMR (CDCl₃) δ: 8.11 (s, 1H, CH-triazole), 7.98 (s, 1H, CH-triazole), 7.64 (d, *J* = 8.5 Hz, 2H, Ar), 7.36 (d, *J* = 8.6 Hz, 1H, Ar), 7.30 (d, *J* = 8.2 Hz, 2H, Ar), 7.02 (d, *J* = 2.2 Hz, 1H, Ar), 6.89 (dd, *J* = 2.3, 8.6 Hz, 1H, Ar), 6.78 (s, 1H, Ar), 6.49 (s, 1H, CH), 4.62 (q, *J* = 2.3 Hz, 2H, CH₂), 1.80 (t, *J* = 2.3 Hz, 3H, CH₃).

¹³C NMR (CDCl₃) δ: 176.61 (C), 157.13 (C), 156.33 (C), 149.85 (C), 140.94 (C), 132.82 (2 x CH), 128.23 (2 x CH), 121.86 (CH), 120.66 (C), 118.06 (C), 113.62 (CH), 113.15 (C), 108.62 (CH), 97.28 (CH), 84.27 (C), 73.57 (C), 61.60 (CH), 57.01 (CH₂), 3.74 (CH₃).

HPLC (method A): 98.58 % at R.T.= 4.60 min.

HRMS (ESI): Calculated 391.1170 [M+Na]⁺, Found 391.1159 [M+Na]⁺.

2.5.3.16. Synthesis of 1-((6-(pent-2-yn-1-yloxy)benzofuran-2-yl)(phenyl)methyl)-1*H*-1,2,4-triazole derivatives (27a, b, c)

(27)

a	R₂ = 4-Cl
b	R₂ = 4-F
c	R₂ = 4-CN
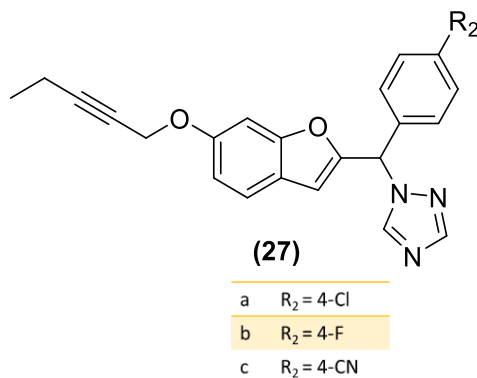
2.5.3.16.1.1. 1-((4-Chlorophenyl)(6-(pent-2-yn-1-yloxy)benzofuran-2-yl)methyl)-1*H*-1,2,4-triazole (27a)

Chemical Formula: $C_{22}H_{18}ClN_3O_2$, Molecular Weight: 391.86

Prepared as described for 1-((4-chlorophenyl)(6-ethoxybenzofuran-2-yl)methyl)-1*H*-1,2,4-triazole (**19a**) using 2-((4-chlorophenyl)(1*H*-1,2,4-triazol-1-yl)methyl)benzofuran-6-ol (**11**) (0.2 g, 0.61 mmol) and 1-bromopent-2-yne (**26**) (0.07 mL g, 0.67 mmol) to afford 1-((4-chlorophenyl)(6-(pent-2-yn-1-yloxy)benzofuran-2-yl)methyl)-1*H*-1,2,4-triazole (**27a**) as a yellow oil. Yield = 0.18 g (75%).

TLC: Petroleum ether – EtOAc 1:1 v/v, R_f = 0.55

¹H NMR (CDCl₃) δ: 8.24 (s, 1H, CH-triazole), 7.98 (s, 1H, CH-triazole), 7.34 (m, 3H, Ar), 7.17 (d, J = 8.4 Hz, 2H, Ar), 7.00 (d, J = 2.0 Hz, 1H, Ar), 6.87 (dd, J = 2.1, 8.5 Hz, 1H, Ar), 6.75 (s, 1H, Ar), 6.45 (s, 1H, CH), 4.62 (t, J = 2.1 Hz, 2H, CH₂), 2.16 (qt, J = 2.1, 7.5 Hz, 2H, CH₂), 1.07 (t, J = 7.5 Hz, 3H, CH₃).

¹³C NMR (CDCl₃) δ: 156.98 (C), 156.26 (C), 151.81 (CH), 150.87 (C), 143.19 (CH), 135.27 (C), 134.17 (C), 129.33 (2 x CH), 128.08 (2 x CH), 121.50 (CH), 120.98 (C), 113.44 (CH), 108.20 (CH), 97.37 (CH), 89.98 (C), 73.87 (C), 61.70 (CH), 57.11 (CH₂), 13.59 (CH₃), 12.51 (CH₂).

HPLC (method A): 94.47 % at R.T.= 4.79 min.

HRMS (ESI): Calculated 392.1165 [M+H]⁺, Found 392.1055 [M+H]⁺.

2.5.3.16.1.2. 1-((4-Fluorophenyl)(6-(pent-2-yn-1-yloxy)benzofuran-2-yl)methyl)-1*H*-1,2,4-triazole (27b)

Chemical Formula: $C_{22}H_{18}FN_3O_2$, molecular Weight: 375.40

Prepared as described for 1-((4-chlorophenyl)(6-ethoxybenzofuran-2-yl)methyl)-1*H*-1,2,4-triazole (**19a**) using 2-((4-fluorophenyl)(1*H*-1,2,4-triazol-1-yl)methyl)benzofuran-6-ol (**13**) (0.2 g, 0.64 mmol) and 1-bromopent-2-yne (**26**) (0.13 mL g, 1.29 mmol) to afford 1-((4-fluorophenyl)(6-(pent-2-yn-1-yloxy)benzofuran-2-yl)methyl)-1*H*-1,2,4-triazole (**27b**) as a yellow oil. Yield = 0.12 g (50%).

TLC: Petroleum ether – EtOAc 1:1 v/v, R_f = 0.43

¹H NMR (DMSO-d_6) δ: 8.72 (s, 1H, CH-triazole), 8.08 (s, 1H, CH-triazole), 7.54 (m, 3H, Ar), 7.32 (s, 1H, Ar), 7.30 (t, *J* = 8.9 Hz, 2H, Ar), 7.21 (d, *J* = 1.9 Hz, 1H, Ar), 6.91 (dd, *J* = 2.2, 8.5 Hz, 1H, Ar), 6.56 (t, *J* = 0.9 Hz, 1H, CH), 4.77 (t, *J* = 2.1 Hz, 2H, CH₂), 2.24 (qt, *J* = 2.2, 7.5 Hz, 2H, CH₂), 1.06 (t, *J* = 7.5 Hz, 3H, CH₃).

¹³C NMR (DMSO-d_6) δ: 163.57 (d, $^1J_{C,F}$ = 243.75 Hz, C), 156.52 (C), 155.89 (C), 153.26 (C), 152.49 (CH), 144.71 (CH), 133.15 (d, $^4J_{C,F}$ = 3.75 Hz, C), 130.67 (d, $^3J_{C,F}$ = 8.75 Hz, 2 x CH), 122.20 (CH), 121.40 (C), 116.26 (d, $^2J_{C,F}$ = 22.5 Hz, 2 x CH), 113.22 (CH), 107.33 (CH), 97.65 (CH), 89.58 (C), 75.27 (C), 59.79 (CH), 56.93 (CH₂), 13.98 (CH₃), 12.14 (CH₂).

HPLC (method B): 100 % at R.T.= 6.70 min.

2.5.3.16.1.3. 4-((6-(Pent-2-yn-1-yloxy)benzofuran-2-yl)(1*H*-1,2,4-triazol-1-yl)methyl)benzonitrile (27c)

Chemical Formula: $C_{23}H_{18}N_4O_2$, molecular Weight: 382.42

Prepared as described for 1-((4-chlorophenyl)(6-ethoxybenzofuran-2-yl)methyl)-1*H*-1,2,4-triazole (**19a**) using 4-((6-hydroxybenzofuran-2-yl)(1*H*-1,2,4-triazol-1-yl)methyl)benzonitrile (**14**) (0.1 g, 0.31 mmol) and 1-bromopent-2-yne (**26**) (0.07 mL g, 0.68 mmol). Gradient column chromatography afforded 4-((6-(pent-2-yn-1-yloxy)benzofuran-2-yl)(1*H*-1,2,4-triazol-1-yl)methyl)benzonitrile (**27c**) at 70% EtOAc as a yellow oil. Yield = 0.02 g (17%).

TLC: Petroleum ether – EtOAc 1:1 v/v, R_f = 0.27

¹H NMR (CDCl₃) δ: 8.11 (s, 1H, CH-triazole), 7.98 (s, 1H, CH-triazole), 7.64 (d, *J* = 8.5 Hz, 2H, Ar), 7.36 (d, *J* = 8.6 Hz, 1H, Ar), 7.30 (d, *J* = 8.2 Hz, 2H, Ar), 7.02 (d, *J* = 2.0 Hz, 1H, Ar), 6.89 (dd, *J* = 2.1, 8.5 Hz, 1H, Ar), 6.78 (s, 1H, Ar), 6.49 (app. s, 1H, CH), 4.63 (t, *J* = 2.1 Hz, 2H, CH₂), 2.19 (qt, *J* = 2.1, 7.5 Hz, 2H, CH₂), 1.08 (t, *J* = 7.5 Hz, 3H, CH₃).

¹³C NMR (CDCl₃) δ: 157.18 (C), 156.34 (C), 152.63 (CH), 149.86 (C), 140.95 (C), 132.82 (2 x CH), 128.23 (2 x CH), 121.83 (CH), 120.78 (C), 118.06 (C), 113.65 (CH), 113.16 (C), 108.63 (CH), 97.35 (CH), 90.04 (C), 73.79 (C), 61.60 (CH), 57.11 (CH₂), 13.58 (CH₃), 12.51 (CH₂).

HPLC (method B): 97.4 % at R.T.= 5.45 min.

2.5.3.17. 2-((4-Chlorophenyl)(1*H*-1,2,4-triazol-1-yl)methyl)benzofuran-6-yl morpholine-4-carboxylate (29a)

Chemical Formula: C₂₂H₁₉ClN₄O₄, Molecular Weight: 438.87
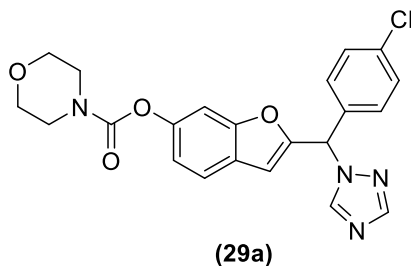
(29a)

Prepared as described for 1-((4-chlorophenyl)(6-ethoxybenzofuran-2-yl)methyl)-1*H*-1,2,4-triazole (**19a**) using 2-((4-chlorophenyl)(1*H*-1,2,4-triazol-1-yl)methyl)benzofuran-6-ol (**11**) (0.15 g, 0.46 mmol) and 4-morpholinecarbonyl chloride (**28**) (0.06 mL g, 0.5 mmol) to afford 2-((4-chlorophenyl)(1*H*-1,2,4-triazol-1-yl)methyl)benzofuran-6-yl morpholine-4-carboxylate (**29a**) as a white solid. Yield = 0.13 g (65%).

TLC: Petroleum ether – EtOAc 1:1 v/v, R_f = 0.2

Melting point: 150-154 ºC

¹H NMR (CDCl₃) δ: 8.23 (s, 1H, CH-triazole), 7.98 (s, 1H, CH-triazole), 7.42 (d, *J* = 8.1 Hz, 1H, Ar), 7.31 (d, *J* = 5.8 Hz, 2H, Ar), 7.19 (m, 3H, Ar), 6.96 (d, *J* = 8.2 Hz, 1H, Ar), 6.76 (s, 1H, Ar), 6.49 (s, 1H, CH), 3.67 (m, 4H, CH₂), 3.61 (m, 4H, CH₂).

¹³C NMR (CDCl₃) δ: 155.24 (C), 153.73 (C), 152.70 (C), 149.35 (C), 135.40 (C), 133.88 (C), 129.39 (2 x CH), 129.20 (2 x CH), 124.87 (C), 121.54 (CH), 118.10 (CH), 108.02 (CH), 105.76 (CH), 66.64 (CH₂), 66.50 (CH₂), 61.64 (CH), 44.94 (CH₂), 44.22 (CH₂).

HPLC (method A): 100 % at R.T.= 4.44 min.

HRMS (ESI): Calculated 461.0992 [M+Na]⁺, Found 461.0987 [M+Na]⁺.

2.5.3.18. 1-((4-Chlorophenyl)(5-(pent-2-yn-1-yloxy)benzofuran-2-yl)methyl)-1*H*-1,2,4-triazole (30)

Chemical Formula: C₂₂H₁₈ClN₃O₂, Molecular Weight: 391.86
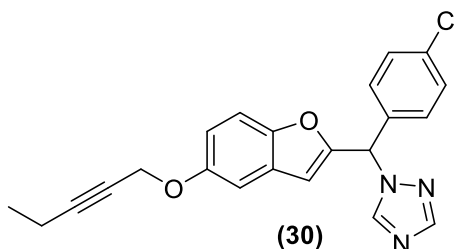
(30)

Prepared as described for 1-((4-chlorophenyl)(6-ethoxybenzofuran-2-yl)methyl)-1*H*-1,2,4-triazole (**19a**) using 2-((4-chlorophenyl)(1*H*-1,2,4-triazol-1-yl)methyl)benzofuran-5-ol (**12**) (0.2 g, 0.61 mmol) and 1-bromopent-2-yne (**26**) (0.07 mL g, 0.67 mmol) to afford 1-((4-chlorophenyl)(5-(pent-2-yn-1-yloxy)benzofuran-2-yl)methyl)-1*H*-1,2,4-triazole (**30**) as a yellow oil. Yield = 0.12 g (50%).

TLC: Petroleum ether – EtOAc 1:1 v/v, R$_f$ = 0.42

¹H NMR (CDCl₃) δ: 8.70 (s, 1H, CH-triazole), 8.08 (s, 1H, CH-triazole), 7.34 (d, *J* = 8.3 Hz, 2H, Ar), 7.28 (d, *J* = 9.1 Hz, 1H, Ar), 7.25 (d, *J* = 8.3 Hz, 2H, Ar), 7.02 (d, *J* = 2.6 Hz, 1H, Ar), 6.94 (dd, *J* = 2.6, 9.0 Hz, 1H, Ar), 6.86 (s, 1H, Ar), 6.51 (s, 1H, CH), 4.60 (t, *J* = 2.2 Hz, 2H, CH₂), 2.18 (qt, *J* = 2.1, 7.5 Hz, 2H, CH₂), 1.07 (t, *J* = 7.5 Hz, 3H, CH₃).

¹³C NMR (CDCl₃) δ: 156.62 (C), 151.90 (C), 150.72 (C), 135.66 (C), 133.38 (C), 129.46 (2 x CH), 129.28 (2 x CH), 127.74 (C), 115.37 (CH), 112.11 (CH), 108.66 (CH), 105.64 (CH), 89.69 (C), 74.16 (C), 62.16 (CH), 57.38 (CH₂), 13.62 (CH₃), 12.50 (CH₂).

HPLC (method B): 92.1 % at R.T.= 8.70 min.

2.5.3.19. 2-((4-Chlorophenyl)(1*H*-1,2,4-triazol-1-yl)methyl)benzofuran-5-yl morpholine-4-carboxylate (31)

Chemical Formula: $C_{22}H_{19}ClN_4O_4$, Molecular Weight: 438.87
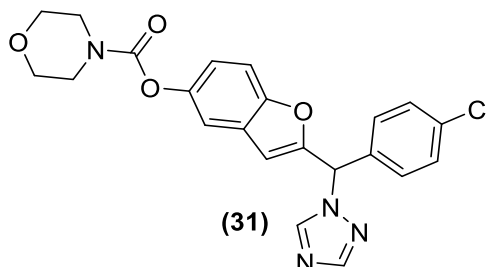
(31)

Prepared as described for 1-((4-chlorophenyl)(6-ethoxybenzofuran-2-yl)methyl)-1*H*-1,2,4-triazole (**19a**) using 2-((4-chlorophenyl)(1*H*-1,2,4-triazol-1-yl)methyl)benzofuran-5-ol (**12**) (0.2 g, 0.61 mmol) and 4-morpholinecarbonyl chloride (**28**) (0.08 mL g, 0.68 mmol) to afford 2-((4-chlorophenyl)(1*H*-1,2,4-triazol-1-yl)methyl)benzofuran-5-yl morpholine-4-carboxylate (**31**) as a white solid. Yield = 0.22 g (81%).

TLC: Petroleum ether – EtOAc 1:1 v/v, R_f = 0.1

Melting point: 158-162 ºC

¹H NMR (CDCl₃) δ: 8.11 (s, 1H, CH-triazole), 7.93 (s, 1H, CH-triazole), 7.30 (d, *J* = 8.9 Hz, 1H, Ar), 7.26 (d, *J* = 8.1 Hz, 2H, Ar), 7.19 (d, *J* = 2.2 Hz, 1H, Ar), 7.13 (d, *J* = 8.1 Hz, 2H, Ar), 6.97 (dd, *J* = 2.2, 8.8 Hz, 1H, Ar), 6.73 (s, 1H, Ar), 6.43 (s, 1H, CH), 3.63 (m, 4H, CH₂), 3.58 (m, 4H, CH₂).

¹³C NMR (CDCl₃) δ: 154.05 (C), 153.46 (C), 152.19 (C), 147.09 (C), 135.52 (C), 133.95 (C), 129.31 (2 x CH), 129.15 (2 x CH), 128.14 (C), 119.64 (CH), 114.35 (CH), 111.90 (CH), 108.04 (CH), 66.58 (CH₂), 66.48 (CH₂), 61.32 (CH), 44.86 (CH₂), 44.18 (CH₂).

HPLC (method B): 100 % at R.T.= 4.76 min.

2.5.3.20. 1-((5-Chlorobenzofuran-2-yl)(4-(pent-2-yn-1-yloxy)phenyl)methyl)-1*H*-1,2,4-triazole (32)

Chemical Formula: $C_{22}H_{18}ClN_3O_2$, Molecular Weight: 391.86
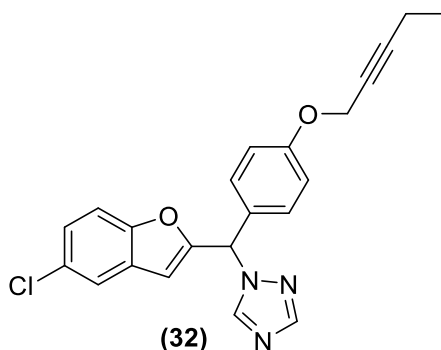
(32)

Prepared as described for 1-((4-chlorophenyl)(6-ethoxybenzofuran-2-yl)methyl)-1*H*-1,2,4-triazole (**19a**) using 4-((5-chlorobenzofuran-2-yl)(1*H*-1,2,4-triazol-1-yl)methyl)phenol (**17**) (0.15 g, 0.69 mmol) and 1-bromopent-2-yne (**26**) (0.07 mL g, 0.69 mmol) to afford 1-((5-chlorobenzofuran-2-yl)(4-(pent-2-yn-1-yloxy)phenyl)methyl)-1*H*-1,2,4-triazole (**32**) as a yellow oil. Yield = 0.08 g (44%).

TLC: Petroleum ether – EtOAc 1:1 v/v, R_f = 0.42

¹H NMR (CDCl₃) δ: 8.21 (s, 1H, CH-triazole), 7.99 (s, 1H, CH-triazole), 7.43 (d, *J* = 1.9 Hz, 1H, Ar), 7.30 (d, *J* = 8.7 Hz, 1H, Ar), 7.22 (m, 3H, Ar), 6.95 (d, *J* = 8.8 Hz, 2H, Ar), 6.73 (s, 1H, Ar), 6.45 (s, 1H, CH), 4.61 (t, *J* = 2.1 Hz, 2H, CH₂), 2.18 (qt, *J* = 2.1, 7.5 Hz, 2H, CH₂), 1.07 (t, *J* = 7.5 Hz, 3H, CH₃).

¹³C NMR (CDCl₃) δ: 158.71 (C), 154.33 (C), 153.66 (C), 151.39 (CH), 142.96 (CH), 129.24 (2 x CH), 128.99 (C), 128.84 (C), 127.26 (C), 125.50 (CH), 121.08 (CH), 115.57 (2 x CH), 112.56 (CH), 107.07 (CH), 90.06 (C), 73.71 (C), 61.91 (CH), 56.63 (CH₂), 13.57 (CH₃), 12.49 (CH₂).

HPLC (method B): 96.1 % at R.T.= 9.17 min.

2.5.3.21. 4-((5-Chlorobenzofuran-2-yl)(1*H*-1,2,4-triazol-1-yl)methyl)phenyl morpholine-4-carboxylate (33)

Chemical Formula: $C_{22}H_{19}ClN_4O_4$, Molecular Weight: 438.87
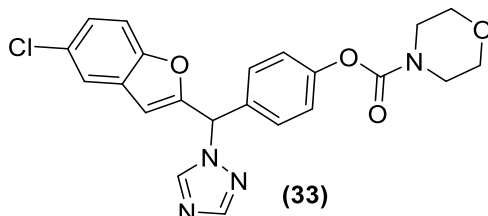
Prepared as described for 1-((4-chlorophenyl)(6-ethoxybenzofuran-2-yl)methyl)-1*H*-1,2,4-triazole (**19a**) using 4-((5-chlorobenzofuran-2-yl)(1*H*-1,2,4-triazol-1-yl)methyl)phenol (**17**) (0.04 g, 0.12 mmol) and 4-morpholinecarbonyl chloride (**28**) (0.02 mL g, 0.18 mmol) to afford 4-((5-chlorobenzofuran-2-yl)(1*H*-1,2,4-triazol-1-yl)methyl)phenyl morpholine-4-carboxylate (**33**) as a yellow oil. Yield = 0.03 g (60%).

TLC: Petroleum ether – EtOAc 1:1 v/v, R_f = 0.1

^{1}H NMR (CDCl₃) δ: 8.48 (s, 1H, CH-triazole), 8.05 (s, 1H, CH-triazole), 7.43 (d, *J* = 1.8 Hz, 1H, Ar), 7.30 (m, 3H, Ar), 7.22 (dd, *J* = 2.1, 8.7 Hz, 1H, Ar), 7.13 (d, *J* = 8.7 Hz, 2H, Ar), 6.83 (s, 1H, Ar), 6.50 (s, 1H, CH), 3.68 (m, 4H, CH₂), 3.59 (m, 4H, CH₂).

^{13}C NMR (CDCl₃) δ: 153.71 (C), 153.31 (C), 153.19 (C), 152.11 (C), 131.58 (C), 129.13 (C), 129.04 (2 x CH), 128.68 (C), 125.78 (CH), 122.58 (2 x CH), 121.19 (CH), 112.62 (CH), 107.75 (CH), 66.61 (CH₂), 66.45 (CH₂), 61.01 (CH), 44.93 (CH₂), 44.18 (CH₂).

HPLC (method B): 97.9 % at R.T.= 5.03 min.

2.5.4. Cell culture

JEG-3 cells were purchased from ATCC and grown in Eagle's Minimal Essential Medium (EMEM) supplemented with 10% fetal calf serum (FCS). MDA-MB-231 cells were grown in Roswell park Memorial Institute medium (RPMI1690) supplemented with 10% FCS. All cells were cultured at 37 ºC under 5% CO₂ in a humidified incubator.

2.5.5. Aromatase Activity assay

Aromatase activity was assayed using a modified method previous reported (Foster *et al.* 2008). JEG-3 cells were grown to approximately 80% confluence in six-well cell culture plates. Androst-4-ene-3,17-dione[1β-^{3}H] was dissolved in serum-free cell culture medium and added into each well. After a 1 h incubation at 37 ℃ followed by a 5-min incubation on ice, 500 µL of culture medium was taken from each well. Medium was vortexed with 2% dextran-treated charcoal (Sigma-Aldrich) in PBS and centrifuged at 4000 rpm. The supernatant containing the product, [^{3}H] H$_2$O, was quantified by scintillation counting. Cell protein concentrations were determined using Pierce BCA assay kit (Thermo Fisher Scientific). Aromatase activity results were determined as a concentration of product formed per mg of protein per hour (pmol/mg/h). Results were shown as a % change in activity compared to control. Each data point was measured in triplicates and the error in the IC$_{50}$ calculations represented as 95% confidence interval.

2.5.6. BrdU-based cell proliferation assay to assess drug toxicity

MDA-MB-231 cells were plated onto 96-well microtiter tissue culture plates in RPMI1690 medium at a density of 5×10^3 cells/well. Groups were treated with either DMSO alone (at no greater than 0.01%) as a vehicle control, or at a dose of 1 µM. Effects of drug treatment on cell growth were detected using the BrdU cell proliferation assay (Roche) according to the manufacturer's recommendations. The BrdU colorimetric immunoassay is a quantitative cell proliferation assay based on the measurement of BrdU incorporation during DNA synthesis. After treatments 20 µL/well of BrdU were added to each well, followed by an incubation of 2 h at 37°C. The cells were subsequently fixed, and the DNA denatured. Anti-BrdU-peroxidase immune complexes were detected by substrate reaction and quantified in an ELISA reader at 370 nm.

Chapter three: Pyridine-based dual binding aromatase inhibitors
3.1.Background

Non-steroidal aromatase inhibitors bind to the enzyme active site through coordination of a heterocyclic nitrogen lone pair with the haem iron. Imidazole was reported to be more efficient in respect to the coordination potential followed by triazole then tetrazole. However, triazole compounds were found to be more selective (Vinh *et al.* 1999). Pyridine nitrogen shows availability of a lone pair with the potential to coordinate the haem iron and the activity was found to fall between triazole and tetrazole moieties making pyridine an interesting heterocycle for the aromatase inhibition due to the increased size, which may lead to a more close interaction with the haem (Saberi *et al.* 2005). A number of studies focused on the ability of pyridine compounds to bind to and inhibit the aromatase enzyme (Kim *et al.* 2004; Stauffer *et al.* 2012; Ertas *et al.* 2018). In a previous study on benzofuran derivatives, the aromatase inhibitory activity was found to be directly proportional to the heterocyclic nitrogen basicity (pKa: imidazole, 14.5; triazole, 10; pyridine, 5.2; tetrazole, 4.8) (**Figure 3.1**) (Saberi *et al.* 2005).

1*H*-imidazole	1*H*-1,2,4-triazole	pyridine	1*H*-tetrazole
pKa 14.5	pKa 10	pKa 5.2	pKa 4.8
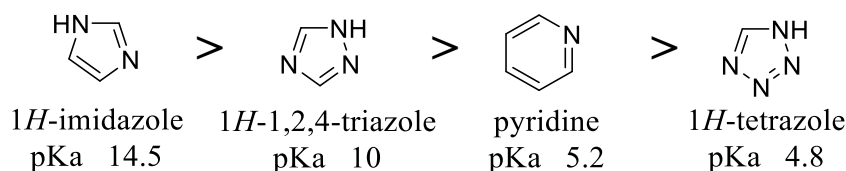
Figure (3.1): Order of basicity of the heterocyclic nitrogen containing compounds.

3.2.Aim of this chapter

To find the right balance between the inhibitory activity against the aromatase enzyme and the toxicity and selectivity of the compounds, it is important to explore other possibilities for optimal aromatase dual binding molecules. This includes replacing the triazole group with another heterocycle i.e. pyridine to investigate the biological consequences of such a structure alteration with respect to the enzyme inhibitory activity, toxicity, and the selectivity over other cytochrome superfamily enzymes.

Objectives to be fulfilled by the end of this chapter:

1. To investigate the possibility of applying the dual binding concept to pyridine-based compounds.
2. To develop synthetic routes to prepare the novel inhibitors.
3. To perform aromatase inhibitory assays to assess the efficacy of novel inhibitors.
4. To establish a clear SAR for the compounds in this study to help further development of novel inhibitors.
5. To perform toxicological studies (MTT assays) to evaluate the safety index of the prepared inhibitors.

A series of pyridine-based benzofuran compounds was designed depending on the parent scaffold previously reported by our research group (**Figure 3.2**) (Saberi *et al.* 2006). Two main modifications were studied, the first of which was varying the substituent on the phenyl ring, 4-bromo and 2,4-dichloro as well as the parent 4-fluoro and 4-chloro, producing four different derivatives to provide better understanding of the SAR. The second modification was achieved by changing the methoxy group on the benzofuran ring with longer chain substituents, namely but-2-ynyloxy and pent-2-ynyloxy, to investigate the binding potential in the access channel of the enzyme active site to provide dual binding aromatase inhibitors.
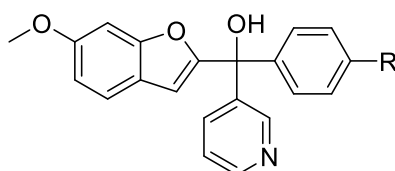
R	IC$_{50}$ (µM)
Cl	0.049
F	0.044

Figure (3.2): Parent pyridine-based aromatase inhibitors with IC$_{50}$ values based on a CYP19 placental assay (Saberi *et al.* 2006).

3.3. Results and discussion

3.3.1. Computational Studies

Protein-ligand complexes were prepared applying the same methods in chapter 2 and MD simulations were performed for 150 ns. Studying the binding profile through the simulation time indicated that the *S*-enantiomer formed interactions with some of the key amino acid residues e.g. Phe221, Met374, Leu477, Ser478 and more importantly formed a robust interaction with the haem iron through the nitrogen of the pyridine ring. On the other hand, the *R*-enantiomer shifted the interaction with the haem iron towards the tertiary alcohol group (**figure 3.3**).
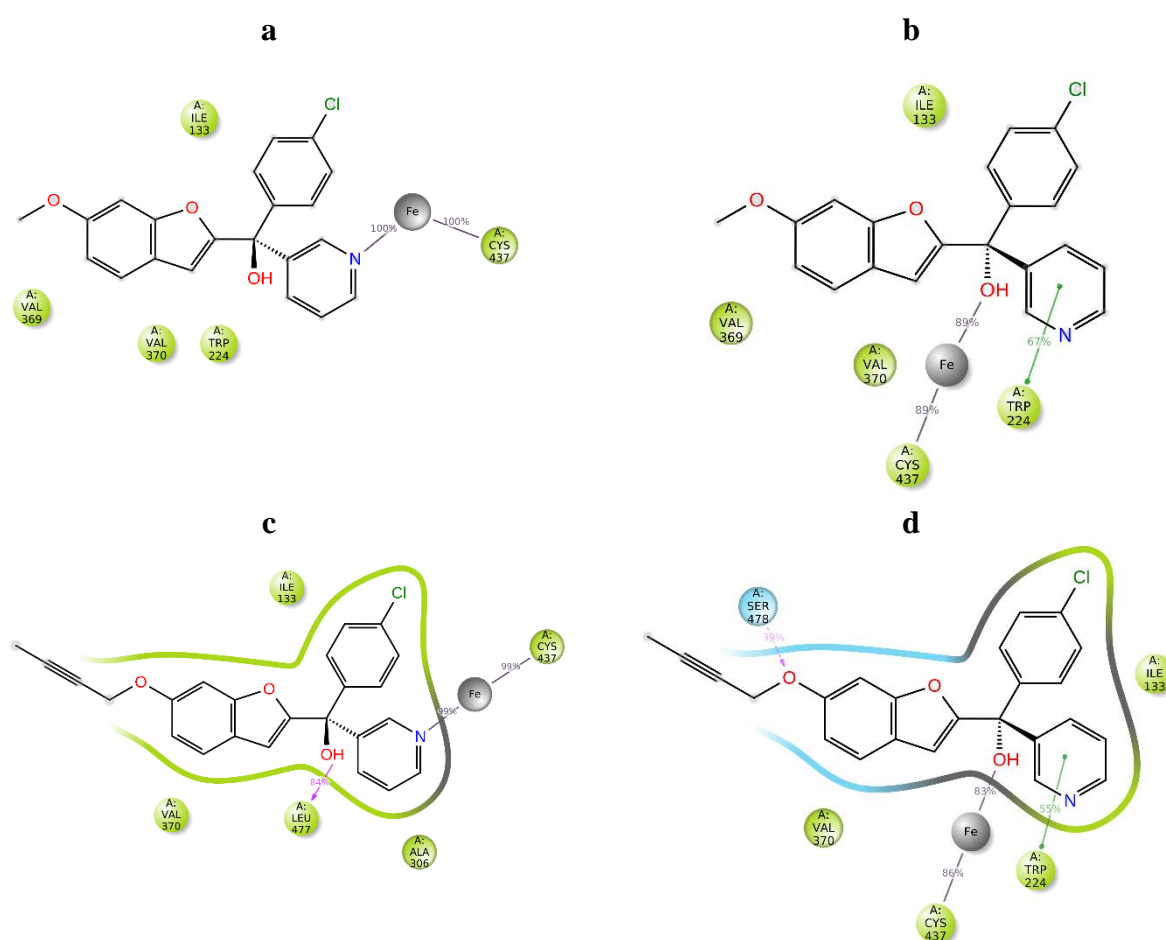
Figure (3.3): Comparing the binding profile showing haem binding over 150 ns MD simulation for (a) *S*-enantiomer of **36a** (b) *R*-enantiomer of **36a** (c) *S*-enantiomer of **43a** (d) *R*-enantiomer of **43a**.

Comparing the secondary substituent on the phenyl ring e.g. compounds **42a-d** showed that all the compounds had comparable binding mode and interactions with the key amino acid residues e.g. Phe221, Met374, Leu477 and Ser478 along with the interaction between the nitrogen of the pyridine ring and the haem iron except **42a**, which theoretically directed the nitrogen away from

the haem (**figure 3.4**). There was no obvious reason for this difference in binding behaviour between the 4-chloro derivative (**42a**) and the closely related analogues (4-fluoro, 4-bromo and 2,4-dichloro (**42b-d**)).
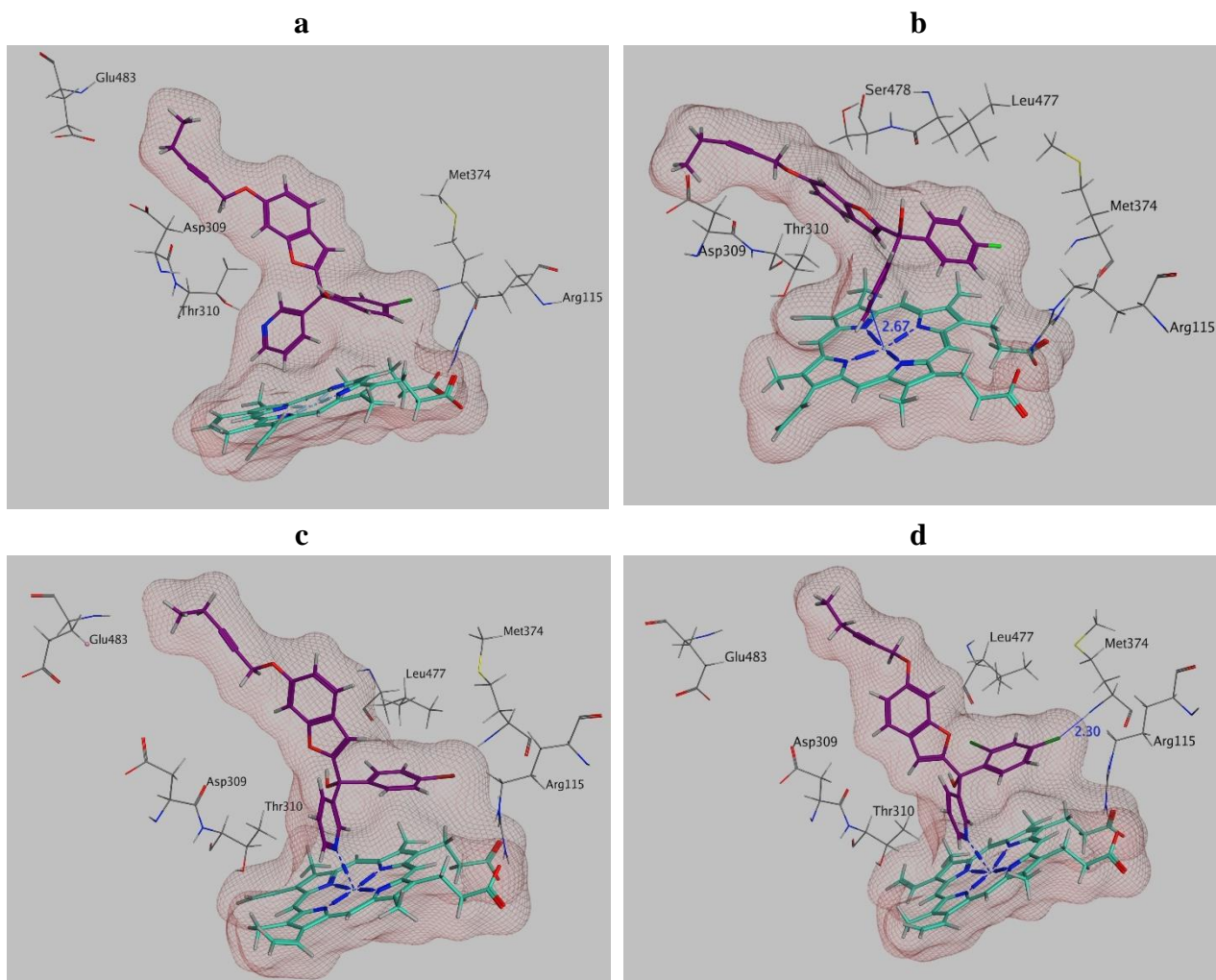
Figure (3.4): Comparing the binding profile after 150 ns MD simulation for (a) *S*-enantiomer of **42a** (b) *S*-enantiomer of **42b** (c) *S*-enantiomer of **42c** (d) *S*-enantiomer of **42d**.

3.3.2. Chemistry

In this part, different synthetic routes for the target compounds will be discussed in detail. The designed compounds were divided into two classes based on the substitution on the 6-position of the benzofuran ring:

➢ Class 1: methoxy-substituted compounds.
➢ Class 2: long chain-substituted compounds.

A two-step synthetic pathway as originally reported was used to prepare the required parent compounds with the 6-methoxy substitution on the benzofuran ring (Saberi *et al.* 2006) (**scheme 3.1**). The first step involved the formation of the benzofuran ketone derivatives (**3**), which were then used in a Grignard reaction with pyridine 3-magnesium bromide, prepared *in situ*, to produce the final compounds (**36**).

	R_1	R_2
2a	Cl	H
2c	F	H
2e	Br	H
2f	Cl	Cl

	R_1	R_2
3a	Cl	H
3d	F	H
3f	Br	H
3g	Cl	Cl

	R_1	R_2
36a	Cl	H
36b	F	H
36c	Br	H
36d	Cl	Cl
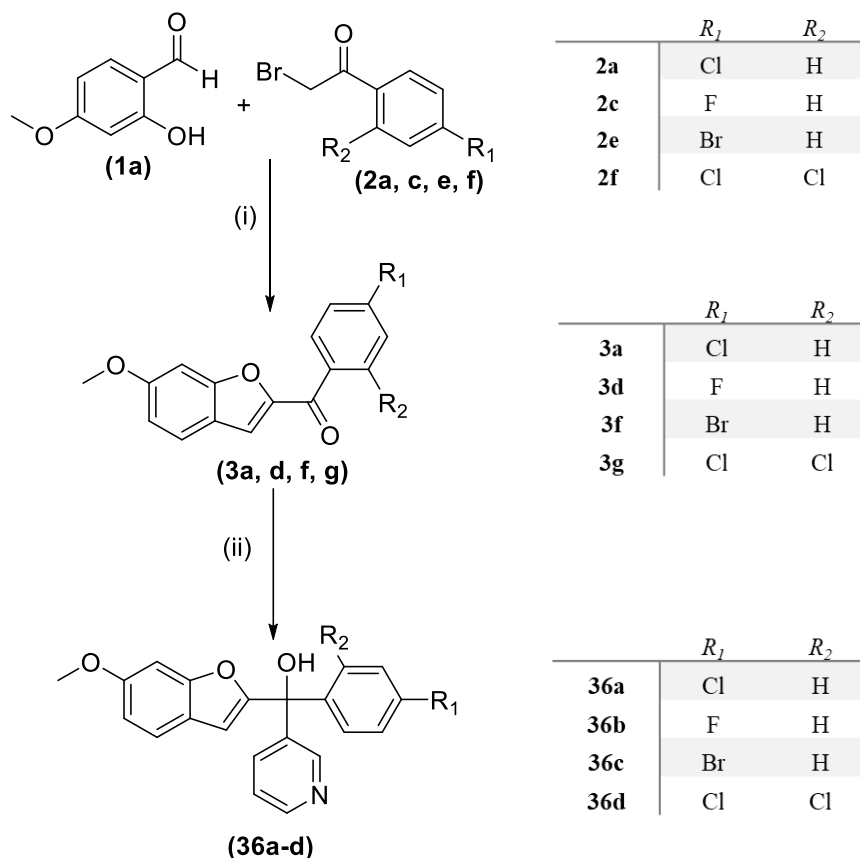
Scheme (3.1): The synthetic pathway for (6-methoxybenzofuran-2-yl)(phenyl)(pyridin-3-yl)methanol derivatives, (i) K_2CO_3, CH_3CN, 70 ℃, 3 h (ii) Pyridine 3-magnesium bromide, THF, 16 h.

Preparation of the longer chain substituted compounds required a different approach with a four-step synthetic pathway. The original suggested pathway (**scheme 3.2**) started with formation of the pyran protected 6-benzofuranol ketone derivative (**9**) followed by Grignard reaction then pyran deprotection to produce 2-(hydroxy(phenyl)(pyridin-3-yl)methyl)benzofuran-6-ol derivatives (**38**), which was meant to provide the required products through a nucleophilic substitution reaction with the corresponding alkynyl halide in a divergent manner. The presence of the free alcoholic OH and the acidity of the benzofuran proton complicated the last step with multiple products produced.

	R_1	R_2
2a	Cl	H
2c	F	H
2e	Br	H
2f	Cl	Cl

	R_1	R_2
9a	Cl	H
9c	F	H
9e	Br	H
9f	Cl	Cl

	R_1	R_2
37a	Cl	H
37b	F	H
37c	Br	H
37d	Cl	Cl

	R_1	R_2
38a	Cl	H
38c	F	H
38d	Br	H
38e	Cl	Cl

	R_1	R_2	R_3
42a	Cl	H	
42b	F	H	pent-2ynyl
42c	Br	H	
42d	Cl	Cl	

	R_1	R_2	R_3
43a	Cl	H	
43b	F	H	but-2ynyl
43c	Br	H	
43d	Cl	Cl	
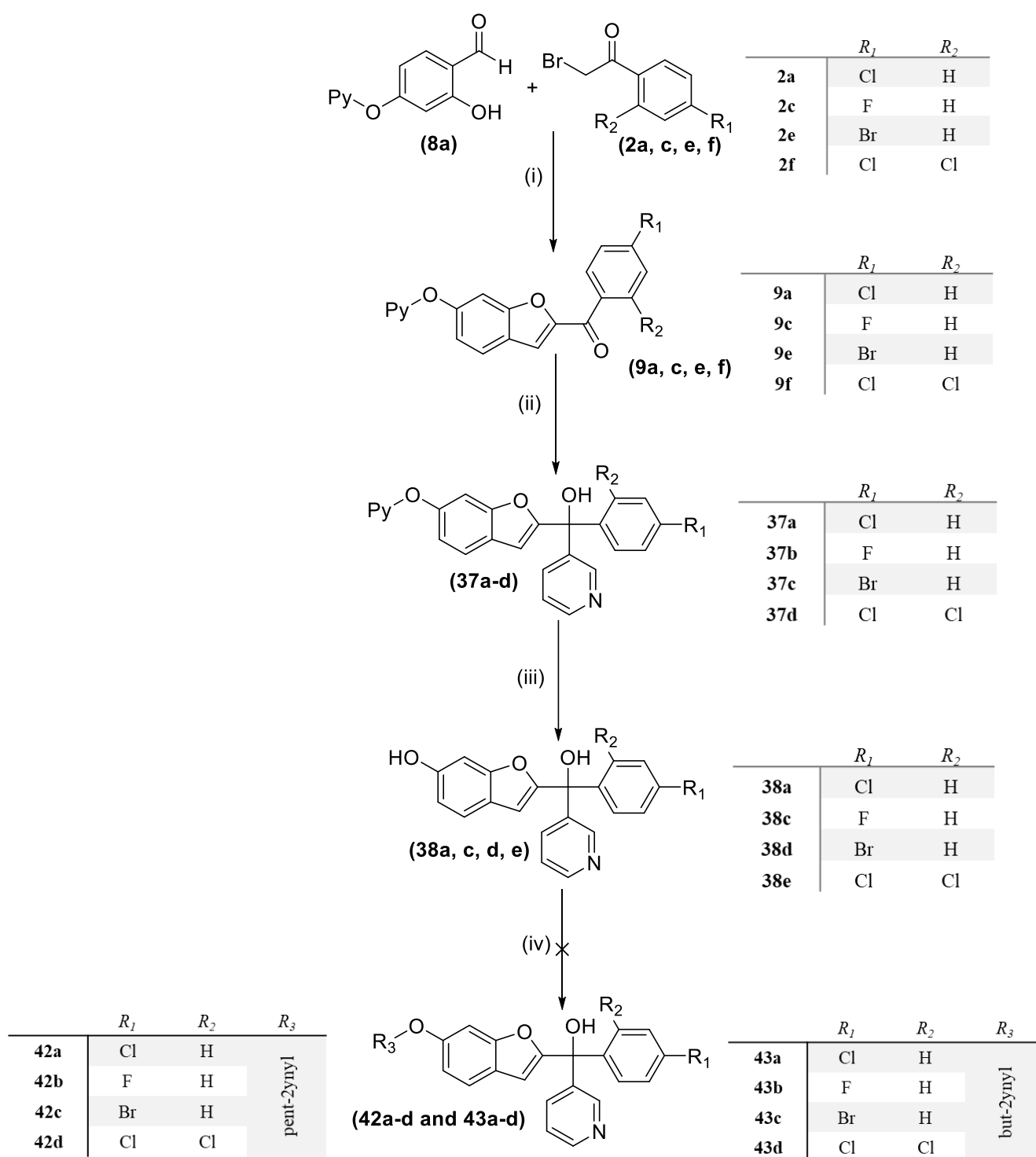
Scheme (3.2): The synthetic pathway for (6-alkynyloxy benzofuran-2-yl)(phenyl)(pyridin-3-yl)methanol derivatives, (i) K_2CO_3, CH_3CN, 70 ℃, 3 h, (ii) pyridine 3-magnesium bromide, THF, 16 h, (iii) HCl/dioxane, 1h, (iv) alkynyl bromide, K_2CO_3, CH_3CN, 70 ℃, 16 h.

To overcome this problem, another less divergent pathway (**scheme 3.3**) was implemented by changing the order of the last three steps to the pyran deprotection followed by the reaction with the alkynyl halide and finally Grignard reaction to prepare the required compounds.

	R_1	R_2
2a	Cl	H
2c	F	H
2e	Br	H
2f	Cl	Cl

	R_1	R_2
9a	Cl	H
9c	F	H
9e	Br	H
9f	Cl	Cl

	R_1	R_2
39a	Cl	H
39b	F	H
39c	Br	H
39d	Cl	Cl

	R_1	R_2
a	Cl	H
b	F	H
c	Br	H
d	Cl	Cl
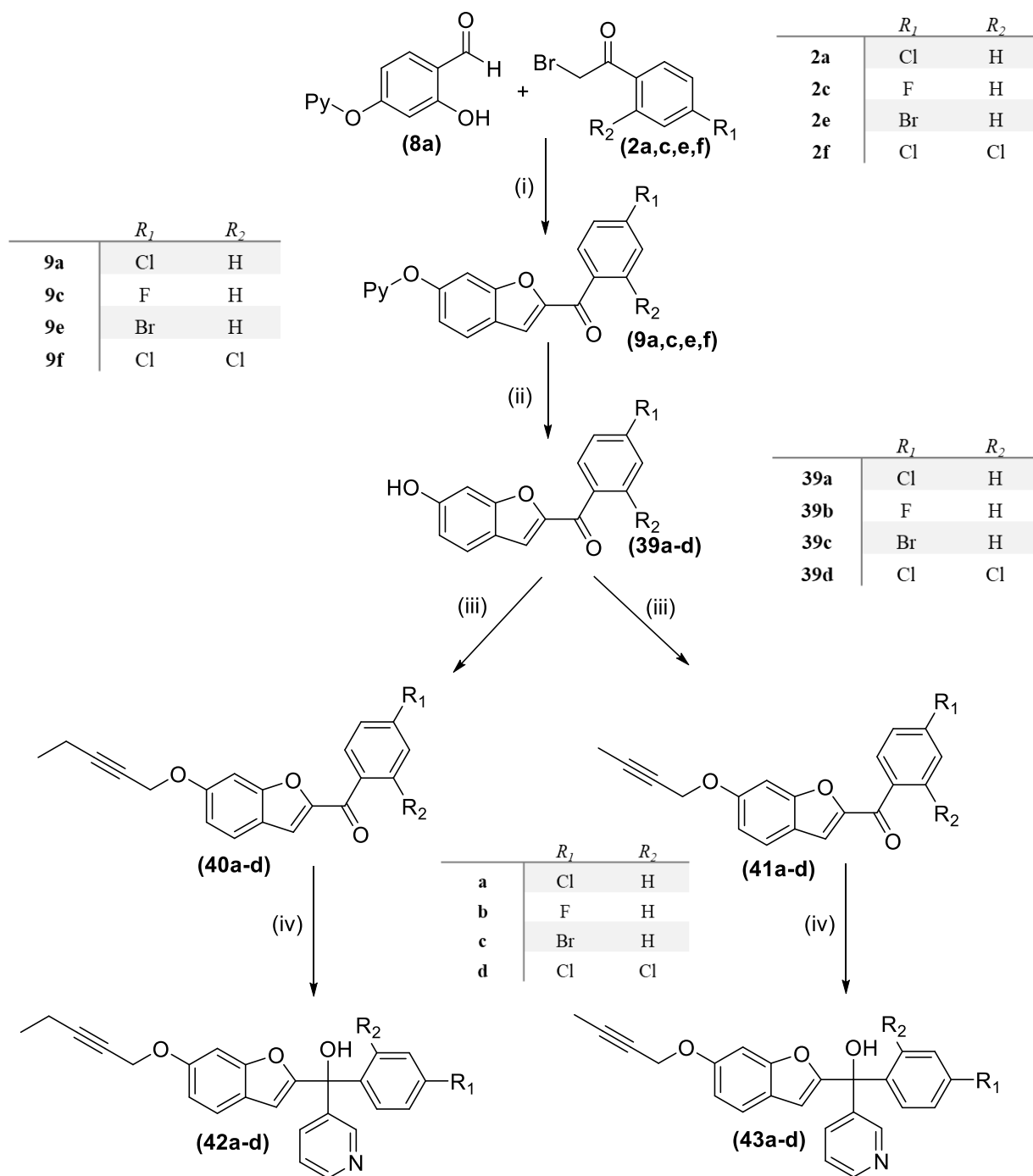
Scheme (3.3): The synthetic pathway for (6-alkynyloxy benzofuran-2-yl)(phenyl)(pyridin-3-yl)methanol derivatives, (i) K$_2$CO$_3$, CH$_3$CN, 70 ℃, 3 h (ii) HCl/dioxane, 1h, (iii) alkynyl bromide, K$_2$CO$_3$, CH$_3$CN, 70 ℃, 16 h, (iv) pyridine 3-magnesium bromide, THF, 16 h.

3.3.2.1. Preparation of the 6-methoxy derivatives: (6-methoxybenzofuran-2-yl)(phenyl)(pyridin-3-yl)methanol derivatives (36a-d) (Saberi *et al.* 2006)

	R_1	R_2
3a	Cl	H
3d	F	H
3f	Br	H
3g	Cl	Cl

	R_1	R_2
36a	Cl	H
36b	F	H
36c	Br	H
36d	Cl	Cl
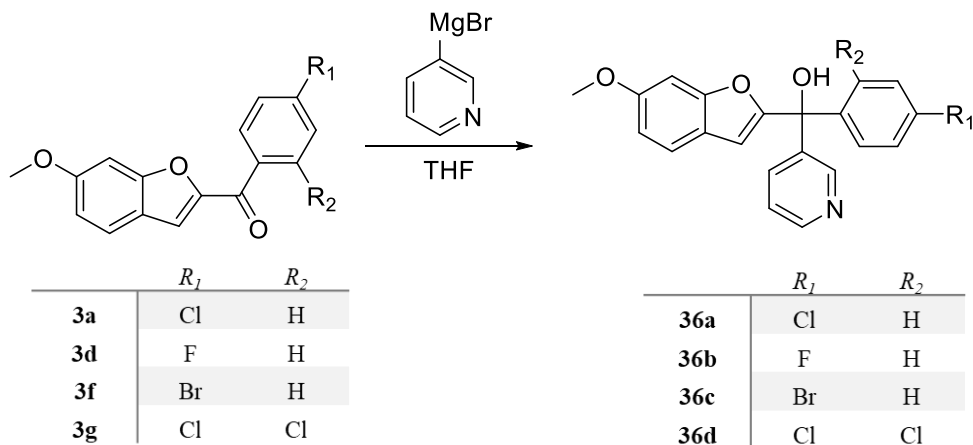
This reaction is a Grignard reaction in which pyridin-3-yl magnesium bromide, prepared *in situ* from the reaction of 3-bromopyridine and magnesium turnings in the presence of a few crystals of iodine, adds to the ketone group through formation of a carbon-carbon bond to form a tertiary alcohol (**Figure 3.5**). The proper ketone starting compounds (**3**) were prepared as described in chapter two.

Formation of Grignard reagent
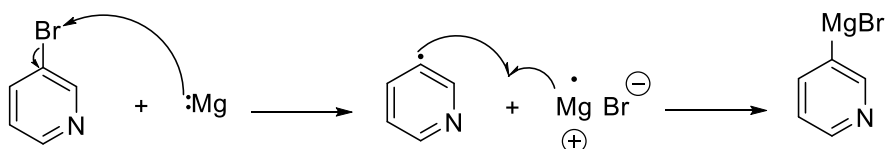
Grignard addition to ketone
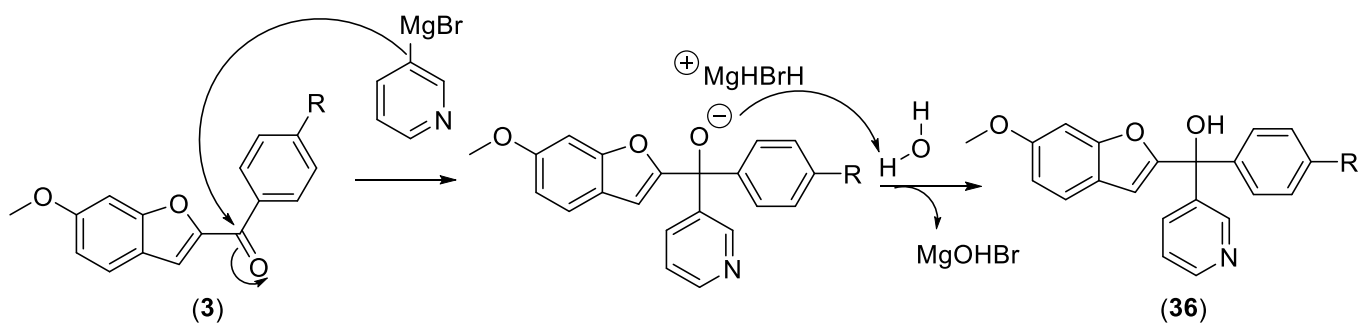
Figure (3.3): Schematic representation of Grignard reaction mechanism.

The yields varied from 25% to 92% (**table 3.1**), which can be attributed to the extent of formation of the Grignard reagent or the time allowed for the reaction. The reaction was monitored by TLC with the addition of excess Grignard reagent until the disappearance of the starting material.

Table (3.1): Yield of compounds **36a-d**

Compound	Yield
36a	92%
36b	83%
36c	25%
36d	32%

The products were identified by ^{1}H and ^{13}C NMR with the appearance of the additional signals downfield in the aromatic area of the spectrum indicating the pyridine ring and a broad singlet corresponding to the tertiary alcohol group. The identity of the products was confirmed by HPLC/HRMS analysis providing the exact molecular weight for each product and with HPLC purity not less than 95%.

3.3.2.2. The divergent synthetic pathway

3.3.2.2.1. Grignard reaction: preparation of (4-chlorophenyl)(pyridin-3-yl)(6-((tetrahydro-2*H*-pyran-2-yl)oxy)benzofuran-2-yl)methanol (37a) (Saberi *et al.* 2006)

(9a)   (37a)
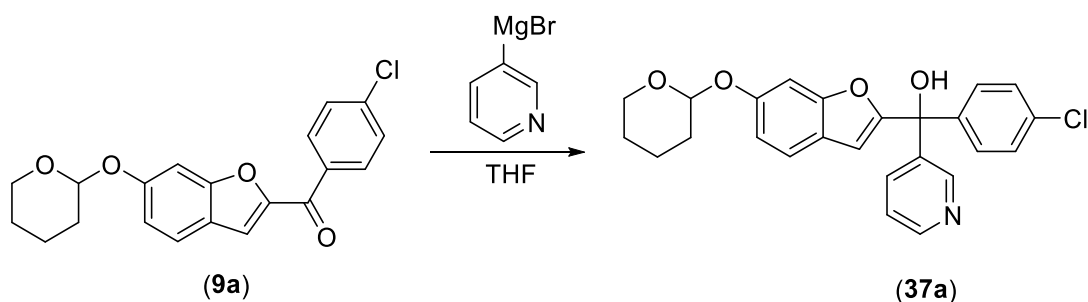
This reaction is a Grignard reaction as described under the preparation of the 6-methoxy derivatives in which the ketone starting compounds (**9**) were prepared from the pyran protected salicylaldehyde derivative (**8a**) as described in chapter two.

The reaction was monitored by TLC with the addition of excess Grignard reagent until the disappearance of the starting material. However, the yield after column chromatography purification was around 30%.

3.3.2.2.2. Pyran deprotection: preparation of 2-((4-chlorophenyl)(hydroxy)(pyridin-3-yl)methyl)benzofuran-6-ol (38a)
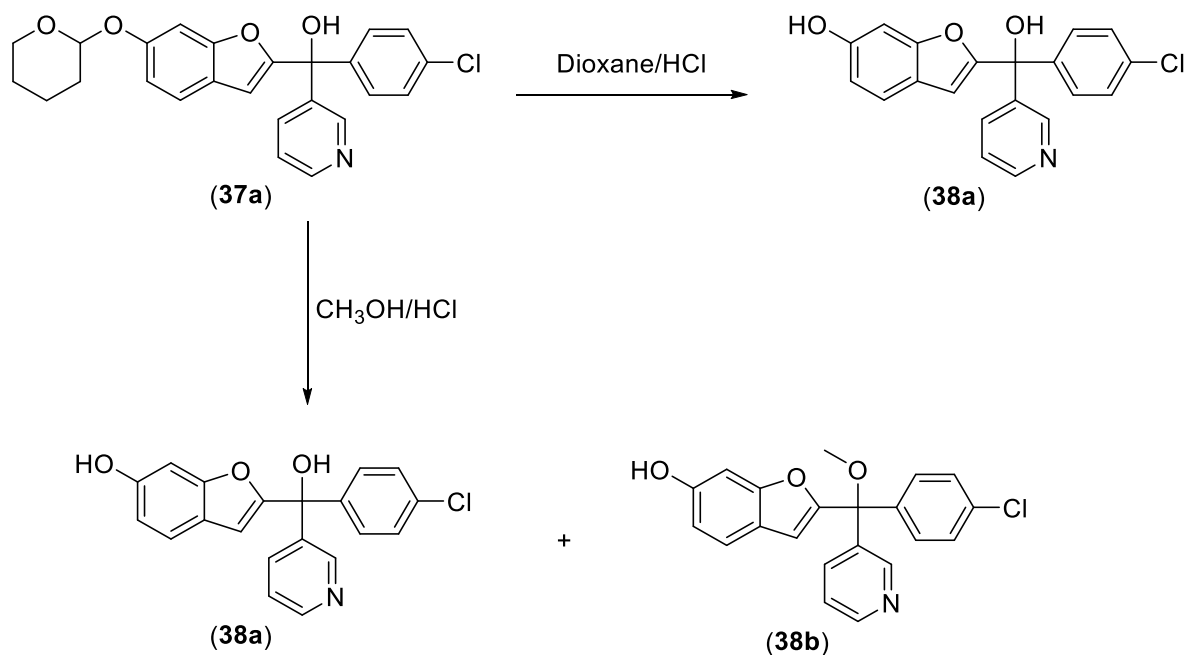
The reaction is acid-catalysed pyran deprotection (Jepsen *et al.* 2011) performed as described in chapter two using HCl and dioxane as the reaction solvent instead of methanol. TLC monitoring showed complete disappearance of the starting material and appearance of a lower spot indicating the formation of the free phenolic OH group.

The identity of the compound was confirmed by ^{1}H NMR, which showed the disappearance of all pyran signals in the aliphatic region of the spectrum and the appearance of a broad singlet signal corresponding to the phenolic OH at around 10.0 ppm.

This reaction was initially attempted using HCl and methanol as the reaction solvent as described (Jepsen *et al.* 2011). However, on monitoring TLC, the intensity of the spot corresponding to the starting material R_f was found to increase over time indicating the formation of a side product. The side product was isolated and analysed to indicate the formation of 2-((4-chlorophenyl)(methoxy)(pyridin-3-yl)methyl)benzofuran-6-ol (**38b**) through acid catalysed ether

formation of the original product 2-((4-chlorophenyl)(hydroxy)(pyridin-3-yl)methyl)benzofuran-6-ol (**38a**) at the tertiary alcoholic OH. The identity of the side product was confirmed by ^{1}H NMR, which showed the disappearance of all pyran signals in the aliphatic region of the spectrum and the appearance of a broad singlet signal corresponding to the phenolic OH at around 10.0 ppm. The only difference between the side product and the product was the disappearance of the broad singlet of the tertiary alcohol at around 7.1 ppm and the appearance of a singlet at around 3.2 ppm representing the methoxy group in the ^{1}HNMR (**figure 3.6**) and the appearance of an extra carbon peak in the ^{13}CNMR.
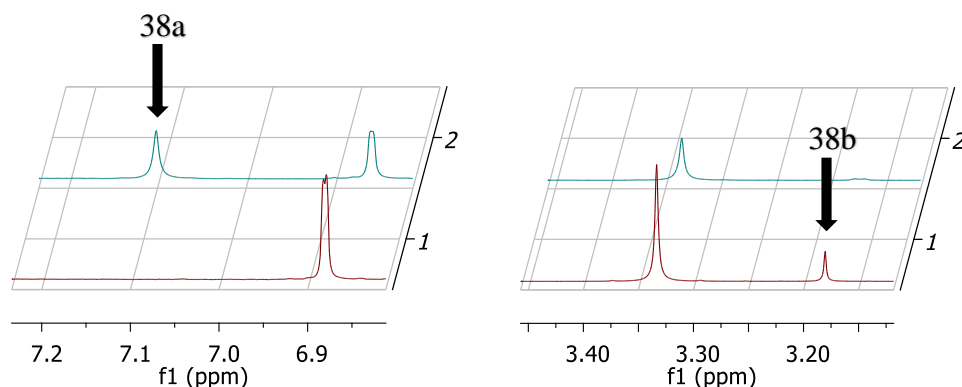
Figure (3.6): Magnification of the difference in ^{1}H NMR for compounds **38a** in green and **38b** in red.

3.3.2.2.3. Preparation of the 6-pentyloxy compounds (42)
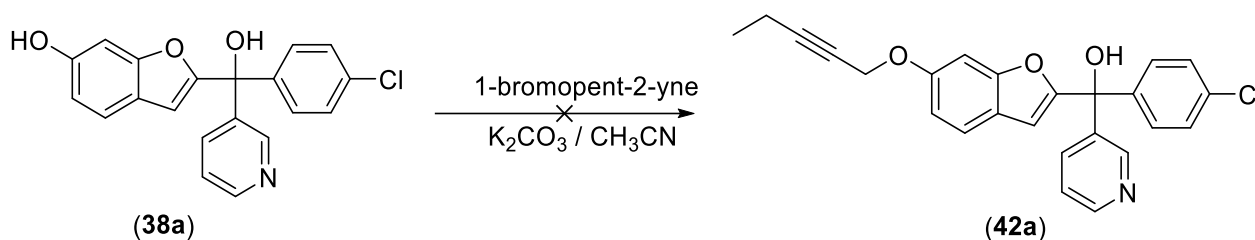
This reaction is a nucleophilic substitution reaction as described earlier in chapter two, where K$_2$CO$_3$ acts as a base to deprotonate the acidic phenolic group. However, the presence of the tertiary alcohol and the acidic benzofuran proton complicated the reaction. The presence of more than one reactive centre led to the formation of multiple products with all sort of combinations (**Figure 3.7**). The complexity of the TLC made it inevitable to shift the synthetic pathway to a less divergent way by changing the order of the reactions to perform this nucleophilic substitution step before the formation of the tertiary alcohol.
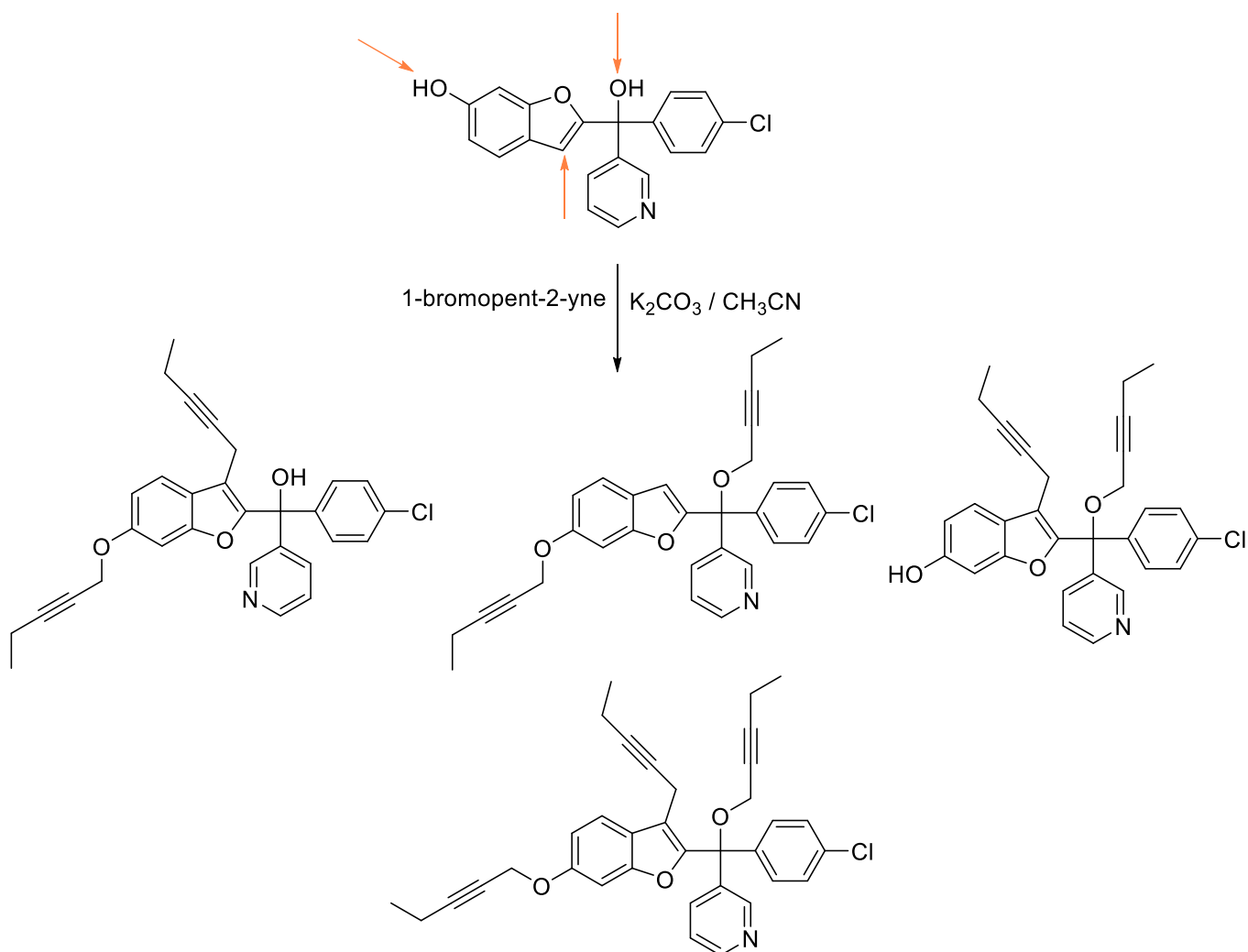
Figure (3.7): The proposed possible multiple products of the nucleophilic substitution reaction for compound **38a** with three reactive centres.

3.3.2.3. The non-divergent synthetic pathway

3.3.2.3.1. Pyran deprotection (Jepsen *et al.* 2011)

	R_1	R_2
9a	Cl	H
9c	F	H
9e	Br	H
9f	Cl	Cl

	R_1	R_2
39a	Cl	H
39b	F	H
39c	Br	H
39d	Cl	Cl
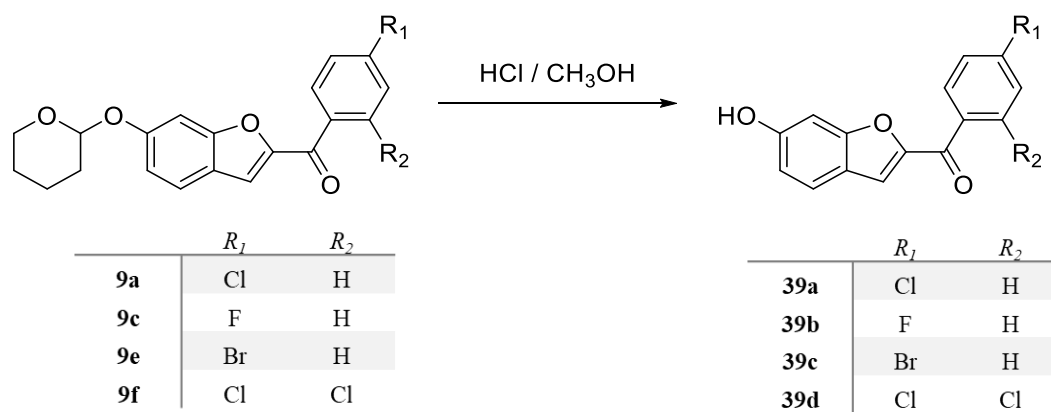
The acid catalysed pyran deprotection reaction was performed as described in chapter two. The identity of the compound was confirmed by ^{1}H NMR, which showed the disappearance of all pyran signals in the aliphatic region of the spectrum and the appearance of a broad singlet signal corresponding to the phenolic OH at around 10.0 ppm. The yield for this reaction and the melting points for the products are indicated in **table 3.2**.

Table (3.2): Yield and melting points for compounds **39a-d**

Compound	Yield	Melting point
39a	64%	208-210 ℃ (lit. m.p. = 222-224 ℃) (Meshram *et al.* 2012)
39b	66%	196-198 ℃
39c	71%	202-206 ℃ (lit. m.p. = 212-214 ℃) (Meshram *et al.* 2012)
39d	66%	192-194 ℃

3.3.2.3.2. Preparation of (6-(pent-2-yn-1-yloxy)benzofuran-2-yl)(phenyl)methanone derivatives (40a-d) and (6-(but-2-yn-1-yloxy)benzofuran-2-yl)(phenyl)methanone derivatives (41a-d)
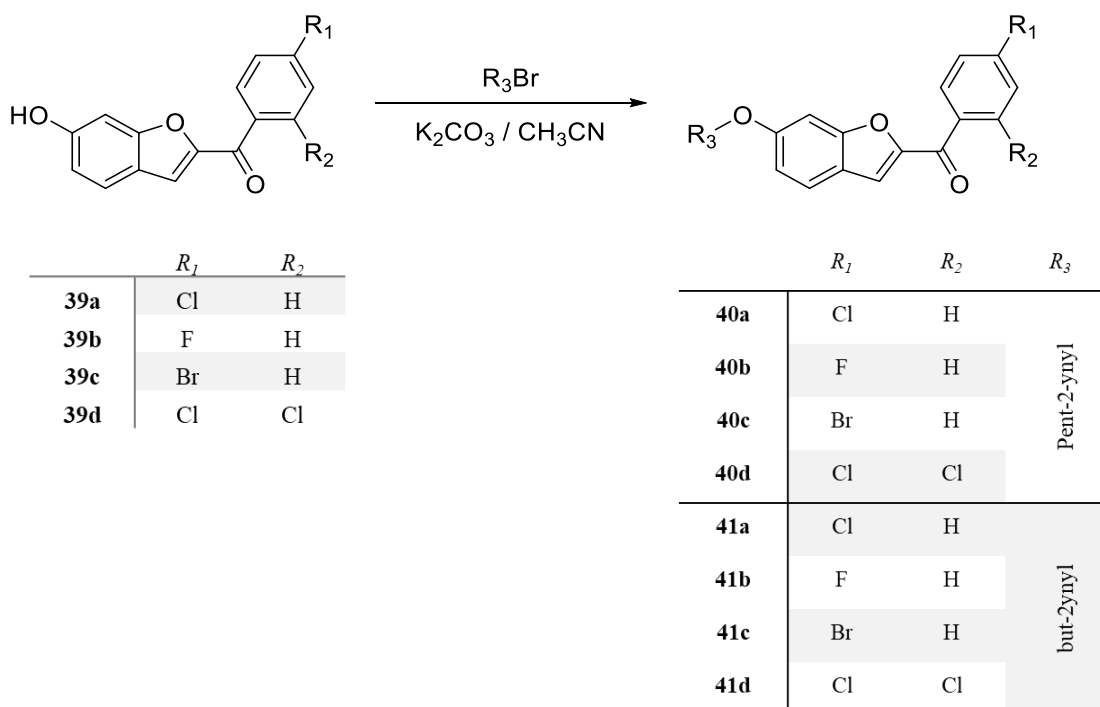
	R_1	R_2
39a	Cl	H
39b	F	H
39c	Br	H
39d	Cl	Cl

	R_1	R_2	R_3
40a	Cl	H	Pent-2-ynyl
40b	F	H	Pent-2-ynyl
40c	Br	H	Pent-2-ynyl
40d	Cl	Cl	Pent-2-ynyl
41a	Cl	H	but-2ynyl
41b	F	H	but-2ynyl
41c	Br	H	but-2ynyl
41d	Cl	Cl	but-2ynyl

The nucleophilic substitution reaction as described earlier in chapter two, where K_2CO_3 acts as a base to deprotonate the acidic phenolic group. ^{1}H and ^{13}C NMR confirmed the identity of the produced white solids by the appearance of the signals representing the alkyne chain in the aliphatic region upfield of the spectrum. The yield for this reaction and the melting points for the products are indicated in **table 3.3**.

Table (3.3): Yield and melting points for compounds **40a-d** and **41a-d**

Compound	Yield	Melting point
40a	35%	106-110 ℃
40b	76%	106-108 ℃
40c	40%	116-118 ℃
40d	75%	Oil
41a	34%	132-134 ℃
41b	61%	162-164 ℃
41c	43%	143-145 ℃
41d	86%	Oil

3.3.2.3.3. Grignard reaction: preparation of (6-(pent-2-yn-1-yloxy)benzofuran-2-yl)(phenyl)(pyridin-3-yl)methanol derivatives (42a-d) and (6-(but-2-yn-1-yloxy)benzofuran-2-yl)(phenyl)(pyridin-3-yl)methanol derivatives (43a-d)

	R_1	R_2	R_3
40a	Cl	H	
40b	F	H	
40c	Br	H	Pent-2-ynyl
40d	Cl	Cl	
41a	Cl	H	
41b	F	H	
41c	Br	H	but-2ynyl
41d	Cl	Cl	

	R1	R2	R3
42a	Cl	H	
42b	F	H	
42c	Br	H	Pent-2-ynyl
42d	Cl	Cl	
43a	Cl	H	
43b	F	H	
43c	Br	H	but-2ynyl
43d	Cl	Cl	
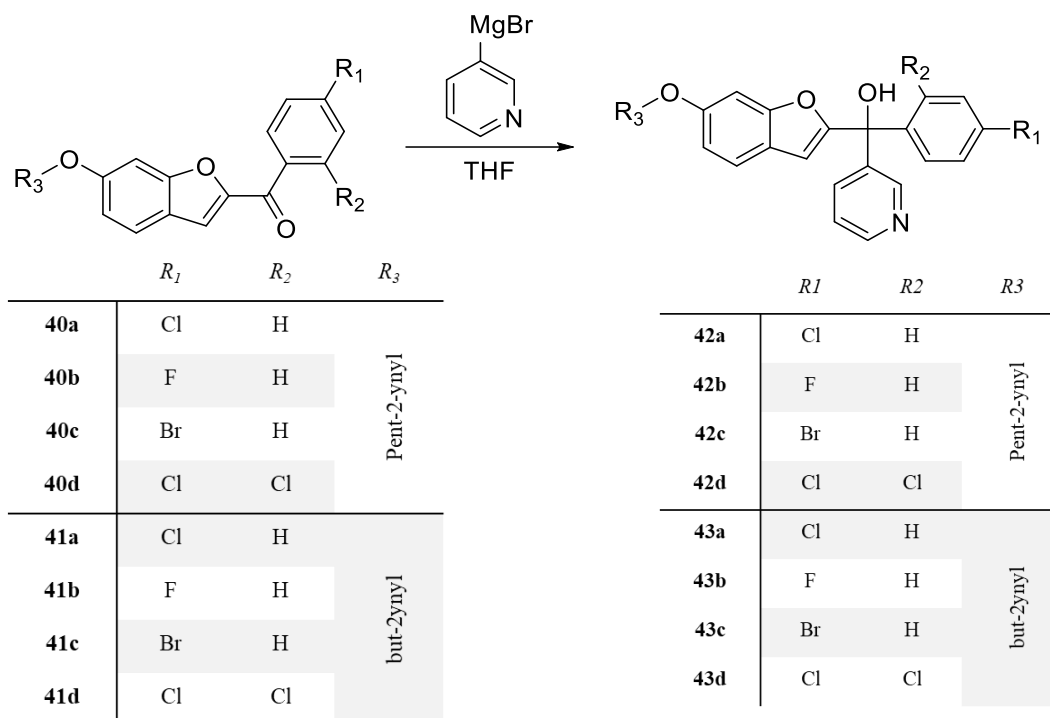
The Grignard reaction (Saberi *et al.* 2006) was performed as described for the preparation of the (6-methoxybenzofuran-2-yl)(phenyl)(pyridin-3-yl)methanol derivatives (**36a-d**). The yield for this reaction is indicated in **table 3.4**.The products were identified by ^{1}H and ^{13}C NMR with the appearance of the signals of the pyridine ring in the aromatic area downfield of the spectrum and a broad singlet corresponding to the tertiary alcohol group.

Table (3.4): Yield for compounds **42a-d** and **43a-d**

Compound	Yield	Compound	Yield
42a	91%	**43a**	94%
42b	20%	**43b**	80%
42c	50%	**43c**	70%
42d	15%	**43d**	34%

3.3.3. Biological evaluation

The twelve prepared compounds were tested for their aromatase inhibitory activity as previously described in chapter 2 at a single concentration (10 nM). Six compounds, namely **36a**, **36c**, **42a**, **42c**, **43a** and **43c**, were selected for more detailed IC_{50} determination (**figure 3.8**).
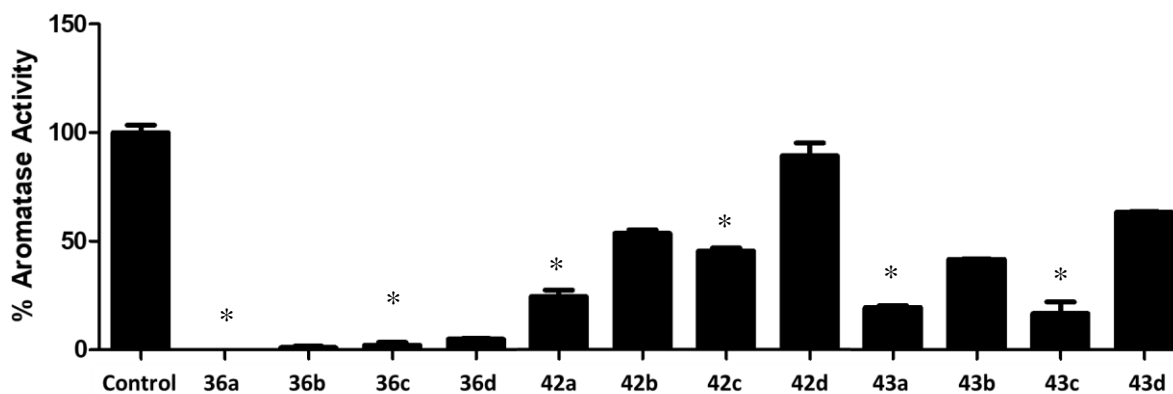
Figure (3.8): Biological results for aromatase activity assay at single concentration (10 nM), compounds selected for IC_{50} indicated by *.

The IC_{50} values indicated in **table 3.5** shows that all compounds except **42c** showed activity at ≤ 1 nM. The methoxy derivatives was generally more potent than the extended compounds with but-2-ynyloxy or pent-2-yn-yloxy groups having the potential of binding the access channel along with the active site. With a chloro group on the phenyl ring, no significant difference was observed between the but-2-ynyloxy (**43a**) or pent-2-ynyloxy (**42a**), however with a bromo group, compound **43c** with a but-2-ynloxy group proved to be better than the pent-2-ynyloxy analogue (**42c**). These results suggest that variation in inhibitory activity could be subjected to size limitations.

Table (3.5): IC$_{50}$ values for the selected compounds (**36a, 36c, 42a, 42c, 43a and 43c**)

Compound	IC$_{50}$ (nM)	95% Confidence interval (nM)	R$_1$	R$_2$	
36a	0.46	0.375 - 0.567	OCH$_3$	Cl	
36c	0.40	0.352 - 0.456	OCH$_3$	Br	
42a	0.92	0.744 - 1.133	Pent-2-ynyloxy	Cl	
42c	4.9	4.093 - 5.971	Pent-2-ynyloxy	Br	
43a	1.05	0.763 - 1.446	But-2-ynyloxy	Cl	
43c	0.83	0.665 - 1.038	But-2-ynyloxy	Br	

Examples of the compounds, namely **36a, 36c, 42a, 42c, 43a, 43c,** and **43d**, were tested at 1 µM over 48 hours along with doxorubicin as positive control by BrdU proliferation assay to evaluate the toxicity against non-oestrogen dependent cells (MDA-MB-231). Statistics using one-way ANOVA followed by a Tukey's Multiple Comparison test comparing all compounds against control showed no significant difference between the tested compounds and the negative control indicating that the compounds had no impact on MDA-MB-231 growth (**Figure 3.9**). These results suggest possible limited off-target effects.
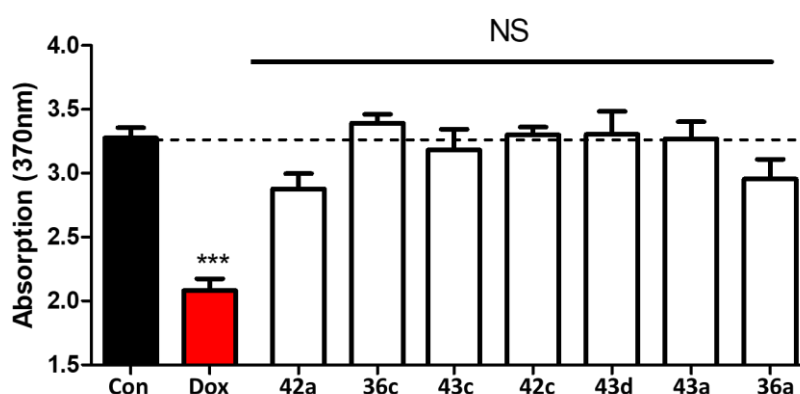
Figure (3.9): Toxicity of pyridine compounds tested at 1 µM for 48 hours treatment followed by BrdU proliferation assay. Stats are one-way ANOVA followed by a Tukey's Multiple Comparison test comparing all compounds against control. Data represents n = 6 technical replicates ± SEM. *** $p < 0.001$ compared to control. NS – Non-significant compared to control.

3.4. Conclusion and future work

Studying the CYP19A1 crystal structure (PDB 3S79) (Ghosh *et al.* 2012) and the binding interactions of the natural substrate showed that hydrogen bonds for the 3- and 17-keto oxygen with Asp309 and Met374 respectively are key ligand interactions along with the other hydrophobic interactions of the ligand with the boundaries of the active site constituted by other residues including Arg115, Ile133, Phe134, Val370, Val373 and Leu477. Docking studies using MOE generated ligand-protein complexes that showed a good fit within the active site pocket. More interestingly, the long chain substitutions with but-2-ynyloxy or pent-2-ynyloxy groups on either the benzofuran or phenyl side were able to theoretically fit in the access channel of the active site, which is lined with Arg192, Val313 and Glu483. MD simulations for the generated complexes showed that generally the 6-position of the benzofuran ring was optimal for long chain substitution to target the access channel. Also, the *S*-enantiomer of the compounds showed better binding than the *R*-enantiomer in terms of binding to the haem through the nitrogen of the pyridine ring.

Synthetic pathways were developed for the designed compounds and modified when needed. Synthesis of class 1 compounds with simple changing of the secondary substituent on the phenyl ring of the parent compounds (**36a, b**) was found to be successful providing four final compounds (**36a-d**). Synthesis of class 2 compounds with the long chain substitutions (but-2-ynyloxy and pent-2-ynyloxy) on the benzofuran ring was found to be more challenging than their triazole analogues prepared in chapter 2 due to the presence of the pyridine ring which complicated the last step with complex multiple substitution products. This required a less divergent synthetic pathway that was successful in all the steps in varying yields, providing the required compounds (**42** and **43**).

Twelve final compounds were successfully prepared, fully characterised and evaluated for aromatase inhibitory activity, which was in nanomolar range for all 12 compounds. Compounds with bromo or chloro substituents were found to be more active than their fluoro or dichloro analogues. Pyridine-based compounds proved to have the dual binding potential, however the results suggest a size limitation for compound **42c** with 4-bromophenyl and pent-2-ynyloxy groups. Compounds **42a** (4-chlorophenyl/pent-2-ynyloxy) and **43c** (4-bromophenyl/but-2-ynyloxy) were found to be of adequate size and low nanomolar IC_{50} values.

❖ **Future work:**

1. Representative examples of the compounds will be tested for selectivity (CYP panel e.g. 1A2, 2C9, 2C19, 2D6 and 3A4).

2. Aromatase inhibitors that 'pass' these assays will be subject to more detailed cell/molecular biology investigations to determine the antiproliferative activity (using aromatase-transfected breast cancer cell line MCF7-AROM (Macaulay *et al.* 1994)).

3. Resistant cell lines for known AIs based on MCF7-AROM will be developed and the compounds evaluated against these resistant cell lines to determine whether they are effective against the resistant cell lines of clinically used AIs.

4. Resistance for the synthesised compounds will be studied to identify the course and mechanism of resistance (if any).

3.5. Experimental

3.5.1. General considerations:

As previously described in section 2.5.1

3.5.2. Computational studies

As previously described in section 2.5.2

3.5.3. Chemistry

3.5.3.1. (4-Bromophenyl)(6-methoxybenzofuran-2-yl)methanone (3f)

Chemical Formula: $C_{16}H_{11}BrO_3$, Molecular Weight: 331.17
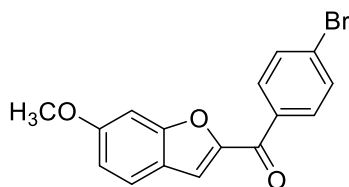
Prepared following the general procedure for the synthesis of benzofuran-2-yl(phenyl)methanone derivatives (**3a-e**) in chapter 2, using 2-hydroxy-4-methoxybenzaldehyde (**1a**) (0.5 g, 3.28 mmol) and 2,4′-dibromoacetophenone (**2e**) (0.91 g, 3.28 mmol) to provide the product as a white solid. Yield = 0.8 g (74%).

Melting Point: 206-208 ºC (lit. m.p. = 176-178 ºC) (Meshram *et al.* 2012)

TLC: Petroleum ether – EtOAc 3:1 v/v, R_f = 0.75

¹H NMR (CDCl₃) δ: 7.84 (d, *J* = 8.6 Hz, 2H, Ar), 8.60 (d, *J* = 8.6 Hz, 2H, Ar), 7.52 (d, *J* = 8.7 Hz, 1H, Ar), 7.40 (d, *J* = 0.9 Hz, 1H, Ar), 7.02 (d, *J* = 1.9 Hz, 1H, Ar), 6.91 (dd, *J* = 2.2, 8.7 Hz, 1H, Ar), 3.82 (s, 3H, OCH₃).

¹³C NMR (CDCl₃) δ: 182.60 (C), 161.43 (C), 157.74 (C), 151.65 (C), 136.20 (C), 131.81 (2 x CH), 130.88 (2 x CH), 127.70 (C), 123.72 (CH), 120.28 (C), 117.31 (CH), 114.75 (CH), 95.60 (CH), 55.78 (CH₃).

3.5.3.2. (2,4-Dichlorophenyl)(6-methoxybenzofuran-2-yl)methanone (3g)

Chemical Formula: C₁₆H₁₀Cl₂O₃, Molecular Weight: 321.15
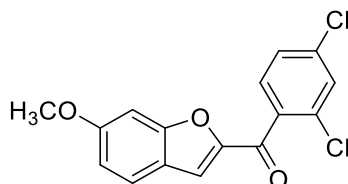
Prepared following the general procedure for the synthesis of benzofuran-2-yl(phenyl)methanone derivatives (**3a-e**) in chapter 2, using 2-hydroxy-4-methoxybenzaldehyde (**1a**) (0.5 g, 3.28 mmol) and 2-bromo-2,4′-diçhloroacetophenone (**2f**) (0.87 g, 3.28 mmol) to provide the product as a white solid. Yield = 0.93 g (88%).

Melting Point: 156 -158 ºC

TLC: Petroleum ether – EtOAc 3:1 v/v, R_f = 0.6

¹H NMR (CDCl₃) δ: 7.57 (d, *J* = 8.7 Hz, 1H, Ar), 7.54 (d, *J* = 1.9 Hz, 1H, Ar), 7.50 (d, *J* = 8.2 Hz, 1H, Ar), 7.40 (dd, *J* = 1.9, 8.2 Hz, 1H, Ar), 7.30 (d, *J* = 0.9 Hz, 1H, Ar), 7.08 (d, *J* = 1.8 Hz, 1H, Ar), 6.99 (dd, *J* = 2.4, 8.7 Hz, 1H, Ar), 3.90 (s, 3H, OCH₃).

¹³C NMR (CDCl₃) δ: 182.00 (C), 161.85 (C), 158.24 (C), 151.37 (C), 137.13 (C), 136.00 (C), 132.90 (C), 130.28 (2 x CH), 127.02 (CH), 123.95 (CH), 120.30 (C), 118.52 (CH), 115.04 (CH), 95.55 (CH), 55.80 (CH₃).

HPLC (method A): 98.15 % at R.T.= 4.90 min.

HRMS (ESI): Calculated 321.0085 [M+H]⁺, Found 321.0079 [M+H]⁺.

3.5.3.3.General procedure for the synthesis of pyridine-3-yl magnesium bromide (Grignard reagent) (35)

To a suspension of dry Mg turnings (0.83 g, 34mmol) in THF (34 mL) was added a few crystals of I_2 followed by 3-bromo pyridine (**34**) (3.3 mL, 34 mmol). The reaction mixture was heated at 70 °C for 5 h to produce the required pyridin-3-yl magnesium bromide (**35**), which was used immediately without any further characterisation.

3.5.3.4.General procedure for the synthesis of (6-methoxybenzofuran-2-yl)(phenyl)(pyridin-3-yl)methanol derivatives (36a-d) (Saberi *et al.* 2006)

(3)   (36)
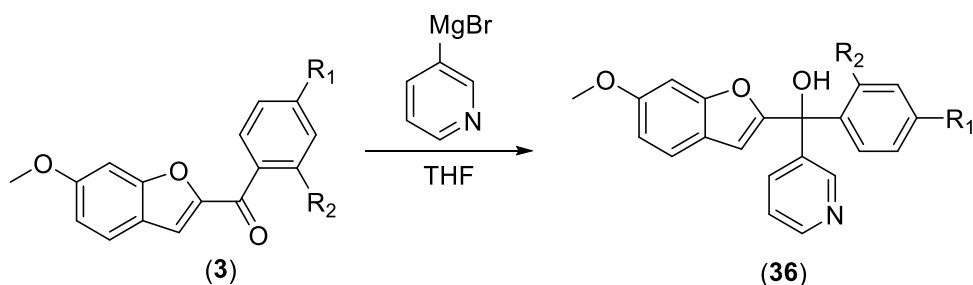
To a solution of (6-methoxybenzofuran-2-yl)(phenyl)methanone derivatives (**3a, d, f, g**) (1 m.eq.) in THF (10 mL/mmol) was added pyridin-3-yl magnesium bromide (**35**) (7 m.eq.). The reaction mixture was heated at 70 °C overnight. The reaction mixture was then concentrated under vacuum. The residue was dissolved in H_2O (50 mL) and extracted with EtOAc (2 x 100 mL). The combined organic layer was dried (MgSO4) and concentrated under vacuum. The product was purified by gradient column chromatography to give (6-methoxybenzofuran-2-yl)(phenyl)(pyridin-3-yl)methanol (**36a-d**) at 60% EtOAc in petroleum ether (v/v) as a colourless or white oil.

3.5.3.4.1.   (4-Chloroophenyl)(6-methoxybenzofuran-2-yl)(pyridin-3-yl)methanol (36a) (Saberi *et al.* 2006)

Chemical Formula: $C_{21}H_{16}ClNO_3$, Molecular Weight: 365.81
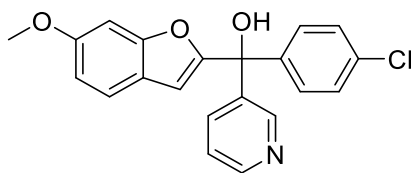
Yield: 0.5 g (92%)

TLC: Petroleum ether – EtOAc 1:1 v/v, R_f = 0.4

¹H NMR (CDCl₃) δ: 8.57 (d, J = 1.7 Hz, 1H, Ar), 8.52 (d, J = 4.7 Hz, 1H, Ar), 7.78 (dt, J = 2.15, 8.1 Hz, 1H, Ar), 7.38 (d, J = 8.6 Hz, 1H, Ar), 7.34 (m, 5H, Ar), 6.96 (d, J = 2.0 Hz, 1H, Ar), 6.90 (dd, J = 2.3, 8.6 Hz, 1H, Ar), 6.27 (d, J = 0.8 Hz, 1H, Ar), 3.84 (s, 3H, OCH₃), 2.37 (bs, 1H, OH).

¹³C NMR (CDCl₃) δ: 158.42 (C), 157.61 (C), 156.28 (C), 148.32 (CH), 148.11 (CH), 141.89 (C), 139.97 (C), 135.55 (CH), 134.22 (C), 128.67 (2 x CH), 128.51 (2 x CH), 123.21 (CH), 121.58 (CH), 120.69 (C), 112.37 (CH), 106.82 (CH), 96.04 (CH), 76.51 (C), 55.72 (CH₃).

HPLC (method A): 100 % at R.T.= 4.73 min.

HRMS (ESI): Calculated 366.0896 [M+H]⁺, Found 366.0891 [M+H]⁺.

3.5.3.4.2. (4-Fluorophenyl)(6-methoxybenzofuran-2-yl)(pyridin-3-yl)methanol (36b) (Saberi *et al.* 2006)

Chemical Formula: $C_{21}H_{16}FNO_3$, Molecular Weight: 349.36
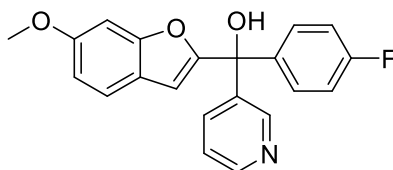
Yield: 0.2 g (83%)

TLC: Petroleum ether – EtOAc 1:1 v/v, R_f = 0.42

¹H NMR (DMSO-*d₆*) δ: 8.52 (m, 2H, Ar), 7.71 (m, 1H, Ar), 7.49 (d, J = 8.6 1H, Ar), 7.41 (m, 3H, Ar), 7.21 (m, 3H, Ar), 7.16 (bs, 1H, OH), 6.88 (dd, J = 2.3, 8.6 Hz, 1H, Ar), 6.47 (d, J = 0.9 Hz, 1H, Ar), 3.77 (s, 3H, OCH₃).

¹³C NMR (DMSO-*d₆*) δ: 162.86 (d, $^1J_{C,F}$ = 243.75 Hz, C), 156.63 (C), 158.23 (C), 156.17 (C), 148.93 (CH), 148.61 (CH), 141.22 (d, $^4J_{C,F}$ = 2.5 Hz, C), 141.00 (C), 135.00 (CH), 129.52 (d, $^3J_{C,F}$ = 8.75 Hz, 2 x CH), 123.56 (CH), 122.05 (CH), 120.96 (C), 115.36 (d, $^2J_{C,F}$ = 21.25 Hz, 2 x CH), 112.50 (CH), 106.10 (CH), 96.44 (CH), 75.86 (C), 56.02 (CH₃).

HPLC (method A): 100 % at R.T.= 4.61 min.

HRMS (ESI): Calculated 350.1187 [M+H]⁺, Found 350.1189 [M+H]⁺.

3.5.3.4.3. (4-Bromophenyl)(6-methoxybenzofuran-2-yl)(pyridin-3-yl)methanol (36c)

Chemical Formula: $C_{21}H_{16}BrNO_3$, Molecular Weight: 410.27
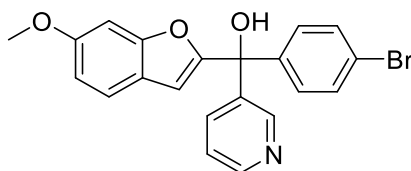
Yield: 0.13 g (25%)

TLC: Petroleum ether – EtOAc 1:1 v/v, R_f = 0.47

^{1}H NMR (DMSO-$d6$) δ: 8.52 (m, 2H, Ar), 7.71 (m, 1H, Ar), 7.58 (d, J = 8.7 Hz, 2H, Ar), 7.49 (d, J = 8.5 Hz, 1H, Ar), 7.41 (m, 1H, Ar), 7.30 (d, J = 8.7 Hz, 2H, Ar), 7.16 (m, 2H, Ar + OH), 6.88 (dd, J = 2.3, 8.5 Hz, 1H, Ar), 6.48 (d, J = 0.9 Hz, 1H, Ar), 3.77 (s, 3H, OCH$_3$).

^{13}C NMR (DMSO-$d6$) δ: 159.26 (C), 158.26 (C), 156.18 (C), 149.01 (CH), 148.58 (CH), 144.38 (C), 140.71 (C), 135.01 (CH), 131.46 (2 x CH), 129.63 (2 x CH), 123.60 (CH), 122.08 (CH), 121.36 (C), 120.94 (C), 112.53 (CH), 106.25 (CH), 96.44 (CH), 75.92 (C), 56.03 (CH$_3$).

HPLC (method A): 98.93 % at R.T.= 4.76 min.

HRMS (ESI): Calculated 410.0391 [M+H]$^+$, Found 410.0387 [M+H]$^+$.

3.5.3.4.4. (2,4-Dichlorophenyl)(6-methoxybenzofuran-2-yl)(pyridin-3-yl)methanol (36d)

Chemical Formula: $C_{21}H_{15}Cl_2NO_3$, Molecular Weight: 400.26
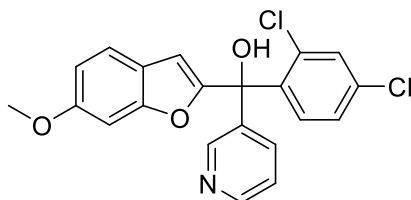
Yield: 0.18 (32%)

TLC: Petroleum ether – EtOAc 1:1 v/v, R_f = 0.5

^{1}H NMR (CDCl$_3$) δ: 8.49 (m, 2H, Ar), 7.69 (m, 1H, Ar), 7.34 (d, J = 2.1 Hz, 1H, Ar), 7.30 (d, J = 8.6 Hz, 1H, Ar), 7.23 (m, 1H, Ar), 7.14 (dd, J = 2.1, 8.5 Hz, 1H, Ar), 7.01 (d, J = 8.5

Hz, 1H, Ar), 6.91 (d, *J* = 2.1 Hz, 1H, Ar), 6.81 (dd, *J* = 2.3, 8.6 Hz, 1H, Ar), 6.22 (d, *J* = 0.9 Hz, 1H, Ar), 4.39 (bs, 1H, OH), 3.75 (s, 3H, OCH$_3$).

^{13}C NMR (CDCl$_3$) δ: 158.42 (C), 156.35 (C), 156.19 (C), 148.99 (CH), 148.56 (CH), 139.06 (C), 138.38 (C), 135.21 (C), 134.82 (CH), 133.89 (C), 131.43 (CH), 131.09 (CH), 127.02 (CH), 123.02 (CH), 121.63 (CH), 120.76 (C), 112.48 (CH), 106.99 (CH), 96.09 (CH), 77.18 (C), 55.72 (CH$_3$).

HPLC (method A): 100 % at R.T.= 4.78 min.

HRMS (ESI): Calculated 422.0326 [M+Na]$^+$, Found 422.0313 [M+Na]$^+$.

3.5.3.5.(4-Bromophenyl)(6-((tetrahydro-2*H*-pyran-2-yl)oxy)benzofuran-2-yl)methanone (9e)

Chemical Formula: C$_{20}$H$_{17}$BrO$_4$, Molecular Weight: 401.26
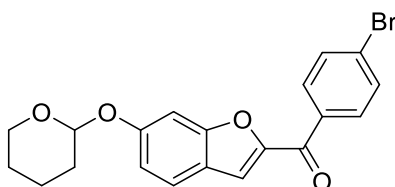
Prepared as described for (**3a-e**) in chapter 2, using 2-hydroxy-4-((tetrahydro-2*H*-pyran-2-yl)oxy) benzaldehyde (**8a**) (0.64 g, 2.88 mmol) and 2, 4′-dibromoacetophenone (**2e**) (0.8 g, 2.88 mmol). The formed solid was purified by recrystallisation from ethanol to afford (4-bromophenyl)(6-((tetrahydro-2*H*-pyran-2-yl)oxy)benzofuran-2-yl)methanone (**9e**) as a white solid. Yield = 1 g (86%).

Melting Point: 180-184 ºC.

TLC: Petroleum ether – EtOAc 3:1 v/v, R$_f$ = 0.67

^{1}H NMR (CDCl$_3$) δ: 7.85 (d, *J* = 8.5 Hz, 2H, Ar), 7.60 (d, *J* = 8.5 Hz, 2H, Ar), 7.52 (d, J = 8.6 Hz, 1H, Ar), 7.41 (d, *J* = 0.85 Hz, 1H, Ar), 7.26 (s, 1H, Ar), 7.01 (dd, *J* = 2.1, 8.6 Hz, 1H, Ar), 5.42 (t, *J* = 3.2 Hz, 1H, CH-pyran), 3.85 (m, 1H, CH$_2$-pyran), 3.58 (m, 1H, CH$_2$-pyran), 1.95 (m, 3H, CH$_2$-pyran), 1.66 (m, 3H, CH$_2$-pyran).

^{13}C NMR (CDCl$_3$) δ: 182.71 (C), 158.62 (C), 157.47 (C), 151.91 (C), 136.10 (C), 131.82 (2 x CH), 130.96 (2 x CH), 127.80 (C), 123.57 (CH), 121.03 (C), 117.16 (CH), 115.72 (CH), 99.34 (CH), 96.95 (CH), 62.22 (CH$_2$), 30.24 (CH$_2$), 25.08 (CH$_2$), 18.71 (CH$_2$).

HPLC (method A): 100 % at R.T.= 5.17 min.

HRMS (ESI): Calculated 401.0382 [M+H]$^+$, Found 401.0388 [M+H]$^+$.

3.5.3.6.(2,4-Dichlorophenyl)(6-((tetrahydro-2*H*-pyran-2-yl)oxy)benzofuran-2-yl)methanone (9f)

Chemical Formula: $C_{20}H_{16}Cl_2O_4$, Molecular Weight: 391.24
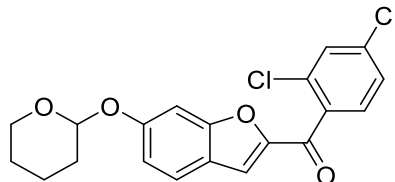
Prepared as described for (**3a-e**) in chapter 2, using 2-hydroxy-4-((tetrahydro-2*H*-pyran-2-yl)oxy) benzaldehyde (**8a**) (0.64 g, 2.88 mmol) and 2-bromo-2′,4′-dichloroacetophenone (**2f**) (0.77 g, 2.88 mmol). The formed solid was purified by recrystallisation from ethanol to afford (2,4-dichlorophenyl)(6-((tetrahydro-2*H*-pyran-2-yl)oxy)benzofuran-2-yl)methanone (**9f**) as yellow crystals. Yield = 0.95 g (85%).

Melting Point: 118-122 ℃

TLC: Petroleum ether – EtOAc 3:1 v/v, R_f = 0.7

¹H NMR (CDCl₃) δ: 7.58 (d, *J* = 8.7 Hz, 1H, Ar), 7.54 (d, *J* = 1.9 Hz, 1H, Ar), 7.49 (d, *J* = 8.2 Hz, 1H, Ar), 7.40 (dd, *J* = 1.9, 8.2 Hz, 1H, Ar), 7.33 (d, *J* = 1.9 Hz, 1H, Ar), 7.30 (d, *J* = 0.9 Hz, 1H, Ar), 7.09 (dd, *J* = 2.1, 8.7 Hz, 1H, Ar), 5.51 (t, *J* = 3.2 Hz, 1H, CH-pyran), 3.93 (m, 1H, CH₂-pyran), 3.66 (m, 1H, CH₂-pyran), 2.036 (m, 1H, CH₂-pyran), 1.93 (m, 2H, CH₂-pyran), 1.75 (m, 3H, CH₂-pyran).

¹³C NMR (CDCl₃) δ: 182.14 (C), 159.03 (C), 157.95 (C), 151.56 (C), 137.15 (C), 135.98 (C), 132.92 (C), 130.29 (CH), 127.01 (CH), 123.80 (CH), 121.03 (C), 118.34 (CH), 115.88 (CH), 99.35 (CH), 96.91 (CH), 62.19 (CH₂), 30.19 (CH₂), 25.05 (CH₂), 18.67 (CH₂).

3.5.3.7.(4-Chlorophenyl)(pyridin-3-yl)(6-((tetrahydro-2*H*-pyran-2-yl)oxy)benzofuran-2-yl)methanol (37)

Chemical Formula: $C_{25}H_{22}ClNO_4$, Molecular Weight: 435.90
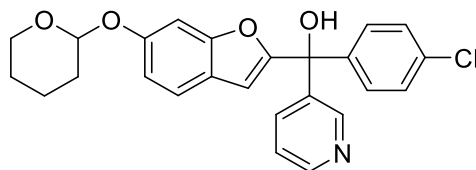
Prepared as described for (**36a-d**) using (4-chlorophenyl)(6-((tetrahydro-2*H*-pyran-2-yl)oxy)benzofuran-2-yl)methanone (**9a**) (1.22 g, 3.4 mmol). The product was purified by gradient column chromatography to give (6-methoxybenzofuran-2-yl)(phenyl)(pyridin-3-yl)methanol (**37**) at 70% EtOAc in petroleum ether (v/v) as a yellow oil. Yield = 0.47 g (31%).

TLC: Petroleum ether – EtOAc 1:1 v/v, R_f = 0.55

¹H NMR (DMSO-*d6*) δ: : 8.51 (m, 2H, Ar), 7.70 (d, *J* = 8.0 Hz, 1H, Ar), 7.50 (d, *J* = 8.5 Hz, 1H, Ar), 7.45 (d, *J* = 8.6, 2H, Ar), 7.41 (m, 1H, Ar), 7.36 (d, *J* = 8.6 Hz, 2H, Ar), 7.21 (s, 1H, Ar), 7.1614 (bs, ex, 1H, OH), 6.96 (dd, *J* = 2.1, 8.5 Hz, 1H, Ar), 6.49 (d, *J* = 4.3 Hz, 1H, Ar), 3.76 (m, 1H, CH_2-pyran), 3.56 (m, 1H, CH_2-pyran), 1.86 (m, 3H, CH_2-pyran), 1.59 (m, 3H, CH_2-pyran).

¹³C NMR (DMSO-*d6*) δ: 159.64 (C), 155.77 (C), 155.11 (C), 149.01 (CH), 148.45 (CH), 143.75 (C), 140.66 (C), 135.10 (CH), 132.80 (C), 129.25 (2 x CH), 128.57 (2 x CH), 123.70 (CH), 122.04 (CH), 121.94 (C), 114.25 (CH), 106.26 (CH), 99.71 (CH), 96.86 (CH), 75.79 (C), 62.11 (CH_2), 30.29 (CH_2), 25.11 (CH_2), 19.11 (CH_2).

3.5.3.8. Deprotection of (4-chlorophenyl)(pyridin-3-yl)(6-((tetrahydro-2*H*-pyran-2-yl)oxy)benzofuran-2-yl)methanol (37)
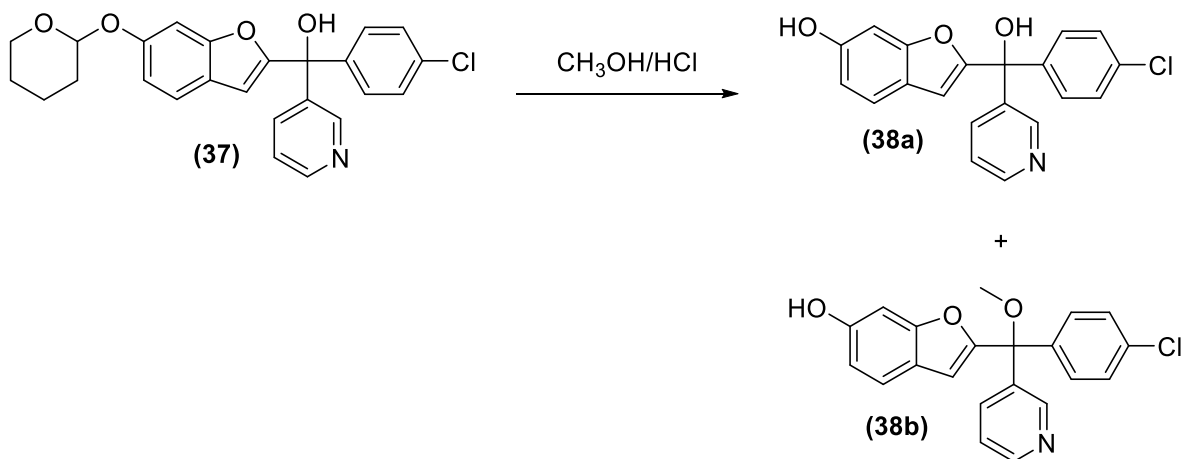
To a solution of (6-methoxybenzofuran-2-yl)(phenyl)(pyridin-3-yl)methanol (**37**) (0.47 g, 1.07 mmol)) in methanol (4 mL), conc. HCl (1 mL) was added and the reaction stirred for 1 h at room temperature. The reaction mixture was concentrated under reduced pressure. The residue neutralised by $NaHCO_3$ and extracted with EtOAc (2 x 100 mL). The combined organic layer was dried ($MgSO_4$) and concentrated under reduced pressure. Purification by gradient column

chromatography afforded 2-((4-chlorophenyl)(methoxy)(pyridin-3-yl)methyl)benzofuran-6-ol (**38b**) at 60% EtOAc in petroleum ether (v/v) as a yellow oil. Yield = 0.15 g (39%) and 2-((4-chlorophenyl)(hydroxy)(pyridin-3-yl)methyl)benzofuran-6-ol (**38a**) at 70% EtOAc in petroleum ether (v/v) as a yellow oil. Yield = 0.1 g (37%).

3.5.3.8.1. 2-((4-Chlorophenyl)(hydroxy)(pyridin-3-yl)methyl)benzofuran-6-ol (38a)

Chemical Formula: $C_{20}H_{14}ClNO_3$, Molecular Weight: 351.79

TLC: Petroleum ether – EtOAc 1:1 v/v, R_f = 0.35

¹H NMR (DMSO-*d6*) δ: : 9.56 (bs, 1H, OH), 8.51 (m, 2H, Ar), 7.69 (dt, *J* = 1.8, 8.0 Hz, 1H, Ar), 7.44 (d, *J* = 8.6 Hz, 2H, Ar), 7.40 (m, 2H, Ar), 7.35 (d, *J* = 8.6 Hz, 2H, Ar), 7.10 (bs, ex, 1H, OH), 6.85 (s, 1H, Ar), 6.73 (dd, *J* = 2.1, 8.4 Hz, 1H, Ar), 6.36 (s, 1H, Ar).

¹³C NMR (DMSO-*d6*) δ: 158.47 (C), 156.26 (C), 155.99 (C), 148.95 (CH), 148.44 (CH), 143.86 (C), 140.76 (C), 135.08 (CH), 132.73 (C), 129.24 (2 x CH), 128.52 (2 x CH), 123.66 (CH), 122.07 (CH), 119.80 (C), 112.72 (CH), 106.40 (CH), 97.97 (CH), 75.74 (C).

3.5.3.8.2. 2-((4-Chlorophenyl)(methoxy)(pyridin-3-yl)methyl)benzofuran-6-ol (38b)

Chemical Formula: $C_{21}H_{16}ClNO_3$, Molecular Weight: 365.81

TLC: Petroleum ether – EtOAc 1:1 v/v, R_f = 0.5

¹H NMR (DMSO-*d6*) δ: : 9.65 (bs, 1H, OH), 8.61 (d, *J* = 1.8 Hz, 1H, Ar), 8.52 (dd, *J* = 1.6, 4.7 Hz, 1H, Ar), 7.80 (m, 1H, Ar), 7.45 (m, 6H, Ar), 6.88 (d, *J* = 1.6, 1H, Ar), 6.77 (dd, *J* = 2.1, 8.4 Hz, 1H, Ar), 6.72 (d, *J* = 0.75 Hz, 1H, Ar), 3.18 (s, 3H, CH₃).

¹³C NMR (DMSO-*d6*) δ: 156.45 (C), 156.36 (C), 154.25 (C), 149.14 (CH), 148.45 (CH), 141.26 (C), 138.53 (C), 135.21 (CH), 132.97 (C), 129.40 (2 x CH), 128.90 (2 x CH), 123.90 (CH), 122.39 (CH), 119.51 (C), 113.03 (CH), 109.88 (CH), 97.99 (CH), 81.95 (C), 52.96 (CH₃).

3.5.3.9.General procedure for the synthesis of (6-hydroxybenzofura-2-yl)(phenyl)methanone derivatives (39a-d)
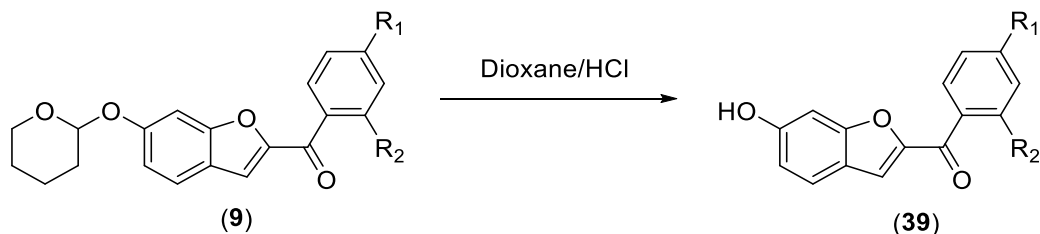
To a solution of (6-((tetrahydro-2*H*-pyran-2-yl)oxy)benzofuran-2-yl)(phenyl)methanone (**9a,c,e,f**) in dioxane (4 mL), conc. HCl (1 mL) was added and the reaction stirred for 1 h at room temperature. The reaction mixture was then concentrated under reduced pressure and the residue washed with CH₂Cl₂ to afford (6-hydroxybenzofura-2-yl)(phenyl)methanone derivatives (**39a, b, c, d**).

3.5.3.9.1. (4-Chlorophenyl)(6-hydroxybenzofura-2-yl)methanone (39a)

Chemical Formula: $C_{15}H_9ClO_3$, Molecular Weight: 272.68
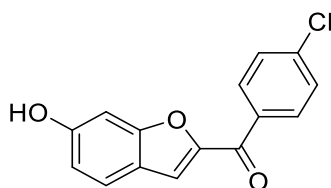
Yield: 0.52 g (64%), white solid.

Melting Point: 208-210 ℃ (lit. m.p. = 222-224 ℃) (Meshram *et al.* 2012)

TLC: Petroleum ether – EtOAc 3:1 v/v, R_f = 0.325

¹H NMR (DMSO-*d6*) δ: 10.26 (bs, 1H, OH), 7.98 (d, *J* = 8.6 Hz, 2H, Ar), 7.71 (d, *J* = 0.9 Hz, 1H, Ar), 7.66 (m, 3H), 7.04 (d, *J* = 1.1 Hz, 1H, Ar), 6.92 (dd, *J* = 2.1, 8.6 Hz, 1H, Ar).

¹³C NMR (DMSO-*d6*) δ: 182.04 (C), 159.99 (C), 157.77 (C), 150.71 (C), 138.03 (C), 136.28 (C), 131.30 (2 x CH), 129.26 (2 x CH), 125.00 (CH), 119.49 (C), 119.01 (CH), 115.24 (CH), 97.92 (CH).

3.5.3.9.2. (4-Fluorophenyl)(6-hydroxybenzofura-2-yl)methanone (39b)

Chemical Formula: $C_{15}H_9FO_3$, Molecular Weight: 256.23
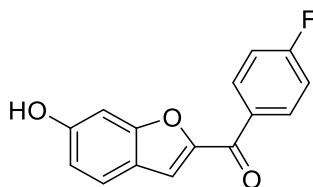
Yield: 0.39 g (66%), white solid.

Melting Point: 196-198 ºC.

TLC: Petroleum ether – EtOAc 3:1 v/v, $R_f = 0.3$

¹H NMR (DMSO-*d6*) δ: 10.23 (bs, 1H, OH), 8.06 (dd, *J* = 5.5, 8.8 Hz, 2H, Ar), 7.69 (d, *J* = 0.8 Hz, 1H, Ar), 7.65 (d, *J* = 8.6 Hz, 1H, Ar), 7.43 (t, *J* = 8.8 Hz, 2H, Ar), 7.03 (s, 1H, Ar), 6.91 (dd, *J* = 2.1, 8.6 Hz, 1H, Ar).

¹³C NMR (DMSO-*d6*) δ: 181.78 (C), 166.16 (d, $^1J_{C,F}$ = 250 Hz, C), 159.91 (C), 157.70 (C), 150.84 (C), 134.23 (d, $^4J_{C,F}$ = 3.75 Hz, C), 132.37(d, $^3J_{C,F}$ = 10 Hz, 2 x CH), 124.89 (CH), 119.49 (C), 118.70 (CH), 116.29 (d, $^2J_{C,F}$ = 21.25 Hz, 2 x CH), 115.17 (CH), 97.95 (CH).

HPLC (method A): 89.79 % at R.T.= 4.96 min.

HRMS (ESI): Calculated 279.0433 [M+Na]⁺, Found 279.0428 [M+Na]⁺.

3.5.3.9.3. (4-Bromophenyl)(6-hydroxybenzofura-2-yl)methanone (39c)

Chemical Formula: $C_{15}H_9BrO_3$, Molecular Weight: 317.14
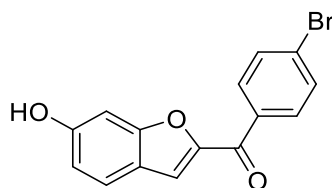
Yield: 0.56 g (71%), white solid.

Melting Point (ºC): 202-206 ºC (lit. m.p. = 212-214 ºC) (Meshram *et al.* 2012)

TLC: Petroleum ether – EtOAc 3:1 v/v, $R_f = 0.32$

¹H NMR (DMSO-*d6*) δ: 10.26 (bs, 1H, OH), 7.89 (d, *J* = 8.6 Hz, 2H, Ar), 7.80 (d, *J* = 8.6 Hz, 2H, Ar), 7.70 (d, *J* = 1.0 Hz, 1H, Ar), 7.65 (d, *J* = 8.6 Hz, 1H, Ar), 7.03 (d, *J* = 1.1 Hz, 1H, Ar), 6.91 (dd, *J* = 2.1, 8.6 Hz, 1H, Ar).

^{13}C NMR (DMSO-*d6*) δ: 182.21 (C), 160.01 (C), 157.78 (C), 150.67 (C), 136.62 (C), 132.20 (2 x CH), 131.41 (2 x CH), 127.09 (C), 125.01 (CH), 119.49 (C), 119.05 (CH), 115.25 (CH), 97.91 (CH).

3.5.3.9.4. (2,4-Dichlorophenyl)(6-hydroxybenzofura-2-yl)methanone (39d)

Chemical Formula: $C_{15}H_8Cl_2O_3$, Molecular Weight: 307.13
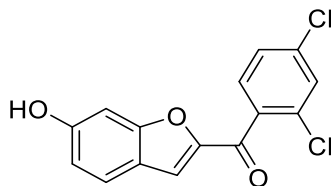
Yield: 0.49 g (66%), yellow solid.

Melting Point: 192-194 ºC

TLC: Petroleum ether – EtOAc 3:1 v/v, R_f = 0.35

^{1}H NMR (DMSO-*d6*) δ: 10.35 (bs, 1H, OH), 7.83 (d, *J* = 1.9 Hz, 1H, Ar), 7.72 (d, *J* = 8.2 Hz, 1H, Ar), 7.62 (m, 2H), 7.51 (d, *J* = 1.0 Hz, 1H, Ar), 7.02 (m, 1H, Ar), 6.90 (dd, *J* = 2.0, 8.6 Hz, 1H, Ar).

^{13}C NMR (DMSO-*d6*) δ: 181.40 (C), 160.55 (C), 158.32 (C), 150.67 (C), 136.60 (C), 136.32 (C), 131.95 (C), 131.30 (CH), 130.09 (CH), 128.01 (CH), 125.25 (CH), 120.65 (CH), 119.47 (C), 115.52 (CH), 97.95 (CH).

HPLC (method A): 100 % at R.T.= 4.72 min.

HRMS (ESI): Calculated 306.9928 [M+H]$^+$, Found 306.9924 [M+H]$^+$.

3.5.3.10. General procedure for the synthesis of (6-(pent-2-yn-1-yloxy)benzofuran-2-yl)(phenyl)methanone derivatives (40a-d)
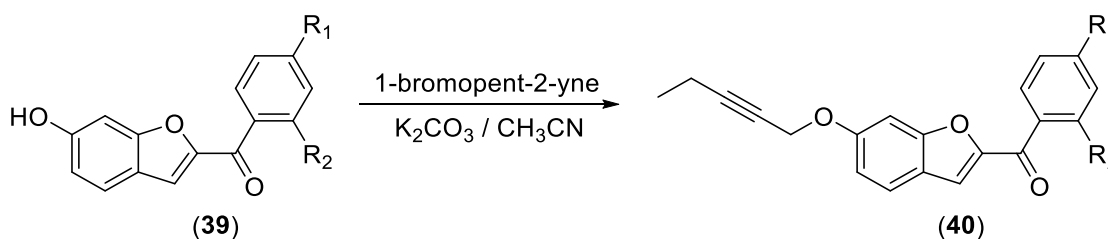
To a solution of (6-hydroxybenzofura-2-yl)(phenyl)methanone derivatives (**39a, b, c, d**)(1 m.eq.) in dry CH_3CN (10 mL/mmol), K_2CO_3 (2.2 m.eq.) was added and the mixture stirred for 1 h at 40 ℃ then 1-bromopent-2-yne (**26**) (2 m.eq.) was added and the reaction mixture stirred at room temperature for 16 h. The reaction mixture was concentrated under reduced pressure and the residue dissolved in EtOAc (100 mL). The organic layer was washed with H_2O (3 x 50 mL), dried ($MgSO_4$) and concentrated under reduced pressure. Purification by gradient column chromatography afforded (6-(pent-2-yn-1-yloxy)benzofuran-2-yl)(phenyl)methanone derivatives (**40a, b, c, d**) at 20% EtOAc in petroleum ether (v/v).

3.5.3.10.1. (4-Chlorophenyl)(6-(pent-2-yn-1-yloxy)benzofuran-2-yl)methanone (40a)

Chemical Formula: $C_{20}H_{15}ClO_3$, Molecular Weight: 338.79
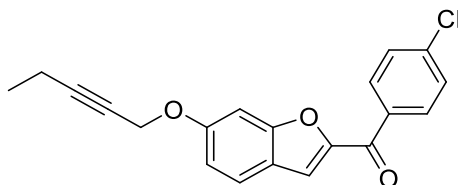
**Yield:** 0.17 g (35%), white solid.

Melting Point: 106-110 ℃

TLC: Petroleum ether – EtOAc 3:1 v/v, R_f = 0.72

¹H NMR (CDCl₃) δ: 8.01 (d, J = 8.6 Hz, 2H, Ar), 7.62 (d, J = 8.7 Hz, 1H, Ar), 7.54 (d, J = 8.6 Hz, 2H, Ar), 7.49 (d, J = 0.9 Hz, 1H, Ar), 7.25 (d, J = 1.8 Hz, 1H, Ar), 7.05 (dd, J = 2.2, 8.7 Hz, 1H, Ar), 4.78 (t, J = 2.1 Hz, 2H, CH₂), 2.29 (qt, J = 2.1, 7.5 Hz, 2H, CH₂), 1.18 (t, J = 7.5 Hz, 3H, CH₃).

¹³C NMR (CDCl₃) δ: 182.52 (C), 159.50 (C), 157.45 (C), 151.78 (C), 139.14 (C), 135.74 (C), 130.77 (2 x CH), 128.86 (2 x CH), 123.70 (CH), 120.70 (C), 117.24 (CH), 115.22 (CH), 97.07 (CH), 90.39 (C), 73.47 (C), 57.06 (CH₂), 13.56 (CH₃), 12.51 (CH₂).

HPLC (method A): 89.32 % at R.T.= 5.06 min.

HRMS (ESI): Calculated 339.0787 [M+H]⁺, Found 339.0784 [M+H]⁺.

3.5.3.10.2. (4-Fluorophenyl)(6-(pent-2-yn-1-yloxy)benzofuran-2-yl)methanone (40b)

Chemical Formula: $C_{20}H_{15}FO_3$, Molecular Weight: 322.34
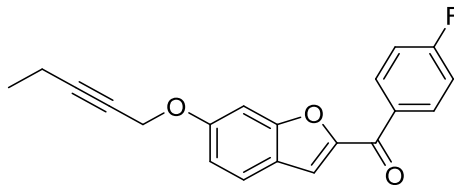
Yield: 0.19 g (76%), white solid.

Melting Point: 106-108 ºC

TLC: Petroleum ether – EtOAc 3:1 v/v, R_f = 0.62

¹H NMR (CDCl₃) δ: 8.01 (dd, J = 5.4, 8.9 Hz, 2H, Ar), 7.52 (d, J = 8.7 Hz, 1H, Ar), 7.40 (d, J = 0.9 Hz, 1H, Ar), 7.15 (m, 3H, Ar), 6.95 (dd, J = 2.2, 8.6 Hz, 1H, Ar), 4.68 (t, J = 2.1 Hz, 2H, CH₂), 2.20 (qt, J = 2.1, 7.5 Hz, 2H, CH₂), 1.08 (t, J = 7.5 Hz, 3H, CH₃).

¹³C NMR (CDCl₃) δ: 182.29 (C), 166.55 (d, $^1J_{,F}$ = 252.5 Hz, C), 159.40 (C), 157.38 (C), 151.88 (C), 133.69 (d, $^4J_{C,F}$ = 3.75 Hz, C), 131.98 (d, $^3J_{C,F}$ = 8.75 Hz, 2 x CH), 123.64 (CH), 120.72 (C), 117.03 (CH), 115.78 (d, $^2J_{C,F}$ = 21.25 Hz, 2 x CH), 115.14 (CH), 97.07 (CH), 90.35 (C), 73.49 (C), 57.05 (CH₂), 13.56 (CH₃), 12.50 (CH₂).

HPLC (method A): 82.69 % at R.T.= 4.94 min.

HRMS (ESI): Calculated 323.1083 [M+H]⁺, Found 323.1077 [M+H]⁺.

3.5.3.10.3. (4-Bromophenyl)(6-(pent-2-yn-1-yloxy)benzofuran-2-yl)methanone (40c)

Chemical Formula: $C_{20}H_{15}BrO_3$, Molecular Weight: 383.24
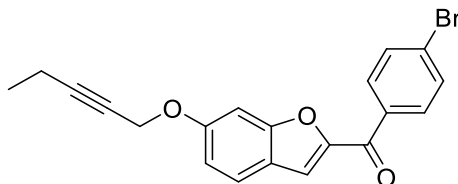
Yield: 0.1 g (40%), white solid.

Melting Point: 116-118 ºC

TLC: Petroleum ether – EtOAc 3:1 v/v, R_f = 0.27

¹H NMR (CDCl₃) δ: 7.84 (d, J = 8.6 Hz, 2H, Ar), 7.61 (d, J = 8.6 Hz, 2H, Ar), 7.53 (d, J = 8.7 Hz, 1H, Ar), 7.40 (d, J = 0.9 Hz, 1H, Ar), 7.16 (d, J = 1.8 Hz, 1H, Ar), 6.95 (dd, J = 2.2,

8.7 Hz, 1H, Ar), 4.69 (t, J = 2.1 Hz, 2H, CH$_2$), 2.20 (qt, J = 2.1, 7.5 Hz, 2H, CH$_2$), 1.09 (t, J = 7.5 Hz, 3H, CH$_3$).

^{13}C NMR (CDCl$_3$) δ: 182.68 (C), 159.51 (C), 157.46 (C), 151.76 (C), 136.18 (C), 131.84 (2 x CH), 130.87 (2 x CH), 127.75 (C), 123.70 (CH), 120.70 (C), 117.29 (CH), 115.24 (CH), 97.06 (CH), 90.39 (C), 73.46 (C), 57.06 (CH$_2$), 13.56 (CH$_3$), 12.50 (CH$_2$).

HPLC (method A): 97.25 % at R.T.= 5.09 min.

HRMS (ESI): Calculated 383.0282 [M+H]$^+$, Found 383.0278 [M+H]$^+$.

3.5.3.10.4. (2,4-Dichlorophenyl)(6-(pent-2-yn-1-yloxy)benzofuran-2-yl)methanone (40d)

Chemical Formula: C$_{20}$H$_{14}$Cl$_2$O$_3$, Molecular Weight: 373.23
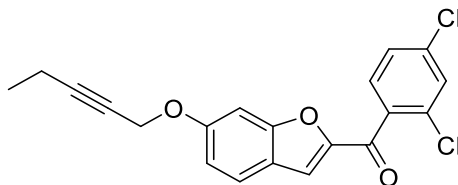
Yield: 0.18 g (75%), yellow oil.

TLC: Petroleum ether – EtOAc 3:1 v/v, R$_f$ = 0.25

^{1}H NMR (CDCl$_3$) δ: 7.49 (d, J = 8.8 Hz, 1H, Ar), 7.45 (d, J = 1.9 Hz, 1H, Ar), 7.40 (d, J = 8.2 Hz, 1H, Ar), 7.31 (dd, J = 1.9, 8.2 Hz, 1H, Ar), 7.20 (d, J = 0.9 Hz, 1H, Ar), 7.12 (d, J = 1.8 Hz, 1H, Ar), 6.94 (dd, J = 2.2, 8.8 Hz, 1H, Ar), 4.68 (t, J = 2.1 Hz, 2H, CH$_2$), 2.19 (qt, J = 2.1, 7.5 Hz, 2H, CH$_2$), 1.08 (t, J = 7.5 Hz, 3H, CH$_3$).

^{13}C NMR (CDCl$_3$) δ: 182.05 (C), 159.51 (C), 157.96 (C), 151.47 (C), 137.18 (C), 135.95 (C), 132.91 (C), 130.31 (CH), 130.28 (CH), 127.03 (CH), 123.94 (CH), 120.69 (C), 118.53 (CH), 115.50 (CH), 97.02 (CH), 90.47 (C), 73.35 (C), 57.06 (CH$_2$), 13.55 (CH$_3$), 12.49 (CH$_2$).

HPLC (method A): 96.52 % at R.T.= 5.06 min.

HRMS (ESI): Calculated 373.0398 [M+H]$^+$, Found 373.0394 [M+H]$^+$.

3.5.3.11. General procedure for the synthesis of (6-(but-2-yn-1-yloxy)benzofuran-2-yl)(phenyl)methanone derivatives (41a-d)

(39) → (41)

1-bromobut-2-yne

K_2CO_3 / CH_3CN
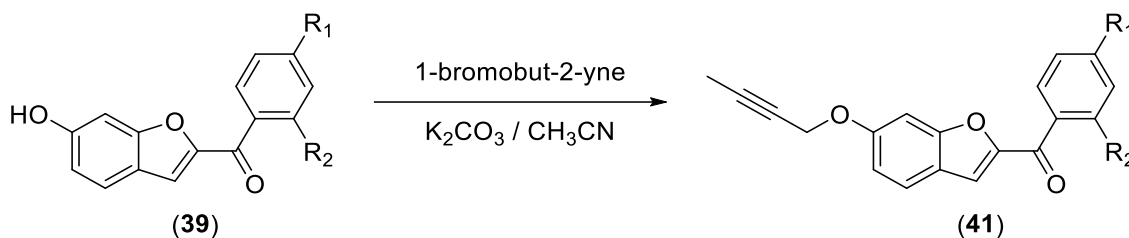
Prepared as described for the synthesis of (6-(pent-2-yn-1-yloxy)benzofuran-2-yl)(phenyl) methanone derivatives (**40a, b, c, d**) using 1-bromobut-2-yne (**22**) (2 m.eq.). Purification by gradient column chromatography afforded (6-(but-2-yn-1-yloxy)benzofuran-2-yl)(phenyl)methanone derivatives (**41a, b, c, d**) at 20% EtOAc in petroleum ether (v/v).

3.5.3.11.1. (6-(But-2-yn-1-yloxy)benzofuran-2-yl)(4-chlorophenyl)methanone (41a)

Chemical Formula: $C_{19}H_{13}ClO_3$, Molecular Weight: 324.76
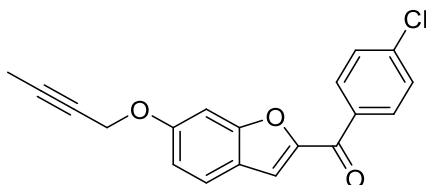
Yield: 0.16 g (34%), white solid.

Melting Point: 132-134 ℃

TLC: Petroleum ether – EtOAc 3:1 v/v, $R_f = 0.7$

^{1}H NMR (CDCl$_3$) δ: 7.90 (d, $J = 8.6$ Hz, 2H, Ar), 7.52 (d, $J = 8.7$ Hz, 1H, Ar), 7.43 (d, $J = 8.6$ Hz, 2H, Ar), 7.39 (d, $J = 0.9$ Hz, 1H, Ar), 7.14 (d, $J = 1.8$ Hz, 1H, Ar), 6.94 (dd, $J = 2.2$, 8.7 Hz, 1H, Ar), 4.66 (q, $J = 2.3$ Hz, 2H, CH$_2$), 1.79 (t, $J = 2.3$ Hz, 3H, CH$_3$).

^{13}C NMR (CDCl$_3$) δ: 182.47 (C), 159.44 (C), 157.43 (C), 151.78 (C), 139.13 (C), 135.71 (C), 130.76 (2 x CH), 128.85 (2 x CH), 123.72 (CH), 120.70 (C), 117.20 (CH), 115.18 (CH), 97.03 (CH), 84.62 (C), 73.33 (C), 56.98 (CH$_2$), 3.72 (CH$_3$).

HPLC (method A): 85.73 % at R.T.= 4.97 min.

HRMS (ESI): Calculated 325.0631 [M+H]$^+$, Found 325.0623 [M+H]$^+$.

3.5.3.11.2. (6-(But-2-yn-1-yloxy)benzofuran-2-yl)(4-fluorophenyl)methanone (41b)

Chemical Formula: $C_{19}H_{13}FO_3$, Molecular Weight: 308.31
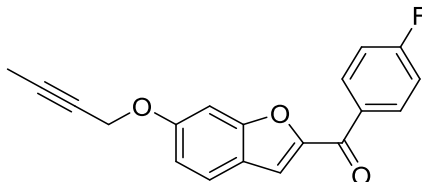
Yield: 0.11 g (61%), white solid.

Melting Point: 162-164 ºC

TLC: Petroleum ether – EtOAc 3:1 v/v, $R_f = 0.6$

¹H NMR (CDCl₃) δ: 8.12 (m, 2H, Ar), 7.62 (d, $J = 8.7$ Hz, 1H, Ar), 7.50 (d, $J = 0.9$ Hz, 1H, Ar), 7.28 (m, 3H, Ar), 7.04 (dd, $J = 2.2, 8.7$ Hz, 1H, Ar), 4.76 (q, $J = 2.3$ Hz, 2H, CH₂), 1.90 (t, $J = 2.3$ Hz, 3H, CH₃).

¹³C NMR (CDCl₃) δ: 182.28 (C), 166.56 (d, $^1J_{C,F} = 252.5$ Hz, C), 159.35 (C), 157.38 (C), 151.90 (C), 133.68 (d, $^4J_{C,F} = 3.75$ Hz, C), 131.99 (d, $^3J_{C,F} = 8.75$ Hz, 2 x CH), 123.67 (CH), 120.73 (C), 117.01 (CH), 115.79 (d, $^2J_{C,F} = 21.25$ Hz, 2 x CH), 115.12 (CH), 97.06 (CH), 84.60 (C), 73.34 (C), 57.98 (CH₂), 3.72 (CH₃).

HPLC (method A): 94.35 % at R.T.= 4.90 min.

HRMS (ESI): Calculated 309.0926 [M+H]⁺, Found 309.0919 [M+H]⁺.

3.5.3.11.3. (6-(But-2-yn-1-yloxy)benzofuran-2-yl)(4-bromophenyl)methanone (41c)

Chemical Formula: $C_{19}H_{13}BrO_3$, Molecular Weight: 369.21
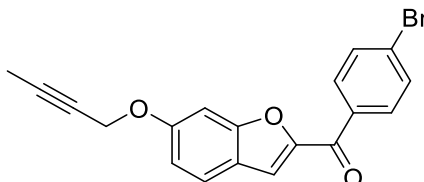
Yield: 0.1 g (43%), white solid.

Melting Point: 143-145 ºC

TLC: Petroleum ether – EtOAc 3:1 v/v, $R_f = 0.37$

¹H NMR (CDCl₃) δ: 7.84 (d, *J* = 8.6 Hz, 2H, Ar), 7.61 (d, *J* = 8.6 Hz, 2H, Ar), 7.53 (d, *J* = 8.7 Hz, 1H, Ar), 7.40 (d, *J* = 0.9 Hz, 1H, Ar), 7.16 (d, *J* = 1.8 Hz, 1H, Ar), 6.95 (dd, *J* = 2.2, 8.7 Hz, 1H, Ar), 4.67 (q, *J* = 2.3 Hz, 2H, CH₂), 1.81 (t, *J* = 2.3 Hz, 3H, CH₃).

¹³C NMR (CDCl₃) δ: 182.48 (C), 159.46 (C), 157.41 (C), 151.76 (C), 136.16 (C), 131.84 (2 x CH), 130.87 (2 x CH), 127.64 (C), 123.73 (CH), 120.71 (C), 117.26 (CH), 115.21 (CH), 97.05 (CH), 84.63 (C), 73.30 (C), 56.99 (CH₂), 3.72 (CH₃).

HPLC (method A): 94.12 % at R.T.= 5.00 min.

HRMS (ESI): Calculated 369.0126 [M+H]⁺, Found 369.0119 [M+H]⁺.

3.5.3.11.4. (6-(But-2-yn-1-yloxy)benzofuran-2-yl)(2,4-dichlorophenyl)methanone (41d)

Chemical Formula: $C_{19}H_{12}Cl_2O_3$, Molecular Weight: 359.20
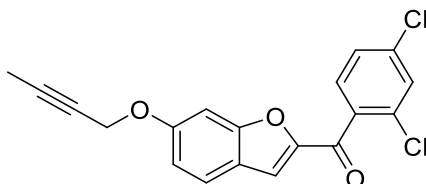
Yield: 0.2 g (86%), yellow oil.

TLC: Petroleum ether – EtOAc 3:1 v/v, R_f = 0.32

¹H NMR (CDCl₃) δ: 7.49 (d, *J* = 8.7 Hz, 1H, Ar), 7.45 (d, *J* = 1.9 Hz, 1H, Ar), 7.40 (d, *J* = 8.2 Hz, 1H, Ar), 7.32 (dd, *J* = 1.9, 8.2 Hz, 1H, Ar), 7.20 (d, *J* = 0.9 Hz, 1H, Ar), 7.13 (d, *J* = 1.9 Hz, 1H, Ar), 6.93 (dd, *J* = 2.2, 8.7 Hz, 1H, Ar), 4.66 (q, *J* = 2.3 Hz, 2H, CH₂), 1.80 (t, *J* = 2.3 Hz, 3H, CH₃).

¹³C NMR (CDCl₃) δ: 182.03 (C), 159.86 (C), 157.95 (C), 151.54 (C), 137.18 (C), 135.94 (C), 132.91 (C), 130.31 (CH), 130.28 (CH), 127.03 (CH), 123.96 (CH), 120.70 (C), 118.50 (CH), 115.47 (CH), 97.01 (CH), 84.72 (C), 73.20 (C), 56.99 (CH₂), 3.71 (CH₃).

HPLC (method A): 100 % at R.T.= 4.98 min.

**HRMS (ESI):** Calculated 359.0241 [M+H]⁺, Found 359.0238 [M+H]⁺.

3.5.3.12. General procedure for the synthesis of (6-(pent-2-yn-1-yloxy)benzofuran-2-yl)(phenyl)(pyridin-3-yl)methanol derivatives (42a-d)
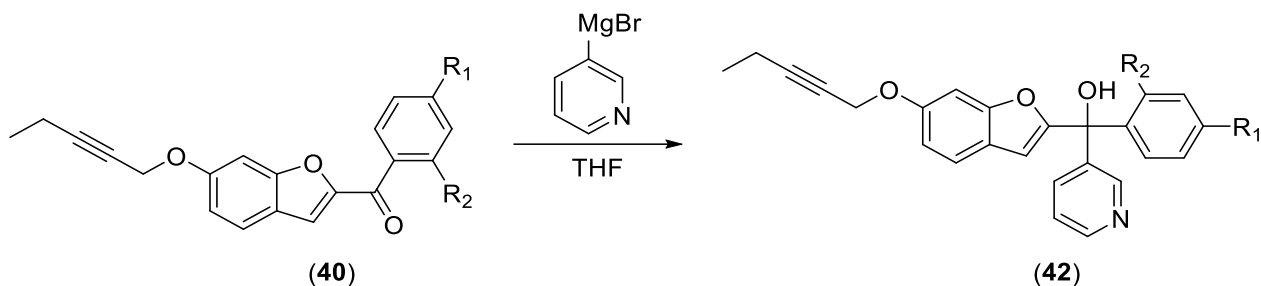
Prepared as described for the synthesis of (6-methoxybenzofuran-2-yl)(phenyl)(pyridin-3-yl)methanol (**36a-d**) using (6-(pent-2-yn-1-yloxy)benzofuran-2-yl)(phenyl)methanone derivatives (**40a-d**) (1 m.eq.) to give (6-(pent-2-yn-1-yloxy)benzofuran-2-yl)(phenyl)(pyridin-3-yl)methanol (**42a-d**) after purification using column chromatography at 60% EtOAc in petroleum ether (v/v) as a colourless or white oil.

3.5.3.12.1. (4-Chlorophenyl)(6-(pent-2-yn-1-yloxy)benzofuran-2-yl)(pyridin-3-yl)methanol (42a)

Chemical Formula: $C_{25}H_{20}ClNO_3$, Molecular Weight: 417.89
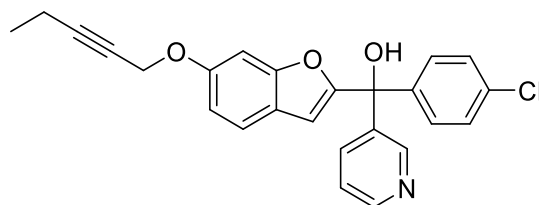
Yield: 0.18 g (91%)

TLC: Petroleum ether – EtOAc 1:1 v/v, $R_f = 0.32$

^{1}H NMR (CDCl$_3$) δ: 8.49 (m, 2H, Ar), 7.64 (m, 1H, Ar), 7.30 (d, $J = 8.6$ Hz, 1H, Ar), 7.26 (m, 5H, Ar), 6.98 (d, $J = 2.0$ Hz, 1H, Ar), 6.86 (dd, $J = 2.3, 8.6$ Hz, 1H, Ar), 6.16 (d, $J = 0.9$ Hz, 1H, Ar),), 4.61 (t, $J = 2.1$ Hz, 2H, CH$_2$), 3.79 (bs, 1H, OH), 2.18 (qt, $J = 2.1, 7.5$ Hz, 2H, CH$_2$), 1.07 (t, $J = 7.5$ Hz, 3H, CH$_3$).

^{13}C NMR (CDCl$_3$) δ: 157.90 (C), 156.61 (C), 156.04 (C), 149.02 (CH), 148.70 (CH), 141.87 (C), 139.46 (C), 134.96 (CH), 134.23 (C), 128.68 (2 x CH), 128.51 (2 x CH), 123.05 (CH),

121.55 (CH), 121.24 (C), 113.05 (CH), 106.86 (CH), 97.48 (CH), 89.87 (C), 76.61 (C), 73.97 (C), 57.13 (CH_2), 13.58 (CH_3), 12.51 (CH_2).

HPLC (method A): 100 % at R.T.= 4.87 min.

HRMS (ESI): Calculated 418.1209 $[M+H]^+$, Found 418.1204 $[M+H]^+$.

3.5.3.12.2. (4-Fluorophenyl)(6-(pent-2-yn-1-yloxy)benzofuran-2-yl)(pyridin-3-yl)methanol (42b)

Chemical Formula: $C_{25}H_{20}FNO_3$, Molecular Weight: 401.44
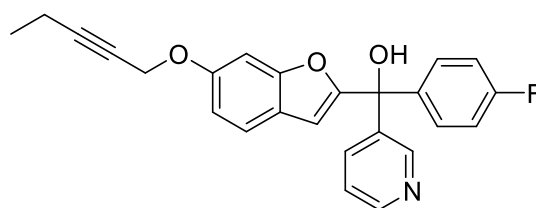
Yield: 0.04 g (20%)

TLC: Petroleum ether – EtOAc 1:1 v/v, R_f = 0.45

¹H NMR (CDCl₃) δ: 8.53 (m, 2H, Ar), 7.66 (d, *J* = 7.9 Hz, 1H, Ar), 7.31 (d, *J* = 8.6 Hz, 1H, Ar), 7.28 (dd, *J* = 5.3, 8.9 Hz, 2H, Ar), 7.19 (obscured by CDCl₃, 1H, Ar), 7.00 (d, *J* = 2.1 Hz, 1H, Ar), 6.99 (t, *J* = 8.7 Hz, 2H, Ar), 6.86 (dd, *J* = 2.3, 8.6 Hz, 1H, Ar), 6.16 (d, *J* = 0.8 Hz, 1H, Ar),), 4.62 (t, *J* = 2.1 Hz, 2H, CH_2), 3.32 (bs, 1H, OH), 2.19 (qt, *J* = 2.1, 7.5 Hz, 2H, CH_2), 1.08 (t, *J* = 7.5 Hz, 3H, CH_3).

¹³C NMR (CDCl₃) δ: 176.59 (C), 163.49 (d, $^1J_{C,F}$ = 247.5 Hz, C), 158.11 (C), 156.58 (C), 156.00 (C), 139.15 (d, $^4J_{C,F}$ = 3.75 Hz, C), 134.83 (CH), 129.17 (d, $^3J_{C,F}$ = 8.75 Hz, 2 x CH), 121.54 (CH), 121.26 (C), 115.33 (d, $^2J_{C,F}$ = 22.5 Hz, 2 x CH), 113.05 (CH), 106.83 (CH), 97.48 (CH), 89.83 (C), 76.76 (C, obscured by CDCl3), 73.94 (C), 57.13 (CH_2), 13.58 (CH_3), 12.51 (CH_2).

* Three CH peaks for Pyridine carbons are too small and require more scan time to be detected.

HPLC (method A): 100 % at R.T.= 4.78 min.

HRMS (ESI): Calculated 402.1505 $[M+H]^+$, Found 402.1501 $[M+H]^+$.

3.5.3.12.3. (4-Bromophenyl)(6-(pent-2-yn-1-yloxy)benzofuran-2-yl)(pyridin-3-yl)methanol (42c)

Chemical Formula: $C_{25}H_{20}BrNO_3$, Molecular Weight: 462.34
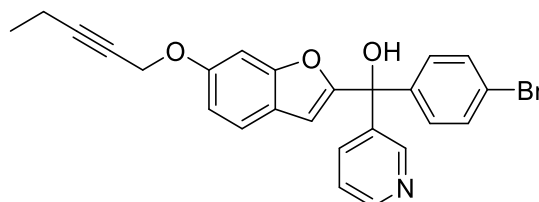
Yield: 0.05 g (50%)

TLC: Petroleum ether – EtOAc 1:1 v/v, $R_f = 0.5$

^{1}H NMR (CDCl$_3$) δ: 8.48 (m, 2H, Ar), 7.64 (d, $J = 8.0$ Hz, 1H, Ar), 7.41 (d, $J = 8.6$ Hz, 2H, Ar), 7.30 (d, $J = 8.6$ Hz, 1H, Ar), 7.20 (m, 3H, Ar), 6.98 (d, $J = 2.1$ Hz, 1H, Ar), 6.86 (dd, $J = 2.3, 8.6$ Hz, 1H, Ar), 6.16 (d, $J = 0.9$ Hz, 1H, Ar),), 4.61 (t, $J = 2.1$ Hz, 2H, CH$_2$), 3.68 (bs, 1H, OH), 2.19 (qt, $J = 2.1, 7.5$ Hz, 2H, CH$_2$), 1.07 (t, $J = 7.5$ Hz, 3H, CH$_3$).

^{13}C NMR (CDCl$_3$) δ: 157.79 (C), 156.62 (C), 156.04 (C), 148.97 (CH), 148.63 (CH), 142.39 (C), 139.49 (C), 135.00 (CH), 131.48 (2 x CH), 129.00 (2 x CH), 123.02 (CH), 122.47 (C), 121.55 (CH), 121.22 (C), 113.06 (CH), 106.90 (CH), 97.47 (CH), 89.87 (C), 76.67 (C), 73.97 (C), 57.13 (CH$_2$), 13.58 (CH$_3$), 12.51 (CH$_2$).

HPLC (method A): 100 % at R.T.= 4.90 min.

HRMS (ESI): Calculated 462.0704 [M+H]$^+$, Found 462.0703 [M+H]$^+$.

3.5.3.12.4. (2,4-Dichlorophenyl)(6-(pent-2-yn-1-yloxy)benzofuran-2-yl)(pyridin-3-yl)methanol (42d)

Chemical Formula: $C_{25}H_{19}Cl_2NO_3$, Molecular Weight: 452.33
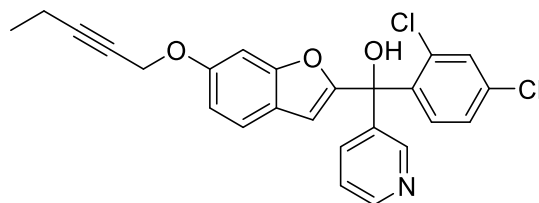
Yield: 0.03 g (15 %)

TLC: Petroleum ether – EtOAc 1:1 v/v, $R_f = 0.37$

¹H NMR (CDCl₃) δ: 8.54 (m, 2H, Ar), 7.69 (d, *J* = 8.0 Hz, 1H, Ar), 7.36 (d, *J* = 2.2 Hz, 1H, Ar), 7.32 (d, *J* = 8.6 Hz, 1H, Ar), 7.26 (m, 1H, Ar), 7.15 (dd, *J* = 2.2, 8.5 Hz, 1H, Ar), 7.03 (d, *J* = 2.1 Hz, 1H, Ar), 7.00 (d, *J* = 8.5 Hz, 1H, Ar), 6.87 (dd, *J* = 2.3, 8.6 Hz, 1H, Ar), 6.22 (d, *J* = 0.8 Hz, 1H, Ar), 4.62 (t, *J* = 2.1 Hz, 2H, CH₂), 4.06 (bs, 1H, OH), 2.19 (qt, *J* = 2.1, 7.5 Hz, 2H, CH₂), 1.08 (t, *J* = 7.5 Hz, 3H, CH₃).

¹³C NMR (CDCl₃) δ: 156.63 (C), 156.48 (C), 155.96 (C), 149.14 (CH), 148.61 (CH), 138.94 (C), 137.56 (C), 135.29 (C), 134.71 (CH), 133.84 (C), 131.45 (CH), 131.13 (CH), 130.68 (CH), 127.06 (CH), 121.62 (CH), 121.27 (C), 113.17 (CH), 107.10 (CH), 97.55 (CH), 89.89 (C), 76.77 (C, obscured by CDCl₃), 73.96 (C), 57.14 (CH₂), 13.58 (CH₃), 12.52 (CH₂).

HPLC (method A): 100 % at R.T.= 4.92 min.

HRMS (ESI): Calculated 452.0820 [M+H]⁺, Found 452.0816 [M+H]⁺.

3.5.3.13. General procedure for the synthesis of (6-(but-2-yn-1-yloxy)benzofuran-2-yl)(phenyl)(pyridin-3-yl)methanol derivatives (43a-d)
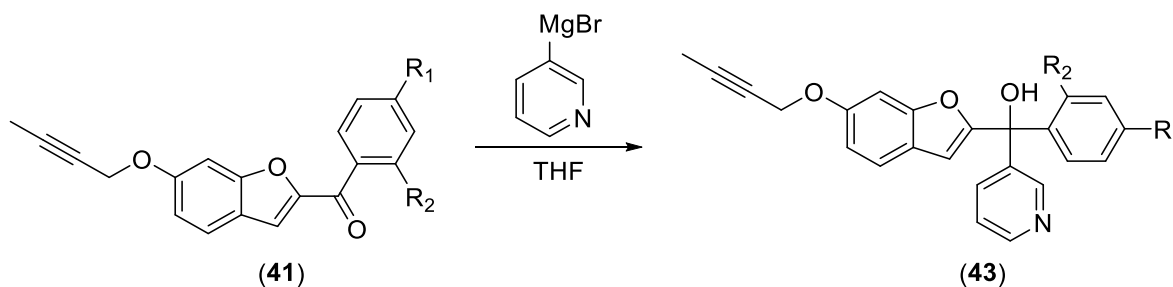
Prepared as described for the synthesis of (6-methoxybenzofuran-2-yl)(phenyl)(pyridin-3-yl)methanol (**36a-d**) using (6-(but-2-yn-1-yloxy)benzofuran-2-yl)(phenyl)methanone derivatives (**41a-d**) (1 m.eq.) to give (6-(but-2-yn-1-yloxy)benzofuran-2-yl)(phenyl)(pyridin-3-yl)methanol (**43a-d**) after purification using column chromatography at 60% EtOAc in petroleum ether (v/v) as a colourless or white oil.

3.5.3.13.1. (6-(But-2-yn-1-yloxy)(4-chlorophenyl)benzofuran-2-yl)(pyridin-3-yl)methanol (43a)

Chemical Formula: $C_{24}H_{18}ClNO_3$, Molecular Weight: 403.86
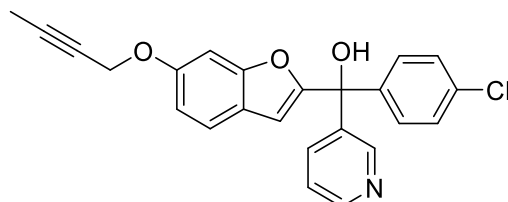
Yield: 0.16 g (94%)

TLC: Petroleum ether – EtOAc 1:1 v/v, R_f = 0.4

^{1}H NMR (CDCl$_3$) δ: 8.60 (m, 2H, Ar), 7.74 (dt, J = 1.6, 8.0 Hz, 1H, Ar), 7.40 (d, J = 8.6 Hz, 1H, Ar), 7.36 (m, 5H, Ar), 7.08 (s, 1H, Ar), 6.95 (dd, J = 2.2, 8.6 Hz, 1H, Ar), 6.26 (s, 1H, Ar), 4.69 (q, J = 2.2 Hz, 2H, CH$_2$), 3.74 (bs, 1H, OH), 1.88 (t, J = 2.2 Hz, 3H, CH$_3$).

^{13}C NMR (CDCl$_3$) δ: 157.84 (C), 156.55 (C), 156.05(C), 149.12 (CH), 148.76 (CH), 141.81 (C), 139.40 (C), 134.92 (CH), 134.27 (C), 128.68 (2 x CH), 128.52 (2 x CH), 123.05 (CH), 121.59 (CH), 121.24 (C), 113.04 (CH), 106.89 (CH), 97.40 (CH), 84.08 (C), 76.65 (C), 73.80 (C), 57.03 (CH$_2$), 3.74 (CH$_3$).

HPLC (method A): 100 % at R.T.= 4.80 min.

HRMS (ESI): Calculated 404.1053 [M+H]$^+$, Found 404.1050 [M+H]$^+$.

3.5.3.13.2. (6-(But-2-yn-1-yloxy)(4-fluorophenyl)benzofuran-2-yl)(pyridin-3-yl)methanol (43b)

Chemical Formula: $C_{24}H_{18}FNO_3$, Molecular Weight: 387.41
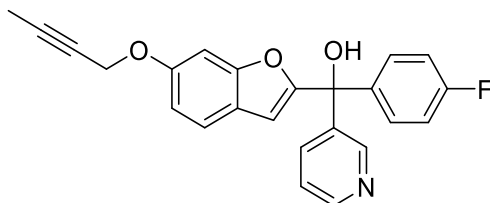
Yield: 0.1 g (80 %)

TLC: Petroleum ether – EtOAc 1:1 v/v, R_f = 0.37

^{1}H NMR (CDCl$_3$) δ: 8.48 (m, 2H, Ar), 7.65 (m, 1H, Ar), 7.30 (d, J = 8.6 Hz, 1H, Ar), 7.26 (dd, J = 5.3, 8.9 Hz, 2H, Ar), 7.20 (m, 1H, Ar), 6.98 (m, 3H, Ar), 6.85 (dd, J = 2.3, 8.6 Hz,

1H, Ar), 6.15 (d, J = 0.8 Hz, 1H, Ar),), 4.59 (q, J = 2.3 Hz, 2H, CH$_2$), 3.90 (bs, 1H, OH), 1.78 (t, J = 2.3 Hz, 3H, CH$_3$).

^{13}C NMR (CDCl$_3$) δ: 163.46 (d, $^1J_{C,F}$ = 246.25 Hz, C), 158.23 (C), 156.52 (C), 156.03 (C), 148.92 (CH), 148.73 (CH), 139.68 (C), 139.24 (d, $^4J_{C,F}$ = 2.5 Hz, C), 134.98 (CH), 129.16 (d, $^3J_{C,F}$ = 8.75 Hz, 2 x CH), 123.02 (CH), 121.55 (CH), 121.29 (C), 115.29 (d, $^2J_{C,F}$ = 21.25 Hz, 2 x CH), 112.96 (CH), 106.72 (CH), 97.41 (CH), 84.06 (C), 76.60 (C), 73.83 (C), 57.02 (CH$_2$), 3.74 (CH$_3$).

HPLC (method A): 100 % at R.T.= 4.70 min.

HRMS (ESI): Calculated 388.1348 [M+H]$^+$, Found 388.1351 [M+H]$^+$.

3.5.3.13.3. (4-Bromophenyl)(6-(but-2-yn-1-yloxy)benzofuran-2-yl)(pyridin-3-yl)methanol (43c)

Chemical Formula: C$_{24}$H$_{18}$BrNO$_3$, Molecular Weight: 448.32
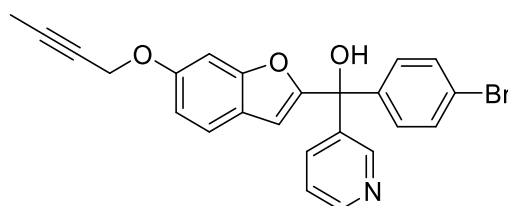
Yield: 0.07 g (70 %)

TLC: Petroleum ether – EtOAc 1:1 v/v, R$_f$ = 0.42

^{1}H NMR (CDCl$_3$) δ: 8.47 (m, 2H, Ar), 7.64 (dt, J = 2.1, 8.1 Hz, 1H, Ar), 7.40 (d, J = 8.7 Hz, 2H, Ar), 7.30 (d, J = 8.6 Hz, 1H, Ar), 7.20 (m, 3H, Ar), 6.97 (d, J = 2.1 Hz, 1H, Ar), 6.85 (dd, J = 2.3, 8.6 Hz, 1H, Ar), 6.16 (d, J = 0.9 Hz, 1H, Ar),), 4.59 (q, J = 2.3 Hz, 2H, CH$_2$), 3.97 (bs, 1H, OH), 1.78 (t, J = 2.3 Hz, 3H, CH$_3$).

^{13}C NMR (CDCl$_3$) δ: 157.87 (C), 156.56 (C), 156.04 (C), 148.98 (CH), 148.66 (CH), 142.43 (C), 139.36 (C), 134.98 (CH), 131.46 (2 x CH), 129.00 (2 x CH), 123.05 (CH), 122.44 (C), 121.58 (CH), 121.24 (C), 113.01 (CH), 106.85 (CH), 97.39 (CH), 84.07 (C), 76.64 (C), 73.82 (C), 57.02 (CH$_2$), 3.75 (CH$_3$).

HPLC (method A): 100 % at R.T.= 4.83 min.

HRMS (ESI): Calculated 448.0548 [M+H]$^+$, Found 448.0543 [M+H]$^+$.

3.5.3.13.4. (6-(But-2-yn-1-yloxy)(2,4-dichlorophenyl)benzofuran-2-yl)(pyridin-3-yl)methanol (43d)

Chemical Formula: $C_{24}H_{17}Cl_2NO_3$, Molecular Weight: 438.30
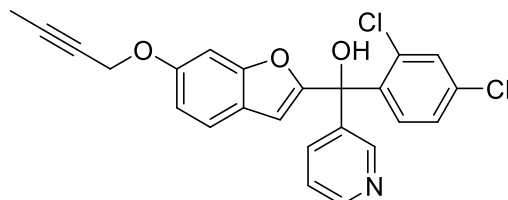
Yield: 0.08 (34 %)

TLC: Petroleum ether – EtOAc 1:1 v/v, $R_f = 0.4$

^{1}H NMR (CDCl$_3$) δ: 8.52 (m, 2H, Ar), 7.69 (dt, $J = 1.8$, 8.2 Hz, 1H, Ar), 7.36 (d, $J = 2.2$ Hz, 1H, Ar), 7.32 (d, $J = 8.6$ Hz, 1H, Ar), 7.25 (m, 1H, Ar), 7.15 (dd, $J = 2.2$, 8.6 Hz, 1H, Ar), 7.03 (d, $J = 2.1$ Hz, 1H, Ar), 7.00 (d, $J = 8.5$ Hz, 1H, Ar), 6.87 (dd, $J = 2.3$, 8.6 Hz, 1H, Ar), 6.23 (d, $J = 0.9$ Hz, 1H, Ar), 4.61 (q, $J = 2.3$ Hz, 2H, CH$_2$), 4.06 (bs, 1H, OH), 1.80 (t, $J = 2.3$ Hz, 3H, CH$_3$).

^{13}C NMR (CDCl$_3$) δ: 156.60 (C), 156.47 (C), 155.97 (C), 149.16 (CH), 148.63 (CH), 138.92 (C), 138.24 (C), 135.29 (C), 134.78 (CH), 133.84 (C), 131.45 (CH), 131.13 (CH), 127.07 (CH), 123.06 (CH), 121.65 (CH), 121.28 (C), 113.13 (CH), 107.09 (CH), 97.47 (CH), 84.09 (C), 76.77 (C, obscured by CDCl$_3$), 73.80 (C), 57.04 (CH$_2$), 3.75 (CH$_3$).

HPLC (method A): 100 % at R.T.= 4.84 min.

HRMS (ESI): Calculated 438.0663 [M+H]$^+$, Found 438.0659 [M+H]$^+$.

3.5.4. Cell culture

As previously described in section 2.5.4

3.5.5. Aromatase activity assay

As previously described in section 2.5.5

3.5.6. BrdU-based cell proliferation assay to assess drug toxicity

As previously described in section 2.5.6

Chapter 4: Dual aromatase sulfatase inhibition

4.1. Background

4.1.1. One molecule – one target – one disease

Traditionally, the aim of drug discovery was the design of molecules that can target a single biological entity with a high degree of selectivity (Ramsay *et al.* 2018). This target, usually a protein, is believed to be crucial for a certain disease providing the basis of a principle dominating the pharmaceutical industry and medicinal chemistry research for several decades in the twentieth century (Ramsay *et al.* 2018; Alcaro *et al.* 2019; Zhou *et al.* 2019). The principle "one molecule – one target – one disease" dictated a target-centric strategy categorising the pharmacological activity of the molecule into desirable "on-target" and undesirable "off-target". This strategy has led to the discovery of many successful selective drugs for unmet medical needs (Bolognesi and Cavalli 2016; Ramsay *et al.* 2018).

4.1.2. Paradigm shift from single target to multi-target therapeutics

Despite the successes of single-target treatments in prolonging lives and sometimes curing the diseases, it was usually found to be inadequate in complex multifactorial diseases such as neurodegenerative and CNS diseases, infections and cancer leading to unsatisfactory therapeutic effect (Alcaro *et al.* 2019; Zhou *et al.* 2019). This resilience could be attributed to the robust nature of cellular networks manifested by the activation of compensatory "back-up" mechanisms preventing major changes in the overall outcome (Zhou *et al.* 2016; Skok *et al.* 2019). Building on these accumulated findings, manipulating two or more targets leading to additive or synergistic effects, known as polypharmacological treatment, has gained more interest with the hope of reduction of resistance development (Bolognesi 2013; Skok *et al.* 2019; Zhou *et al.* 2019).

Polypharmacology includes two approaches; mixture of monotherapies and multi-target directed ligands (MTDLs) (**Figure 4.1**). Mixture of monotherapies can be either a drug cocktail (combination of different formulas each containing one active ingredient) or multicomponent drug (combination drug i.e.: one formula containing multiple active ingredients) (Bolognesi 2013; Zhou *et al.* 2019). In this combination therapy approach, smaller doses of the individual drugs would be required leading to decreased side effects when compared with each individual drug alone (Mokhtari *et al.* 2017; Skok *et al.* 2019). The downside of this strategy is always related to patient compliance, potential drug-drug interactions and complex pharmacokinetic and pharmacodynamic profile

(Proschak *et al.* 2019; Zhou *et al.* 2019). The second approach of polypharmacology i.e. MTDLs, also commonly referred to as multimodal, multi-functional, dual and triple acting agents, designed multitarget ligands or multitarget drugs, could avoid some of these pitfalls requiring only a single molecule, triggering academic and industrial interest over the last couple of decades (Morphy *et al.* 2004; Morphy and Rankovic 2005; Youdim and Buccafusco 2005; Morphy and Rankovic 2007; Millan 2009; Morphy and Rankovic 2009; Morphy and Rankovic 2003; Bolognesi 2013; Zhou *et al.* 2019).
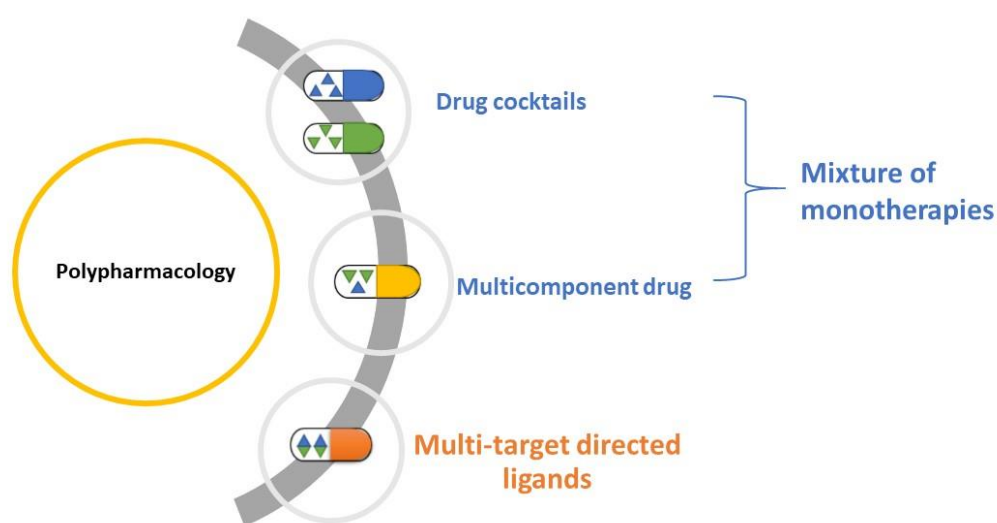
Figure (4.1): Three scenarios of polypharmacology contained into two approaches, where mixture of monotherapies is labelled in blue and multi-target directed ligands is labelled in orange.

The success of multi-target drugs can be clearly illustrated by the rise of their percentage in the new molecular entities approved by the US Food and Drug Administration (FDA) (**Figure 4.2**) from 16% (2000-2015) to 21% (2015-2017). Newly approved combinations also represented 10%, while single-target drugs represented 34%. Adding the scores of the two polypharmacology approaches together produces 31% of all approved new molecular entities approaching the percentage of the single-target drugs (Ramsay *et al.* 2018).
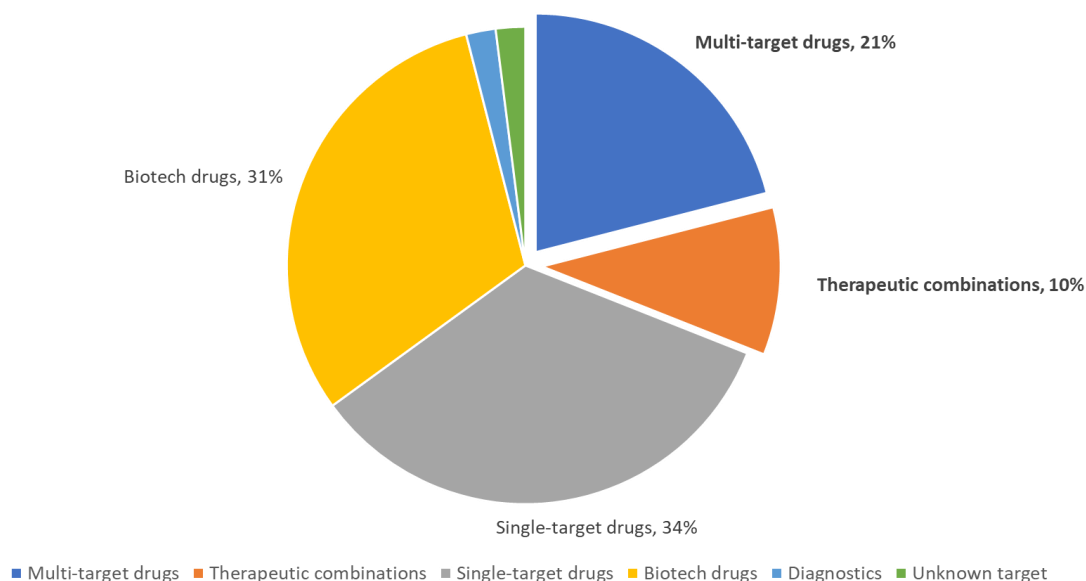
Figure (4.2): New molecular entities approved from 2015 to 2017 by the FDA, data adapted from (Ramsay *et al.* 2018).

4.1.3. Multi-target drugs history: from serendipity to rational design

Retrospective studies discovered that the high therapeutic efficacy of some of our oldest small molecule drugs is due to their multi-target potential (Mei and Yang 2018; Proschak *et al.* 2019). Paracetamol, metformin and even aspirin are three examples of long known drugs that interact with multiple targets accounting for their additive or synergistic effects (Proschak *et al.* 2019). Statins, a relatively newer drug class, also show some anti-inflammatory effects not mediated by their main target of action but supporting their clinical efficacy (Proschak *et al.* 2019; Skok *et al.* 2019). From the beginning of this century with the rise of polypharmacology and beneficial off-target activity, multi-target drug discovery witnessed a shift towards a more rational design process (Mei and Yang 2018; Proschak *et al.* 2019; Zhou *et al.* 2019). However, rational multi-target drug design encompasses two big challenges; selection of targets and ligand discovery (Ramsay *et al.* 2018).

4.1.4. Rational selection of multiple targets

Deciding the proper target combination is crucial for the rational discovery of MTDLs. This requires an in-depth understanding of the disease related pathways and the relationship of the target to the therapeutic and adverse events (Ramsay *et al.* 2018; Zhou *et al.* 2019). The additive or synergistic effects is decided by the relation between the target pathways. Targets sharing the same

pathway are expected to produce additive effects, while belonging to complementary pathways could provide synergistic effects (Ramsay *et al.* 2018). Target combinations can be validated by clinical observations of drug cocktails leading to MTDLs. Other rational approaches include phenotypic screening or *in silico* techniques (Proschak *et al.* 2019; Zhou *et al.* 2019).

4.1.5. Multi-target ligand discovery

The multi-target ligand discovery process goes through ligand identification then optimisation. Identification can be achieved by either screening approaches or by the predominant method, which is the knowledge-based approach. This approach combines the essential pharmacophores of different ligands for single targets into one single compound to form MTDL (Proschak *et al.* 2019; Zhou *et al.* 2019). The ligands can be classified by the manner of their combination into three distinct types: linked pharmacophores, fused pharmacophores, and merged pharmacophores (**Figure 4.3**).
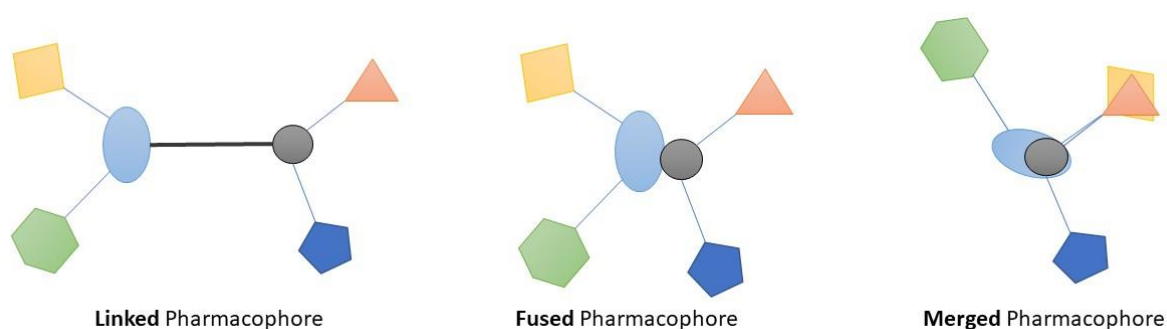
Figure (4.3): Different types of multi-target designed ligands.

The linked type is simply achieved by conjugating the two active pharmacophores by a linker that can be cleavable or non-cleavable (Morphy *et al.* 2004; Zhou *et al.* 2019). However, this usually ends up with a large molecule, which can make them less favourable in terms of bioavailability or can be associated with other drawbacks related to the position and composition of the linker in a way that can hinder interactions with the required targets (Morphy and Rankovic 2005; Morphy and Rankovic 2009; Zhou *et al.* 2019). This type is currently popular with antibody drug conjugates where the antibody acts as a delivering agent for the small molecule to its target of action (Proschak *et al.* 2019).

Conjugation of pharmacophores without a linker with partial pharmacophore overlapping produces the second type; fused pharmacophores, which also may have large molecular weights and may suffer from excessive lipophilicity (Proschak *et al.* 2019; Zhou *et al.* 2019). Raising the level of pharmacophore overlapping provides the most advantageous merged pharmacophore type as it possesses smaller molecular weights. Apart from being highly demanding in the design process, a simpler structure increases their drug likeliness and usually fulfils Lipinski's rule of five (Lipinski *et al.* 1997; Proschak *et al.* 2019; Zhou *et al.* 2019).

Another huge challenge for multi-target designing is the optimisation of the ligand to keep the balance of activity between the different required targets. Design-in and design-out are the two approaches for optimisation. Design-in is the incorporation of the pharmacophore of one ligand into the molecular architecture of a selective ligand to the other target enhancing the affinity for the new target while keeping the other target activity optimal. Design-out is the opposite of the design-in approach as it starts with unselective ligand acting on multiple targets and raising the selectivity to the desired targets by reducing the affinity towards undesired ones (Zhou *et al.* 2016; Proschak *et al.* 2019; Zhou *et al.* 2019).

4.1.6. MTDL progress and applications

At this point, it is quite challenging to tell which multi-target drug was intended and which was a matter of luck as in many cases the complex multi-targeting profile was detected in a retrospective manner. Nevertheless, according to Proschak *et al.*, we can only assume that luck only meets excellent knowledge and hard work (Proschak *et al.* 2019). One good representative is aspirin. Aspirin, one of the earliest described nonsteroidal anti-inflammatory drugs, started to reveal its complexity of multiple activities around 23 centuries after it was first used. Beside its cyclooxygenase (COX) inhibition, it was found to beneficially inhibit platelet thromboxane A_2, NF-κB and regulate MAPKs along with other activities (Amin *et al.* 1999; Dzeshka *et al.* 2016; Proschak *et al.* 2019). Although designing such a multi-target ligand against unrelated targets represents a challenging scenario, the structural similarity between the COX-2 ligand, arachidonic acid, and thromboxane A2 (**Figure 4.4**) suggested that thromboxane A2 receptor and the COX-2 enzyme could accommodate a multi-targeted ligand. Consequently, some derivatives of Lumiracoxib, a COX-2 selective inhibitor (**Figure 4.5**), were rationally designed to act as dual inhibitors (Bertinaria *et al.* 2012; Proschak *et al.* 2019).
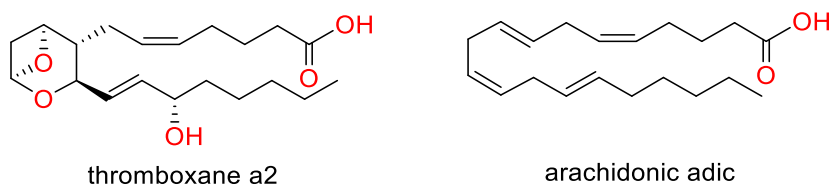
Figure (4.4): Structural similarity between arachidonic acid and thromboxane A2.

A good example for serendipity followed by rational design of a dual acting molecule is CBS-3595, a dual P38α/MAPK and phosphodiesterase inhibitor (**Figure 4.5**). During the testing of several P38α/MAPK inhibitors, one candidate showed significantly better *in vivo* efficacy, which could not be anticipated from *in vitro* studies. Another target was identified as phosphodiesterase and was found to be responsible for the improvement of activity. SAR studies and rational modifications led to the discovery of the dual inhibitor that synergistically affects the release of TNFα, which might be of help in chronic inflammatory diseases (Albrecht *et al.* 2017; Proschak *et al.* 2019).
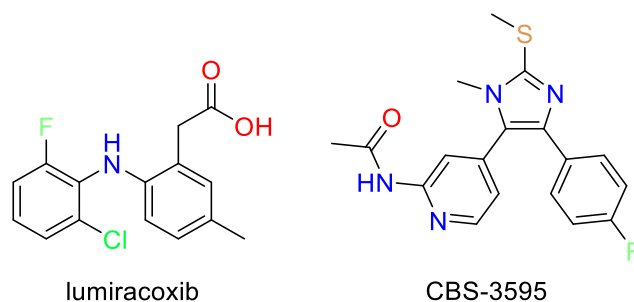
Figure (4.5): Anti-inflammatory compounds.

In the field of infectious diseases, the need for multi-target designed ligands is growing due to antimicrobial resistance (Bolognesi and Cavalli 2016; Proschak *et al.* 2019). In the 1960s, a combination protocol was adopted for the treatment of tuberculosis (Wang *et al.* 2007; Zhou *et al.* 2019) and later the same combination concept was extended to acquired immunodeficiency syndrome (AIDS) (Zhou *et al.* 2019). Human immunodeficiency virus (HIV), the causative agent for AIDS, has two crucial enzymes for its replication for which dual inhibitors were designed from selective single-target inhibitors (**Figure 4.6**). These enzymes are integrase (IN), which integrates the pathogen DNA into the host, and reverse transcriptase (RT), which transcribes RNA to double stranded DNA (Wang *et al.* 2007; Wang and Vince 2008; Bolognesi 2013; Zhou *et al.* 2019).
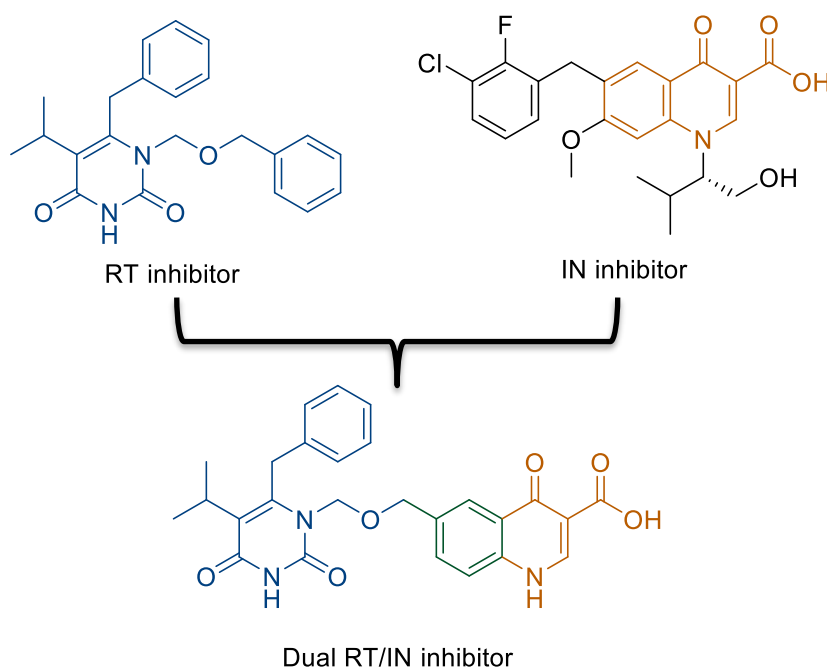
Figure (4.6): Derivatisation of a dual RT/IN inhibitor from selective single inhibitors.

A leading example of MTDL successes is in the arena of antipsychotics. Initially, targeting dopamine D2-like receptors led to undeniable side effects especially extrapyramidal motor symptoms (EPS). The combination with antiserotonergic 5-HT$_{2A}$ activity dramatically reduced the side effects. Efforts on activity modulation led to the successful antipsychotics, aripiprazole and cariprazine (**Figure 4.7**) (Proschak *et al.* 2019).
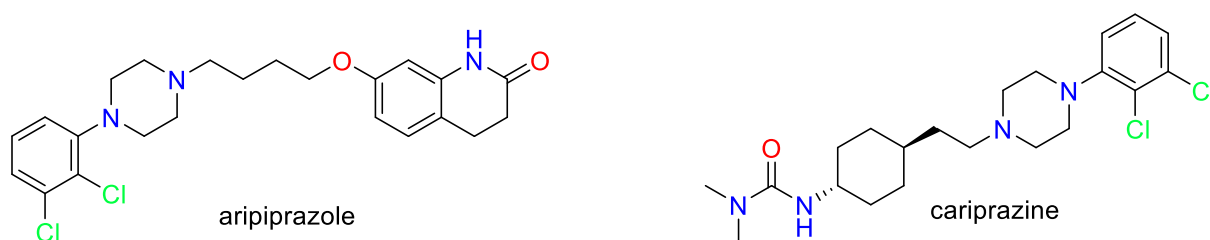
Figure (4.7): Antipsychotic drugs with multi-target activity.

After a century now from the date of Ehrlich's hypothesis that combination of two or more chemotherapeutic agents would be superior to single treatments as it would help prevent resistance (Ehrlich 1913), many attempts to design multi-target agents were performed against several targets *e.g.* histone deacetylases (HDACs) (Bolognesi 2013; Ramsay *et al.* 2018). Although, the most extensively investigated protocol of multi-targeting in cancer therapy are multi-kinase inhibitors *e.g.*

sunitinib, sorafenib, lenvatinib and imatinib (**Figure 4.8**), as with all other fields of drug discovery research, efforts were previously directed towards the development of more selective kinase inhibitors. However, it is now widely believed that interacting with multiple kinases is crucial for their anti-cancer activity as resistance is rising against single targets in most cancer diseases (Ramsay *et al.* 2018; Skok *et al.* 2019).
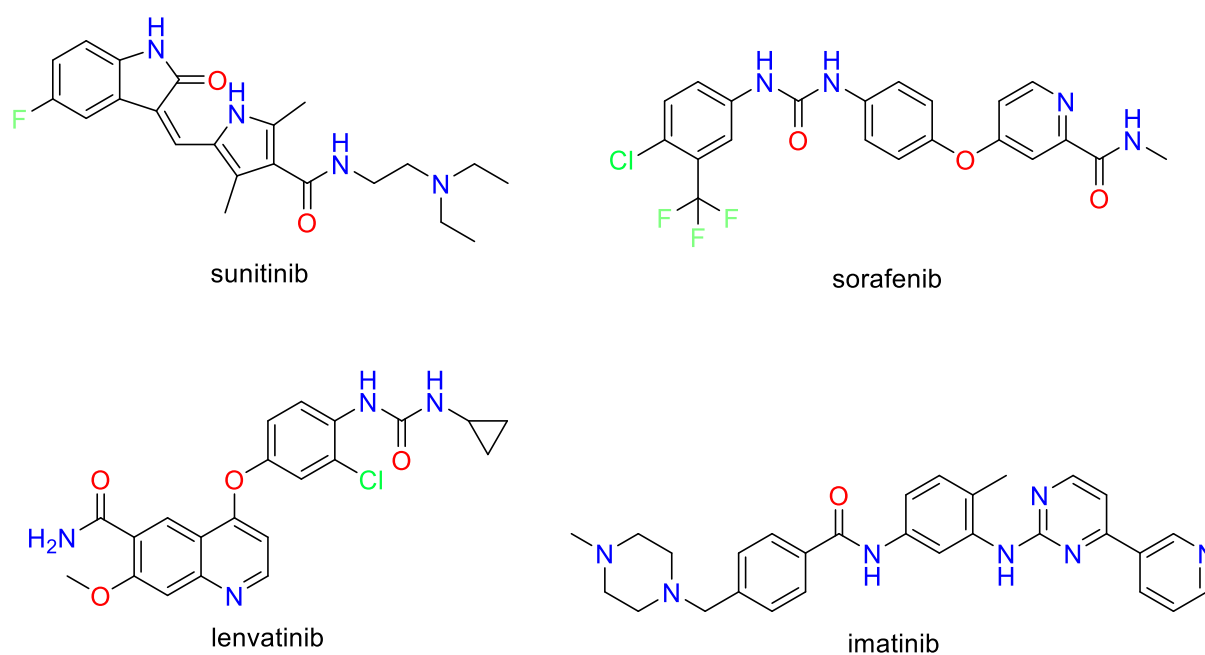
Figure (4.8): Examples of multi-kinase inhibitors.

4.1.7. MTDL in Breast cancer

In the breast cancer setting, multi-targeting is a very popular approach of study due to resistance issues leading to a wide variety of multi-targeted drugs. Oestrogen receptor (ER), HER-2, EGFR, VEGFR, PI3K, mTOR, 17β-HSD1, aromatase enzyme and steroid sulfatase enzyme have all been targets for development of dual acting inhibitors (Proschak *et al.* 2019; Tripathi *et al.* 2019; Zhou *et al.* 2019; Salah *et al.* 2017). Each of the dual inhibitor target combinations was inspired by the crucial role played by the target in the welfare of the tumour in different subclasses of breast cancer. In HER-2+ breast cancer, lapatinib, a tyrosine kinase inhibitor (**Figure 4.9a**), possesses a beneficial dual inhibitory activity against HER-2 and EGFR (Burris 2004). AZD-8055 and OSI-027 (**Figure 4.9b**) demonstrated dual inhibition of mTOR1 and mTOR2 and promising activity in TNBC (Chresta *et al.* 2010; Bhagwat *et al.* 2011). Various multi-kinase inhibitors against angiogenesis

pathway receptors have been described, including axitinib, motesanib, pazopanib, vandetanib and cediranib (**Figure 4.9c**).
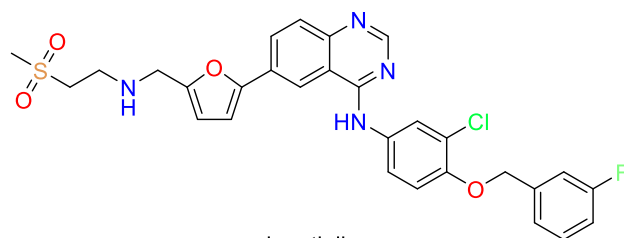
lapatinib

(a) Dual HER-2/EGFR inhibitor
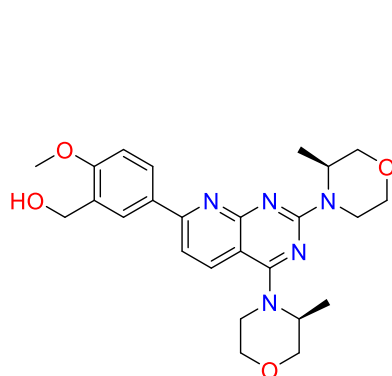
AZD-8055
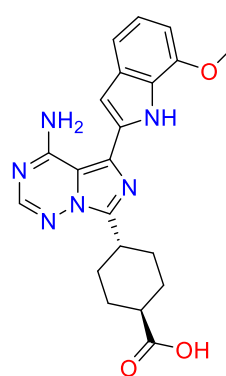
OSI-027

(b) Dual mTOR1/mTOR2 inhibitors
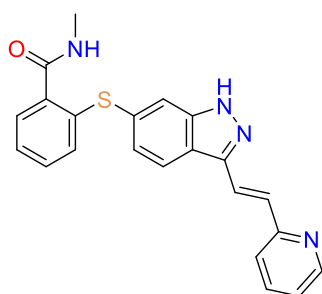
axitinib
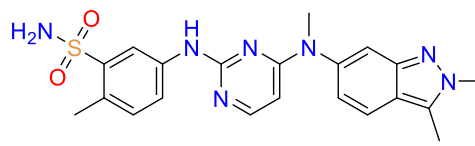
pazopanib
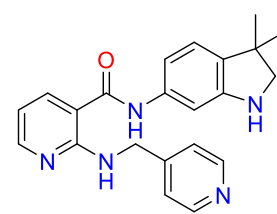
motesanib
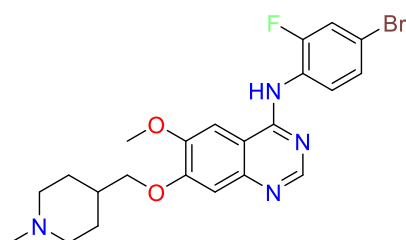
vandetanib
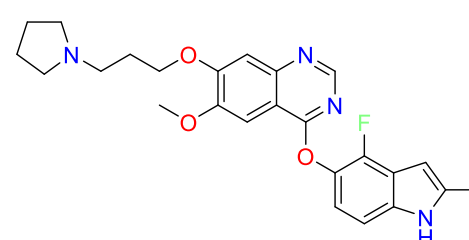
cediranib

(c) Multikinase inhibitors against angiogenesis

Figure (4.9): Some of the MTDL examples in the breast cancer setting.

Dual inhibitors of PI3K and mTOR *e.g.* GSK2126458 and VS-5584 (**Figure 4.10a**) are effective in both TNBC and ER⁺ breast cancer (Knight *et al.* 2010; Kolev *et al.* 2015; Tripathi *et al.* 2019). A combination of a SERM (tamoxifen) and a VEGFR-2 inhibitor (brivanib alaninate) (**Figure 4.10b**) improved efficacy and helped to prevent SERM resistance inspiring some research to develop a dual inhibitor against ERα and VEGFR-2 using a linked pharmacophore approach demonstrating *in vitro* antiproliferative activity alongside *in vivo* antiangiogenetic activity (Patel *et al.* 2010; Tang *et al.* 2014; Zhou *et al.* 2019). Also, combination between steroid sulfatase (STS) inhibitors and aromatase inhibitors proved beneficial in a phase II clinical trial, the IRIS study, using Irosustat with aromatase inhibitors (Palmieri *et al.* 2017).

GSK2126458

VS-5584

(a) Dual PI3K/mTOR inhibitors

Brivanib Alaninate

(b) VEGFR-2 inhibitor

Irosustat

(c) Steroid sulfatase inhibitor
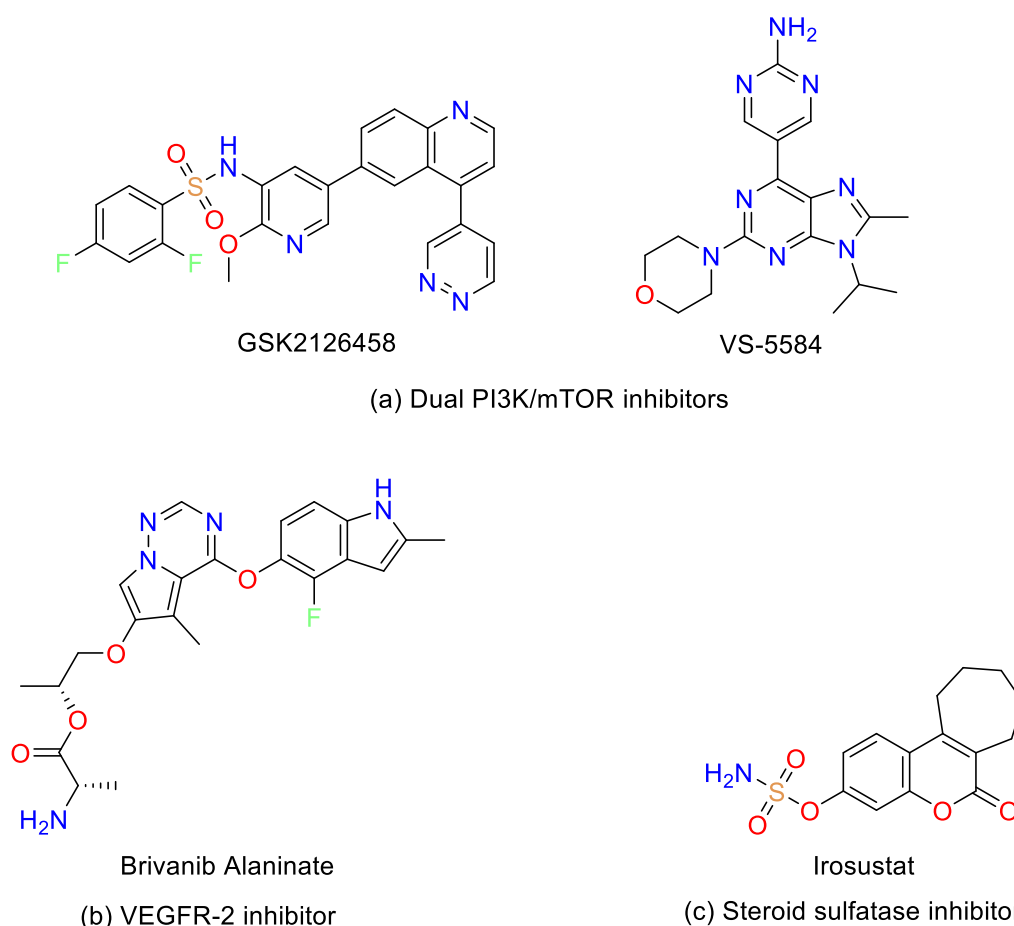
Figure (4.10): Examples of compounds used in ER⁺ breast cancer.

In oestrogen dependant breast cancer, dual inhibition of oestrogen synthesis from androgens through the aromatase enzyme and oestrogen sulphate stores through the sulfatase enzyme simultaneously, was an interesting approach leading to the development of several dual

aromatase/sulfatase inhibitors (DASIs) (Begam *et al.* 2017). Merging the pharmacophores responsible for inhibition of the two enzymes was achieved by incorporation of a phenol sulfamate moiety responsible for sulfatase activity into an aromatase inhibitor scaffold depending upon X-ray structures of enzyme-ligand complexes, docking and extensive SAR studies. Various DASIs were developed over time with activity ranging between reasonable nanomolar range to outstanding picomolar values (**Figure 4.11**) (Woo *et al.* 2003; Jackson *et al.* 2007; Woo *et al.* 2007; Woo *et al.* 2010; Woo *et al.* 2011; Wood *et al.* 2011; Proschak *et al.* 2019).
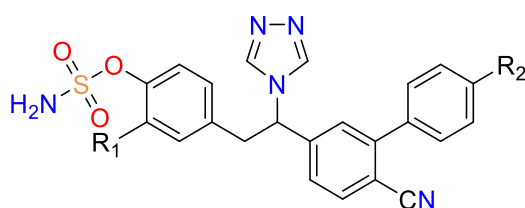
R_1	R_2	Aromatase IC$_{50}$ (nM)	STS IC$_{50}$ (nM)
Cl	H	**0.015**	**0.83**
Br	H	**0.018**	**0.13**
H	OCH$_3$	0.015	22

Figure (4.11): Picomolar active DASIs.

4.2. Objectives of this chapter

In an attempt to circumvent the development of resistance in anti-hormonal treatment, a clear research question was raised, whether it is possible to make use of the potent aromatase inhibitor benzofuran/triazole scaffold to build dual aromatase-sulfatase inhibitors.

Objectives to be fulfilled by the end of this chapter:

1- To understand the binding requirements of the sulfatase enzyme and use of the knowledge gained to design dual aromatase-sulfatase inhibitors.
2- To develop synthetic routes to synthesise the novel inhibitors.
3- To perform enzyme inhibitory experiments to assess the efficacy of novel inhibitors.

4.3. Design of dual aromatase sulfatase inhibitors

The natural substrates of aromatase and sulfatase enzymes (oestrogen and oestrogen sulphate) share a high degree of structural similarity with just one extra group: the sulphate group in the substrate of the sulfatase enzyme making the design-in technique an appropriate method to build the DASIs. This involved the incorporation of the sulfamoyl group, required for sulfatase activity, into the phenol scaffold of the aromatase inhibitors (**Figure 4.12**).
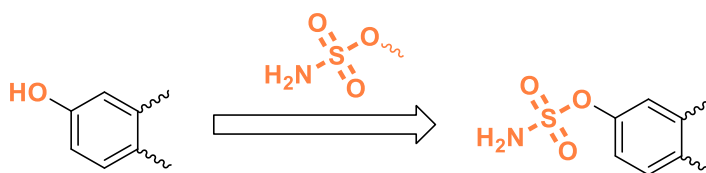
Figure (4.12): Incorporation of sulfamoyl group (orange) to the phenolic scaffold of aromatase inhibitors.

The general idea was to compare three different positions for the sulfamate group: the parent C6 of the benzofuran ring, C5 of the benzofuran ring and C4 of the phenyl ring. Also, varying the substituent on the C4 of the phenyl ring in the parent compound from chloro to fluoro or cyano groups to help build a clearer SAR (**Figure 4.13**).
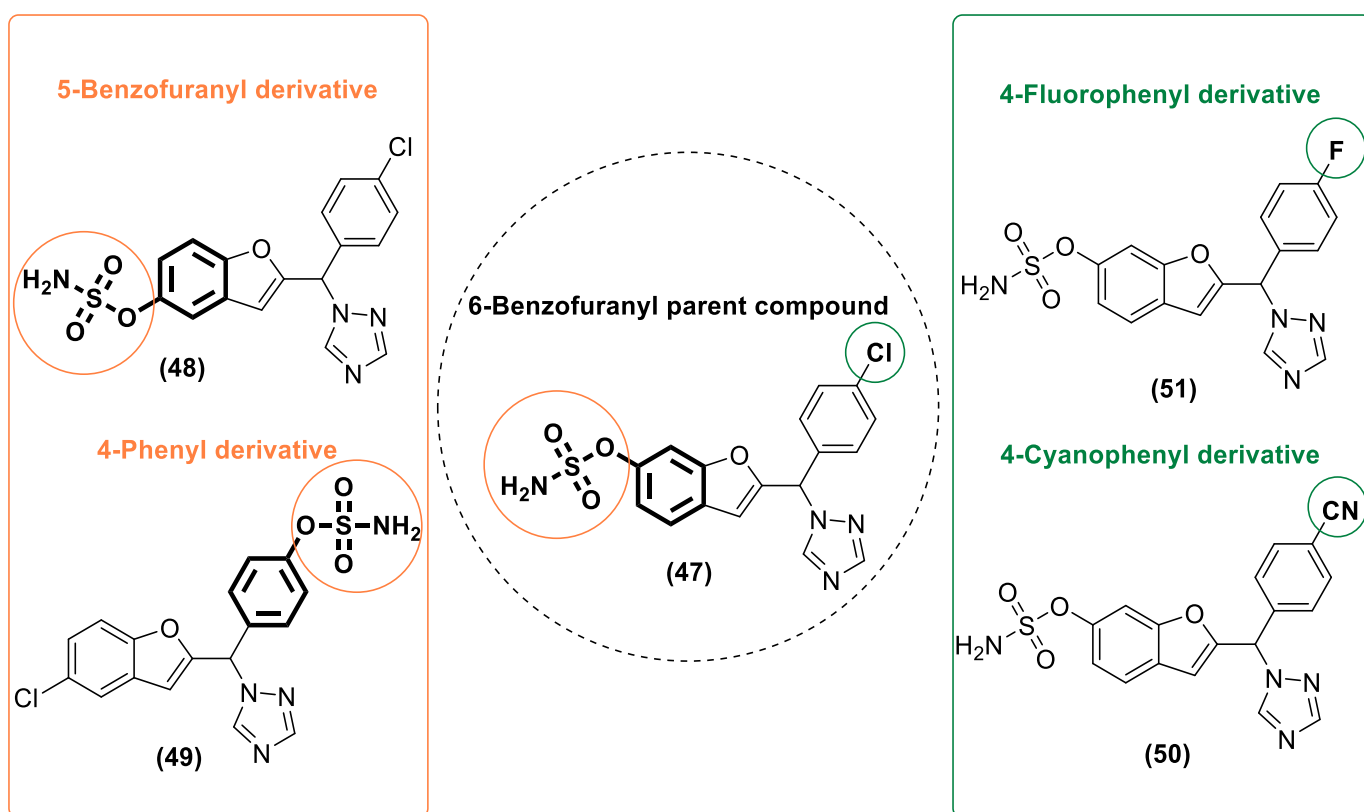
Figure (4.13): Two sets of comparisons with the structure variations represented in bold; varying the position of sulfamate indicated in orange and varying the phenyl substituent indicated in green.

4.4. Results and discussion

4.4.1. Computational Studies

Ligand complexes with the aromatase enzyme prepared in MOE as previously described in chapter two were subjected to MD simulations for 150 ns. The results showed that the *S*-enantiomer had the ability to bind the haem iron through the N4 of the triazole ring, however the *R*-enantiomer interacted through the N2 of the triazole ring suggesting improved binding interactions of the *S*-enantiomer for the haem (**figure 4.14**).
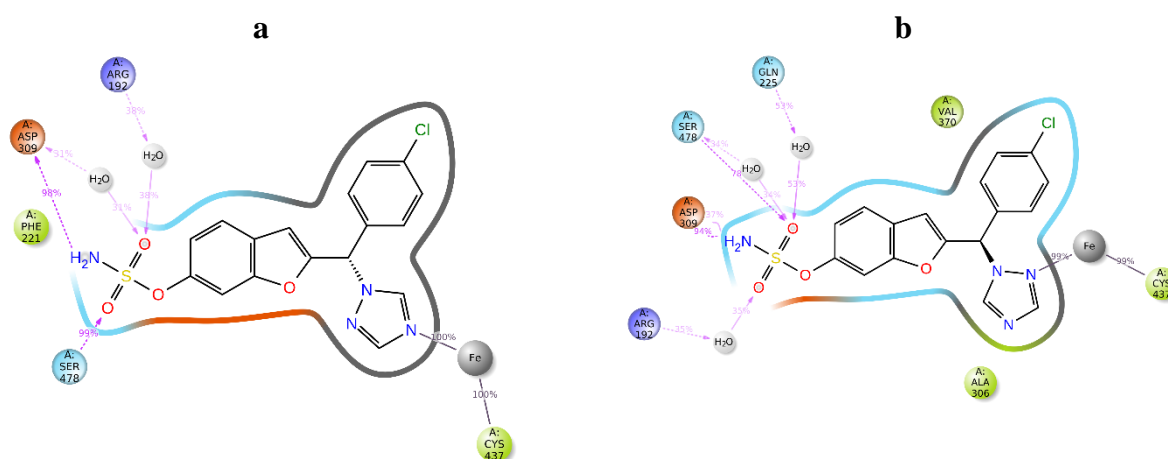
Figure (4.14): Comparing the haem binding between the enantiomers of sulfamate compound **47** over the course of 150 ns MD simulations (a) *S*-enantiomer of **47** (b) *R*-enantiomer of **47**.

The ligand-protein complex formed between compound **47** (*S*-enantiomer) and aromatase enzyme was generally stable during the simulation time with RMSD values ranging from (P/L 1.18/0.95 Å) at the beginning to (P/L 1.87/1.12) towards the end of the simulation (**figure 4.15**).
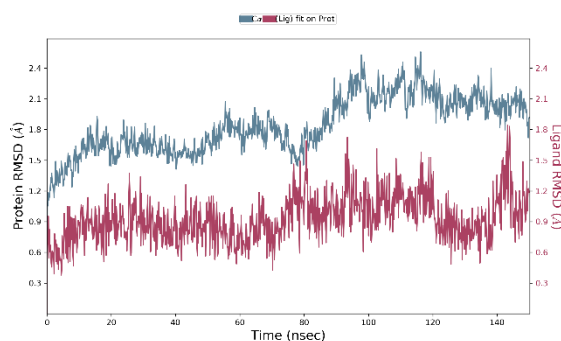
Figure (4.15): Protein-ligand RMSD plot for the *S*-enantiomer of compound **47** with aromatase enzyme showing the stability of the complex through the simulation time, ligand RMSD in red and protein RMSD in blue.

The results also revealed the potential for the sulfamate group to form hydrogen bond interactions with some of the key amino acid residues, Arg 192, Asp 309 and Ser 478 as shown in **figure 4.16**.
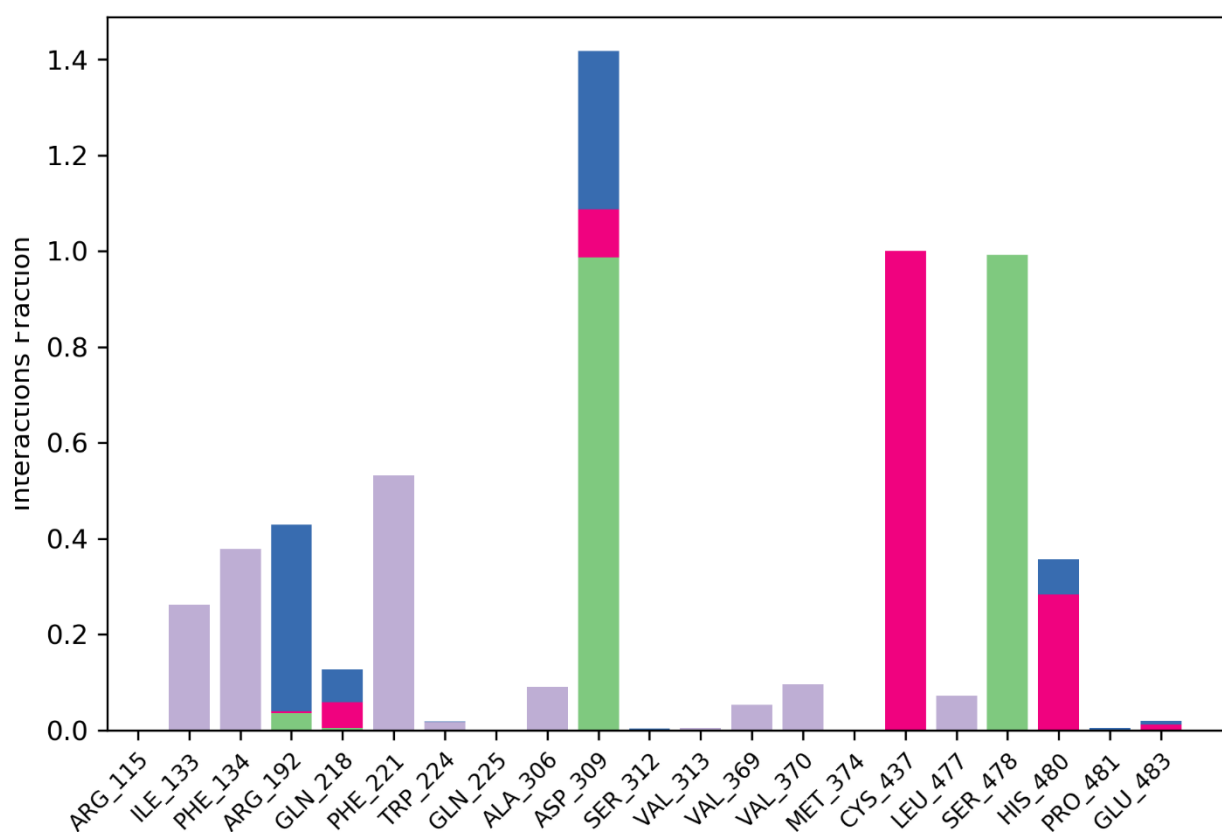
Figure (4.16): Protein-ligand interactions through the whole simulation time showing amino acid residues interactions, including Arg 192 (mainly through water bridges), Asp 309 and Ser 478 (through hydrogen bonds).

Computational studies using the crystal structure of the human steroid sulfatase enzyme (PDB 1P49) were far less successful than the aromatase enzyme. The gem diol of formyl glycine residue 75 was obtained by manually deleting the sulphate group and the docking process was performed for the well-known STS inhibitor (Irosustat) after the active site was selected by the site finder tool in MOE to include Leu 74, Als 75, Arg 98, Thr 99, Gly 100, Val 101, Leu 103, Lys 134, His 136, Thr 165, Asn 166, Leu 167, Arg 168, Val 177, Phe 178, Thr 179, Thr 180, Gly 181, His 290, Thr 291, His 346, Glu 349, Lys 368, Thr 484, His 485, Val 486 and Phe 488. MD simulations were performed for the generated complex for 150 ns with the results showed impracticality of modelling the STS inhibition positioning the sulfamate group far away from the gem diol group of formyl glycine residue 75 which plays the main role in both the activity and inhibition of the enzyme (**figure 4.17**) (Reed *et al.* 2005; Recksiek *et al.* 1998).
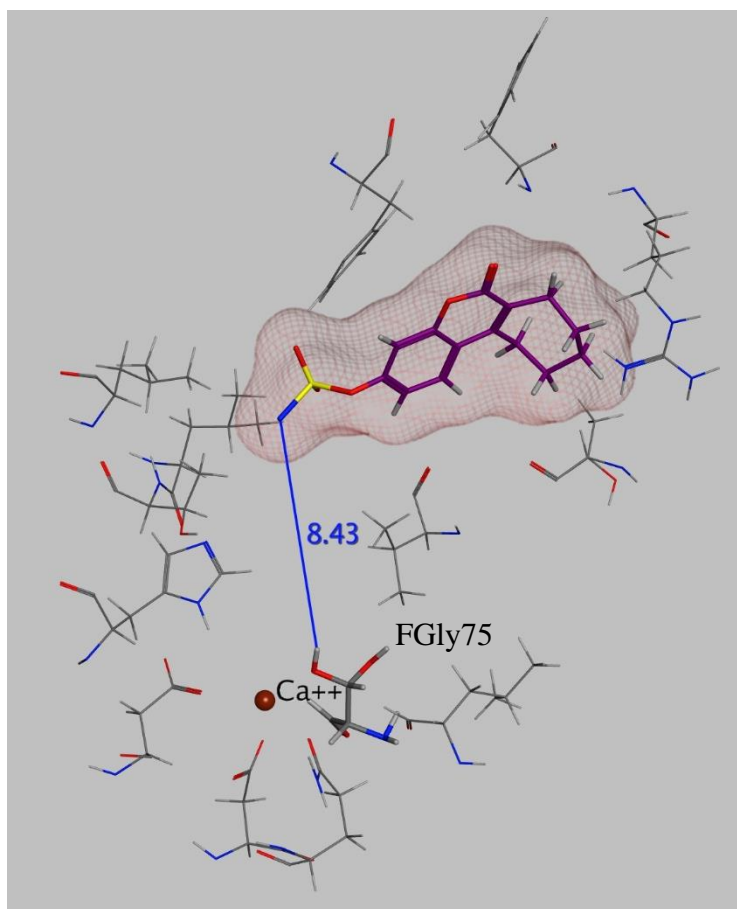
Figure (4.17): Final frame after 150 ns MD simulations for Irosustat with the sulfatase enzyme showing distance in Å between sulfamate group and the gem diol of formyl glycine 75 residue.

4.4.2. Chemistry

Starting with the phenol scaffold of the aromatase inhibitors, preparing the DASI involved two consecutive steps. The first of which was the preparation of the sulfamoyl chloride (**46**), which was then reacted with the phenolic compounds (**11, 12, 13, 14, 17**) in a nucleophilic substitution reaction to produce the required sulfamate compounds (**47-51**).
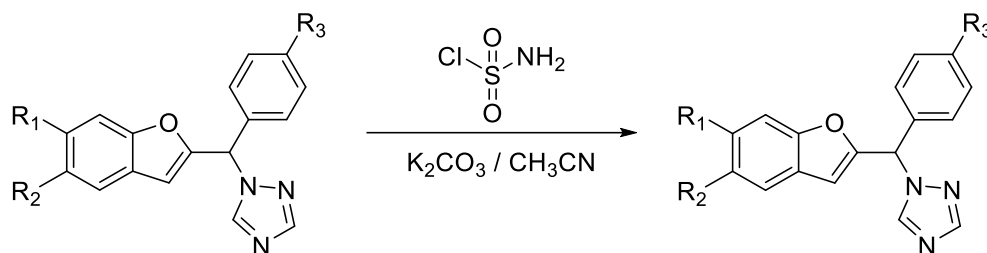
Compound	R$_1$	R$_2$	R$_3$
11	OH	H	Cl
12	H	OH	Cl
17	H	Cl	OH
14	OH	H	CN
13	OH	H	F

Compound	R$_1$	R$_2$	R$_3$
47	OSO$_2$NH$_2$	H	Cl
48	H	OSO$_2$NH$_2$	Cl
49	H	Cl	OSO$_2$NH$_2$
49b	H	Cl	OCONH$_2$
50	OSO$_2$NH$_2$	H	CN
50b	OCONH$_2$	H	CN
51	OSO$_2$NH$_2$	H	F

Five different sulfamate derivatives were successfully prepared through this synthetic pathway. A carbamate compound (**49b, 50b**) was formed as a side product with the sulfamate compound in two different occasions. The interesting side product **50b** was then intentionally prepared through different reaction conditions and included for biological investigations raising the number of biologically tested compounds against both aromatase and sulfatase enzymes to seven compounds. The detailed aromatase activity will be discussed later however lack of sulfatase activity for these seven compounds raised a question about the reason. To try to address the answer to this question a truncated analogue (**56a-f**) was prepared based on the ketone species formed in the first step (**9a-k**) of the aromatase inhibitors synthetic pathway, after pyran deprotection giving compound **39a-j**.

4.4.2.1. **Sulfamoylation of Phenolic compounds** (Wood *et al.* 2011; Ahmed *et al.* 2002; Appel and Berger 1958)
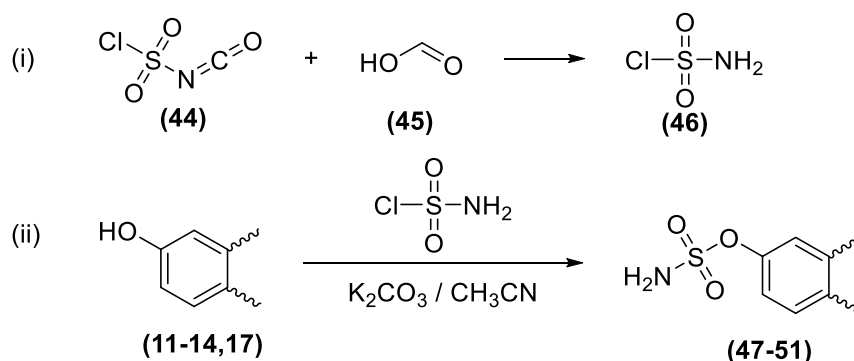
The sulfamoyl chloride (**46**) prepared *in situ* from the reaction of chlorosulfonyl isocyanate (**44**) and formic acid (**45**) (Wood *et al.* 2011; Ahmed *et al.* 2002; Appel and Berger 1958) was used without purification or characterisation. This reaction is extremely sensitive to moisture. Using dry solvents and freshly opened, well preserved chemicals were crucial to the formation of the required product in relatively good yield. Sulfamoyl chloride was added to the phenolic compound (**11-14, 17**) in the presence of K_2CO_3 as a base to deprotonate the phenolic group leading to a nucleophilic substitution reaction to provide the required sulfamate compounds (**47-51**). The reaction was tracked by TLC to monitor the progress. However, even with the addition of excess base and/or excess sulfamoyl chloride, the reaction was not complete with yields ranging from 16% to 39%.

The identity of the compounds was confirmed by ^{1}H NMR, which showed the appearance of a broad singlet signal integrating for two protons of the amine group at around 8.0 ppm, with the disappearance of the broad singlet integrating for one proton of the phenolic OH in the range 9-10 ppm.

An unexpected carbamate side product (**49b, 50b**) was formed in two of the derivatives. This may be attributed to the presence of moisture in the reaction. The carbamate side product was identified by ^{1}H NMR, which showed the appearance of two separate broad singlet signals each integrating for one proton between 6.5 and 7.5 ppm (**Figure 4.18**). This may be attributed to the tautomerism of the amidic group leading to the inequality between the two protons. Also, ^{13}C NMR supported this assumption by the presence of an extra quaternary carbon when compared with the ^{13}C NMR spectrum of the sulfamate compound.
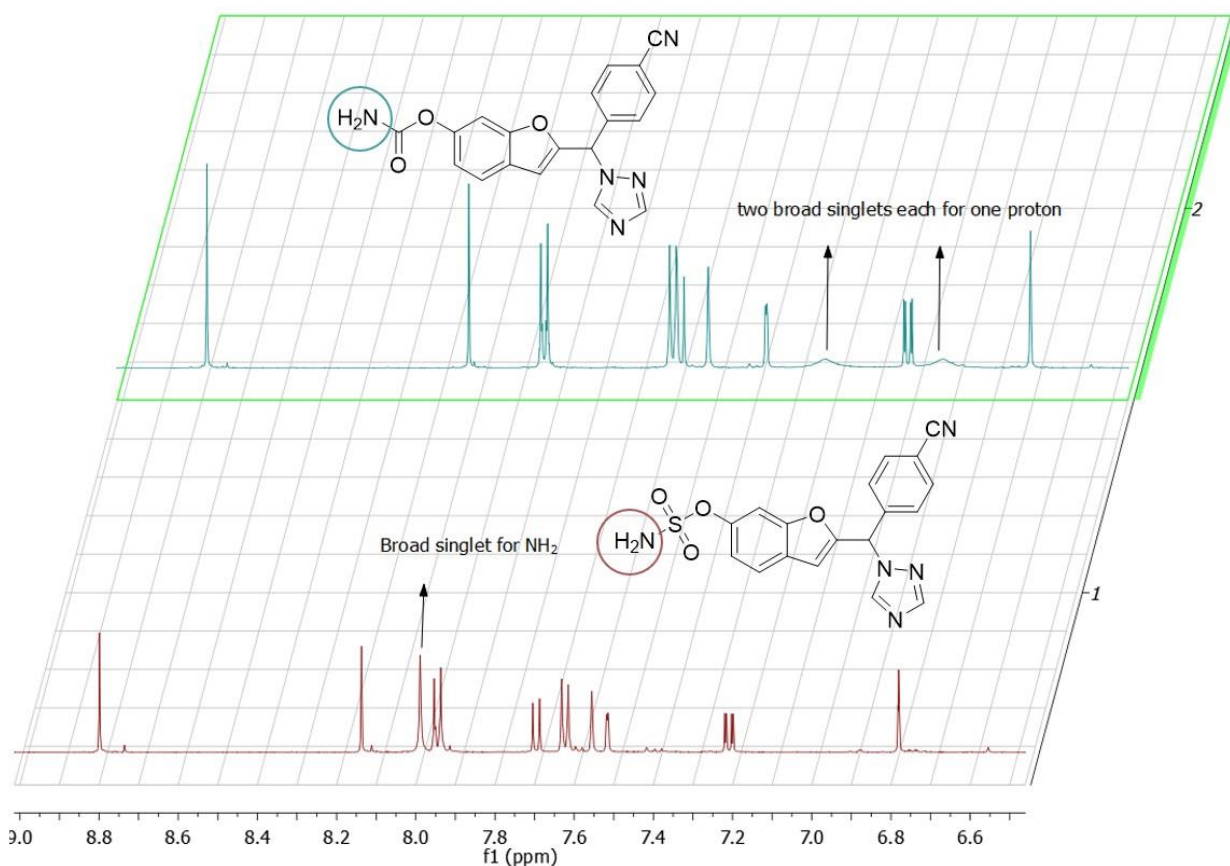
Figure (4.18): Comparison between the ^{1}H NMR spectra of the sulfamate and carbamate products indicating the difference in the amino group signals.

Verification of the carbamate side product was performed by the intentional synthesis of the carbamate compound (Singh *et al.* 2016) using chlorosulfonyl isocyanate/H$_2$O instead of sulfamoyl chloride and comparing the product from the two methods.

The identity of the sulfamate compound and the carbamate side product was confirmed by HRMS with a difference of 36 between the weight of the sulfamate and the carbamate.

4.4.3. Biological evaluation

Seven compounds including two carbamate side products were investigated for their aromatase and sulfatase enzymes inhibitory activity. Knowing that the parent compounds had strong aromatase inhibitory activity, the compounds were preliminarily tested for aromatase inhibitory activity at 10 nM to check that they retained aromatase inhibitory activity after the incorporation of the sulfamoyl group. All compounds, except compound **48**, showed more than

50% aromatase inhibition and were further investigated for IC_{50} confirming retention of aromatase inhibitory activity at low nanomolar range (**Table 4.1**).

Table (4.1): Aromatase inhibitory activity of the compounds displayed in nM with the most active compounds indicated by (*).

Compound	Aromatase IC_{50} (nM)	95% Confidence interval (nM)
47	1.4*	1.060 – 1.848
48	>10	-
49	5.49	-
49b	4.1	3.646 – 4.797
50	1.52*	1.427 – 1.628
50b	0.65*	0.603 – 0.696
51	8.4	6.672 – 10.620

The results not only provided some preliminary SAR in terms of position and nature of substituents, but also showed that the carbamate side product (**49b, 50b**) was more active against the aromatase enzyme. There was clear superiority for the 6- benzofuran for the sulfamate group over the 5- benzofuran or the 4-phenyl positions. Also, the chloro and cyano derivatives were better than the fluoro derivative (**Figure 4.19**).
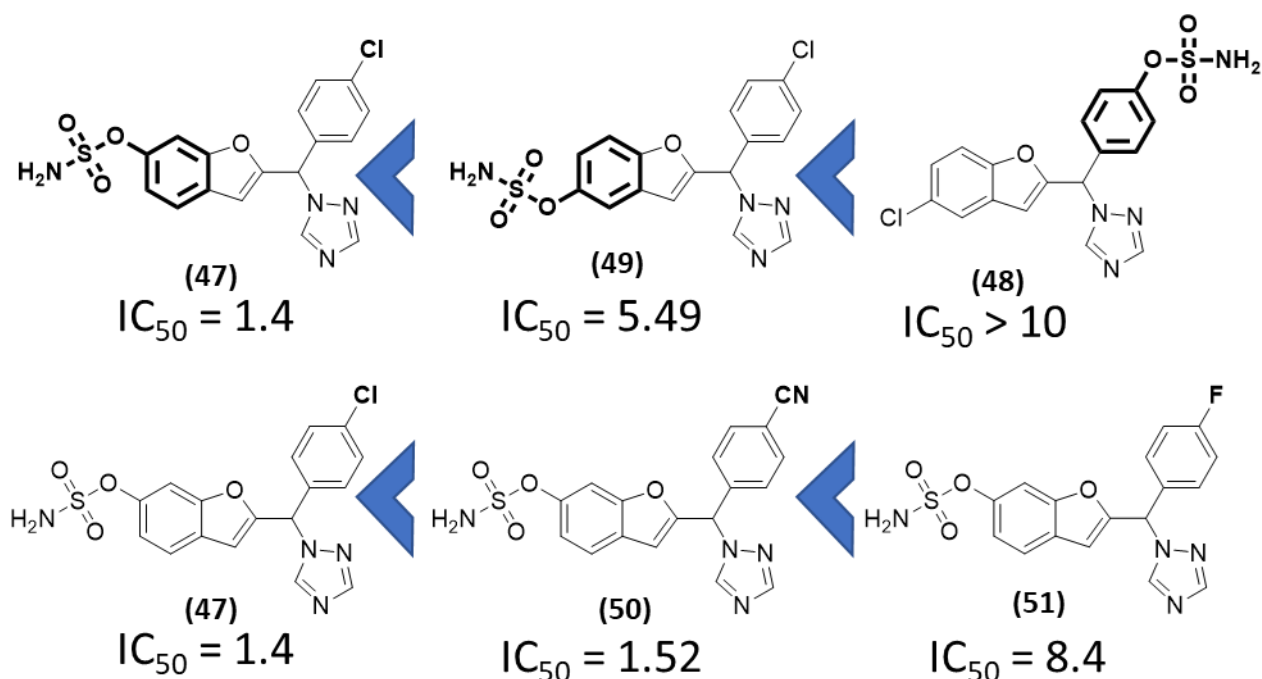
Figure (4.19): Order of aromatase activity of the sulfamate compounds represented in IC_{50} showing the SAR.

Despite this low nanomolar aromatase activity, when it came to the sulfatase enzyme, all the compounds showed complete loss of activity at 10 µM (**Figure 4.20**).
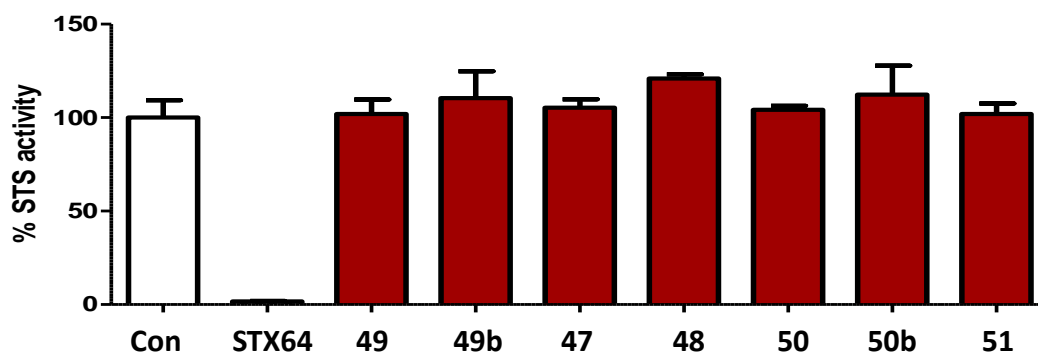
Figure (4.20): Sulfatase activity of the compounds showing the lack of activity for all test compounds compared with the positive and negative control.

At first, these results were quite surprising and required further investigation to understand. However, literature evidence allowed a rationale for the results obtained. A vorozole-derived sulfamate having a similar geometry to the benzofuran derivatives described here showed the same result of nanomolar aromatase activity and sulfatase activity more than 10 µM (**Figure 4.21**) (Wood *et al.* 2011). Also Jackson *et al.* 2007 suggested that the presence of the triazole group in the compounds reported in that publication may cause steric hinderance within the STS active site.

IC_{50} ^{arom} = 29 nM
IC_{50} ^{STS} > 10000nM
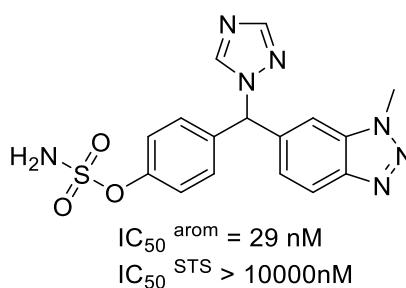
Figure (4.21): IC_{50} against both aromatase and sulfatase for compound reported by (Wood *et al.* 2011).

4.4.4. Design of the ketone sulfamate compounds
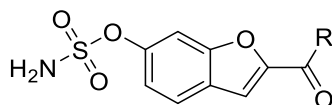
R	Compound
4-Chlorophenyl	**56a**
4-Fluorophenyl	**56b**
4-Bromophenyl	**56c**
2,4-Dichlorophenyl	**56d**
Thiophene	**56e**
Adamantane	**56f**

To investigate the relation between the lack of sulfatase activity and the geometric orientation of the compounds (**47-51**), a series of truncated compounds (**56a-f**), lacking the triazole group but retaining the benzofuran scaffold, were designed based on the STX64 (Irosustat) structural similarity (**Figure 4.22**). These truncated compounds had the triazole group replaced by a carbonyl group to offer some planarity and rigidity to the structure.
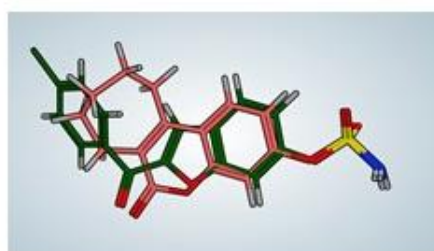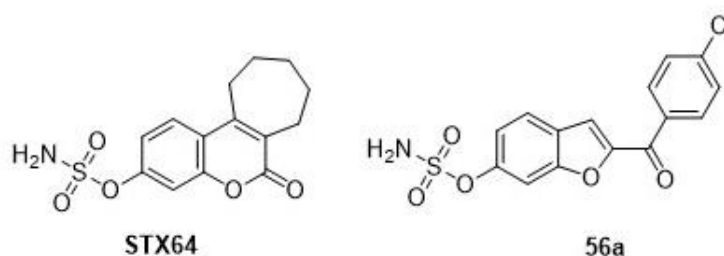
Figure (4.22): Structural similarity between compound **56a** and STX64 through flexible alignment of the 3D structure, where compound **56a** is represented in green and Irosustat in pink.

4.4.5. Synthesis of the ketone sulfamate compounds

A three-step synthetic pathway was used to prepare the final compounds (**56**). The first step involved the benzofuran ketone derivative formation followed by a pyran deprotection step. The produced phenolic compounds (**39**) were subjected to sulfamoylation step to produce the final products (**56**).

	R
2a	4-Chlorophenyl
2b	4-Methoxyphenyl
2c	4-Fluorophenyl
2d	4-benzonitrile
2e	4-Bromophenyl
2f	2,4-Dichlorophenyl
52	Phenyl
53	Pyridin-3-yl
54	Thiophen-3-yl
55	Adamantan-1-yl

	R
9a	4-Chlorophenyl
9c	4-Fluorophenyl
9d	4-benzonitrile
9e	4-Bromophenyl
9f	2,4-Dichlorophenyl
9g	Phenyl
9h	4-Methoxyphenyl
9i	Pyridin-3-yl
9j	Thiophen-3-yl
9k	Adamantan-1-yl

	R
39a	4-Chlorophenyl
39b	4-Fluorophenyl
39c	4-Bromophenyl
39d	2,4-Dichlorophenyl
39e	Phenyl
39f	4-Methoxyphenyl
39g	4-benzonitrile
39h	Pyridin-3-yl
39i	Thiophen-3-yl
39j	Adamantan-1-yl

	R
56a	4-Chlorophenyl
56b	4-Fluorophenyl
56c	4-Bromophenyl
56d	2,4-Dichlorophenyl
56e	Thiophen-3-yl
56f	Adamantan-1-yl

Scheme (4.1): The synthetic pathway for the sulfamate derivatives (**56a-f**), (i) K_2CO_3, CH_3CN, 70 °C, 3 h (ii) HCl/dioxane, 1h, (iii) sulfamoyl chloride, K_2CO_3, CH_3CN, 16h.

4.4.5.1. Benzofuran ketone formation
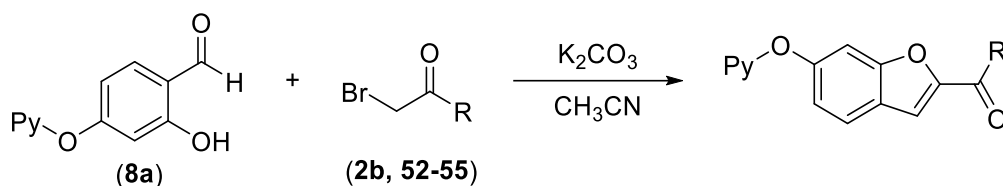
R	Compound
Phenyl	**9g**
4-Methoxyphenyl	**9h**
Pyridyl	**9i**
Thiophene	**9j**
Adamantane	**9k**

This reaction is a Rap-Stoermer formation (Pestellini *et al.* 1988; Mahboobi *et al.* 2007) as described in chapter 2 for the synthesis of (4-substitutedphenyl)(5- or 6-substitutedbenzofuran-2-yl) methanone (**3a-e**). The adamantane and thiophene derivatives followed the same behaviour as their phenyl analogues. The only exception was pyridin-3-yl(6-((tetrahydro-2*H*-pyran-2-yl)oxy)benzofuran-2-yl)methanone (**9i**), which had a more complex reaction as indicated by TLC which required column chromatography to afford the product with a much lower yield than all other family members (34%).

4.4.5.2. Pyran deprotection
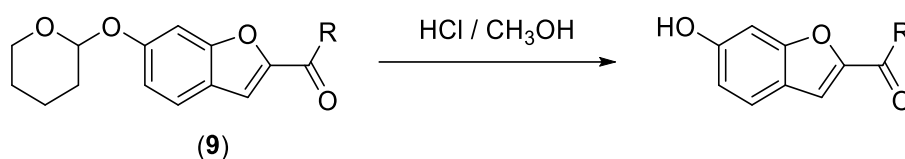
R	Compound
Phenyl	**39e**
4-methoxyphenyl	**39f**
4-cyanophenyl	**39g**
Pyridyl	**39h**
Thiophene	**39i**
Adamantane	**39j**

This reaction is a fast acid catalysed pyran deprotection reaction (Jepsen *et al.* 2011), which only took 1h at room temperature as identified by TLC tracking, which showed complete disappearance of the starting material and appearance of a lower spot indicating the formation of the free phenolic OH group.

The identity of the compound was confirmed by ^{1}H NMR, which showed the disappearance of all pyran signals in the aliphatic region of the spectrum and the appearance of a broad singlet signal corresponding to the phenolic OH at around 10.0 ppm.
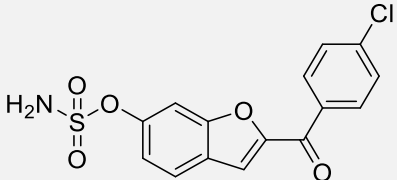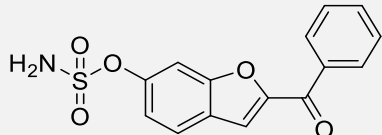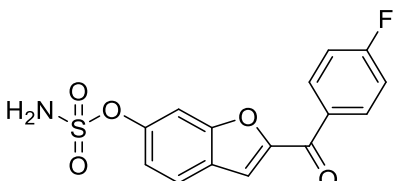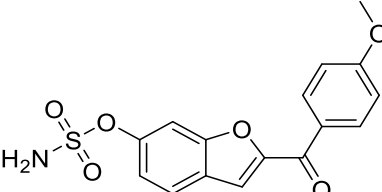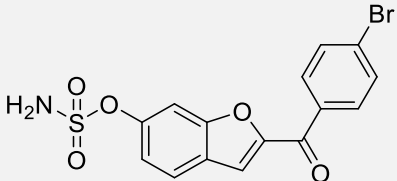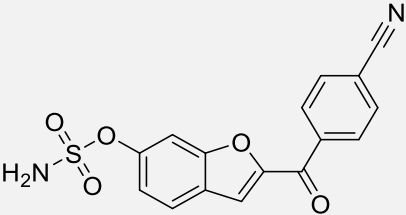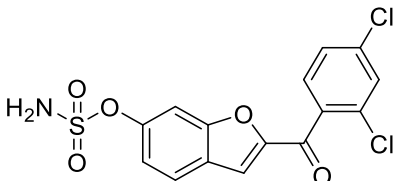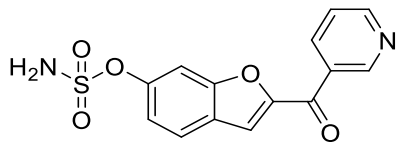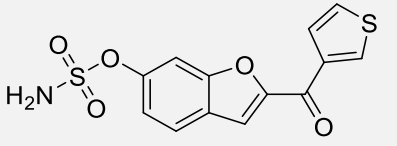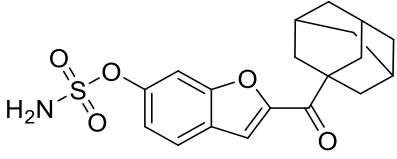
4.4.5.3. Preparation of the Sulfamate final compounds
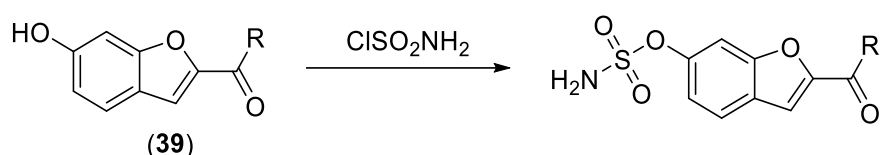
(**39**)

R	Compound
4-Chlorophenyl	**56a**
4-Fluorophenyl	**56b**
4-Bromophenyl	**56c**
2,4-Dichlorophenyl	**56d**
Thiophene	**56e**
Adamantane	**56f**

The general method for sulfamoylation of phenolic compounds used in this chapter included the *in situ* formation of sulfamoyl chloride (Wood *et al.* 2011; Ahmed *et al.* 2002; Appel and Berger 1958). However, applying the exact same method in the preparation of the sulfamate analogues of the benzofuran ketone compounds was not successful with a trace reaction detected by TLC. This may be attributed to the general lower reactivity of the ketone species when compared to their triazole analogues. The strength of the base used, which is K_2CO_3, would also be expected to be a determining factor in this reaction. The use of a stronger base, such as NaH, would have been expected to improve the reactivity, however it is not an option with these compounds due to the acidity of the C3 benzofuran proton. The use of commercially available sulfamoyl chloride slightly improved the yield in some derivatives especially those derivatives having electron withdrawing groups on the phenyl group. However, it was not possible to separate the pyridyl, unsubstituted phenyl, methoxy phenyl, or benzonitrile derivatives. The successful compounds suffered from extremely low yields (few

milligrams) which complicated the purification process. This would suggest that the current method is not optimal for the preparation of the required compounds. **Table 4.2** summarises the yield of the obtained compounds and the status of other compounds which were not separated.

Obtained compounds	*Yield*	*Other compounds*	*Status*
56a	6%	2-benzoylbenzofuran-6-yl sulfamate	Very faint spot
56b	3%	2-(4-methoxybenzoyl)benzofuran-6-yl sulfamate	Very faint spot
56c	4%	2-(4-cyanobenzoyl)benzofuran-6-yl sulfamate	Complex reaction
56d	4%	2-nicotinoylbenzofuran-6-yl sulfamate	No reaction
56e	7%		
56f	4%		

The percentage of purity suggested by HPLC analysis did not reflect the anticipated purity from TLC and NMR for all these compounds (**figure 4.23**), showing another peak overlapped with the peak of the compound with slightly higher retention time.
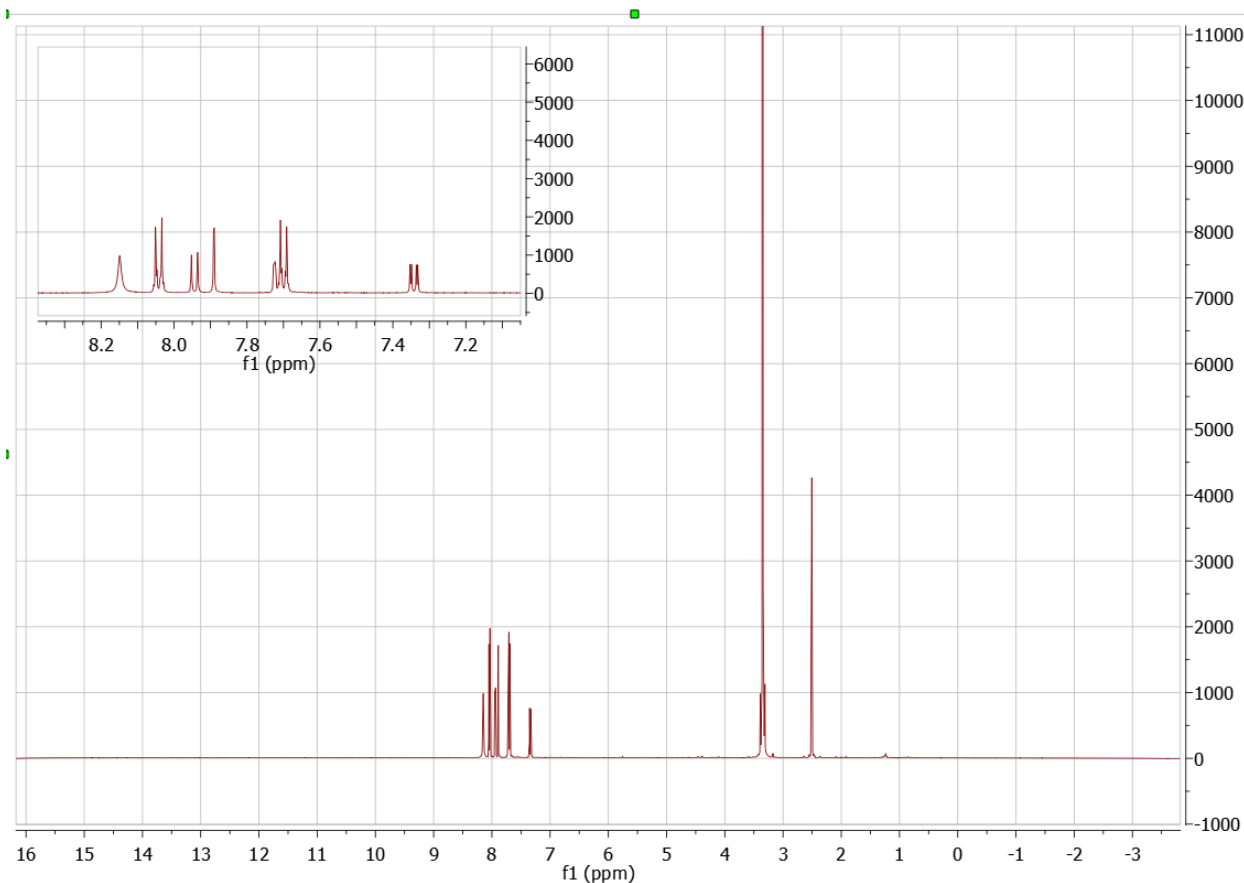
Figure (4.23): ^{1}H NMR for compound **56a** as an example for the sulfamate compounds to indicate purity.

HPLC indicated a second peak very close to the main peak as indicated in **figure 4.24**. Even compound **56e**, with 100% purity indicated by HPLC, showed a shoulder peak suggesting the presence of the same peak underneath but with lower difference in polarity so was not manually separated (**Figure 4.24(b)**)

a

b

The peak shoulder
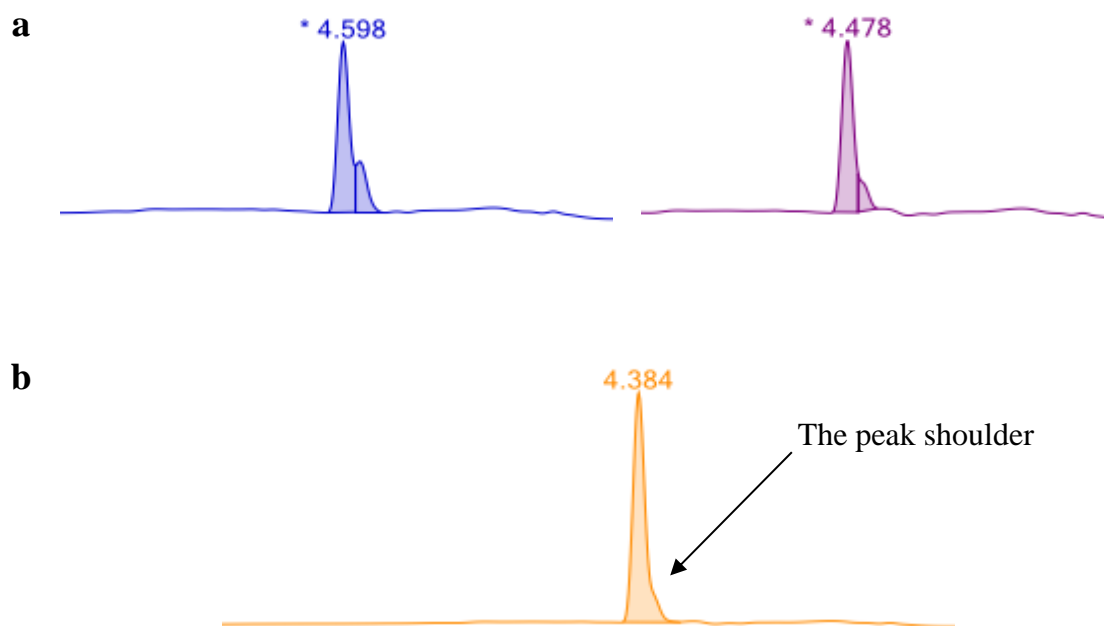
Figure (4.24): Magnified HPLC peaks of sulfamate compounds showing splitting of peaks (a) compounds **56a** and **56b** (b) compound **56e**.

This pattern of overlap was thought to be either due to instability of the compounds in the conditions of the HPLC or more probably due to tautomerism at the sulfamate group to sulfurimidate (**figure 4.25**). To validate the purity of these compounds, microanalysis for the available two compounds (**56a** and **56e**) were performed to find the exact CHN%. The results showed to be inconsistent with HPLC data with compound **56a** passed and **56e** failed. These results showed that the structure identity of the prepared compounds could be confirmed by NMR and HRMS, however the purity and stability of the products were questionable leading to non-reliable biological data.

Sulfamate form

Hydrogen sulfurimidate form
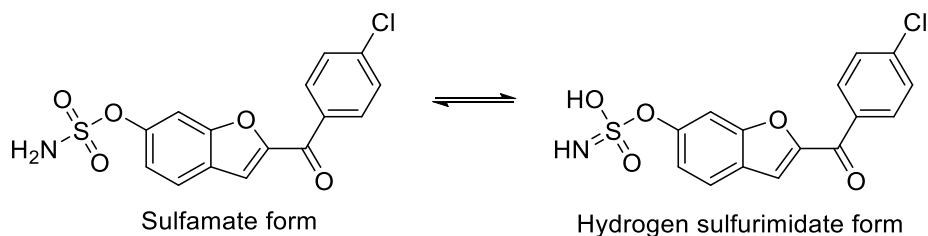
Figure (4.25): The tautomerism of compound **56a** between sulfamate and sulfurimidate forms.

4.4.6. Biological evaluation of the ketone sulfamate compounds

Compound **56a** was tested for both aromatase and sulfatase activity. As expected for aromatase, there was a decrease in activity to between 1 μM and 10 nM due to the lack of the triazole group in the compounds, which is important for haem interaction. However, the compound gained STS activity with IC_{50} around 400 nM (**Figure 4.26**) complying with the postulation of the steric hinderance. These findings were interesting in terms of providing a new lead compound for dual aromatase sulfatase inhibition. Further modifications and investigations are required to add to the SAR understanding of this scaffold.
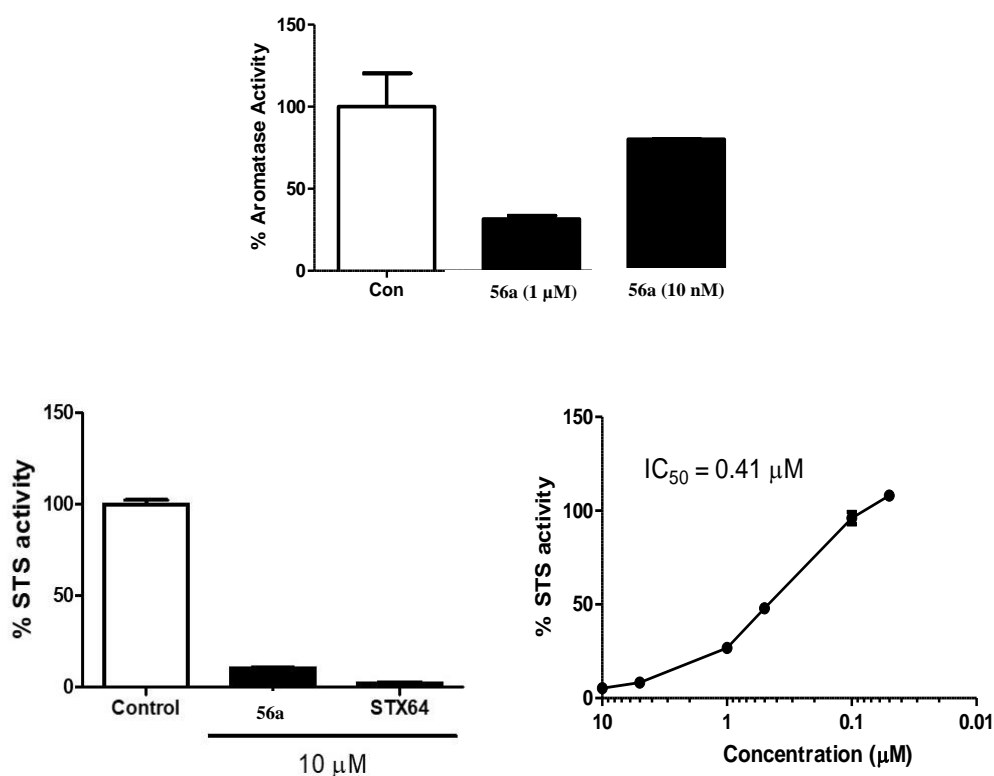
Figure (4.26): Aromatase and sulfatase activity of compound **56a**.

4.5. Conclusion and future work

Five triazole based sulfamate compounds (**47-51**) were successfully prepared using the suggested one step pathway from the analogous phenolic compound along with two carbamate side products (**49b, 50b**). All the prepared compounds were biologically evaluated against aromatase and sulfatase enzymes with IC_{50} values ranging from low nanomolar to picomolar values for the aromatase

inhibitory activity. However, none of the triazole derivatives showed any activity against the sulfatase enzyme. The lack of sulfatase activity was attributed to the steric hindrance caused by the tetrahedral geometry of the stereo-centric carbon atom.

Computational studies provided extra evidence for the biological results. MD simulations for compound **49a** with the aromatase enzyme showed good binding potential with the haem iron and hydrogen bonding potential with key amino acid residues. However, computational modelling with the sulfatase enzyme proved to be impractical using the current available techniques. As a result, flexible alignment with the known inhibitor Irosustat was found to be a better approach.

Compounds **56a-f** were prepared and evaluated against aromatase and sulfatase enzymes showing promising nanomolar activity against both enzymes. However, the synthetic scheme for these compounds was not optimal either owing to poor reactivity of starting material and/or questionable purity of the products, however it provides a lead compound to build upon with different variations on the phenyl side to add some heterocyclic moieties to investigate the possibility of optimising the aromatase activity through interactions with the haem iron as future work.

4.6. Experimental

4.6.1. General considerations

As previously described in section 2.5.1

4.6.2. Computational studies

Docking for the sulfatase enzyme: The crystal structure of human placental oestrone sulfatase (PDB 1P49) was downloaded from the protein data bank (https://www.rcsb.org). The gem diol of formyl glycine residue 75 was obtained by manually deleting the sulphate group. The 3D structures of compounds were generated using MOE builder, energy minimised and saved in a dataset ready for docking studies. The docking process was performed after the active site was selected by the site finder tool in MOE to include Leu74, FGly75, Arg98, Thr99, Gly100, Val101, Leu103, Lys134, His136, Thr165, Asn166, Leu167, Arg168, Val177, Phe178, Thr179, Thr180, Gly181, His290, Thr291, His346, Glu349, Lys368, Thr484, His485, Val486 and Phe488.

Docking for the aromatase enzyme: As previously described in section 2.5.2

Molecular Dynamics: As previously described in section 2.5.2

4.6.3. Chemistry

4.6.3.1. Sulfamoyl chloride (46) (Wood *et al.* 2011; Ahmed *et al.* 2002; Appel and Berger 1958)

$$Cl-\underset{\underset{O}{\|}}{\overset{\overset{O}{\|}}{S}}-NH_2$$
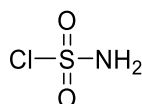
To chlorosulfonyl isocyanate (**44**) (2.31 mL, 26.5 mmol) cooled in an ice bath was added dropwise formic acid (**45**) (1 mL, 26.5 mmol) leading to evolution of gas. After cessation of gas evolution, the reaction mixture solidified, then dry toluene (20 mL) was added, and the reaction mixture was stirred at room temperature for 1 h. The produced solution of sulfamoyl chloride (**46**) was then used immediately without further purification or characterisation.

4.6.3.2. General procedure for sulfamoylation of phenolic compounds (Wood *et al.* 2011; Ahmed *et al.* 2002; Appel and Berger 1958)

To a solution of phenolic compound (**11, 12, 13, 14, 17**) (0.43 mmol) in dry CH_3CN (5 mL), K_2CO_3 (2.35 mmol) was added and the mixture stirred for 1 h at 40 ºC, then a freshly prepared solution of sulfamoyl chloride (**46**) (2.15 mmol) was added and the reaction mixture stirred at room temperature for 16 h. The reaction mixture was concentrated under reduced pressure and the residue dissolved in EtOAc (100 mL). The organic layer was washed with H_2O (3 x 50 mL), dried ($MgSO_4$) and concentrated under reduced pressure. Purification by gradient column chromatography afforded the required sulfamate at 80% EtOAc in petroleum ether (v/v) as a colourless oil.

4.6.3.2.1. 2-((4-Chlorophenyl)(1*H*-1,2,4-triazol-1-yl)methyl)benzofuran-6-yl sulfamate (47) Chemical Formula: $C_{17}H_{13}ClN_4O_4S$, Molecular Weight: 404.83
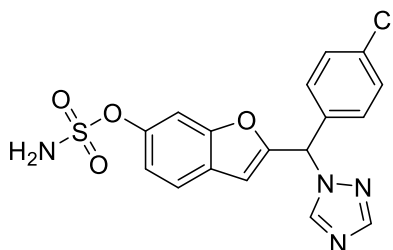
Yield: 40 mg (23%)

TLC: Petroleum ether – EtOAc 1:1 v/v, R_f = 0.13

^{1}H NMR (DMSO-*d6*) δ: 8.77 (s, 1H, CH-triazole), 8.11 (s, 1H, CH-triazole), 7.99 (bs, 2H, NH$_2$), 7.69 (d, *J* = 8.5 Hz, 1H, Ar), 7.54 (d, *J* = 8.6 Hz, 2H, Ar), 7.51 (d, *J* = 1.6 Hz, 1H, Ar), 7.49 (d, *J* = 8.6 Hz, 1H, Ar), 7.42 (s, 1H, CH), 7.21 (dd, *J* = 2.1, 8.5 Hz, 1H, Ar), 6.74 (s, 1H, Ar).

^{13}C NMR (DMSO-*d6*) δ: 155.25 (C), 154.64 (C), 152.63 (CH), 148.17 (C), 144.94 (CH), 135.59 (C), 134.09 (C), 130.29 (2 x CH), 129.40 (2 x CH), 126.33 (C), 122.45 (CH), 118.79 (CH), 107.50 (CH), 106.35 (CH), 59.62(CH).

HPLC (method B): 97.9 % at R.T.= 3.99 min.

4.6.3.2.2. 2-((4-Chlorophenyl)(1*H*-1,2,4-triazol-1-yl)methyl)benzofuran-5-yl sulfamate (48) Chemical Formula: C$_{17}$H$_{13}$ClN$_4$O$_4$S, Molecular Weight: 404.83
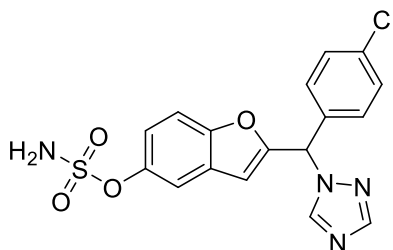
Yield: 50 mg (29%)

TLC: Petroleum ether – EtOAc 1:1 v/v, R_f = 0.13

^{1}H NMR (DMSO-*d6*) δ: 8.76 (s, 1H, CH-triazole), 8.11 (s, 1H, CH-triazole), 7.92 (bs, 2H, NH$_2$), 7.65 (d, *J* = 8.9 Hz, 1H, Ar), 7.56 (d, *J* = 2.5 Hz, 1H, Ar), 7.54 (d, *J* = 8.6 Hz, 2H, Ar), 7.49 (d, *J* = 8.6 Hz, 2H, Ar), 7.43 (s, 1H, CH), 7.23 (dd, *J* = 2.5, 8.9 Hz, 1H, Ar), 6.76 (s, 1H, Ar).

^{13}C NMR (DMSO-*d6*) δ: 155.62 (C), 153.04 (C), 152.65 (CH), 146.52 (C), 135.55 (C), 134.09 (C), 130.31 (2 x CH), 129.40 (2 x CH), 128.58 (C), 120.25 (CH), 115.69 (CH), 112.53 (CH), 107.90 (CH), 59.65(CH).

HPLC (method B): 97.5 % at R.T.= 3.92 min.

4.6.3.2.3. 4-((5-Chlorobenzofuran-2-yl)(1*H*-1,2,4-triazol-1-yl)methyl)phenyl sulfamate (49) Chemical Formula: $C_{17}H_{13}ClN_4O_4S$, Molecular Weight: 404.83
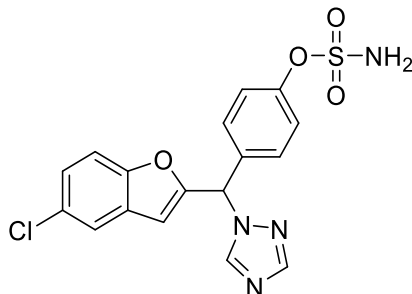
Yield: sulfamate (**49**) 20 mg (16%) and carbamate (**49b**) 10 mg (9%)

TLC: Petroleum ether – EtOAc 1:3 v/v, R_f = 0.35

¹H NMR (DMSO-*d6*) δ: 8.77 (s, 1H, CH-triazole), 8.11 (s, 1H, CH-triazole), 8.05 (bs, 2H, NH₂), 7.73 (d, J = 2.3 Hz, 1H, Ar), 7.63 (d, J = 8.9 Hz, 1H, Ar), 7.58 (d, J = 8.6 Hz, 2H, Ar), 7.43 (s, 1H, CH), 7.37 (m, 3H, Ar), 6.69 (t, J = 0.9 Hz, 1H, Ar).

¹³C NMR (DMSO-*d6*) δ: 155.85 (C), 153.56 (C), 152.65 (CH), 150.81 (C), 134.76 (C), 130.08 (2 x CH), 129.55 (C), 128.09 (C), 125.45 (CH), 123.17 (2 x CH), 121.56 (CH), 113.41 (CH), 107.22 (CH), 59.75(CH).

HPLC (method B): 100% at R.T.= 4.13 min.

4.6.3.2.4. 4-((5-Chlorobenzofuran-2-yl)(1*H*-1,2,4-triazol-1-yl)methyl)phenyl carbamate (49b) Chemical Formula: $C_{18}H_{13}ClN_4O_3$, Molecular Weight: 368.78
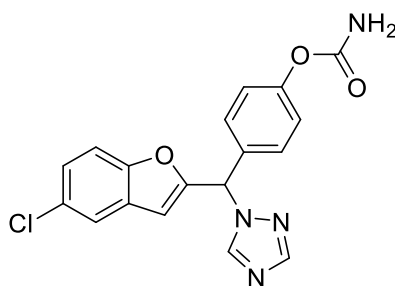
TLC: Petroleum ether – EtOAc 1:3 v/v, R_f = 0.52

¹H NMR (CDCl₃) δ: 8.16 (s, 1H, CH-triazole), 8.06 (s, 1H, CH-triazole), 7.54 (d, *J* = 2.1 Hz, 1H, Ar), 7.40 (d, *J* = 8.8 Hz, 1H, Ar), 7.36 (d, *J* = 8.7 Hz, 2H, Ar), 7.31 (dd, *J* = 2.1, 8.8 Hz, 1H, CH), 7.24 (d, *J* = 8.7 Hz, 2H, Ar), 6.84 (s, 1H), 6.58 (s, 1H, Ar), 5.02 (bs, 2H, NH₂).

¹³C NMR (CDCl₃) δ: 154.32 (C), 153.94 (C), 153.68 (C), 152.36 (CH), 151.43 (C), 132.38 (C), 129.05 (C), 128.92 (2 x CH), 128.77 (C), 125.62 (CH), 122.42 (2 x CH), 121.14 (CH), 112.59 (CH), 107.37 (CH), 61.55 (CH).

HPLC (method A): 90% at R.T.= 4.44 min.

HRMS (EI): Calculated 391.0573 [M+Na]⁺, Found 391.0568 [M+Na]⁺.

4.6.3.2.5. 2-((4-Cyanophenyl)(1*H*-1,2,4-triazol-1-yl)methyl)benzofuran-6-yl sulfamate (50) Chemical Formula: C₁₈H₁₃N₅O₄S, Molecular Weight: 395.39
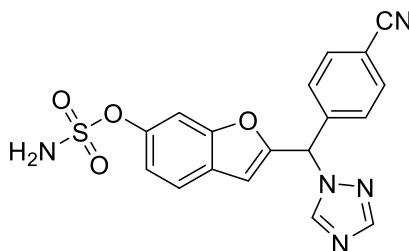
Yield: 60 mg (23%)

TLC: Petroleum ether – EtOAc 1:1 v/v, R$_f$ = 0.2

¹H NMR (DMSO-*d6*) δ: 8.79 (s, 1H, CH-triazole), 8.14 (s, 1H, CH-triazole), 7.99 (bs, 2H, NH₂), 7.95 (d, *J* = 8.5 Hz, 2H, Ar), 7.70 (d, *J* = 8.5 Hz, 1H, Ar), 7.63 (d, *J* = 8.2 Hz, 2H, Ar), 7.56 (s, 1H, CH), 7.52 (d, *J* = 1.7 Hz, 1H, Ar), 7.22 (dd, *J* = 2.1, 8.5 Hz, 1H, Ar), 6.78 (t, *J* = 0.9 Hz, 1H, Ar).

¹³C NMR (DMSO-*d6*) δ: 154.68 (C), 154.52 (C), 152.79 (CH), 148.25 (C), 145.13 (CH), 141.73 (C), 133.38 (2 x CH), 129.29 (2 x CH), 126.25 (C), 122.54 (CH), 118.87 (CH), 112.18 (C), 107.89 (CH), 106.38 (CH), 60.22 (C), 59.75(CH).

HPLC (method A): 100% at R.T.= 3.94 min.

HRMS (EI): Calculated 396.0766 [M+H]⁺, Found 396.0761 [M+H]⁺.

4.6.3.2.6. 2-((4-Fluorophenyl)(1*H*-1,2,4-triazol-1-yl)methyl)benzofuran-6-yl sulfamate (51) Chemical Formula: $C_{17}H_{13}FN_4O_4S$, Molecular Weight: 388.37
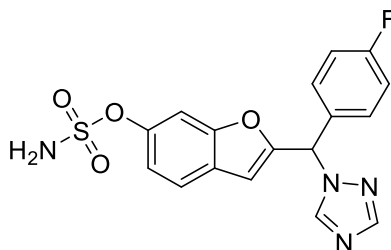
Yield: 70 mg (39%)

TLC: Petroleum ether – EtOAc 1:1 v/v, R_f = 0.15

^{1}H NMR (DMSO-*d6*) δ: 8.81 (s, 1H, CH-triazole), 8.16 (s, 1H, CH-triazole), 8.03 (bs, 2H, NH$_2$), 7.75 (d, *J* = 8.5 Hz, 1H, Ar), 7.61 (dd, *J* = 5.4, 8.8 Hz, 2H, Ar), 7.56 (d, *J* = 1.8 Hz, 1H, Ar), 7.46 (s, 1H), 7.37 (t, *J* = 8.9 Hz, 2H, Ar), 7.26 (dd, *J* = 2.1, 8.5 Hz, 1H, Ar), 6.77 (t, *J* = 0.9 Hz, 1H, Ar).

^{13}C NMR (DMSO-*d6*) δ: 163.64 (d, $^1J_{C,F}$ = 243.75 Hz, C), 155.57 (C), 154.62 (C), 152.59 (CH), 148.13 (C), 144.85 (CH), 132.88 (d, $^4J_{C,F}$ = 2.5 Hz, C), 130.74 (d, $^3J_{C,F}$ = 7.5 Hz, 2 x CH), 126.35 (C), 122.42 (CH), 118.78 (CH), 116.35 (d, $^2J_{C,F}$ = 22.5 Hz, 2 x CH), 107.33(CH), 106.34 (CH), 59.63 (CH).

HPLC (method B): 100% at R.T.= 3.69 min.

4.6.3.2.7. 2-((4-Cyanophenyl)(1*H*-1,2,4-triazol-1-yl)methyl)benzofuran-6-yl carbamate (50b) Chemical Formula: $C_{19}H_{13}N_5O_3$, Molecular Weight: 359.35
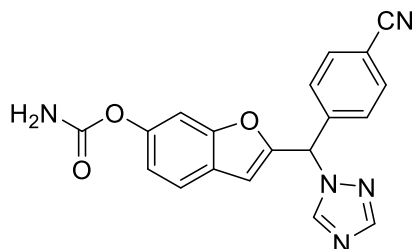
To a solution of phenolic compound (**4.7**) (0.1 g, 0.32 mmol)) in dry CH$_3$CN (5 mL), chlorosulfonyl isocyanate (**1**) (0.14 mL, 1.58 mmol) was added and the reaction stirred for 3 h at

room temperature. The reaction mixture was then concentrated under reduced pressure and the residue dissolved in ice-water (10 mL) containing crushed ice and stirred for 1 h. The mixture was extracted with EtOAc (100 mL), washed with H_2O (2 x 100 mL), dried ($MgSO_4$) and concentrated under reduced pressure to afford the product as a white low melting point solid.

Yield: 90 mg (81%)

TLC: Petroleum ether – EtOAc 1:1 v/v, R_f = 0.22

^{1}H NMR (DMSO-*d6*) δ: 8.79 (s, 1H, CH-triazole), 8.13 (s, 1H, CH-triazole), 7.95 (d, *J* = 8.5 Hz, 2H, Ar), 7.62 (d, *J* = 8.2 Hz, 2H, Ar), 7.60 (d, *J* = 8.7 Hz, 1H, Ar), 7.52 (s, 1H, CH), 7.38 (d, *J* = 1.6 1H, Ar), 7.23 (bs, 1H, NH_2), 7.03 (dd, *J* = 2.1, 8.5 Hz, 1H, Ar), 6.93 (bs, 1H, NH_2), 6.71 (t, *J* = 1.0, 1H, Ar).

^{13}C NMR (DMSO-*d6*) δ: 155.32 (C), 155.01 (C), 153.67 (C), 152.75 (CH), 149.45 (C), 145.13 (CH), 141.88 (C), 133.35 (2 x CH), 129.28 (2 x CH), 124.78 (C), 121.89 (CH), 118.88 (C), 118.70 (CH), 112.11 (C), 107.91 (CH), 106.09 (CH), 59.85 (CH).

HRMS (EI): Calculated 382.0916 $[M+Na]^+$, Found 382.0908 $[M+Na]^+$.

4.6.3.3. Phenyl(6-((tetrahydro-2*H*-pyran-2-yl)oxy)benzofuran-2-yl)methanone

(9g) Chemical Formula: $C_{20}H_{18}O_4$, Molecular Weight: 322.36
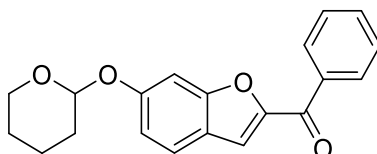
Prepared as described for (**3a-e**) using 2-hydroxy-4-((tetrahydro-2*H*-pyran-2-yl)oxy) benzaldehyde (**8a**) (0.25 g, 1.12 mmol) and 2-chlorooacetophenone (**52**) (0.17 g, 1.12 mmol) to afford phenyl(6-((tetrahydro-2*H*-pyran-2-yl)oxy)benzofuran-2-yl)methanone (**9g**) as a white solid.

Yield: 0.35 g (97%).

Melting Point: 119-122 ºC

TLC: Petroleum ether – EtOAc 3:1 v/v, R_f = 0.67

^{1}H NMR (DMSO-*d6*) δ: 7.98 (m, 2H, Ar), 7.76 (d, *J* = 8.7 Hz, 1H, Ar), 7.73 (m, 2H, Ar), 7.62 (t, *J* = 8.0 Hz, 2H), 7.41 (d, *J* = 1.6 Hz, 1H, Ar), 7.11 (dd, *J* = 2.2, 8.7 Hz, 1H, Ar), 5.63 (t, *J* = 3.4

Hz, 1H, CH-pyran), 3.80 (m, 1H, CH_2-pyran), 3.62 (m, 1H, CH_2-pyran), 1.92 (m, 3H, CH_2-pyran), 1.67 (m, 3H, CH_2-pyran).

^{13}C NMR (DMSO-*d6*) δ: 183.43 (C), 158.31 (C), 157.07 (C), 151.73 (C), 137.49 (C), 133.32 (CH), 129.49 (2 x CH), 129.18 (2 x CH), 124.74 (CH), 121.39 (C), 118.16 (CH), 115.92 (CH), 99.50 (CH), 96.61 (CH), 62.15 (CH_2), 30.14 (CH_2), 25.07 (CH_2), 18.99 (CH_2).

HRMS (ESI): Calculated 345.1102 $[M+Na]^+$, Found 345.1098 $[M+Na]^+$.

4.6.3.4. (4-Methoxyphenyl)(6-((tetrahydro-2*H*-pyran-2-yl)oxy)benzofuran-2-yl)methanone (9h) Chemical Formula: $C_{21}H_{20}O_5$, Molecular Weight: 352.39
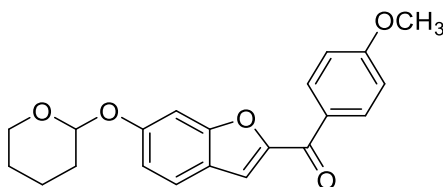
Prepared as described for (**3a-e**) using 2-hydroxy-4-((tetrahydro-2*H*-pyran-2-yl)oxy) benzaldehyde (**8a**) (0.25 g, 1.12 mmol) and 2-bromo-4′-methoxyacetophenone (**2b**) (0.25 g, 1.12 mmol) to afford (4-methoxyphenyl)(6-((tetrahydro-2*H*-pyran-2-yl)oxy)benzofuran-2-yl)methanone (**9h**) as a white solid.

Yield: 0.37 g (95%).

Melting Point: 108-112 ℃

TLC: Petroleum ether – EtOAc 3:1 v/v, R_f = 0.5

^{1}H NMR (DMSO-*d6*) δ: 8.03 (d, *J* = 8.9 Hz, 2H, Ar), 7.75 (d, *J* = 8.7 Hz, 1H, Ar), 7.70 (d, *J* = 0.9 Hz, 1H, Ar), 7.40 (d, *J* = 1.8 Hz, 1H, Ar), 7.14 (d, *J* = 8.9 Hz, 2H, Ar), 7.11 (dd, *J* = 2.2, 8.7 Hz, 1H, Ar), 5.62 (t, *J* = 3.4 Hz, 1H, CH-pyran), 3.88 (s, 3H, OCH_3), 3.80 (m, 1H, CH_2-pyran), 3.62 (m, 1H, CH_2-pyran), 1.92 (m, 3H, CH_2-pyran), 1.66 (m, 3H, CH_2-pyran).

^{13}C NMR (DMSO-*d6*) δ: 181.85 (C), 163.59 (C), 158.03 (C), 156.81 (C), 152.12 (C), 131.99 (2 x CH), 129.87 (C), 124.49 (CH), 121.39 (C), 116.93 (CH), 115.79 (CH), 114.53 (2 x CH), 99.52 (CH), 96.64 (CH), 62.14 (CH_2), 56.07 (CH_3), 30.16 (CH_2), 25.08 (CH_2), 19.00 (CH_2).

HRMS (ESI): Calculated 353.1389 $[M+H]^+$, Found 353.1384 $[M+H]^+$.

4.6.3.5. Pyridin-3-yl(6-((tetrahydro-2*H*-pyran-2-yl)oxy)benzofuran-2-yl)methanone (9i) Chemical Formula: C$_{19}$H$_{17}$NO$_4$, Molecular Weight: 323.35
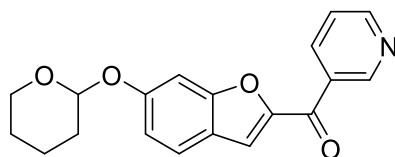
Prepared as described for (**3a-e**) using 2-hydroxy-4-((tetrahydro-2*H*-pyran-2-yl)oxy) benzaldehyde (**8a**) (0.4 g, 1.80 mmol) and 3-bromoacetylpyridine HBr (**53**) (0.5 g, 1.80 mmol). Purification by gradient column chromatography afforded pyridin-3-yl(6-((tetrahydro-2*H*-pyran-2-yl)oxy)benzofuran-2-yl)methanone (**9i**) at 70% EtOAc in petroleum ether (v/v) as a white solid.

Yield: 0.2 g (34%).

Melting Point: 114-116 ºC

TLC: Petroleum ether – EtOAc 3:1 v/v, R$_f$ = 0.17

^{1}H NMR (CDCl$_3$) δ: 9.30 (s, 1H, Ar), 8.86 (d, *J* = 3.6 Hz, 1H, Ar), 8.35 (dt, *J* = 1.9, 8.0 Hz, 1H, Ar), 7.64 (d, *J* = 8.7 Hz, 1H, Ar), 7.58 (d, *J* = 0.9 Hz, 1H, Ar), 7.52 (dd, *J* = 4.8, 7.8 Hz, 1H, Ar), 7.37 (d, *J* = 1.8 Hz, 1H, Ar), 7.11 (dd, *J* = 2.1, 8.7 Hz, 1H, Ar), 5.52 (t, *J* = 3.2 Hz, 1H, CH-pyran), 3.94 (m, 1H, CH$_2$-pyran), 3.68 (m, 1H, CH$_2$-pyran), 2.12 (m, 3H, CH$_2$-pyran), 1.76 (m, 3H, CH$_2$-pyran).

^{13}C NMR (CDCl$_3$) δ: 181.84 (C), 158.85 (C), 157.62 (C), 153.00 (CH), 151.82 (C), 150.30 (C), 136.82 (CH), 133.11 (C), 123.69 (CH), 123.55 (CH), 120.97 (C), 117.44 (CH), 115.89 (CH), 99.29 (CH), 96.95 (CH), 62.21 (CH$_2$), 30.21 (CH$_2$), 25.06 (CH$_2$), 18.69 (CH$_2$).

HPLC (method A): 96.07 % at R.T.= 4.72 min.

HRMS (ESI): Calculated 324.1235 [M+H]$^+$, Found 324.1232 [M+H]$^+$.

4.6.3.6. (6-((Tetrahydro-2*H*-pyran-2-yl)oxy)benzofuran-2-yl)(thiophen-3-yl)methanone (9j) Chemical Formula: C$_{18}$H$_{16}$O$_4$S, Molecular Weight: 328.38
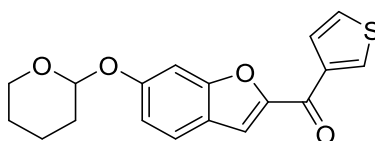
Prepared as described for (**3a-e**) using 2-hydroxy-4-((tetrahydro-2*H*-pyran-2-yl)oxy) benzaldehyde (**8a**) (0.35 g, 1.57 mmol) and 3-bromoacetyl thiophene (**54**) (0.32 g, 1.57 mmol) to afford (6-((tetrahydro-2*H*-pyran-2-yl)oxy)benzofuran-2-yl)(thiophen-3-yl)methanone (**9j**) as a yellow solid.

Yield: 0.51 g (99 %).

Melting Point: 120-124 ºC

TLC: Petroleum ether – EtOAc 3:1 v/v, R_f = 0.67

¹H NMR (DMSO-*d6*) δ: 8.73 (dd, J = 1.3, 2.8 Hz, 1H, Ar), 7.85 (dd, J = 1.0 Hz, 1H, Ar), 7.75 (m, 2H, Ar), 7.69 (dd, J = 1.3, 5.1 Hz, 1H, Ar), 7.43 (d, J = 1.8 Hz, 1H, Ar), 7.11 (dd, J = 2.2, 8.7 Hz, 1H, Ar), 5.62 (t, J = 3.4 Hz, 1H, CH-pyran), 3.80 (m, 1H, CH_2-pyran), 3.62 (m, 1H, CH_2-pyran), 1.92 (m, 3H, CH_2-pyran), 1.68 (m, 3H, CH_2-pyran).

¹³C NMR (DMSO-*d6*) δ: 176.37 (C), 158.14 (C), 156.89 (C), 152.32 (C), 140.10 (C), 135.10 (CH), 128.24 (CH), 127.97 (CH), 124.50 (CH), 121.13 (C), 116.45 (CH), 115.90 (CH), 99.58 (CH), 96.66 (CH), 62.15 (CH_2), 30.17 (CH_2), 25.08 (CH_2), 18.99 (CH_2).

HRMS (ESI): Calculated 351.0667 [M+Na]⁺, Found 351.0662 [M+Na]⁺.

4.6.3.7. Adamantan-1-yl(6-((tetrahydro-2*H*-pyran-2-yl)oxy)benzofuran-2-yl)methanone (9k) Chemical Formula: $C_{24}H_{28}O_4$, Molecular Weight: 380.48
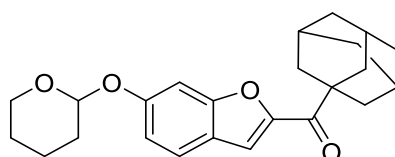
Prepared as described for (**3a-e**) using 2-hydroxy-4-((tetrahydro-2*H*-pyran-2-yl)oxy) benzaldehyde (**8a**) (0.4 g, 1.80 mmol) and 1-adamantyl bromomethyl ketone (**55**) (0.46 g, 1.80 mmol) to afford adamantan-1-yl(6-((tetrahydro-2*H*-pyran-2-yl)oxy)benzofuran-2-yl)methanone (**9k**) as a white semisolid.

Yield: 0.68 g (99%).

TLC: Petroleum ether – EtOAc 3:1 v/v, R_f = 0.75

¹H NMR (CDCl₃) δ: 7.57 (d, J = 8.6 Hz, 1H, Ar), 7.50 (d, J = 0.9 Hz, 1H, Ar), 7.31 (d, J = 1.7 Hz, 1H, Ar), 7.05 (dd, J = 2.2, 8.6 Hz, 1H, Ar), 5.51 (t, J = 3.2 Hz, 1H, CH-pyran), 3.96 (m, 1H, CH₂-pyran), 3.69 (m, 1H, CH₂-pyran), 2.15 (m, 21H, 3 x CH₂-pyran + 15H adamantane).

¹³C NMR (CDCl₃) δ: 196.00 (C), 157.87 (C), 156.11 (C), 152.82 (C), 123.07 (CH), 120.85 (C), 115.23 (CH), 113.91 (CH), 99.15 (CH), 96.83 (CH), 62.07 (CH₂), 46.07 (C), 38.24 (3 x CH₂), 36.74 (3 x CH₂), 30.28 (CH₂), 28.16 (3 x CH), 25.14 (CH₂), 18.64 (CH₂).

HRMS (ESI): Calculated 403.1885 [M+Na]⁺, Found 403.1878 [M+Na]⁺.

4.6.3.8.   (6-Hydroxybenzofura-2-yl)(phenyl)methanone (39e) Chemical Formula: $C_{15}H_{10}O_3$, Molecular Weight: 238.24
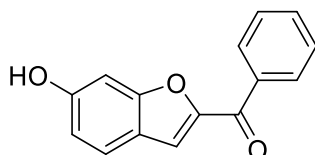
Prepared as described for the synthesis of (6-hydroxybenzofura-2-yl)(phenyl)methanone derivatives (**39a-d**) in chapter 3 using phenyl(6-((tetrahydro-2*H*-pyran-2-yl)oxy)benzofuran-2-yl)methanone (**9g**) (0.34 g, 1.1 mmol) to provide (6-hydroxybenzofura-2-yl)(phenyl)methanone (**39e**) as pale yellow solid.

Yield: 0.15 g (60 %).

Melting point: 214-216 ℃ (lit. m.p = 160.2-160.8 ℃) (Zhao *et al.* 2013)

TLC: Petroleum ether – EtOAc 3:1 v/v, R_f = 0.25

¹H NMR (DMSO-*d6*) δ: 10.23 (bs, 1H, OH), 7.95 (m,2H, Ar), 7.71 (m, 1H, Ar), 7.67 (d, J = 0.9 Hz, 1H, Ar), 7.65 (d, J = 8.5 Hz, 1H, Ar), 7.60 (t, J = 7.9 Hz, 2H, Ar), 7.04 (m, 1H, Ar), 6.91 (dd, J = 2.1, 8.6 Hz, 1H, Ar).

¹³C NMR (DMSO-*d6*) δ: 183.25 (C), 159.89 (C), 157.70 (C), 150.95 (C), 137.72 (C), 133.13 (CH), 129.38 (2 x CH), 129.13 (2 x CH), 124.91 (CH), 119.52 (C), 118.78 (CH), 115.13 (CH), 97.95 (CH).

4.6.3.9. (6-Hydroxybenzofura-2-yl)(4-methoxyphenyl)methanone (39f)

Chemical Formula: C$_{16}$H$_{12}$O$_4$, Molecular Weight: 268.27
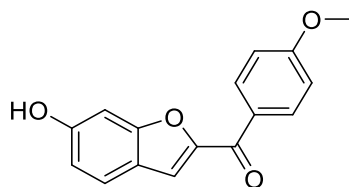
Prepared as described for the synthesis of (6-hydroxybenzofura-2-yl)(phenyl)methanone derivatives (**39a-d**) in chapter 3 using (4-methoxyphenyl)(6-((tetrahydro-2*H*-pyran-2-yl)oxy)benzofuran-2-yl)methanone (**9h**) (0.36 g, 1.0 mmol) to provide 6-hydroxybenzofura-2-yl)(4-methoxyphenyl)methanone (**39f**) as pale yellow solid.

Yield: 0.18 g (62 %).

Melting point: 196-198 ℃ (lit. m.p = 201-203 ℃) (Meshram *et al.* 2012)

TLC: Petroleum ether – EtOAc 3:1 v/v, R$_f$ = 0.17

¹H NMR (DMSO-*d6*) δ: 10.17 (bs, 1H, OH), 8.00 (d, *J* = 8.9 Hz, 2H, Ar), 7.65 (m, 1H, Ar), 7.13 (d, *J* = 8.9 Hz, 2H, Ar), 7.03 (m, 1H), 6.90 (dd, *J* = 2.1, 8.6 Hz, 1H, Ar), 3.88 (s, 3H, OCH$_3$).

¹³C NMR (DMSO-*d6*) δ: 181.73 (C), 163.44 (C), 159.56 (C), 157.43 (C), 151.30 (C), 131.85 (2 x CH), 130.08 (C), 124.65 (CH), 119.50 (C), 117.51 (CH), 114.95 (CH), 114.48 (2 x CH), 97.96 (CH), 56.05 (CH$_3$).

4.6.3.10. 4-(6-Hydroxybenzofura-2-carbonyl)benzonitrile (39g) Chemical Formula: C$_{16}$H$_9$NO$_3$, Molecular Weight: 263.25
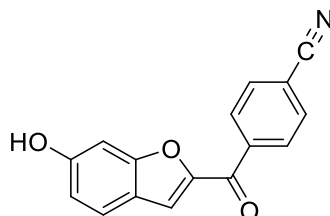
Prepared as described for the synthesis of (6-hydroxybenzofura-2-yl)(phenyl)methanone derivatives (**39a-d**) in chapter 3 using 4-(hydroxy(6-((tetrahydro-2*H*-pyran-2-yl)oxy)benzofuran-2-

yl)methyl)benzonitrile (**9d**) (0.3 g, 0.8 mmol) to provide 4-(6-hydroxybenzofura-2-carbonyl)benzonitrile (**39g**) as white solid.

Yield: 0.17 g (75 %).

Melting point: 276-278 ºC

**TLC:** Petroleum ether – EtOAc 3:1 v/v, R_f = 0.2

¹H NMR (DMSO-*d6*) δ: 10.32 (bs, 1H, OH), 8.10 (m, 4H, Ar), 7.72 (d, *J* = 0.8 Hz, 1H, Ar), 7.66 (d, *J* = 8.6 Hz, 1H, Ar), 7.04 (d, *J* = 0.8 Hz, 1H, Ar), 6.92 (dd, *J* = 2.1, 8.6 Hz, 1H, Ar).

¹³C NMR (DMSO-*d6*) δ: 183.03 (C), 160.32 (C), 158.00 (C), 150.49 (C), 141.41 (C), 133.11 (2 x CH), 130.01 (2 x CH), 125.14 (CH), 119.90 (CH), 119.50 (C), 118.67 (C), 115.41 (CH), 115.04 (C), 97.94 (CH).

HPLC (method A): 100 % at R.T.= 4.42 min.

HRMS (ESI): Calculated 264.0660 [M+H]⁺, Found 264.0654 [M+H]⁺.

4.6.3.11. (6-Hydroxybenzofura-2-yl)(pyridin-3-yl)methanone (39h) Chemical Formula: $C_{14}H_9NO_3$, Molecular Weight: 239.23
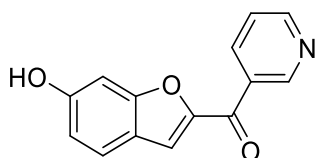
Prepared as described for the synthesis of (6-hydroxybenzofura-2-yl)(phenyl)methanone derivatives (**39a-d**) in chapter 3 using pyridin-3-yl(6-((tetrahydro-2*H*-pyran-2-yl)oxy)benzofuran-2-yl)methanone (**9i**) (0.19 g, 0.58 mmol) to provide (6-hydroxybenzofuran-2-yl)(pyridin-3-yl)methanone (**39h**) as white solid.

Yield: 0.07 g (38 %).

Melting point: 262-264 ºC

TLC: Petroleum ether – EtOAc 1:1 v/v, R_f = 0.27

¹H NMR (DMSO-*d6*) δ: 10.28 (bs, 1H, OH), 9.08 (d, *J* = 1.6 Hz, 1H, Ar), 8.85 (dd, *J* = 1.6, 4.8 Hz, 1H, Ar), 8.32 (m, 1H, Ar), 7.78 (d, *J* = 1.0 Hz, 1H, Ar), 7.67 (d, *J* = 8.6 Hz, 1H, Ar), 7.64 (ddd, *J* = 0.9, 4.8, 3.1 Hz, 1H, Ar), 7.05 (m, 1H, Ar), 6.92 (dd, *J* = 2.1, 8.6 Hz, 1H, Ar).

¹³C NMR (DMSO-*d6*) δ: 181.73 (C), 160.19 (C), 157.92 (C), 153.36 (CH), 150.74 (C), 149.87 (CH), 137.02 (CH), 133.47 (C), 125.09 (CH), 124.26 (CH), 119.55 (C), 119.48 (CH), 115.34 (CH), 97.96 (CH).

HPLC (method A): 100 % at R.T.= 4.18 min.

HRMS (ESI): Calculated 240.0660 [M+H]⁺, Found 240.0657 [M+H]⁺.

4.6.3.12.   (6-Hydroxybenzofura-2-yl)(thiophen-3-yl)methanone (39i) Chemical Formula: $C_{13}H_8O_3S$, Molecular Weight: 244.26
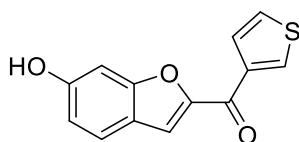
Prepared as described for the synthesis of (6-hydroxybenzofura-2-yl)(phenyl)methanone derivatives (**39a-d**) in chapter 3 using (6-(((tetrahydro-2*H*-pyran-2-yl)oxy)benzofuran-2-yl)(thiophen-3-yl)methanone (**9j**) (0.5 g, 1.5 mmol) to provide (6-hydroxybenzofuran-2-yl)(thiophen-3-yl)methanone (**39i**) as yellow solid.

Yield: 0.2 g (54 %).

Melting point: 176-178 ºC

TLC: Petroleum ether – EtOAc 3:1 v/v, R_f = 0.25

¹H NMR (DMSO-*d6*) δ: 10.20 (bs, 1H, OH), 8.67 (dd, *J* = 1.3, 2.8 Hz, 1H, Ar), 7.80 (d, *J* = 0.9 Hz, 1H, Ar), 7.73 (dd, *J* = 2.8, 5.1 Hz, 1H, Ar), 7.67 (dd, *J* = 1.3, 5.1 Hz, 1H, Ar), 7.65 (d, *J* = 8.6 Hz, 1H, Ar), 7.06 (d, *J* = 1.5 Hz, 1H, Ar), 6.91 (dd, *J* = 2.1, 8.6 Hz, 1H, Ar).

¹³C NMR (DMSO-*d6*) δ: 176.25 (C), 159.67 (C), 157.52 (C), 151.55 (C), 140.26 (C), 134.65 (CH), 128.24 (CH), 127.86 (CH), 124.66 (CH), 119.48 (C), 116.99 (CH), 115.07 (CH), 98.06 (CH).

HPLC (method A): 98.84 % at R.T.= 4.47 min.

HRMS (ESI): Calculated 245.0272 [M+H]$^+$, Found 245.0271 [M+H]$^+$.

4.6.3.13. Adamantan-1-yl(6-hydroxybenzofuran-2-yl)methanone (39j) Chemical Formula: $C_{19}H_{20}O_3$, Molecular Weight: 296.37
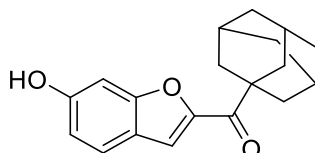
Prepared as described for the synthesis of (6-hydroxybenzofura-2-yl)(phenyl)methanone derivatives (**39a-d**) in chapter 3 using adamantan-1-yl(6-((tetrahydro-2*H*-pyran-2-yl)oxy)benzofuran-2-yl)methanone (**9k**) (0.66 g, 1.73 mmol) to provide adamantan-1-yl(6-hydroxybenzofuran-2-yl)methanone (**39j**) as white solid.

Yield: 0.15 g (29 %).

Melting point: 202-204 ºC

TLC: Petroleum ether – EtOAc 3:1 v/v, $R_f = 0.25$

¹H NMR (CDCl₃) δ: 7.55 (m,2H, Ar), 7.21 (d, *J* = 1.4 Hz, 1H, Ar), 6.92 (dd, *J* = 2.1, 8.5 Hz, 1H, Ar), 6.20 (bs, 1H, OH), 2.16 (s, 9H, adamantane), 1.83 (s, 6H, adamantane).

¹³C NMR (CDCl₃) δ: 196.43 (C), 157.12 (C), 156.26 (C), 151.86 (C), 123.63 (CH), 120.23 (C), 114.53 (CH), 113.99 (CH), 98.56 (CH), 46.14 (C), 38.63 (3 x CH₂), 37.71 (3 x CH₂), 20.16 (3 x CH).

HPLC (method A): 87.18 % at R.T.= 4.96 min.

HRMS (ESI): Calculated 297.1490 [M+H]$^+$, Found 297.1490 [M+H]$^+$.

4.6.3.14. 2-(4-Chlorobenzoyl)benzofuran-6-yl sulfamate (56a) Chemical

Formula: $C_{15}H_{10}ClNO_5S$, Molecular Weight: 351.76
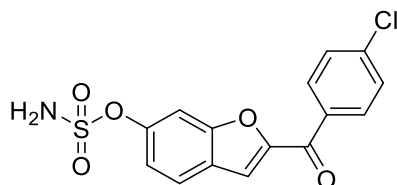
Prepared as the described in the general procedure of sulfomylation of phenolic compounds using (4-chlorophenyl)(6-hydroxybenzofura-2-yl)methanone (**39a**) (0.2 g, 0.74 mmol). Purification by gradient column chromatography at 30% EtOAc in petroleum ether (v/v) followed by a preparative TLC afforded the product as a white solid.

Yield: 16 mg (6 %)

TLC: Petroleum ether – EtOAc 3:1 v/v, $R_f = 0.2$

¹H NMR (DMSO-*d6*) δ: 8.15 (bs, 2H, NH₂), 8.05 (d, $J = 8.7$ Hz, 2H, Ar), 7.95 (d, $J = 8.6$ Hz, 1H, Ar), 7.89 (d, $J = 1.0$, 1H, Ar), 7.73 (d, $J = 1.6$ 1H, Ar), 7.71 (d, $J = 8.7$ Hz, 2H, Ar), 7.35 (dd, $J = 2.1, 8.6$ Hz, 1H, Ar).

¹³C NMR (DMSO-*d6*) δ: 182.52 (C), 155.62 (C), 152.83 (C), 150.88 (C), 138.62 (C), 135.70 (C), 131.60 (2 x CH), 129.40 (2 x CH), 125.66 (C), 125.09 (CH), 119.93 (CH), 117.54 (CH), 106.93 (CH).

HPLC (method A): 78.07 % at R.T.= 4.60 min.

HRMS (ESI): Calculated 352.0046 [M+H]⁺, Found 352.0039 [M+H]⁺.

4.6.3.15. 2-(4-Fluorobenzoyl)benzofuran-6-yl sulfamate (56b) Chemical

Formula: $C_{15}H_{10}FNO_5S$, Molecular Weight: 335.31
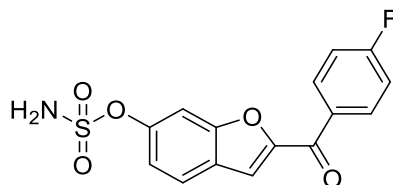
Prepared as the described in the general procedure of sulfomylation of phenolic compounds using (4-fluorophenyl)(6-hydroxybenzofura-2-yl)methanone (**39b**) (0.13 g, 0.52 mmol). Purification by

gradient column chromatography at 30% EtOAc in petroleum ether (v/v) followed by a preparative TLC afforded the product as a white solid.

Yield: 6 mg (3 %)

TLC: Petroleum ether – EtOAc 3:1 v/v, $R_f = 0.12$

^{1}H NMR (DMSO-*d6*) δ: 8.13 (m, 4H, 2 x CH + NH$_2$), 7.94 (d, $J = 8.6$ Hz, 1H, Ar), 7.87 (d, $J = 1.0$ Hz, 1H, Ar), 7.72 (m, 1H, Ar), 7.48 (d, $J = 8.6$ Hz, 2H, Ar), 7.35 (dd, $J = 2.1, 8.6$ Hz, 1H, Ar).

^{13}C NMR (DMSO-*d6*) δ: 182.23 (C), 166.51 (d, $^1J_{C,F} = 251.25$ Hz, C), 155.59 (C), 152.90 (C), 150.80 (C), 133.63 (d, $^4J_{C,F} = 3.75$ Hz, C), 132.75 (d, $^3J_{C,F} = 8.75$ Hz, 2 x CH), 125.67 (C), 125.02 (CH), 119.90 (CH), 117.30 (CH), 116.48 (d, $^2J_{C,F} = 21.25$ Hz, 2 x CH), 106.93 (CH).

HPLC (method A): 87.07 % at R.T.= 4.60 min.

HRMS (ESI): Calculated 336.0341 [M+H]$^+$, Found 336.0338 [M+H]$^+$.

4.6.3.16. 2-(4-Bromobenzoyl)benzofuran-6-yl sulfamate (56c) Chemical Formula: C$_{15}$H$_{10}$BrNO$_5$S, Molecular Weight: 396.21
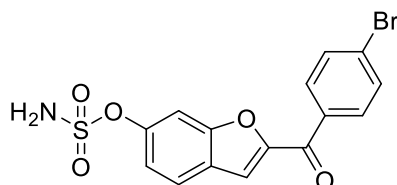
Prepared as the described in the general procedure of sulfomylation of phenolic compounds using (4-bromophenyl)(6-hydroxybenzofura-2-yl)methanone (**39c**) (0.13 g, 0.37 mmol). Purification by gradient column chromatography at 30% EtOAc in petroleum ether (v/v) followed by a preparative TLC afforded the product as a white solid.

Yield: 6 mg (4 %)

TLC: Petroleum ether – EtOAc 3:1 v/v, $R_f = 0.12$

^{1}H NMR (DMSO-*d6*) δ: 8.13 (bs, 2H, NH$_2$), 7.96 (m, 3H, Ar), 8.89 (d, $J = 1.0$ Hz, 1H, Ar), 7.85 (d, $J = 8.7$ Hz, 2H, Ar), 7.72 (m, 1H, Ar), 7.35 (dd, $J = 2.1, 8.6$ Hz, 1H, Ar).

¹³C NMR (DMSO-*d6*) δ: 182.69 (C), 155.62 (C), 152.80 (C), 150.89 (C), 138.03 (C), 132.34 (2 x CH), 131.68 (2 x CH), 127.74 (C), 125.65 (C), 125.08 (CH), 119.93 (CH), 117.56 (CH), 106.93 (CH).

HPLC (method A): 58.35 % at R.T.= 4.63 min.

HRMS (ESI): Calculated 395.9541 [M+H]⁺, Found 395.9533 [M+H]⁺.

4.6.3.17. 2-(2,4-Dichlorobenzoyl)benzofuran-6-yl sulfamate (56d) Chemical Formula: $C_{15}H_9Cl_2NO_5S$, Molecular Weight: 386.20
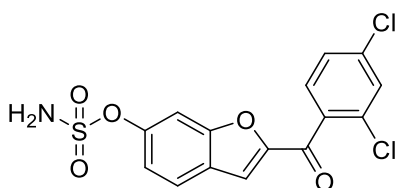
Prepared as the described in the general procedure of sulfomylation of phenolic compounds using (2,4-dichlorophenyl)(6-hydroxybenzofura-2-yl)methanone (**39d**) (0.15 g, 0.48 mmol). Purification by gradient column chromatography at 30% EtOAc in petroleum ether (v/v) followed by a preparative TLC afforded the product as a white solid.

Yield: 8.5 mg (4 %)

TLC: Petroleum ether – EtOAc 3:1 v/v, R_f = 0.15

¹H NMR (DMSO-*d6*) δ: 8.14 (bs, 2H, NH₂), 7.91 (d, *J* = 8.7 Hz, 1H, Ar), 7.87 (d, *J* = 1.9 Hz, 1H, Ar), 7.79 (d, *J* = 8.3 Hz, 1H, Ar), 7.73 (d, *J* = 1.0 Hz, 1H, Ar), 7.71 (m, 1H, Ar), 7.66 (dd, *J* = 2.0, 8.3 Hz, 1H, Ar), 7.34 (dd, *J* = 2.0, 8.6 Hz, 1H, Ar).

¹³C NMR (DMSO-*d6*) δ: 182.35 (C), 156.07 (C), 152.71 (C), 151.31 (C), 136.82 (C), 136.04 (C), 131.99 (C), 131.48 (CH), 130.23 (CH), 128.16 (CH), 125.59 (C), 125.35 (CH), 120.14 (CH), 119.07 (CH), 107.00 (CH).

HPLC (method A): 60.72 % at R.T.= 4.63 min.

HRMS (ESI): Calculated 385.9656 [M+H]⁺, Found 385.9646 [M+H]⁺.

4.6.3.18.   2-(Thiophene-3-carbonyl)benzofuran-6-yl sulfamate (56e) Chemical Formula: $C_{13}H_9NO_5S_2$, Molecular Weight: 323.34
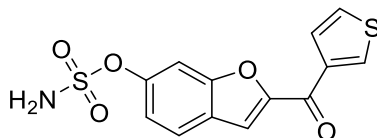
Prepared as described in the general procedure of sulfomylation of phenolic compounds using (6-hydroxybenzofuran-2-yl)(thiophen-3-yl)methanone (**39i**) (0.2 g, 0.82 mmol). Purification by gradient column chromatography at 30% EtOAc in petroleum ether (v/v) followed by a preparative TLC afforded the product as white solid.

Yield: 20 mg (7 %)

TLC: Petroleum ether – EtOAc 3:1 v/v, R_f = 0.67

¹H NMR (DMSO-*d6*) δ: 8.80 (dd, *J* = 1.3, 2.8 Hz, 1H, Ar), 8.13 (bs, 2H, NH₂), 7.96 (d, *J* = 0.9 Hz, 1H, Ar), 7.94 (d, *J* = 8.6 Hz, 1H, Ar), 7.77 (dd, *J* = 2.8, 5.1 Hz, 1H, Ar), 7.74 (m, 1H, Ar), 7.72 (dd, *J* = 1.3, 5.1 Hz, 1H, Ar), 7.34 (dd, *J* = 2.1, 8.6 Hz, 1H, Ar).

¹³C NMR (DMSO-*d6*) δ: 176.51 (C), 155.41 (C), 153.64 (C), 150.60 (C), 139.82 (C), 135.89 (CH), 128.22 (CH), 128.19 (CH), 125.69 (C), 124.81 (CH), 119.86 (CH), 115.73 (CH), 107.03 (CH).

HPLC (method A): 100 % at R.T.= 4.38 min.

HRMS (ESI): Calculated 345.9819 [M+Na]⁺, Found 345.9815 [M+Na]⁺.

4.6.3.19.   2-(Adamantane-1-carbonyl)benzofuran-6-yl sulfamate (56f) Chemical Formula: $C_{19}H_{21}NO_5S$, Molecular Weight: 375.44
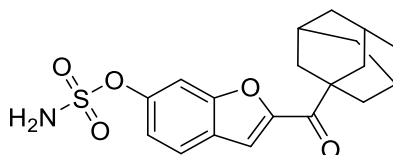
Prepared as described in the general procedure of sulfomylation of phenolic compounds using adamantan-1-yl(6-hydroxybenzofuran-2-yl)methanone (**39j**) (0.15 g, 0.5 mmol). Purification by gradient column chromatography at 30% EtOAc in petroleum ether (v/v) followed by a preparative TLC afforded the product as a white solid.

Yield: 7 mg (4 %)

TLC: Petroleum ether – EtOAc 3:1 v/v, R_f = 0.25

^{1}H NMR (CDCl$_3$) δ: 7.64 (d, J = 8.6 Hz, 1H, Ar), 7.55 (d, J = 1.5 Hz, 1H, Ar), 7.45 (d, J = 0.9 Hz, 1H, Ar), 7.22 (dd, J = 2.1, 8.6 Hz, 1H, Ar), 5.00 (bs, 2H, NH$_2$), 2.05 (s, 9H, adamantane), 1.75 (s, 6H, adamantane).

^{13}C NMR (CDCl$_3$) δ: 196.12 (C), 154.58 (C), 154.52 (C), 149.47 (C), 125.78 (C), 123.64 (CH), 118.59 (CH), 113.16 (CH), 106.69 (CH), 46.27 (C), 38.02 (3 x CH$_2$), 36.65 (3 x CH$_2$), 28.03 (3 x CH).

HPLC (method A): 41.89 % at R.T.= 5.49 min.

HRMS (ESI): Calculated 376.1218 [M+H]$^+$, Found 376.1209 [M+H]$^+$.

4.6.4. Cell culture

As previously described in section 2.5.4

4.6.5. Aromatase activity assay

As previously described in section 2.5.6

4.6.6. Steroid sulfatase assay

STS inhibitory assays were performed as described previously (El-Gamal *et al.* 2020; Purohit *et al.* 1995). Briefly, the ability of a compound to inhibit STS activity was determined using the lysate of JEG-3, a human placenta choriocarcinoma cell line which has high STS activity. To ascertain STS inhibition, enzyme activity was measured in the absence and presence of the inhibitor (0.0001–1 μM) using [^{3}H] oestrone sulphate (E1S; 4×10^5 dpm, Perkin Elmer) adjusted to 20 μM with unlabelled E1S substrate. After incubation of the substrate and inhibitor with JEG-3 lysate (125 μg of protein/mL) for 1 h, the product formed, oestrone (E1), was separated from the mixture by extraction with toluene. [4–^{14}C] E$_1$ (American Radiolabelled Chemicals) was also used throughout the assay to monitor procedural losses. An organic phase aliquot was added to scintillation fluid and the ^{3}H and ^{14}C content measured by scintillation spectrometry. The mass of E1S hydrolysed was calculated from the ^{3}H counts detected (corrected for the volume of medium and organic solvent used and for recovery of ^{14}C counts) and the specific activity of the substrate.

Chapter 5: General conclusion

This thesis consists of five chapters; a general introduction, three results chapters and a general conclusion. The general introduction discussed breast cancer as a common disease, incidence, risk factors, different classes, the treatment options, and resistance suggesting the need for a new generation of aromatase inhibitors. Each of the three results chapters represents an attempt to answer the research question of the thesis investigating the possibility of developing dual binding inhibitors to act as 4th generation aromatase inhibitors for the treatment of breast cancer. An iterative design process of three main elements was used; Computational studies, chemistry and aromatase inhibitory activity.

The computational component involved studying the CYP19A1 crystal structure (PDB 3S79) (Ghosh *et al.* 2012) and the binding requirements indicating that hydrogen bonds for the 3- and 17-keto oxygen with Asp309 and Met374 respectively, the hydrophobic interactions of other residues including Arg115, Ile133, Phe134, Val370, Val373 and Leu477 and haem iron binding are key ligand interactions for the non-steroidal aromatase inhibitors. Docking studies using MOE and MD simulations using Desmond provided theoretical evidence of the possibility of dual binding of the active site and access channel, as shown by the ability of the long chain substitutions, but-2-ynyloxy or pent-2-ynyloxy, to fit in the access channel of the active site, which is lined with Arg192, Val313 and Glu483. This was accompanied by more favourable results generated for the *S*-enantiomer of the compounds than the *R*-enantiomer in terms of binding to the haem through N4 of the triazole ring (chapter two and four) or through the pyridine nitrogen (chapter three).

In total, 45 compounds were prepared using various synthetic pathways. Chapter two, triazole based compounds, which was based on the reported parent compound **6a**, focused on identifying the optimal nature, position, and length of the substitutions. After synthesis and biological evaluation of 22 compounds, a clear SAR could be concluded with the alkynyl chain substituent on the 6-position of the benzofuran ring optimal for activity and the but-2-ynyloxy group provided the optimal length for dual binding compounds. The secondary substituent on the phenyl side showed comparable aromatase inhibitory activity for the nitrile and fluoro, which was better than their chloro analogues. The prepared compounds were found to be potent

inhibitors with 4-((6-(but-2-yn-1-yloxy)benzofuran-2-yl)(1*H*-1,2,4-triazol-1-yl)methyl)benzonitrile (**23c**) showing the best activity at picomolar level (0.09 nM = 90 pM).

Expanding on the dual binding concept discussed in chapter two, a series of 12 pyridine-based inhibitors with different chain length and secondary substituents was prepared and biologically evaluated. Despite being generally less active than the triazole-based compounds, the pyridine compounds with long chain substituents proved to be potent inhibitors with activity in the low nanomolar range indicating the possibility of applying the same dual binding concept implemented in chapter two.

In quite a different approach, eleven sulfamate-based compounds were prepared in chapter four to investigate the dual aromatase/sulfatase inhibition potential. Six compounds were derivatised from the parent compounds (**11-14** and **17**) by replacing the phenolic hydroxy group with a sulfamate group, however these compounds were only active against the aromatase enzyme. This lack of activity against the sulfatase enzyme was attributed to the steric hindrance caused by the tetrahedral geometry of the stereo-centric carbon atom. As a result, the ketone sulfamate compounds **56a-f** were prepared and evaluated against aromatase and sulfatase enzymes showing promising nanomolar activity against both enzymes. However, the synthetic scheme for these compounds was not optimal either owing to poor reactivity of starting material and/or questionable purity of the products.

❖ **Future work:**

1- Representative examples of the compounds will be tested for selectivity (CYP panel e.g. 1A2, 2C9, 2C19, 2D6 and 3A4).

2- Aromatase inhibitors that 'pass' these assays will be subject to more detailed cell/molecular biology investigations to investigate the antiproliferative activity (using aromatase-transfected breast cancer cell line MCF7-AROM (Macaulay *et al.* 1994)).

3- Resistant Cell lines for known AIs based on MCF7-AROM will be developed and the compounds evaluated against these resistant cell lines to determine whether they are effective against the resistant cell lines of clinically used AIs.

4- Resistance for the synthesised compounds will be studied to identify the course and mechanism of resistance (if any).

5- Investigation and optimisation of the synthetic pathway for the sulfamate compounds.

References

De Abreu, F.B., Schwartz, G.N., Wells, W.A. and Tsongalis, G.J. (2014). Personalized therapy for breast cancer. *Clinical Genetics* **86**:62–67.

Ahmed, S., James, K., Owen, C.P. and Patel, C.K. (2002). Synthesis and biochemical evaluation of novel and potent inhibitors of the enzyme oestrone sulphatase (ES). *The Journal of Steroid Biochemistry and Molecular Biology* **80**:419–427.

Akhtar, M., Calder, M.R., Corina, D.L. and Wright, J.N. (1982). Mechanistic studies on C-19 demethylation in estrogen biosynthesis. *Biochemical Journal* **201**:569–580.

Albrecht, W., Unger, A., Bauer, S.M. and Laufer, S.A. (2017). Discovery of N-{4-[5-(4-fluorophenyl)-3-methyl-2-methylsulfanyl-3H-imidazol-4-yl]-pyridin-2-yl}-acetamide (CBS-3595), a dual p38α MAPK/PDE-4 inhibitor with activity against TNFα-related diseases. *Journal of Medicinal Chemistry* **60**:5290–5305.

Alcaro, S., Bolognesi, M.L., García-Sosa, A.T. and Rapposelli, S. (2019). Editorial: Multi-Target-Directed Ligands (MTDL) as challenging research tools in drug discovery: From design to pharmacological evaluation. *Frontiers in Chemistry* **7**:71.

Amin, A.R., Attur, M.G., Pillinger, M. and Abramson, S.B. (1999). The pleiotropic functions of aspirin: Mechanisms of action. *Cellular and Molecular Life Sciences* **56**:305–312.

Appel, R. and Berger, G. (1958). Hydrazinsulfonsaure-Amide. 1. Uber Das Hydrazodisulfamid. *Chemische Berichte-Recueil* **91**:1339–1341.

Beatson, G.T. (1896). On the treatment of inoperable cases of carcinoma of the mamma: suggestions for a new method of treatment with illustrative cases. *Lancet* **II**:104–107.

Begam, A.J., Jubie, S. and Nanjan, M.J. (2017). Estrogen receptor agonists/antagonists in breast cancer therapy: a critical review. *Bioorganic Chemistry* **71**:257–274.

Bertinaria, M., Shaikh, M.A.A.G., Buccellati, C., Cena, C., Rolando, B., Lazzarato, L., Fruttero, R., Gasco, A., Hoxha, M., Capra, V., Sala, A. and Rovati, G.E. (2012). Designing multitarget anti-inflammatory agents: Chemical modulation of the lumiracoxib structure toward dual thromboxane antagonists-COX-2 inhibitors. *ChemMedChem* **7**:1647–1660.

Bhagwat, S. V, Gokhale, P.C., Crew, A.P., Cooke, A., Yao, Y., Mantis, C., Kahler, J., Workman, J., Bittner, M., Dudkin, L., Epstein, D.M., Gibson, N.W., Wild, R., Arnold, L.D., Houghton, P.J. and Pachter, J.A. (2011). Preclinical characterization of OSI-027, a potent and selective inhibitor of mTORC1 and mTORC2: Distinct from rapamycin. *Molecular Cancer Therapeutics* **10**:1394–1406.

Bolognesi, M.L. (2013). Polypharmacology in a single drug: Multitarget drugs. *Current Medicinal Chemistry* **20**:1639–1645.

Bolognesi, M.L. and Cavalli, A. (2016). Multitarget drug discovery and polypharmacology. *ChemMedChem* **11**:1190–1192.

Bonfield, K., Amato, E., Bankemper, T., Agard, H., Steller, J., Keeler, J.M., Roy, D., McCallum, A., Paula, S. and Ma, L. (2012). Development of a new class of aromatase inhibitors: design, synthesis and inhibitory activity of 3-phenylchroman-4-one (isoflavanone) derivatives. *Bioorganic and Medicinal Chemistry* **20**:2603–2613.

Bowers, K.J., Chow, D.E., Xu, H., Dror, R.O., Eastwood, M.P., Gregersen, B.A., Klepeis, J.L., Kolossvary, I., Moraes, M.A. and Sacerdoti, F.D. (2006). Scalable algorithms for molecular dynamics simulations on commodity clusters. In: *SC'06: Proceedings of the 2006 ACM/IEEE Conference on Supercomputing*. IEEE, p. 43.

Schrödinger Release 2020-4: Desmond Molecular Dynamics System, D. E. Shaw Research, New York, NY, 2020. Maestro-Desmond Interoperability Tools, Schrödinger, New York, NY, 2020.

Bray, F., Ferlay, J., Soerjomataram, I., Siegel, R.L., Torre, L.A. and Jemal, A. (2018). Global cancer statistics 2018: GLOBOCAN estimates of incidence and mortality worldwide for 36 cancers in 185 countries. *CA: A Cancer Journal for Clinicians* **68**:394–424.

Brodie, A.M.H., Garrett, W.M., Hendrickson, R., Marcotte, P.A. and Robinson, C.H. (1981). Inactivation of aromatase in vitro by 4-hydroxy-4-androstene-3,17-dione and 4-acetoxy-4-androstene-3,17-dione and sustained effects in vivo. *Steroids* **38**:693–702.

Brodie, A.M.H. and Njar, V.C.O. (1998). Review aromatase inhibitors in advanced breast cancer : mechanism of action and clinical implications. *Journal of Steroid Biochemistry and Molecular Biology* **66**:1–10.

Brooks, P.R., Wirtz, M.C., Vetelino, M.G., Rescek, D.M., Woodworth, G.F., Morgan, B.P. and Coe, J.W. (1999). Boron trichloride/tetra-n-butylammonium iodide: A mild, selective combination reagent for the cleavage of primary alkyl aryl ethers. *Journal of Organic Chemistry* **64**:9719–9721.

Cancer Research UK (2017). *Breast Cancer Statistics*.

Cetin, I. and Topcul, M. (2014). Triple negative breast cancer. *Asian Pacific Journal of Cancer Prevention* **15**:2427–2431.

Chresta, C.M., Davies, B.R., Hickson, I., Harding, T., Cosulich, S., Critchlow, S.E., Vincent, J.P., Ellston, R., Jones, D., Sini, P., James, D., Howard, Z., Dudley, P., Hughes, G., Smith, L., Maguire, S., Hummersone, M., Malagu, K., Menear, K., Jenkins, R., Jacobsen, M., Smith, G.C.M., Guichard, S. and Pass, M. (2010). AZD8055 is a potent, selective, and orally bioavailable ATP-competitive mammalian target of rapamycin kinase inhibitor with in vitro and in vivo antitumor activity. *Cancer Research* **70**:288–298.

Chumsri, S., Howes, T., Bao, T., Sabnis, G. and Brodie, A. (2011). Aromatase, aromatase inhibitors, and breast cancer. *Journal of Steroid Biochemistry and Molecular Biology* **125**:13–22.

Claridge, T.D.W. (2009). Chapter 4 - One-dimensional techniques. In: Claridge, T. D. W. B. T.-T. O. C. S. (ed.) *High-Resolution NMR Techniques in Organic Chemistry*. Elsevier, pp. 99–128.

Cole, M.P., Jones, C.T.A. and Todd, I.D.H. (1971). A new anti-oestrogenic agent in late breast cancer an early clinical appraisal of ICI46474. *British Journal of Cancer* **25**:270–275.

Conley, A. and Hinshelwood, M. (2001). Mammalian aromatases. *Reproduction* **121**:685–695.

Dixon, J.M. (2014). Endocrine resistance in breast cancer. *New Journal of Science* **2014**:1–27.

Dzeshka, M.S., Shantsila, A. and Lip, G.Y.H. (2016). Effects of aspirin on endothelial function and hypertension. *Current Hypertension Reports* **18**:83.

Edge, S.B. and Compton, C.C. (2010). The American Joint Committee on Cancer: the 7th Edition of the AJCC Cancer Staging Manual and the Future of TNM. *Annals of Surgical Oncology* **17**:1471–1474.

Egbuta, C., Lo, J. and Ghosh, D. (2014). Mechanism of Inhibition of Estrogen Biosynthesis by Azole Fungicides. **155**:4622–4628.

Ehrlich, P. (1913). Chemotherapeutics: scientific principles, methods, and result. *Lancet* **16**:445–451.

El-Gamal, M.I., Zaraei, S.O., Foster, P.A., Anbar, H.S., El-Gamal, R., El-Awady, R. and Potter, B.V.L. (2020). A new series of aryl sulfamate derivatives: Design, synthesis, and biological evaluation. *Bioorganic and Medicinal Chemistry* **28**:115406.

Ertas, M., Sahin, Z., Berk, B., Yurttas, L., Biltekin, S.N. and Demirayak, S. (2018). Pyridine-substituted thiazolylphenol derivatives: Synthesis, modeling studies, aromatase inhibition, and antiproliferative activity evaluation. *Archiv der Pharmazie* **351**:1–11.

Ferlay, J., Ervik, M., Lam, F., Colombet, M., Mery, L., Piñeros, M., Znaor, A., Soerjomataram, I. and Bray, F. (2018). *Global Cancer Observatory: Cancer Today.Lyon, France: International Agency for Research on Cancer. Available from: Https://Gco.Iarc.Fr/Today, Accessed [11 June 2019].*

Ferlay, J., Soerjomataram, I., Dikshit, R., Eser, S., Mathers, C., Rebelo, M., Parkin, D.M., Forman, D. and Bray, F. (2015). Cancer incidence and mortality worldwide: sources, methods and major patterns in GLOBOCAN 2012. *International Journal of Cancer* **136**:E359–E386.

Foster, P.A., Chander, S.K., Newman, S.P., Woo, L.W.L., Sutcliffe, O.B., Bubert, C., Zhou, D., Chen, S., Potter, B.V.L., Reed, M.J. and Purohit, A. (2008). A new therapeutic strategy against hormone-dependent breast cancer: The preclinical development of a dual aromatase and sulfatase inhibitor. *Clinical Cancer Research* **14**:6469–6477.

Ghosh, D., Egbuta, C. and Lo, J. (2018). Journal of Steroid Biochemistry and Molecular Biology Testosterone complex and non-steroidal ligands of human aromatase. *Journal of Steroid Biochemistry and Molecular Biology* **181**:11–19.

Ghosh, D., Griswold, J., Erman, M. and Pangborn, W. (2009). Structural basis for androgen specificity and oestrogen synthesis in human aromatase. *Nature* **457**:219–223.

Ghosh, D., Lo, J. and Egbuta, C. (2016). Recent progress in the discovery of next generation inhibitors of aromatase from the structure-function perspective. *Journal of Medicinal Chemistry* **59**:5131–5148.

Ghosh, D., Lo, J., Morton, D., Valette, D., Xi, J., Griswold, J., Hubbell, S., Egbuta, C., Jiang, W., An, J. and Davies, H.M.L. (2012). Novel aromatase inhibitors by structure-guided design. *Journal of Medicinal Chemistry* **55**:8464–8476.

Gilardi, G. and Di Nardo, G. (2017). Heme iron centers in cytochrome P450: structure and catalytic activity. *Rendiconti Lincei* **28**:159–167.

Gobbi, S., Zimmer, C., Belluti, F., Rampa, A., Hartmann, R.W., Recanatini, M. and Bisi, A. (2010). Novel highly potent and selective nonsteroidal aromatase inhibitors: synthesis, biological evaluation and structure-activity relationships investigation. *Journal of Medicinal Chemistry* **53**:5347–5351.

Goss, P.E., Ingle, J.N., Pritchard, K.I., Ellis, M.J., Sledge, G.W., Budd, G.T., Rabaglio, M., Ansari, R.H., Johnson, D.B., Tozer, R., D'Souza, D.P., Chalchal, H., Spadafora, S., Stearns, V., Perez, E.A., Liedke, P.E.R., Lang, I., Elliott, C., Gelmon, K.A., Chapman, J.-A.W. and Shepherd, L.E. (2013). Exemestane versus anastrozole in postmenopausal women with early breast cancer: NCIC CTG MA.27--a randomized controlled phase III trial. *Journal of clinical oncology : official journal of the American Society of Clinical Oncology* **31**:1398–1404.

Guengerich, F.P. (2015). Human cytochrome P450 enzymes. In: de Montellano, P. R. (ed.) *Cytochrome P450: Structure, Mechanism, and Biochemistry*. Cham: Springer International Publishing, pp. 523–785.

Guengerich, F.P., Waterman, M.R. and Egli, M. (2016). Recent structural insights into cytochrome P450 function. *Trends in Pharmacological Sciences* **37**:625–640.

Hackett, J.C., Brueggemeier, R.W. and Hadad, C.M. (2005). The final catalytic step of cytochrome P450 aromatase: a density functional theory study. *Journal of the American Chemical Society* **127**:5224–5237.

Hayashi, S. and Kimura, M. (2015). Mechanisms of hormonal therapy resistance in breast cancer. *International Journal of Clinical Oncology* **20**:262–267.

Herschkowitz, J.I., Simin, K., Weigman, V.J., Mikaelian, I., Usary, J., Hu, Z., Rasmussen, K.E., Jones, L.P., Assefnia, S., Chandrasekharan, S., Backlund, M.G., Yin, Y., Khramtsov, A.I., Bastein, R., Quackenbush, J., Glazer, R.I., Brown, P.H., Green, J.E., Kopelovich, L., Furth, P.A., Palazzo, J.P., Olopade, O.I., Bernard, P.S., Churchill, G.A., Van Dyke, T. and Perou, C.M. (2007). Identification of conserved gene expression features between murine mammary carcinoma models and human breast tumors. *Genome Biology* **8**:1–17.

Hiscox, S., Davies, E.L. and Barrett-Lee, P. (2009). Aromatase inhibitors in breast cancer. *Maturitas* **63**:275–279.

Hu, Z., Fan, C., Oh, D.S., Marron, J.S., He, X., Qaqish, B.F., Livasy, C., Carey, L.A., Reynolds, E., Dressler, L., Nobel, A., Parker, J., Ewend, M.G., Sawyer, L.R., Wu, J., Liu, Y., Nanda, R., Tretiakova, M., Orrico, A.R., Dreher, D., Palazzo, J.P., Perreard, L., Nelson, E., Mone, M., Hansen, H., Mullins, M., Quackenbush, J.F., Ellis, M.J., Olopade, O.I., Bernard, P.S. and Perou, C.M. (2006). The molecular portraits of breast tumors are conserved across microarray platforms. *BMC Genomics* **7**:1–12.

Jackson, T., Woo, L.W.L., Trusselle, M.N., Chander, S.K., Purohit, A., Reed, M.J. and Potter, B.V.L. (2007). Dual aromatase-sulfatase inhibitors based on the anastrozole template: Synthesis, in vitro SAR, molecular modelling and in vivo activity. *Organic and Biomolecular Chemistry* **5**:2940–2952.

Jepsen, T.H., Larsen, M., Jørgensen, M., Solanko, K.A., Bond, A.D., Kadziola, A. and Nielsen, M.B. (2011). Synthesis of functionalized dibenzothiophenes- An efficient three-step approach based on Pd-catalyzed C-C and C-S bond formations. *European Journal of Organic Chemistry* **2011**:53–57.

Jessie, W., Zeruesenay, L. and Flockhart, D.A. (2012). Tamoxifen metabolites as active inhibitors of aromatase in the treatment of breast cancer. *Breast Cancer Research and treatment* **131**:473–481.

Kang, H., Xiao, X., Huang, C., Yuan, Y., Tang, D., Dai, X. and Zeng, X. (2018). Potent aromatase inhibitors and molecular mechanism of inhibitory action. *European Journal of Medicinal Chemistry* **143**:426–437.

Kim, Y.W., Hackett, J.C. and Brueggemeier, R.W. (2004). Synthesis and aromatase inhibitory activity of novel pyridine-containing isoflavones. *Journal of Medicinal Chemistry* **47**:4032–4040.

Knight, S.D., Adams, N.D., Burgess, J.L., Chaudhari, A.M., Darcy, M.G., Donatelli, C.A., Luengo, J.I., Newlander, K.A., Parrish, C.A., Ridgers, L.H., Sarpong, M.A., Schmidt, S.J., Van Aller, G.S., Carson, J.D., Diamond, M.A., Elkins, P.A., Gardiner, C.M., Garver, E., Gilbert, S.A., Gontarek, R.R., Jackson, J.R., Kershner, K.L., Luo, L., Raha, K., Sherk, C.S., Sung, C.-M., Sutton, D., Tummino, P.J., Wegrzyn, R.J., Auger, K.R. and Dhanak, D. (2010). Discovery of GSK2126458, a highly potent inhibitor of PI3K and the mammalian target of rapamycin. *ACS Medicinal Chemistry Letters* **1**:39–43.

Kolev, V.N., Wright, Q.G., Vidal, C.M., Ring, J.E., Shapiro, I.M., Ricono, J., Weaver, D.T., Padval, M. V, Pachter, J.A. and Xu, Q. (2015). PI3K/mTOR Dual inhibitor VS-5584 preferentially targets cancer stem cells. *Cancer Research* **75**:446–455.

Lipinski, C.A., Lombardo, F., Dominy, B.W. and Feeney, P.J. (1997). Experimental and computational approaches to estimate solubility and permeability in drug discovery and development settings. *Advanced Drug Delivery Reviews* **23**:3–25.

Maas, P., Barrdahl, M., Joshi, A.D., Auer, P.L., Gaudet, M.M., Milne, R.L., Schumacher, F.R., Anderson, W.F., Check, D., Chattopadhyay, S., Baglietto, L., Berg, C.D., Chanock, S.J., Cox, D.G., Figueroa, J.D., Gail, M.H., Graubard, B.I., Haiman, C.A., Hankinson, S.E., Hoover, R.N., Isaacs, C., Kolonel, L.N., Marchand, L. Le, Lee, I., Lindström, S., Overvad, K., Romieu, I., Sanchez, M., Southey, M.C., Stram, D.O., Tumino, R., Vanderweele, T.J., Willett, W.C., Zhang, S., Buring, J.E., Canzian, F., Gapstur, S.M., Henderson, B.E., Hunter, D.J., Giles, G.G., Prentice, R.L., Ziegler, R.G., Kraft, P., Garcia-closas, M. and Chatterjee, N. (2019). Breast Cancer Risk From Modifiable and Nonmodifiable Risk Factors Among White Women in the United States. *JAMA Oncology* **21205**:1295–1302.

Macaulay, V.M., Nicholls, J.E., Gledhill, J., Rowlands, M.G., Dowsett, M. and Ashworth, A. (1994). Biological effects of stable overexpression of aromatase in human hormone-dependent breast cancer cells. *British Journal of Cancer* **69**:77–83.

Macedo, L.F., Sabnis, G.J., Goloubeva, O.G. and Brodie, A. (2008). Combination of anastrozole with fulvestrant in the intratumoral aromatase xenograft model. *Cancer Research* **68**:3516–3522.

Magistrato, A., Sgrignani, J., Krause, R. and Cavalli, A. (2017). Single or Multiple Access Channels to the CYP450s Active Site? An Answer from Free Energy Simulations of the Human Aromatase Enzyme. *The Journal of Physical Chemistry Letters* **8**:2036–2042.

Mahboobi, S., Sellmer, A., Höcher, H., Garhammer, C., Pongratz, H., Maier, T., Ciossek, T. and Beckers, T. (2007). 2-Aroylindoles and 2-aroylbenzofurans with N-hydroxyacrylamide substructures as a novel series of rationally designed histone deacetylase inhibitors. *Journal of Medicinal Chemistry* **50**:4405–4418.

Mak, P.J. and Denisov, I.G. (2018). Spectroscopic studies of the cytochrome P450 reaction mechanisms. *Biochimica et Biophysica Acta - Proteins and Proteomics* **1866**:178–204.

Malhotra, G.K., Zhao, X., Band, H. and Band, V. (2010). Histological, molecular and functional subtypes of breast cancers. *Cancer Biology & Therapy* **10**:955–960.

Manikandan, P. and Nagini, S. (2018). Cytochrome P450 structure, function and clinical significance: a Review. *Current Drug Targets* **19**:38–54.

Di Matteo, M., Ammazzalorso, A., Andreoli, F., Caffa, I., De Filippis, B., Fantacuzzi, M., Giampietro, L., Maccallini, C., Nencioni, A., Parenti, M.D., Soncini, D., Del Rio, A. and Amoroso, R. (2016). Synthesis and biological characterization of 3-(imidazol-1-ylmethyl)piperidine sulfonamides as aromatase inhibitors. *Bioorganic and Medicinal Chemistry Letters* **26**:3192–3194.

Maurelli, S., Chiesa, M., Giamello, E., Di Nardo, G., Valentina, V.E., Gilardi, G. and Van Doorslaer, S. (2011). Direct spectroscopic evidence for binding of anastrozole to the iron heme of human aromatase. Peering into the mechanism of aromatase inhibition. *Chemical Communications* **47**:10737–10739.

Mavaddat, N., Antoniou, A.C., Easton, D.F. and Garcia-Closas, M. (2010). Genetic susceptibility to breast cancer. *Molecular Oncology* **4**:174–191.

Mei, Y. and Yang, B. (2018). Rational application of drug promiscuity in medicinal chemistry. *Future Medicinal Chemistry* **10**:1835–1851.

Meshram, H.M., Reddy, B.C., Prasad, B.R. V, Goud, P.R., Kumar, G.S. and Kumar, R.N. (2012). DABCO-promoted efficient and convenient synthesis of benzofurans. *Synthetic Communications* **42**:1669–1676.

Millan, M.J. (2009). Dual- and triple-acting agents for treating core and co-morbid symptoms of major depression: novel concepts, new Drugs. *Neurotherapeutics* **6**:53–77.

Miller, W.L. and Auchus, R.J. (2011). The molecular biology, biochemistry, and physiology of human steroidogenesis and its disorders. *Endocrine Reviews* **32**:81–151.

Miller, W.R. (1999). Biology of aromatase inhibitors : pharmacology / endocrinology within the breast. *Endocrine-Related Cancer* **6**:187–195.

Miller, W.R. and Larionov, A.A. (2012). Understanding the mechanisms of aromatase inhibitor resistance. *Breast Cancer Research* **14**:201.

Mojaddami, A., Sakhteman, A., Fereidoonnezhad, M., Faghih, Z., Najdian, A., Khabnadideh, S., Sadeghpour, H. and Rezaei, Z. (2017). Binding mode of triazole derivatives as aromatase inhibitors based on docking, protein ligand interaction fingerprinting, and molecular dynamics simulation studies. *Research in Pharmaceutical Sciences* **12**:21–30.

Mokhtari, R.B., Homayouni, T.S., Baluch, N., Morgatskaya, E., Kumar, S., Das, B. and Yeger, H. (2017). Combination therapy in combating cancer. *Oncotarget* **8**:38022–38043.

Molecular Operating Environment (MOE), 2019.01; Chemical Computing Group ULC, 1010 Sherbooke St. West, Suite #910, Montreal, QC, Canada, H3A 2R7, **2020**.

Morphy, R., Kay, C. and Rankovic, Z. (2004). From magic bullets to designed multiple ligands. *Drug Discovery Today* **9**:641–651.

Morphy, R. and Rankovic, Z. (2005). Designed multiple ligands. An emerging drug discovery paradigm. *Journal of Medicinal Chemistry* **48**:6523–6543.

Morphy, R. and Rankovic, Z. (2009). Designing multiple ligands – Medicinal chemistry strategies and challenges. *Current Pharmaceutical Design* **15**:587–600.

Morphy, R. and Rankovic, Z. (2007). Fragments, network biology and designing multiple ligands. *Drug Discovery Today* **12**:156–160.

Morphy, R. and Rankovic, Z. (2003). Medicinal chemistry approaches for multitarget drugs. In: *Burger's Medicinal Chemistry and Drug Discovery*. American Cancer Society, pp. 249–274.

Murray, J., Young, O.E., Renshaw, L., White, S., Williams, L., Evans, D.B., Thomas, J.S.J., Dowsett, M. and Dixon, J.M. (2009). A randomised study of the effects of letrozole and anastrozole on oestrogen receptor positive breast cancers in postmenopausal women. *Breast Cancer Research and Treatment* **114**:495–501.

Di Nardo, G., Castrignanò, S., Sadeghi, S.J., Baravalle, R. and Gilardi, G. (2015). Bioelectrochemistry as a tool for the study of aromatization of steroids by human aromatase. *Electrochemistry Communications* **52**:25–28.

Di Nardo, G. and Gilardi, G. (2013). Human aromatase: perspectives in biochemistry and biotechnology. *Biotechnology and Applied Biochemistry* **60**:92–101.

Omura, T. and Sato, R. (1962). Liver microsomes spermidine in the extraction of the deoxyribosyl-synthesizing system from Escherichia. *Journal of Bological Chemistry* **237**:1375–1376.

Palmieri, C., Stein, R.C., Liu, X., Hudson, E., Nicholas, H., Sasano, H., Guestini, F., Holcombe, C., Barrett, S., Kenny, L., Reed, S., Lim, A., Hayward, L., Howell, S. and Coombes, R.C. (2017). IRIS study: a phase II study of the steroid sulfatase inhibitor Irosustat when added to an aromatase inhibitor in ER-positive breast cancer patients. *Breast Cancer Research and Treatment* **165**:343–353.

Patel, R.R., Sengupta, S., Kim, H.R., Klein-Szanto, A.J., Pyle, J.R., Zhu, F., Li, T., Ross, E.A., Oseni, S., Fargnoli, J. and Jordan, V.C. (2010). Experimental treatment of oestrogen receptor (ER) positive breast cancer with tamoxifen and brivanib alaninate, a VEGFR-2/FGFR-1 kinase inhibitor: A potential clinical application of angiogenesis inhibitors. *European Journal of Cancer* **46**:1537–1553.

Perou, C.M., Sørile, T., Eisen, M.B., Van De Rijn, M., Jeffrey, S.S., Ress, C.A., Pollack, J.R., Ross, D.T., Johnsen, H., Akslen, L.A., Fluge, Ø., Pergammenschlkov, A., Williams, C., Zhu, S.X., Lønning, P.E., Børresen-Dale, A.-L., Brown, P.O. and Botstein, D. (2000). Molecular portraits of human breast tumours. *Nature* **406**:747–752.

Pestellini, V., Giolitti, A., Pasqui, F., Abelli, L., Cutrufo, C., De Salvia, G., Evangelista, S. and Meli, A. (1988). Synthesis and hypolipidemic activity of new substituted (benzofuran-2-yl)-phenyl-carbinols. *European Journal of Medicinal Chemistry* **23**:203–206.

Plattner, J.J., Martin, Y.C., Smital, J.R., Lee, C.M., Fung, A.K.L., Horrom, B.W., Crowley, S.R., Pernet, A.G., Bunnell, P.R. and Kim, K.H. (1985). [(Aminomethyl)aryloxy]acetic Acid Esters. a new class of high-ceiling diuretics. 3. variation in the bridge between the aromatic rings to complete mapping of the receptor. *Journal of Medicinal Chemistry* **28**:79–93.

Polyak, K. (2011). Heterogeneity in breast cancer. *The Journal of Clinical Investigation* **121**:3786–3788.

Porubsky, P.R., Meneely, K.M. and Scott, E.E. (2008). Structures of human cytochrome P-450 2E1: insights into the binding of inhibitors and both small molecular weight and fatty acid substrates. *Journal of Biological Chemistry* **283**:33698–33707.

Proschak, E., Stark, H. and Merk, D. (2019). Polypharmacology by design: A medicinal chemist's perspective on multitargeting compounds. *Journal of Medicinal Chemistry* **62**:420–444.

Purohit, A. and Foster, P.A. (2012). Steroid sulfatase inhibitors for estrogen- and androgen-dependent cancers. *Journal of Endocrinology* **212**:99–110.

Purohit, A., Williams, G.J., Howarth, N.M., Potter, B.V.L. and Reed, M.J. (1995). Inactivation of steroid sulfatase by an active site-directed inhibitor, estrone-S-O-sulfamate. *Biochemistry* **34**:11508–11514.

Ramsay, R.R., Popovic-Nikolic, M.R., Nikolic, K., Uliassi, E. and Bolognesi, M.L. (2018). A perspective on multi-target drug discovery and design for complex diseases. *Clinical and Translational Medicine* **7**:3–16.

Recksiek, M., Selmer, T., Dierks, T., Schmidt, B. and Von Figura, K. (1998). Sulfatases, trapping of the sulfated enzyme intermediate by substituting the active site formylglycine. *Journal of Biological Chemistry* **273**:6096–6103.

Reed, M.J., Purohit, A., Woo, L.W.L., Newman, S.P. and Potter, B.V.L. (2005). Steroid sulfatase: Molecular biology, regulation, and inhibition. *Endocrine Reviews* **26**:171–202.

Rowland, P., Blaney, F.E., Smyth, M.G., Jones, J.J., Leydon, V.R., Oxbrow, A.K., Lewis, C.J., Tennant, M.G., Modi, S., Eggleston, D.S., Chenery, R.J. and Bridges, A.M. (2006). Crystal structure of human cytochrome P450 2D6. *Journal of Biological Chemistry* **281**:7614–7622.

Saberi, M.R., Shah, K. and Simons, C. (2005). Benzofuran- and furan-2-yl-(phenyl)-3-pyridylmethanols: Synthesis and inhibition of P450 aromatase. *Journal of Enzyme Inhibition and Medicinal Chemistry* **20**:135–141.

Saberi, M.R., Vinh, T.K., Yee, S.W., Griffiths, B.J.N., Evans, P.J. and Simons, C. (2006). Potent CYP19 (aromatase) 1-(benzofuran-2-yl)(phenylmethyl)pyridine, -imidazole, and -triazole inhibitors: synthesis and biological evaluation. *Journal of Medicinal Chemistry* **49**:1016–1022.

Salah, M., Abdelsamie, A.S. and Frotscher, M. (2017). First Dual Inhibitors of Steroid Sulfatase (STS) and 17β-Hydroxysteroid Dehydrogenase Type 1 (17β-HSD1): Designed Multiple Ligands as Novel Potential Therapeutics for Estrogen-Dependent Diseases. *Journal of Medicinal Chemistry* **60**:4086–4092.

Salomé, C., Narbonne, V., Ribeiro, N., Thuaud, F., Serova, M., De Gramont, A., Faivre, S., Raymond, E. and Désaubry, L. (2014). Benzofuran derivatives as a novel class of inhibitors of mTOR signaling. *European Journal of Medicinal Chemistry* **74**:41–49.

Sastry, G.M., Adzhigirey, M., Day, T., Annabhimoju, R. and Sherman, W. (2013). Protein and ligand preparation: Parameters, protocols, and influence on virtual screening enrichments. *Journal of Computer-Aided Molecular Design* **27**:221–234.

Schrödinger Release 2020-4: Protein Preparation Wizard; Epik, Schrödinger, LLC, New York, NY, 2016; Impact, Schrödinger, LLC, New York, NY, 2016; Prime, Schrödinger, LLC, New York, NY, 2020.

Schmidt, B., Riemer, M. and Schilde, U. (2014). Chroman-4-ones via Microwave-Promoted Domino Claisen Rearrangement–Oxa-Michael Addition: Synthesis of Tabchromones A and B. *Synlett* **25**:2943–2946.

Schoch, G.A., Yano, J.K., Sansen, S., Dansette, P.M., Stout, C.D. and Johnson, E.F. (2008). Determinants of cytochrome P450 2C8 substrate binding: structures of complexes with montelukast, troglitazone, felodipine, and 9-cis-retinoic acid. *Journal of Biological Chemistry* **283**:17227–17237.

Sen, K. and Hackett, J.C. (2012). Coupled electron transfer and proton hopping in the final step of CYP19-catalyzed androgen aromatization. *Biochemistry* **51**:3039–3049.

Sgrignani, J., Bon, M., Colombo, G. and Magistrato, A. (2014). Computational approaches elucidate the allosteric mechanism of human aromatase inhibition: a novel possible route to small-molecule regulation of CYP450s activities? *Journal of Chemical Information and Modeling* **54**:2856–2868.

Singh, R., Nagesh, K. and Parameshwar, M. (2016). Rhodium(II)-Catalyzed Undirected and Selective C(sp2)-H Amination en Route to Benzoxazolones. *ACS Catalysis* **6**:6520–6524.

Skok, Z., Zidar, N., Kikelj, D. and ILAŠ, J. (2019). Dual inhibitors of human DNA topoisomerase II and other cancer-related targets. *Journal of Medicinal Chemistry* **63**:884–904.

Sohl, C.D. and Guengerich, F.P. (2010). Kinetic analysis of the three-step steroid aromatase reaction of human cytochrome P450 19A1. *Journal of Biological Chemistry* **285**:17734–17743.

Spinello, A., Martini, S., Berti, F., Pennati, M., Pavlin, M., Sgrignani, J., Grazioso, G., Colombo, G., Zaffaroni, N. and Magistrato, A. (2019). European Journal of Medicinal Chemistry Rational design of allosteric modulators of the aromatase enzyme : An unprecedented therapeutic strategy to fi ght breast cancer. *European Journal of Medicinal Chemistry* **168**:253–262.

Stauffer, F., Furet, P., Floersheimer, A. and Lang, M. (2012). New aromatase inhibitors from the 3-pyridyl arylether and 1-aryl pyrrolo[2,3-c]pyridine series. *Bioorganic and Medicinal Chemistry Letters* **22**:1860–1863.

Takahashi, S., Nagano, S., Nogawa, T., Kanoh, N., Uramoto, M., Kawatani, M., Shimizu, T., Miyazawa, T., Shiro, Y. and Osada, H. (2014). Structure-function analyses of cytochrome P450revI involved in reveromycin A biosynthesis and evaluation of the biological activity of its substrate, reveromycin T. *Journal of Biological Chemistry* **289**:32446–32458.

Tang, Z., Niu, S., Liu, F., Lao, K., Miao, J., Ji, J., Wang, X., Yan, M., Zhang, L., You, Q., Xiao, H. and Xiang, H. (2014). Synthesis and biological evaluation of 2,3-diaryl isoquinolinone derivatives as anti-breast cancer agents targeting ERα and VEGFR-2. *Bioorganic & Medicinal Chemistry Letters* **24**:2129–2133.

Tokunaga, E., Hisamatsu, Y., Tanaka, K., Yamashita, N., Saeki, H., Oki, E., Kitao, H. and Maehara, Y. (2014). Molecular mechanisms regulating the hormone sensitivity of breast cancer. *Cancer Science* **105**:1377–1383.

Tripathi, S., Srivastava, G. and Sharma, A. (2019). Computational design of multi-target drugs against breast cancer. In: Roy, K. (ed.) *Multi-Target Drug Design Using Chem-Bioinformatic Approaches*. New York, NY: Springer New York, pp. 443–458.

Vargo-Gogola, T. and Rosen, J.M. (2007). Modelling breast cancer: one size does not fit all. *Nature Reviews Cancer* **7**:659–672.

Vinh, T.K., Ahmadi, M., Delgado, P.O.L., Perez, S.F., Walters, H.M., Smith, H.J., Nicholls, P.J. and Simons, C. (1999). 1-[(Benzofuran-2-yl) phenylmethyl]-triazoles and-tetrazoles-potent competitive inhibitors of aromatase. *Bioorganic & medicinal chemistry letters* **9**:2105–2108.

Waks, A.G. and Winer, E.P. (2019). Breast Cancer Treatment: A Review. *JAMA* **321**:288–300.

Wang, Z., Bennett, E.M., Wilson, D.J., Salomon, C. and Vince, R. (2007). Rationally designed dual inhibitors of HIV reverse transcriptase and integrase. *Journal of Medicinal Chemistry* **50**:3416–3419.

Wang, Z. and Vince, R. (2008). Synthesis of pyrimidine and quinolone conjugates as a scaffold for dual inhibitors of HIV reverse transcriptase and integrase. *Bioorganic and Medicinal Chemistry Letters* **18**:1293–1296.

Werck-Reichhart, D. and Feyereisen, R. (2000). Cytochromes P450: a success story. *Genome Biology* **1**:1–9.

Williams, P.A. (2004). Crystal structures of human cytochrome P450 3A4 bound to metyrapone and progesterone. *Science* **305**:683–686.

Woo, L.W.L., Bubert, C., Purohit, A. and Potter, B.V.L. (2011). Hybrid dual aromatase-steroid sulfatase inhibitors with exquisite picomolar inhibitory activity. *ACS Medicinal Chemistry Letters* **2**:243–247.

Woo, L.W.L., Bubert, C., Sutcliffe, O.B., Smith, A., Chander, S.K., Mahon, M.F., Purohit, A., Reed, M.J. and Potter, B.V.L. (2007). Dual aromatase-steroid sulfatase inhibitors. *Journal of Medicinal Chemistry* **50**:3540–3560.

Woo, L.W.L., Jackson, T., Putey, A., Cozier, G., Leonard, P., Ravi Acharya, K., Chander, S.K., Purohit, A., Reed, M.J. and Potter, B.V.L. (2010). Highly potent first examples of dual aromatase-steroid sulfatase inhibitors based on a biphenyl template. *Journal of Medicinal Chemistry* **53**:2155–2170.

Woo, L.W.L., Sutcliffe, O.B., Bubert, C., Grasso, A., Chander, S.K., Purohit, A., Reed, M.J. and Potter, B.V.L. (2003). First dual aromatase-steroid sulfatase inhibitors. *Journal of Medicinal Chemistry* **46**:3193–3196.

Wood, P.M., Woo, L.W.L., Thomas, M.P., Mahon, M.F., Purohit, A. and Potter, B.V.L. (2011). Aromatase and dual aromatase-steroid sulfatase inhibitors from the letrozole and vorozole templates. *ChemMedChem* **6**:1423–1438.

Wouters, W., Snoeck, E. and Coster, R. De (1994). Vorozole, a specific non-steroidal aromatase inhibitor. *Breast Cancer Research and Treatment* **30**:89–94.

Yano, J.K., Wester, M.R., Schoch, G.A., Griffin, K.J., Stout, C.D. and Johnson, E.F. (2004). The structure of human microsomal cytochrome P450 3A4 determined by X-ray crystallography to 2.05 Å resolution. *Journal of Biological Chemistry* **279**:38091–38094.

Yoshizawa, K., Toyota, S., Toda, F. and Csöregh, I. (2003). Preparative and mechanistic studies of solvent-free Rap-Stoermer reactions. *Green Chemistry* **5**:353–356.

Youdim, M.B.H. and Buccafusco, J.J. (2005). Multi-functional drugs for various CNS targets in the treatment of neurodegenerative disorders. *Trends in Pharmacological Sciences* **26**:27–35.

Zhao, S., Wang, X. and Zhang, L. (2013). Polyethylene glycol (PEG-400) as an efficient and recyclable reaction medium for the synthesis of 2-aroylbenzofurans. *Organic Preparations and Procedures International* **45**:421–428.

Zhou, J., Jiang, X., He, S., Jiang, H., Feng, F., Liu, W., Qu, W. and Sun, H. (2019). Rational design of multitarget-directed ligands: strategies and emerging paradigms. *Journal of Medicinal Chemistry* **62**:8881–8914.

Zhou, J., Li, Q., Wu, M., Chen, C. and Cen, S. (2016). Progress in the rational design for polypharmacology drug. *Current Pharmaceutical Design* **22**:3182–3189.